Developing the potential of airborne lidar systems for the sustainable management of forests : Accounting for and managing the impacts of lidar scan angle on ABA model predictions of forest attributes

Karun Dayal

THÈSE POUR OBTENIR LE GRADE DE DOCTEUR DE L'INSTITUT NATIONAL DES SCIENCES ET INDUSTRIES DU VIVANT ET DE L'ENVIRONNEMENT - AGROPARISTECH

N° : 2022 AGPT 0011

Géomatique

École doctorale GAIA – Biodiversité, Agriculture, Alimentation, Environnement, Terre, Eau – n°584
Portée par l'Université de Montpellier

Unité de recherche TETIS

Titre de la thèse

Developing the potential of airborne lidar systems for the sustainable management of forests: Accounting for and managing the impacts of lidar scan angle on ABA model predictions of forest attributes

Présentée par Karun Reuel DAYAL
Le 19 Septembre 2022

Sous la direction de Sylvie DURRIEU et du co-encadrant Marc BOUVIER

Devant le jury composé de

Sylvie DURRIEU, ICPEF, INRAE	Directrice de thèse
Marc BOUVIER, Ingénieur de recherche, IRD	Co-encadrant de thèse
Jocelyn CHANUSSOT, Professeur, Grenoble INP	Rapporteur
Felix MORSDORF, Maître de conférences, Université de Zurich	Rapporteur
Richard FOURNIER, Professeur, Université de Sherbrooke	Membre du jury
Pierre COUTERON, Directeur de Recherche, IRD	Président

AgroParisTech

UNIVERSITÉ DE MONTPELLIER

Foreword

This PhD was carried out at the *Unité Mixte de Recherche (UMR) – TETIS (Territoires, environnement, télédétection et information spatiale)* at *La Maison de la Télédétection*, in Montpellier, France. The *Région Occitanie* and INRAE co-funded the PhD scholarship. This PhD was also carried out in the framework of the PROTEST project, supported by the French Agency for Ecological Transition (ADEME) (grant 1703C0069, GRAINE program) and the FRISBEE project, supported by the TOSCA Continental Surface program of the Centre National d'Etudes Spatiales (CNES) (order N° 4500070632).

Abstract

Information measured by lidar depends on the observed vegetation and the acquisition geometry, which is a function of the acquisition parameters and the terrain properties. The thesis aims to understand the relationship between lidar acquisition geometry and forest attribute predictions, focusing on the assessment and management of impacts of lidar scan angle on lidar metrics and ABA models. Four different forest types were studied with three forest types (broadleaf, coniferous and mixed) in mountainous terrain and one forest type (riparian) in relatively flat terrain. The thesis was divided into three parts. The first part assessed the effect of lidar scan angle on lidar metrics commonly used in ABA predictions. It was observed that different lidar metrics behave differently under changing scan angles. Subsequently, the effect of including metrics with different sensitivities to scan angle was investigated in the second part of the study. A model involving a set of predefined metrics with different sensitivities to scan angle was used. Existing lidar datasets were resampled based on the flight lines 1) to simulate lidar acquisitions with different scan geometries, 2) to build models for a set of scan patterns and 3) to further compare the quality of estimations resulting from each scan pattern. These comparisons highlighted that introducing metrics sensitive to scan angle led to a decrease in model robustness. Also, the variation in the accuracy of ABA models was found to be higher for datasets consisting of point clouds scanned from only one flight line as opposed to those consisting of point clouds scanned from multiple flight lines. The normalisation of lidar metrics sensitive to scan angle was also attempted using voxelisation. Voxel-based metrics contributed by increasing either the precision or the accuracy, or both. In the last part of the study, the terrain properties and acquisition parameters were considered explicitly. As the interaction between lidar acquisition parameters, terrain, and vegetation properties can be complex, neural networks were used to model the relationships between various lidar metrics and the acquisition geometry, resulting in significantly better ABA predictions.

Keywords: lidar, forest, scan angle, voxelisation, neural networks, sustainable management

Résume

L’information mesurée par Lidar aéroporté dépend de la végétation observée et de la géométrie de l'acquisition lidar, elle-même fonction des paramètres d'acquisition et des propriétés du terrain. Cette thèse vise à comprendre la relation entre la géométrie d'acquisition du lidar et les prédictions d'attributs forestiers en se focalisant sur l'évaluation et la gestion des impacts de l'angle de balayage du lidar sur les métriques lidar et les modèles construits à l’échelle du peuplement (i.e. approches surfaciques ou ABA). Quatre types de forêts différents ont été étudiés, dont trois types de forêts (feuillus, conifères et mixtes) en terrain montagneux et un type de forêt (ripisylve) en terrain relativement plat. La thèse est divisée en trois parties. La première partie évalue l'effet de l'angle de balayage du lidar sur les mesures lidar couramment utilisées dans les prédictions de type ABA. On a ainsi montré que les différentes métriques lidar ne sont pas impactées de la même façon par des changements d'angle de balayage. La deuxième partie de l'étude s’intéresse aux conséquences sur la qualité des modèles de l’introduction dans ces modèles de métriques lidar présentant des sensibilités différentes à l'angle de balayage. Un modèle basé sur un jeu de métriques Lidar prédéfinies, plus ou moins sensibles aux angles de balayage, est utilisé.

Les jeux de données lidar existants sont ré-échantillonnés selon les lignes de vol pour 1) simuler des acquisitions lidar avec différentes configurations de balayage, 2) construire des modèles pour une série de configurations de balayage différentes, et 3) comparer la qualité des estimations qui résultent de chaque configuration d’acquisition. Ces comparaisons montrent que l’introduction de métriques sensibles à l’angle de balayage diminue la robustesse des modèles. De plus, la variation de la précision des modèles ABA s’est révélée être plus élevée pour les jeux de données composés de nuages de points acquis depuis une seule ligne de vol que pour ceux composés de nuages de points obtenus en combinant les mesures de plusieurs lignes de vol.

Nous avons aussi tenté de normaliser les métriques lidar en utilisant des méthodes de voxellisation pour limiter les impacts des changements d’angles de balayage. Les métriques issues des données voxellisées contribuent à augmenter la précision des prédictions ou à augmenter leur justesse, ou, dans certains cas, les deux en même temps. Dans la dernière partie de l'étude, les propriétés du terrain (topographie) et les paramètres d'acquisition sont explicitement pris en compte dans les modèles. Comme les interactions entre les paramètres d'acquisition lidar, le terrain et les propriétés de la végétation peuvent être complexes, un réseau de neurone (perceptron multicouche) est utilisé pour modéliser les relations entre les attributs forestiers et les métriques lidar en tenant compte de ces interactions entre métriques lidar et géométrie d'acquisition. Cela a permis d'améliorer significativement les prédictions ABA.

Mots clés: lidar, forêt, angle de scan, voxellisation, réseau de neurones, gestion durable

Table of contents

Acknowledgements

I want to express my gratitude to my supervisors, Sylvie Durrieu and Marc Bouvier, for considering me suitable for this study. They have been incredibly kind and encouraging right since the very beginning of this journey. They have always treated all my ideas, good or bad, with due consideration, which has helped me nurture my desire to ask questions and wonder. I hope I have lived up to at least some of their expectations.

I would especially like to thank Sylvie again, with whom I frequently interacted at MTD during the study. Coming from a completely different environment, I was unsure of the challenges I would face. Sylvie indeed went above and beyond in guiding and motivating me with inspirational kindness and patience. Thank you for sharing your knowledge with me.

I want to express my gratitude to Felix Morsdorf and Jocelyn Chanussot for agreeing to be a part of the jury and review my thesis. I would also like to thank Richard Fournier for agreeing to be a part of the jury to assess my work. Their constructive and positive comments on this study were highly motivating as I take my first steps as a young researcher.

I want to mention Pierre-Yves Vion and Marie-Laure Morel for helping me complete the formalities needed from the other side of the world. It would not have been possible without you.

I would especially like to thank the members of my '*comité de suivi de thèse*', Pierre Couteron, Samuel Alleaume, Cédric Vega and Jean-Pierre Renaud, for guiding me with their suggestions. Thank you, Jean-Pierre, for always being available to help me with statistics. Thank you, François Pimont, David Sheeren and Michel Chartier, for contributing diverse ideas and perspectives to my work.

I had a wonderful time on the field trips with Eric and Samuel. Thank you for the experience and the memories. I want to thank Jean-Matthieu Monnet, Dino and Florian for sharing their technical expertise when I needed it.

Arriving in a new environment was understandably overwhelming sometimes. Milo and Jacques always reached out to me to ensure I felt comfortable in and outside the lab. Thank you for always inviting me to be a part of events and sharing many memorable times with my fellow students.

I would like to mention Milo, Sara, Mehtab, Camille, Larissa and Kamel, with whom I shared the office at different times. Thank you for all the memories. Thank you, Anouk, for all the help and the memorable interactions. I wish you all the success in the future.

A big thank you to everyone at MTD and INRAE who may have had a role to play, directly or indirectly, in helping me complete this journey.

Rowan, this would not have been possible without you. The three most challenging years of my life were navigable only because of your support and constant belief in my abilities when mine would waver. Having met you and your family, it felt like a home away from home. I will forever remember all the little souls we were able to help together and that compassion and kindness are uncompromisable ideals.

When I left India, a place dear to me, little did I know that I would not be returning for three years. A lot has passed in those years. My family always supported and encouraged me through successes, failures, losses, joys and sorrows. I thank them for their patience and understanding.

Un très grand merci à tous les gens en France. Ce pays sera toujours spécial pour moi.

List of figures

Chapter 1

Chapter 2

Chapter 3

Chapter 4

List of tables

Chapter 2

Chapter 3

Chapter 4

Acronyms

ABA: Area-based Approach

ALS: Airborne Laser Scanning

ANN: Artificial Neural Networks

BA: Basal area

DBH: Diameter at breast height

EFI: Enhanced Forest Inventory

FOV: Field of View

ITD: Individual Tree Detection

LAD/PAD: Leaf/Plant Area Density

LAI/PAI: Leaf/Plant Area Index

MFI: Multisource Forest Inventory

MLP: Multilayer perceptron

MSA: Mean Scan Angle

NFI: National Forest Inventory

PRF: Pulse Repetition Frequency

RF: Random Forest

RWE: Return Waveform Energy

UAV: Unmanned Aerial Vehicle

V_{st}: Stem volume

V_{tot}: Total volume

Résumé long en Français

Développement du potentiel du Lidar aéroporté pour la gestion durable des forêts : prise en compte et gestion des effets de l'angle de balayage sur les prédictions d'attributs forestiers à l'aide de modèles surfaciques (ABA)

Contexte et objectifs de la thèse

Contexte

Nos vies quotidiennes sont étroitement liées aux écosystèmes forestiers, de par les nombreuses ressources que nous en tirons, telles que le papier, le bois, l'énergie, ou la nourriture. En outre, les forêts permettent la subsistance de plus d'un milliard de personnes dans le monde et le maintien de nombreuses populations autochtones (Bernier et Schoene, 2009). Les forêts abritent également une grande diversité d'espèces végétales et animales. Cette biodiversité est essentielle à la préservation des équilibres écologiques et doit être préservée tout en assurant le maintien des fonctions économiques et sociales de la forêt (FAO, 2020). Dans le contexte du changement climatique, les forêts constituent d'importants puits de carbone naturels indispensables à la réduction des émissions de gaz à effet de serre. Elles contribuent également à lutter contre le réchauffement climatique grâce au refroidissement par évaporation (Bonan, 2008). Parallèlement, les forêts sont constamment menacées par des pressions d'origine anthropique (déforestation, fragmentation et pollution) et climatique (changements phénologiques, déplacements d'aires de répartition, épisodes de dépérissement, infestations d'insectes) ou une combinaison des deux (disparition d'espèces animales, incendies, changements de composition des peuplements et de productivité primaire nette, changements biogéochimiques) (Prăvălie, 2018). Aujourd'hui, les écosystèmes forestiers subissent constamment des perturbations et il est devenu primordial de les gérer avec la volonté de maintenir cet équilibre fragile entre les facteurs socio-économiques et écologiques (Kuuluvainen et al., 2021 ; Lazdinis et al., 2019 ; MacDicken et al., 2015 ; Prăvălie, 2018).

Historiquement, la gestion des forêts était principalement motivée et guidée par un objectif de production de bois et d'autres ressources naturelles (Gadow et al., 2000). Autour des années 1990, la biodiversité est devenue une composante essentielle de la gestion forestière (ONU, 1992). L'adaptation aux impacts du changement climatique sur les écosystèmes forestiers a, quant à elle, pris une importance considérable au XXIe siècle (Bernier et Schoene, 2009 ; Jandl et al., 2019 ; Spittlehouse et Stewart, 2003). Avec l'accroissement constant de la population humaine, les milieux forestiers doivent ainsi être gérés dans une perspective à long terme. Dans un contexte de changement climatique, la préservation des forêts et des services écosystémiques qu'elles procurent nécessitera de guider l'élaboration des plans de gestion par les dernières connaissances scientifiques (Bergeron et al., 2004 ; Seidl et al., 2011 ; Torres-Rojo et al., 2016 ; Williamson et Edwards, 2014). Ainsi, une information actualisée en

permanence est au cœur de la gestion durable des forêts. Une partie de cette information peut être collectée par le biais d'inventaires forestiers réalisés à plusieurs échelles (Kangas et Maltamo, 2006).

Différents pays disposent de programmes d'inventaire forestier national (IFN) pour quantifier les ressources forestières et élaborer des politiques de gestion forestière adaptées (Barrett et al., 2016 ; Bohn et Huth, 2017 ; Breidenbach et Astrup, 2012 ; McRoberts et Tomppo, 2007; Nilsson et al., 2017).

Traditionnellement, l'inventaire forestier implique l'identification des espèces et la prise de mesures sur les arbres individuels pour estimer des attributs au niveau des peuplements forestiers. Ces attributs comprennent la hauteur dominante des arbres (m), la hauteur moyenne (m), la surface terrière ($m^2\ ha^{-1}$), la densité des tiges (nombre de tiges par ha), le volume total brut ($m^3\ ha^{-1}$), la biomasse aérienne totale (Kg ha-1) (McRoberts et Tomppo, 2007). Ces relevés sont parfois complétés par des informations concernant la végétation arbustive et herbacée. La collecte de mesures sur le terrain est longue et coûteuse, et est donc effectuée sur un échantillon de placettes dont la surface reste limitée (typiquement de l'ordre de 250 à 700 m² en forêt tempérée). Cet échantillon est représentatif des forêts de la zone inventoriée. Les informations sont ensuite extrapolées à l'ensemble de la zone forestière afin d'obtenir des estimations des différents attributs forestiers, du niveau local au niveau national (McRoberts et Tomppo, 2007 ; White et al., 2017).

La télédétection aéroportée et spatiale permet d'acquérir des informations exhaustives sur de grandes surfaces et facilite la mise à l'échelle des inventaires forestiers (passage du terrain aux échelles régionales ou nationales). Grâce à la télédétection, l'inventaire forestier traditionnel est amélioré au niveau régional et national (White et al., 2017 ; Wulder et al., 2012a). La télédétection fait ainsi partie intégrante des méthodes d'inventaires modernes et est utilisée selon trois modalités : 1) comme support aux relevés terrain et source d'informations complémentaires, 2) comme source de données auxiliaires pour améliorer la précision des inventaires et produire des estimations sur de petits territoires et 3) pour la cartographie (McRoberts and Tomppo, 2007)

Dans ce contexte, la technologie Lidar (« light detection and ranging ») présente un potentiel particulièrement intéressant pour caractériser les forêts. Les Lidars sont des systèmes de télédétection active basés sur l'émission-réception d'un signal laser. Pour couvrir de grandes surfaces, des capteurs équipés de systèmes à balayages sont montés sur des plates-formes aéroportées (ALS (airborne laser scanning) ou laser à balayage aéroporté) ou, depuis plus récemment, des capteurs pouvant acquérir des données le long d'un nombre limité de traces ont été embarqués sur des engins spatiaux, par exemple la mission ICESat1 (Schutz et al., 2005), qui a acquis des données entre 2003 et 2009, et les missions GEDI (Dubayah et al., 2020) et ICESat2 (Magruder et al., 2021) actuellement opérationnelles.

Les systèmes aéroportés (ALS) sont reconnus pour leur capacité à générer des mesures spatialisées de la structure en 3D de la végétation plus précises et denses que les autres technologies de télédétection (Holmgren and Nilsson, 2003; Nelson, 2013). Ces mesures sont généralement produites sous la forme

de nuages de points 3D géolocalisés, dont la densité varie de moins d'un point par m² à plusieurs dizaines de points par m². La position de chaque point indique la présence d'éléments de végétation (feuilles, bois ou tronc) ou du sol ayant interagi avec le faisceau laser émis par le système. Le Lidar permet ainsi de détecter le haut de la canopée et le sol, d'estimer la hauteur des peuplements forestiers (Dubayah and Drake, 2000; Hudak et al., 2009; Næsset, 1997; Nelson, 2013; Rempel and Parker, 1964) et d'en déduire d'autres informations comme la surface terrière, le volume de bois, la biomasse.

Les approches dites surfaciques (ABA en anglais pour Area Based Approaches) sont couramment utilisées pour produire des informations forestières au niveau peuplement (par opposition aux approches au niveau de l'arbre). Elles consistent à établir, à l'aide d'un modèle de régression, une relation entre des attributs forestiers issus des mesures de terrain et des variables Lidar calculées à partir des nuages de points 3D au niveau des placettes de terrain (Næsset, 2002; White et al., 2017; Wulder et al., 2012). Les métriques Lidar peuvent être ensuite calculées en tout point de l'espace et les modèles appliqués pour cartographier les attributs forestiers d'intérêt.

Les métriques Lidar utilisées dans les modèles sont un « résumé » des milliers de points qui représentent le peuplement au niveau d'une placette forestière. Si le peuplement ne change pas, on pourrait s'attendre à avoir systématiquement le même nuage de point. Cependant la distribution des points est fortement dépendante des conditions et paramètres d'acquisition, incluant le système (e.g. la longueur d'onde, la puissance et la divergence du laser, les caractéristiques du récepteur) et les spécifications de l'acquisition, comme la hauteur de vol, la fréquence d'émission du système, l'angle maximum de balayage (ou de scan), le recouvrement entre ligne de vols.

L'avantage des approches surfaciques est qu'elles restent performantes même pour traiter des jeux de données Lidar ayant des densités de points faibles (e.g., de l'ordre 1 point/m²). Et elles ne nécessitent pas, comme c'est le cas pour les approches à l'arbre, d'étape de segmentation, coûteuse en temps et ressources de calcul pour des résultats de qualité très variable. Cependant, un paramètre d'acquisition susceptible d'affecter la qualité des modèles surfaciques et la précision des résultats a été encore assez peu étudié. Il s'agit de l'angle de balayage ou angle de scan. L'étude de l'impact de ce paramètre sur la qualité des modèles surfaciques et sur la fiabilité des prédictions des attributs forestiers qui en découle est au cœur de ce travail de thèse.

Questions de recherche et objectifs de la thèse

Alors que l'angle de scan est reconnu comme étant un paramètre susceptible d'impacter les modèles surfaciques, il semble y avoir deux écoles de pensée concernant l'angle de scan : l'une, dominante, qui recommande de limiter l'angle de scan à des acquisitions quasi-nadir (< 15°) et l'autre qui soutient qu'accroître les angles de scan peut apporter de nouvelles informations et connaissances sur les peuplements forestiers.

Depuis le début de l'utilisation du Lidar en forêt, la tendance a été de recommander de limiter l'angle de scan à maximum 15° afin de favoriser la pénétration du signal jusqu'au sol et les mesures de hauteur des arbres. Ainsi, la plupart des études qui ont analysé l'impact de l'angle de scan ont été faites à partir de jeux de données avec des angles ne dépassant pas 15°-20°. Plusieurs études ont ainsi conclu au faible impact de l'angle de scan sur les modèles de terrain sous couvert (Ahokas et al. (2005) avec des angles < 15°), sur les estimations des hauteurs des arbres (Magnussen and Boudewyn (1998) avec des angles < 12°), sur le taux de trouées (Chen et al. (2014) avec des angles < 15°). Keränen et al., (2016) ont trouvé que la prédiction des hauteurs moyennes des arbres et des volumes de bois étaient plus précises avec des angles limités à 15° qu'avec des angles allant jusqu'à 20°. Certaines études se sont appuyées sur la simulation de données Lidar pour analyser des données caractérisées par une gamme d'angles de scan plus large que celle des données expérimentales habituellement disponibles (Disney et al., 2010; Holmgren et al., 2003; Qin et al., 2017). Qin et al. (2017) ont ainsi montré que des angles de 20° permettaient de mieux reconstruire les profils de distribution des feuilles que des angles plus faibles. A partir de données expérimentales, van Lier et al., (2021) ont récemment conclu qu'utiliser des données avec des angles de scan allant jusqu'à 30° avait peu d'impact sur les prédictions des attributs forestiers, même si les métriques Lidar pouvaient être significativement impactées par les changements d'angles. Kamoske et al., (2019) ont aussi suggéré que des angles de scans plus élevés permettraient de mieux comprendre la distribution des trouées dans la canopée.

Par ailleurs, on constate qu'au fil du temps les angles de scan maximums ont tendance à augmenter dans les jeux de données Lidar, probablement en raison de l'évolution des capteurs et de considérations pratiques visant à limiter les coûts. De plus en plus de pays planifient des acquisitions au niveau national pour répondre à plusieurs objectifs applicatifs, y compris le suivi des forêts. Pour ces acquisitions sur de vastes territoires, les angles maximums sont généralement ≥ 30°. En parallèle les acquisitions par Lidar embarqués sur drone en forêt se développent, pour des études au niveau local, avec des angles de scans élevés (>20°) en raison de la faible hauteur de vol (Cao et al., 2019; Liu et al., 2018; Lu et al., 2020; Ma et al., 2022).

En raison de la complexité de la végétation, mesurer sa structure par Lidar dépend fortement de la géométrie de l'acquisition. Ainsi, alors qu'un effet probable de l'angle de scan sur les modèles surfaciques est reconnu, il n'y a pas de consensus sur les limites acceptables pour ce paramètre, ni sur l'importance de son impact sur les modèles surfaciques en milieu forestier. De plus, très peu d'études se sont intéressées à des stratégies pour traiter des données caractérisées par des angles de scan supérieur à 20°, alors même que de telles données commencent à se multiplier.

Ces constats soulignent le besoin d'améliorer notre compréhension de l'impact de l'angle de scan sur les mesures Lidar en forêt et sur la qualité de prédiction des attributs forestiers afin de déterminer si plus

d'attention doit être portée à ce paramètre lors de l'analyse des données Lidar et du développement de modèles surfaciques.

Pour cela, deux hypothèses de travail ont été formulées :

H1 : les prédictions d'attributs forestiers à l'aide de modèles surfaciques ne seront pas fiables si l'impact de l'angle de scan n'est pas pris en compte lors de la modélisation de la relation entre attribut forestiers et variables Lidar.

La question de recherche principale découlant de cette hypothèse est : « Quels sont les impacts des angles de scan sur les métriques Lidar et sur les prédictions des modèles surfaciques ? »

H2 : La normalisation des métriques Lidar par rapport aux changements de la géométrie d'observation ou l'incorporation des caractéristiques de cette géométrie dans les modèles peuvent aider à atténuer l'impact des angles de scan sur la qualité des prédictions.

La question de recherche principale découlant de cette hypothèse est : « Comment gérer l'impact des angles de scan sur les prédictions des modèles surfaciques ? »

Dans le cadre de ces deux hypothèses, l'objectif principal de la thèse est de comprendre si la prise en compte de l'impact de l'angle de scan sur les données Lidar est essentiel pour le développement de modèles surfaciques robustes et précis pour la prédiction d'attributs forestiers.

Les sous-objectifs suivants ont été définis pour ce travail de thèse :

1) Evaluer l'impact des angles de scan sur la qualité des modèles Lidar surfaciques pour différents peuplements forestiers complexes
    a. En estimant l'impact de ces angles sur des métriques Lidar communément utilisées dans les modèles
    b. En estimant l'impact de l'utilisation de métriques explicatives mais sensibles à l'angle de scan sur la qualité des prédictions des modèles.
2) Développer des méthodes pour gérer les effets des angles de scan sur les modèles de prédiction
    a. En considérant différentes combinaisons de géométries d'acquisition (angles de scan)
    b. En utilisant des métriques calculées après avoir mobilisé des approches de voxellisation pour normaliser des effets des angles de scan
    c. En modélisant les effets complexes des angles de scan grâce à des réseaux de neurones artificiels avec, en entrée des modèles, les caractéristiques de la géométrie d'acquisition en plus des métriques Lidar.
3) Proposer, sur la bases des résultats obtenus, des recommandations et des perspectives, pour une utilisation opérationnelle des données Lidar pour des applications forestières.

Cette thèse comprend quatre chapitres qui sont résumés dans ce qui suit. Les trois premiers ont été rédigés sous forme d'article de journal. Le dernier chapitre résume les résultats de la thèse et propose des pistes pour de futures recherches.

Chapitre 2 : Impact de l'angle de scan sur les métriques Lidar utilisées dans les modèles de prédiction des caractéristiques des peuplements forestiers : une analyse basée sur un découpage des données selon une grille régulière.

Le sous-objectif 1-a est au cœur de ce chapitre qui aborde la question suivante : Quel est l'impact des angles de scan sur les métriques Lidar communément utilisées dans les modèles surfaciques?

Ce chapitre a été publié dans « International Archives of the Photogrammetry, Remote Sensing and Spatial Information Sciences » (Dayal et al., 2020).

Les approches dites surfaciques (ABA) s'appuient sur des modèles de régression pour établir une relation entre les attributs forestiers d'intérêt et des variables dérivées des données Lidar, encore appelées métriques Lidar. Les modalités d'acquisition des données Lidar déterminent la qualité et les caractéristiques des nuages de points 3D utilisés pour le calcul des métriques. Ces caractéristiques peuvent varier d'une acquisition à l'autre mais aussi localement au sein d'un même jeu de données.

L'angle de balayage, ou angle de scan, est l'une des caractéristiques des données qui peut avoir un impact sur l'estimation des métriques Lidar et donc sur les modèles surfaciques qui utilisent ces métriques. Les métriques standards les plus utilisées comprennent les caractéristiques des distributions de la hauteur et de l'intensité des points Lidar, telles que la moyenne, l'écart-type, les percentiles, ainsi que des métriques de densités par strates de hauteur ou des métriques de rugosité du sommet de la canopée (Rumple index). Ces métriques standards sont parfois complétées par des métriques spécifiques développées pour mieux représenter certaines caractéristiques du peuplement, par exemple le taux de couvert ou le taux de trouées. Ces métriques sont calculées sur une surface représentative du peuplement local, i.e. similaire à celle utilisée pour les inventaires de terrain. C'est donc à cette échelle qu'il est important d'étudier la façon dont les métriques Lidar varient en fonction de l'angle de scan. Une forte sensibilité à ce paramètre traduirait un manque de robustesse des variables explicatives pour la construction des futurs modèles.

L'objectif de ce chapitre est d'évaluer, au niveau d'un peuplement, l'impact de l'angle de scan sur 11 métriques (9 métriques de hauteur des points et 2 autres métriques communément utilisées).

La zone d'étude est la ripisylve du Ciron, dans les Landes, dans le Sud-Ouest de la France. Sur ce site, caractérisé par des peuplements feuillus et des mélanges feuillus/pins de structure complexe, l'acquisition de données Lidar a été faite à l'aide d'un système Lidar léger embarqué sur ULM en

favorisant un recouvrement entre lignes de vol supérieur à 35% et en passant à plusieurs reprises sur certaines zones. Ainsi, une part significative de la zone a été observée depuis plusieurs points de vue. La zone d'étude a été divisée selon une grille définissant des cellules carrées de 30 m de côté. Dans chaque cellule, les lignes de vol ayant produit un nuage de points couvrant au moins 90% de la surface de la cellule ont été identifiées et retenues. Puis, pour chaque nuage de points issu d'une de ces lignes de vol, une classe d'angle de scan est attribuée, sur la base de l'angle de scan moyen des points contenus dans la cellule. Quatre classes ont été définies : 0°-10°, 10°-20°, 20°-30° and 30°- 40°. Pour les cellules contenant plusieurs nuages de points affectés à la même classe d'angle, seul celui dont l'angle moyen est le plus proche du centre de la classe a été retenu. Les 11 métriques Lidar ont ensuite été calculées par ligne de vol - et donc par classe d'angle - pour chaque cellule, résultant en un maximum de 4 valeurs par cellule et par métrique. La comparaison de ces valeurs permet d'évaluer l'évolution des métriques en fonction de l'angle de scan. Cette comparaison a été faite à l'aide de tests de Student (t-test) appariés et de régressions linéaires.

Les résultats montrent que, pour la plupart des métriques, les valeurs diminuent lorsque l'angle de scan augmente, les valeurs au nadir étant prises comme référence. Le taux de trouées et l'indice de rugosité de la canopée (Rumple index) sont plus impactés par l'angle de scan que l'écart-type des hauteurs des points. La hauteur maximale s'est révélée être peu sensible à l'angle de scan. Parmi les percentiles de la distribution des hauteurs, les percentiles les plus élevés se sont révélés moins sensibles à l'angle de scan que les percentiles les plus bas. Ces résultats montrent que l'angle de scan peut impacter de façon significative certaines métriques couramment utilisées dans les modèles surfaciques. L'impact susceptible d'en résulter sur les modèles eux-mêmes doit être étudié et fait l'objet du prochain chapitre.

Chapitre 3 : Analyse de l'impact des angles de scan Lidar sur la prédiction des attributs forestiers dans différents environnements forestiers

Ce chapitre aborde les trois questions suivantes :

- Quel est l'effet de l'inclusion de métriques Lidar sensibles à l'angle de scan sur les modèles ABA? (sous-objectif 1-b)

- Peut-on gérer les effets des angles de scan sur la qualité des modèles en combinant des nuages de points acquis selon différents points de vue? (sous-objectif 2-a)

- Peut-on gérer les effets des angles de scan sur la qualité des modèles en normalisant les métriques Lidar par rapport aux effets de ces angles grâce à la voxellisation ? (sous-objectif 2-b)

Il a fait l'objet d'une publication, soumise à la revue « Journal of Photogrammetry and Remote Sensing (P&RS) » de l'ISPRS (International Society for Photogrammetry and Remote Sensing). La publication a été acceptée et resoumise après prise en compte des corrections et avis des évaluateurs.

Des études, dont celle présentée au chapitre précédent, ayant démontré que plusieurs métriques dérivées des données Lidar et couramment utilisées dans les approches surfaciques étaient sensibles aux angles de scan, les deux objectifs suivants ont été fixés pour cette partie de la thèse :

1) Analyser l'impact de cette sensibilité sur les prédictions des attributs forestiers obtenues par des modèles surfaciques;
2) Évaluer le potentiel d'approches de voxellisation pour normaliser les métriques Lidar des changements dus aux angles de scan et atténuer l'effet de ces angles sur la qualité des modèles surfaciques.

L'étude a porté sur quatre environnements forestiers complexes, une ripisylve (29 placettes) pour le site du Ciron, dans le Sud-Ouest de la France, et trois peuplements de montagne, pour le site du Parc Naturel Régional du massif des Bauges (PNR des Bauges) situé dans les Alpes françaises (feuillus (42 placettes), résineux (31 placettes) et mixtes (45 placettes)).

Pour atteindre nos objectifs, nous avons sélectionné un modèle basé sur quatre métriques Lidar présentant différents niveaux de sensibilité aux angles de scan, i.e. la moyenne et la variance des hauteurs au-dessus du sol des points Lidar de végétation (μ_{CH} et σ^2_{CH}), le taux de trouées (P_f) et le coefficient de variation du profil de densité de surface foliaire (CV_{LAD}). Pour chaque placette, nous avons considéré indépendamment les nuages de points scannés à partir de lignes de vols différentes. Chaque nuage a été caractérisé par l'angle de scan moyen des points le composant et classé dans l'une des trois classes suivantes selon la valeur de cet angle moyen : A ($0° \leq MSA < 10°$), B ($10° \leq MSA < 20°$) ou C ($20° \leq MSA < 30°$).

Un dispositif expérimental comprenant neuf scénarios a été conçu pour étudier l'impact sur les modèles surfaciques du nombre de lignes de vol (scénarios fl1, fl2 et fl3 pour, respectivement, une, deux et trois lignes de vol) et de l'angle de scan prédominant (scénarios A, B ou C) ou de la combinaison de deux angles de scan prédominants (scénarios (A et B), (A et C), ou (B et C)). Pour les mêmes placettes forestières, nous avons produit pour chaque scénario 5000 jeux de données par tirage aléatoire dans l'ensemble des combinaisons de lignes de vol disponibles par placettes. Pour chaque jeu de données, trois modèles surfaciques ont été construits et validés par validation croisée (LOO cross validation) pour prédire trois attributs forestiers, i.e. le volume de tronc (Vst), le volume total (Vtot) et la surface terrière (BA). Trois critères permettant d'évaluer le bon ajustement des modèles ont été calculés : le coefficient de détermination (R^2), l'erreur quadratique moyenne relative (rRMSE) et l'erreur moyenne en pourcentage (MPE).

Les distributions de ces critères de qualité ont été comparées pour les différents scenarios afin d'évaluer le comportement des modèles de prédiction lorsque : 1) le nombre de lignes de vol (i.e. d'angles de scan) par placette augmente (fl1, fl2, fl3) ; 2) le jeu de données Lidar est caractérisé par des angles de scan spécifiques (A, B ou C) ou une combinaison spécifique d'angles de scan (AB, AC ou BC) ; 3) la voxellisation est utilisée pour calculer le taux de trouées (P_f) et le coefficient de variation du profil de densité foliaire (CV_{LAD}), deux variables ayant montré dans certains peuplements une assez forte sensibilité aux changements d'angles de scan.

Les résultats montrent que les modèles construits avec des nuages de points issus de directions de scan multiples, i.e., acquis depuis plusieurs lignes de vol, sont plus robustes, avec un écart type plus faible pour les critères mesurant le bon ajustement des modèles. En moyenne, en considérant tous les types de forêts, les écarts types des distributions de R^2 pour fl2 et fl3 sont inférieurs de 42 % et 77 % à ceux obtenus pour fl1. Nous avons également observé qu'un jeu de données avec une configuration d'acquisition privilégiant des angles de scan au nadir (i.e. scénario A), ne donnait pas toujours de meilleures prédictions (e.g., R^2 moyen plus élevé de 0.08, 0.07, 0.04 avec le scénario B pour les feuillus, les conifères et les peuplements mixtes). Ces analyses montrent qu'un modèle d'estimation d'attributs forestiers construit sur la base d'un ensemble de placettes d'étalonnage (calibration/validation du modèle) dépend fortement de la géométrie des acquisitions Lidar sur ces placettes. Ainsi, lors de l'application du modèle pour cartographier les attributs forestiers sur une zone complète, la fiabilité des prédictions n'est pas garantie, même pour des peuplements similaires à ceux ayant fait l'objet de relevés terrain au niveau des placettes d'étalonnage. Le risque est particulièrement élevé dans le cas d'acquisitions Lidar réalisées avec un faible taux de recouvrement entre lignes de vol, conduisant à de nombreuses zones observées depuis un seul point de vue (i.e., un seul angle de scan).

Le remplacement dans les modèles des variables P_f et CV_{LAD} calculées directement à partir des nuages de points par celles calculées après voxellisation du nuage de points et construction de profils de végétation a permis d'atténuer les impacts des changements d'angles de scan. La voxellisation corrige des effets d'occlusion et prend en la longueur du trajet du faisceau laser dans la végétation, et donc l'angle de scan. Avec ces nouvelles variables, nous avons ainsi observé a) une augmentation des moyennes des distributions des R^2 et une diminution des moyennes des erreurs, indiquant une amélioration de la justesse des prédictions, ou b) une diminution des écarts types des critères mesurant l'ajustement des modèles, indiquant une augmentation de la précision des prédictions, ou c) les deux en même temps. Ces résultats soulignent le potentiel de la voxellisation à normaliser les métriques Lidar des effets des angles de scan et l'intérêt de cette normalisation pour développer des modèles plus robustes.

Chapitre 4 : Amélioration de la prédiction d'attributs forestiers à partir de données Lidar par la prise en compte de l'angle de scan et de la topographie dans des modèles basés sur des réseaux de neurones.

Ce chapitre aborde l'objectif 2-c au travers de la question suivante : Comment intégrer la géométrie des acquisitions Lidar dans les modèles surfaciques ?

Une infinité de métriques Lidar décrivant les peuplements forestiers peuvent être intégrées dans les modèles surfaciques. Ces métriques sont, la plupart du temps, utilisées sans que l'on connaisse leur sensibilité aux changements d'angles de scan. Plutôt que de considérer cette sensibilité comme une contrainte, elle pourrait être vue comme une opportunité de caractériser plus finement les propriétés de la végétation.

Pendant de nombreuses années, il a été recommandé de limiter l'angle de scan maximum à 15-20 degrés lors de l'acquisition de données Lidar destinées à des applications forestières. Restreindre l'angle de scan entraîne une réduction de la fauchée et donc de la surface couverte au sol à chaque passage de l'avion. Ainsi, pour réduire les coûts (i.e. optimiser le temps de vol pour couvrir un territoire donné), la limitation de l'angle maximum de scan peut être accompagnée d'une réduction du taux de recouvrement entre lignes de vol. Au cours des dernières années, on a pu constater une augmentation des angles de scan dans les jeux de données Lidar utilisés pour le suivi des forêts. D'une part, de nombreux pays ont réalisé des acquisitions Lidar au niveau national avec des angles de scan maximums de 30° et plus. Ces acquisitions ont pour vocation d'être utilisées pour différentes applications, y compris forestières. D'autre part, les acquisitions par systèmes légers se multiplient pour des études au niveau local et s'accompagnent d'angles de scan plus élevés que les acquisitions aériennes traditionnelles. Cependant, des études ont montré que les métriques Lidar présentent des sensibilités différentes aux angles de scan qui peuvent affecter la robustesse des modèles de prédiction basés sur les approches surfaciques (ABA) et leur fiabilité lors de leur application pour générer des cartes d'attributs forestiers. De plus, la topographie affecte également les métriques Lidar.

Il apparait donc essentiel de pouvoir prendre en compte l'impact combiné de la géométrie d'observation (angles de scan et azimut des faisceaux Lidar) et de la topographie sur les métriques Lidar pour améliorer les modèles surfaciques. Dans cette partie du travail de thèse, nous faisons l'hypothèse que les réseaux de neurones artificiels ont la capacité de gérer ces interactions complexes.

Le site d'étude est le Parc Naturel Régional du *massif des Bauges* dans les Alpes françaises. Ce site de haute montagne est caractérisé par la présence de forêts de feuillus, de conifères et mixtes. Les mesures terrain ont été collectées au niveau de 291 placettes circulaires de 15 m de rayon échantillonnant les trois types de forêts. Les données Lidar ont été acquises avec des recouvrements multiples entre lignes

de vol, et chaque placette de terrain a été scannée depuis plusieurs lignes de vol. Les nuages de point 3D de chaque placette terrain ont été divisés en fonction des lignes de vol, résultant en 1095 observations pour lesquelles 55 métriques Lidar standards ont été calculées pour caractériser la végétation. De plus, des variables ont été introduites pour décrire la topographie au niveau des placettes et les caractéristiques de la géométrie d'acquisition (angle de scan et azimut). Chaque nuage de points obtenu avec une ligne de vol, et les métriques Lidar correspondantes, sont le résultat d'une interaction spécifique entre les paramètres d'acquisitions, les propriétés du terrain et les caractéristiques de végétation et peuvent donc être considérés comme une observation unique et indépendante dans les modèles surfaciques. Cette façon de procéder peut être apparentée à une méthode d'augmentation de données appliquée en amont du développement d'un modèle.

Nous avons utilisé un perceptron multicouche (MLP) avec deux couches cachées pour modéliser la surface terrière (*BA*) et le volume totale (V_{tot}). Ce réseau de neurones est supposé pouvoir mieux modéliser les interactions complexes entre les métriques Lidar de végétation (e.g., métriques de distributions des hauteurs et des intensités des points Lidar, densités de points par strates de hauteur, métriques de canopée, i.e. rugosité du sommet de la canopée et taux de couvert), la topographie locale (pente, orientation, altitude), et la géométrie de l'acquisition par le Lidar (angles de scan et azimut de la visée, distance entre le terrain et l'avion).

La division des données en un jeu pour l'étalonnage du modèle (calibration/validation) et un jeu pour son évaluation (test) a été définie sur la base des identifiants des placettes afin d'éviter qu'une placette ne contribue à la fois à l'étalonnage et au test des modèles. 30 itérations ont été réalisées avec des jeux d'étalonnage et de test différents. A chaque itération, pour chaque placette du jeu de test, chaque attribut forestier (i.e., BA et Vtot) est prédit autant de fois que le nombre de nuages de points disponibles, i.e. le nombre de lignes de vol à partir desquelles des données ont été acquises pour la placette. La médiane des prédictions est utilisée pour évaluer la performance des modèles à l'aide de critères standard, i.e. le coefficient de détermination R^2 et des mesures d'erreurs. Plusieurs jeux de données sont considérés : 1) standard (*std*), avec les métriques issues des nuages de points composés des points provenant de toutes les lignes de vol, 2) augmenté (*aug*) en distinguant les observations issues de chaque ligne de vol, 3) standard et augmenté complétés avec les informations de topographie ($std_{terrain}$, et $aug_{terrain}$) 4) augmenté complété des informations de topographie et de la géométrie d'acquisition ($aug_{terrain+scan}$). Les performances des différents modèles MLP ont été comparées à celles de modèles construit avec un algorithme de Forêt Aléatoire (ou Random Forest, RF), une approche de régression non-paramétrique couramment utilisée et prise ici comme référence.

Pour le MLP, les R^2 pour les prédictions avec le jeu de données $aug_{terrain+scan}$ (R^2 de 0.83 et 0.85 pour *BA* et V_{tot}) sont supérieurs à ceux obtenus avec le jeu de données $std_{terrain}$, i.e. sans diviser les nuages de points selon leur géométrie de scan (R^2 de 0.77 pour *BA* et V_{tot}). Les résultats de ce modèle (MLP avec

$aug_{terrain+scan}$) sont aussi nettement meilleurs que ceux du MLP basé sur le jeu de données standard (*std*) (R^2 de 0.66 et 0.71 pour *BA* et V_{tot}, respectivement) qui n'intègre ni variables topographiques, ni géométrie d'acquisition. Dans tous les scénarios, y compris celui basé sur le jeu de données $aug_{terrain+scan}$, le MLP surpasse le RF (R^2 de 0.6 et 0.64 pour *BA* et V_{tot} pour le RF appliqué aux données $aug_{terrain+scan}$). Ces résultats, obtenus avec un réseau de neurones MLP à deux couches, soulignent le potentiel des méthodes d'apprentissage profond à fournir une solution efficace pour modéliser les interactions complexes entre les signaux Lidar et la végétation, qui sont régies par le changement de la géométrie d'acquisition et de la topographie.

Chapitre 5 : Conclusion et perspectives

Par sa capacité à fournir des mesures de la structure en 3D de la végétation sur de vastes surfaces, le Lidar aéroporté est une technologie particulièrement adaptée pour fournir des informations utiles à la gestion des forêts. L'utilisation croissante du Lidar pour les applications forestières, et en particulier pour l'inventaire forestier et la cartographie d'attributs forestiers, témoigne de ce potentiel. Construire des modèles reliant des données issues de mesures de terrain au niveau de placettes forestières et des variables issues des nuages de points 3D Lidar est la façon la plus courante de produire des estimations de paramètres forestiers et des cartes à grande échelle. Cette approche est appelée approche surfacique (ou ABA, pour Area Based Approach en anglais).

Cependant, de par le mécanisme d'acquisition par balayage des données Lidar, il est difficile d'obtenir des nuages de points avec les mêmes caractéristiques de densité et d'angles de balayage (ou de scan) en tout point de l'espace. L'impact de l'angle de scan sur la qualité des données en forêt et des modèles de prédiction a été assez peu étudié. Cependant, ces dernières années, on constate qu'une importance croissante est accordée à la compréhension de l'influence des angles de scan sur les métriques Lidar. Par convention, l'angle de scan maximum a été limité à 15-20° pour la plupart des études en milieu forestier. Une telle limitation est très contraignante (mauvais rapport coût/surface) pour la réalisation de couvertures au niveau national qui visent une efficience opérationnelle. Même à une échelle plus locale, autoriser un angle de scan maximum plus élevé permettrait de diminuer les coûts d'acquisition. Par ailleurs, l'utilisation de systèmes légers tend à se développer en forêt et implique en général des angles de scan maximums plus élevés qu'avec des systèmes aéroportés qui opèrent à plus haute altitude.

Pour ces raisons il est important d'étudier et de mieux comprendre l'effet des angles de scan sur la qualité des nuages de points au regard des applications forestières. Dans cette thèse, l'impact de différentes géométries d'acquisition sur les modèles surfaciques Lidar développés pour la prédictions d'attributs forestiers a été étudié dans différents environnements forestiers complexes.

L'étude a été menée selon deux axes de travail. Le premier axe s'est focalisé sur l'étude de l'impact de l'angle de scan sur les métriques Lidar et sur la qualité des modèles surfaciques basés sur ces métriques.

Le second axe s'est concentré sur l'exploration de différentes stratégies pour mieux gérer les effets des angles de scan.

Les résultats obtenus ont montré que l'angle de scan peut impacter de façon significative certaines métriques couramment utilisées dans les modèles surfaciques. Ils ont aussi souligné le manque de robustesse des modèles construits à partir de jeux de données de calibration constitués de nuages de points issus d'une seule ligne de vol (i.e. un seul angle d'observation) au niveau des placettes de référence et le risque d'erreurs non maîtrisées qui en découle, lorsque ces modèles sont utilisés pour cartographier les attributs forestiers. Il est ainsi apparu impératif de gérer les effets des angles de scan lors de l'élaboration et de l'utilisation des modèles.

Pour se faire trois stratégies ont été évaluées.

La première stratégie, et la plus simple en théorie, est de s'assurer que l'acquisition des données est faite de façon à ce que tout point de la zone d'étude est scanné depuis au moins deux lignes de vol, trois voire plus si possible, pour compenser les biais de représentation de la végétation liés aux angles de scan. Les résultats ont en effet montré que les modèles construits avec des nuages de points issus de directions de scan multiples étaient plus robustes. Cependant, pour des questions de coût des acquisitions, cette solution n'est pas envisageable dans un contexte opérationnel.

La seconde stratégie, est de s'assurer que les modèles utilisent des métriques Lidar peu sensibles aux angles de scan. Dans cette optique, les résultats obtenus ont montré que la voxellisation, basée sur des approches de suivi de rayons, était une option intéressante pour normaliser les métriques Lidar des effets des angles de scan et augmenter ainsi la robustesse et la fiabilité des modèles. La voxellisaiton peut être appliquée à l'échelle des placettes de terrain pour élaborer les modèles, mais aussi sur l'ensemble d'une zone d'étude pour appliquer le modèle et produire des cartes d'attributs forestiers plus fiables. Les approches de voxellisation ont aussi le potentiel de caractériser la végétation avec plus de précision. Des développements méthodologiques sont cependant encore nécessaires pour les optimiser et les intégrer dans des procédures opérationnelles d'inventaires forestiers améliorés combinant données terrain et Lidar.

La troisième stratégie consiste à prendre directement en compte dans les modèles la géométrie des acquisitions, en la décrivant au travers de variables spécifiques (e.g. angle de scan, azimut de visée pour l'acquisition) et en intégrant aussi la morphologie du terrain (pente, orientation, altitude). Les résultats, obtenus avec un réseau de neurones MLP à deux couches, ont permis de montrer le potentiel des méthodes d'apprentissage profond pour modéliser les interactions complexes entre les signaux Lidar et la végétation qui sont modulées par la géométrie des acquisition et de la scène observée. Le déploiement de ces approches n'est cependant pas toujours possible en raison de la difficulté de disposer de suffisamment de données de référence terrain contemporaines des acquisitions Lidar, les inventaires terrain étant longs et couteux à réaliser.

Les résultats de cette thèse soulignent l'importance de poursuivre les recherches pour améliorer notre compréhension des interactions Lidar/végétation et notre capacité à gérer les effets des angles de scan sur les données Lidar et les modèles de prédiction d'attributs forestiers dans des contextes forestiers variés (types de peuplements et topographie). Les stratégies visant à normaliser les métriques Lidar et à s'appuyer sur des méthodes d'apprentissage profond pour gérer les effets des angles de scan ont été évaluées indépendamment mais pourraient être combinées afin de tirer parti des bénéfices des deux approches. Faire appel à des données Lidar simulées ouvre aussi des perspectives intéressantes pour, d'une part, analyser de façon plus systématique les effets des angles de scan sur les métriques Lidar dans différents types de peuplements forestiers et, d'autre part, produire des données de référence additionnelles pour favoriser le déploiement de méthodes d'apprentissage profond.

.

Chapter 1: Introduction

1.1 Sustainable Forest Management

"Sustainable forest management means the stewardship and use of forests and forest lands in a way, and at a rate, that maintains their biodiversity, productivity, regeneration capacity, vitality and their potential to fulfil, now and in the future, relevant ecological, economic and social functions, at local, national, and global levels, and that does not cause damage to other ecosystems."

- Resolution H1 of the Helsinki Ministerial Conference on the Protection of Forests in Europe, 1992

A broad understanding of the definition above tells us that we interact with forests on two levels: socio-economic and ecological. Our daily lives are inextricably linked with forest ecosystems because of the numerous resources we derive from forests, such as wood, fuel, paper, food and many more. Moreover, forests are responsible for providing livelihoods to more than a billion people worldwide and sustaining numerous indigenous populations (Bernier and Schoene, 2009). In Europe alone, about 2.6 million people depend on various industries linked to forests (Forest Europe, 2020). Forests are also home to diverse species of plants and animals that make up the biological biodiversity critical for maintaining an ecological balance while providing many economic benefits (FAO, 2020). In the context of global climate change, forests are also crucial carbon sinks, and they help tackle global warming through evaporative cooling (Bonan, 2008). At the same time, forests are under constant threat due to anthropogenic (deforestation, fragmentation and pollution), climatic factors (phenological shifts, range shifts, die-off events, insect infestations) or a combination of both (defaunation, fires, composition shifts, net primary productivity shifts, biogeochemical shifts) (Prăvălie, 2018). Forests constantly undergo disruptive changes; therefore, their management to maintain a balance between the socio-economic and ecological factors assumes increased importance (Kuuluvainen et al., 2021; Lazdinis et al., 2019; MacDicken et al., 2015; Prăvălie, 2018).

Forest management plans identify the activities to be carried out per the goals and objectives of the forest managers (Bettinger et al., 2017). With the ever-increasing human population, forest environments must be managed with long-term perspectives. Historically, forest management was mainly driven by the primacy of timber production and other natural resources (Gadow et al., 2000). For example, in countries such as Finland and Sweden, the idea of sustainability was limited to economic sustainability, allowing them to make up around 15% of global sawn wood and paper pulp production with only 2% of the international forest area (Kuuluvainen et al., 2021). Such intensive practices are known to jeopardise the biodiversity of forests due to degradation of habitats and loss and reduced structural and species variability (Kuuluvainen et al., 2021). Around the 1990s, biodiversity became an essential component of forest management (UN, 1992). While a balance between the extraction of resources and ecological considerations may only be achieved if efficient management plans guide forest management practices, climate change considerations are crucial in the present and the future. Adapting

to the effects of climate change on forest ecosystems has assumed significant importance over the 21st century (Bernier and Schoene, 2009; Jandl et al., 2019; Spittlehouse and Stewart, 2003). The evolution of forests in the context of climate change will require the development of scientifically guided plans for effective decision-making concerning harvest levels prediction, resource consumption optimisation and maintenance of forest health (Bergeron et al., 2004; Seidl et al., 2011; Torres-Rojo et al., 2016; Williamson and Edwards, 2014). Therefore, information is at the heart of sustainable forest management and is obtained through forest inventories (Kangas and Maltamo, 2006).

1.2 The role of remote sensing in enhancing forest inventory

Forest inventory and mapping form crucial components of sustainable forest management by providing periodic information about the availability of natural resources and the state of the forest in general. It involves collecting data on forest resources within an area, whether local, national or global. The quantity and quality of forest information are vital components of forest management. Forest information is collected through forest inventory conducted at several geographic levels, which is typically carried out through field measurement of forest attributes at sample field plots. Forest attributes are modelled using the information from sample locations and extrapolated spatially to understand the current state of forests and their evolution over time. Different countries have national forest inventory (NFI) programs to quantify forest resources and develop suitable forest management policies (Barrett et al., 2016; Bohn and Huth, 2017; Breidenbach and Astrup, 2012; McRoberts and Tomppo, 2007; Nilsson et al., 2017).

Traditionally, forest inventory involves species identification and measurements made on individual trees (and smaller vegetation) for the estimation of forest attributes such as tree heights (m), mean height (m), basal area (m^2 ha^{-1}), stem density (stems ha^{-1}), Gross total volume (m^3 ha^{-1}), Total aboveground biomass (kg ha^{-1}) (McRoberts and Tomppo, 2007). The measurements can be intensive and costly and are therefore made on sample plots. The information is extrapolated to the entire forest area to derive estimates of the various forest attributes from local to national levels (McRoberts and Tomppo, 2007; White et al., 2017). In traditional forest inventory, accuracy depends on the number of sampling units and their stratification to ensure even representation, which in turn depend on cost and time constraints. Moreover, tree measurements are not made for all the trees in the forests, and wall-to-wall coverage is not practical.

Remote sensing solves the problem of scaling forest inventories as sensors mounted on aircrafts or satellites are used to make measurements over large areas. Traditional forest inventory becomes the enhanced forest inventory (EFI) at the regional and national level with the support of remote sensing (White et al., 2017; Wulder et al., 2012a). In general, remote sensing involves two main components, a) acquisition of data, and b) interpretation of data. Data acquisition involves the use of different kinds of

sensors such as optical, infrared, thermal, microwave or lidar to acquire data about forests (Lillesand et al., 2004). Sensors collecting such data are mounted on different platforms such as terrestrial and ground-based, aerial and satellite, depending on the application, data properties or coverage area (Figure 1).

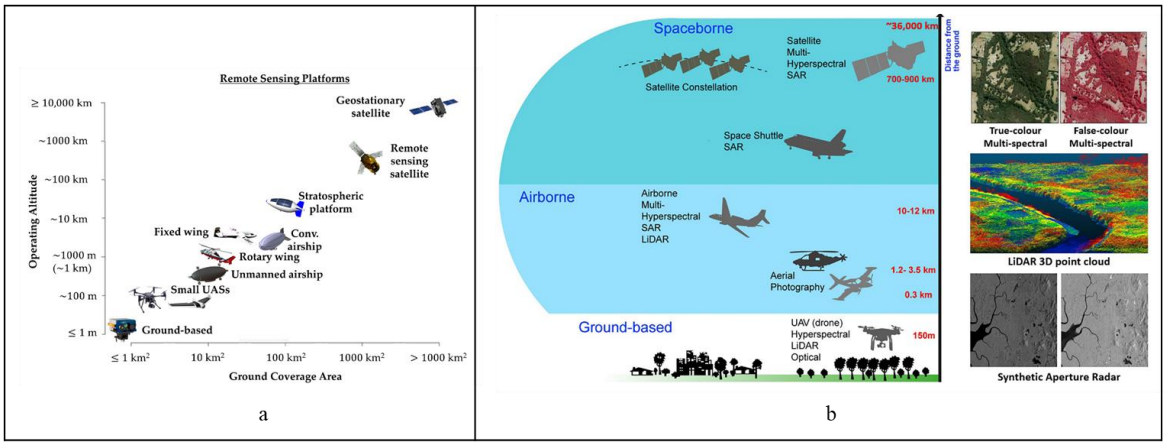

Figure 1: (a) Various remote sensing platforms based on their area of coverage and operation altitudes (Gili et al., 2021)*; (b) Classification of remote sensing platforms based on their operations (left) and different types of data resulting from optical, infrared, lidar and microwave sensors (right)* (Lechner et al., 2020).

Interpretation of data may range from a basic visual interpretation to using advanced modelling techniques to derive useful information about the forests. Studies have used various sensors to extract information about forests, such as land-use land-cover (LULC), vegetation structure, biodiversity and vegetation cover, among others (Cartus et al., 2012; Dubayah and Drake, 2000; Foody et al., 2003; Hall et al., 2006; Le Toan et al., 1992; Magnussen and Boudewyn, 1998; Neumann et al., 2010). Multisource forest inventories (MFI) combine NFI information with auxiliary data, mainly remote sensing data or forest maps derived from remote sensing data, to increase inventories' speed and cost efficiency while reducing uncertainties of forest characteristics estimates. MFIs provide accurate results at more local scales without increasing the effort in the field. Remote sensing data contributes to the support of modern NFIs through three main applications: (1) surrogates for field observation or measurement; (2) ancillary data to improve the precision of traditional inventory areal estimates; and (3) mapping (McRoberts and Tomppo, 2007).

1.3 Enhanced forest inventory with lidar

Lidar is an active remote sensing method that involves the emission of monochromatic energy pulses with wavelengths, usually in the infrared region for earth observation. Lidar sensors are also mounted on different platforms (Figure 1). For large-scale coverages, sensors are mounted on airborne platforms, i.e. airborne laser scanning (ALS) or, since more recently, on spacecraft, e.g. the ICESat1 mission (Schutz et al., 2005), which operated from 2003 to the end of 2009, and the ongoing GEDI (Dubayah et al., 2020) and ICESat2 missions (Magruder et al., 2021). ALS sensors, in particular, have gained

recognition for their ability to generate the most accurate, spatially explicit and dense measurements of vegetation (Holmgren and Nilsson, 2003; Nelson, 2013). The pulses are emitted towards objects of interest, such as buildings, vegetation etc. and the roundtrip time of the pulse is used to measure the distances of the objects from the sensor. Part of the laser pulse strikes an object (a group of leaves, for example), which is returned as an echo, and the remaining portion of the pulse continues further. This process repeats to generate a waveform, which is the entire backscatter signal (Figure 2). It is possible to have multiple echoes or returns, with the first return generally corresponding to the top of the vegetation and the last return corresponding to the ground or lower parts of the vegetation closer to the ground. The intermediate returns make lidar scanning exceptionally proficient in sensing the internal canopy regions of the vegetation. The full waveforms generated as a result of the interaction of the pulses with the objects possess the range information and information about the physical backscattering properties of the objects (Mallet and Bretar, 2009). From waveforms, a discrete set of georeferenced points called point clouds sampled on the surfaces of the objects in three-dimensional space are obtained along with the intensity of returns (Lillesand et al., 2004; Vosselman and Maas, 2010).

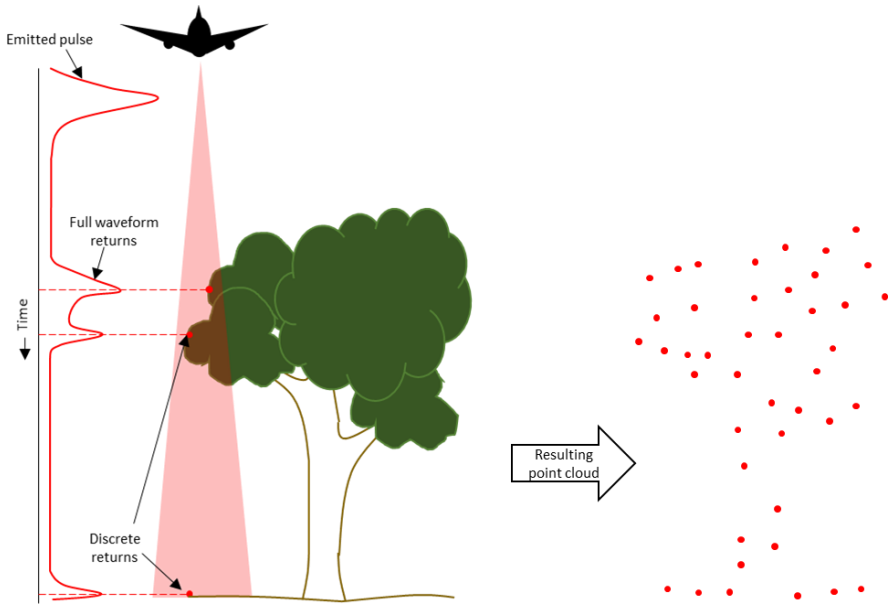

Figure 2: Illustration of an airborne lidar scanning (ALS) setup. The principle is the same for terrestrial scanners.

The ability of lidar to accurately detect the top and bottom (ground) of the vegetation has been used for several decades, with earlier studies focused on measuring the height of the vegetation (Dubayah and Drake, 2000; Hudak et al., 2009; Næsset, 1997a; Nelson, 2013; Rempel and Parker, 1964), thereby enabling estimation of biophysical parameters such biomass and forest structural information such as basal area and wood volume. Recent developments in lidar scanning allow for acquiring very high-density point clouds. Identifying individual trees and directly measuring their physical characteristics, such as crown diameter or height, is possible. This method is called the individual tree detection (ITD) approach. Although lidar sensors now have very high pulse frequencies that result in dense point clouds (Figure 3), it is challenging to identify individual trees in dense canopies due to the complexities in the

shapes of different crowns and difficulties in developing robust algorithms. Furthermore, the density of the points in lower parts of the forests reduces, making it challenging to identify suppressed trees (Räty, 2020). However, there has been significant progress in ITD methods over the years (Ferraz et al., 2016; Jeronimo et al., 2018; Koch et al., 2006; Kwak et al., 2007; Picos et al., 2020; Véga et al., 2014; Zhen et al., 2016)

Figure 3: Dense point cloud obtained for one of the field plots in this study. The point cloud was normalised using a digital terrain model (DTM) to convert point altitudes to point heights above ground. Converting these dense representations to useful information in the form of trees can be challenging.

An alternate option is an area-based approach (ABA) (Figure 4), wherein statistical relationships, also known as models, are developed between field measurements for representative forest areas (field reference plots) and lidar metrics derived for points clouds corresponding to those areas (Næsset, 2002; White et al., 2017; Wulder et al., 2012b). The statistical relationships could be parametric regression models (Hudak et al., 2006; Woods et al., 2011) or non-parametric regression methods such as random forests (Nurminen et al., 2013; Yu et al., 2015), k-NN (Chirici et al., 2016; LeMay and Temesgen, 2005; Packalén and Maltamo, 2007; Vastaranta et al., 2013), and, in recent years, deep learning-based methods (Lahssini et al., 2022; Liu et al., 2021; Martins-Neto et al., 2021). The advantage of ABA approaches lies in the fact that they are known to perform well even with datasets with low pulse densities. The lidar metrics can be in the form of statistical descriptors of the vertical distribution of points or of the distribution of intensity values of the points, canopy structural parameters (Hopkinson and Chasmer, 2009), vegetation profiles (Bouvier et al., 2015; Fischer et al., 2019), voxels (Carrasco et al., 2019; Pearse et al., 2019), or any metrics meant to capture the structural characteristics of the vegetation. Figure 5 illustrates different ways in which lidar data could be summarised.

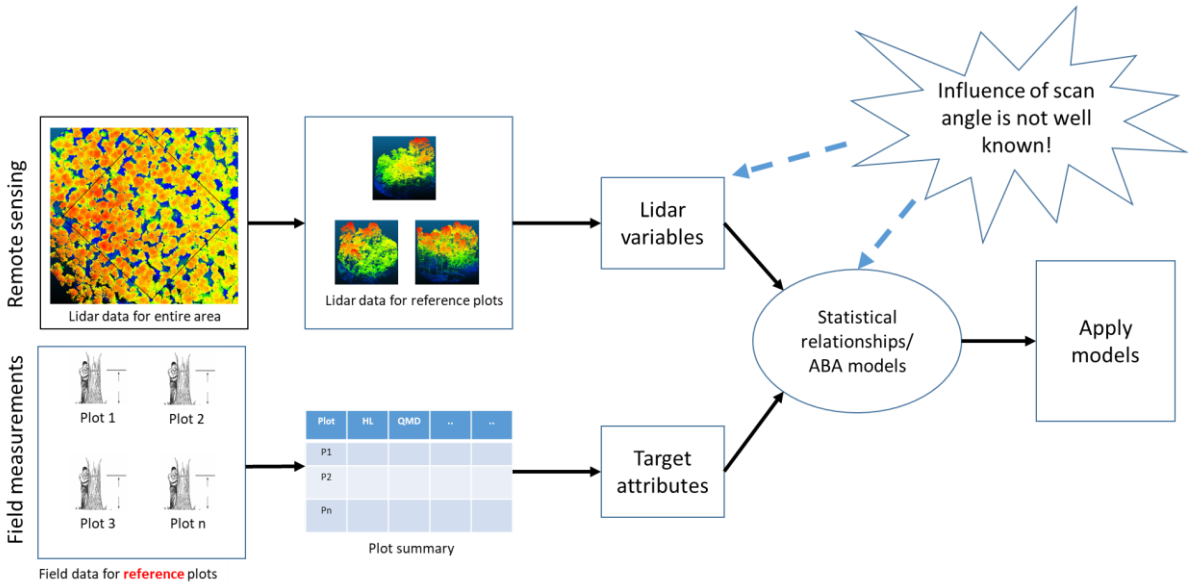

Figure 4: Illustration of area-based approaches.

Lidar metrics are nothing but summaries of the several thousands of points in the point cloud that represent a given plot of forest. If the forest plot remains constant, one would expect the lidar metrics to stay constant. This would be true if lidar data acquisitions were carried out with the same system and constant acquisition parameters. However, by its very nature, lidar scanning can be highly variable. Lidar scanning is governed by parameters such as the flying height, pulse repetition rate of the transmitter, overlap requirements and the scan angle (or the field of view), and other sensor-related properties, e.g. wavelength, beam divergence, power and recorder type. These parameters are dynamic and can vary across different acquisitions, collectively governing the quality of the point clouds. Furthermore, the relationship between lidar metrics and forest parameters also depends on the forest type and terrain characteristics. The latter has been shown to impact point distributions and the ABA model based on distributional metrics (Hansen et al., 2017).

Voxel-based metrics are alternatives to standard lidar metrics. They have also been explored in recent years to summarise and characterise vegetation more accurately. Point clouds are subdivided into smaller three-dimensional units called voxels. A voxel (volumetric pixel) is analogous to a pixel in image data, wherein each pixel contains some summary information of the area it represents. The three-dimensional distribution of vegetation elements is captured better by discretising the point clouds using voxels (Pearse et al., 2019; Yan et al., 2019). The number of points in each voxel can also be related to the distribution of foliage to obtain a simplified but more accurate spatial distribution of the vegetation (Béland et al., 2011; Carrasco et al., 2019; Grau et al., 2017; Soma et al., 2018). Voxel-based metrics have been demonstrated to improve the accuracy of forest attribute predictions (Kim et al., 2016; Pearse et al., 2019). Their use in ABA models has given rise to exciting possibilities in the future. ITD or ABA approaches depend on a specific minimum point density related to the pulse density. Nonetheless, studies have found that ABA methods tend to perform well even in low pulse densities (Bouvier et al.,

2019; Disney et al., 2010; Jakubowski et al., 2013; Lovell et al., 2005; Qin et al., 2017). ITD approaches, on the other hand, need higher pulse densities (>5 pulses /m²) for the delineation of different trees (Räty, 2020).

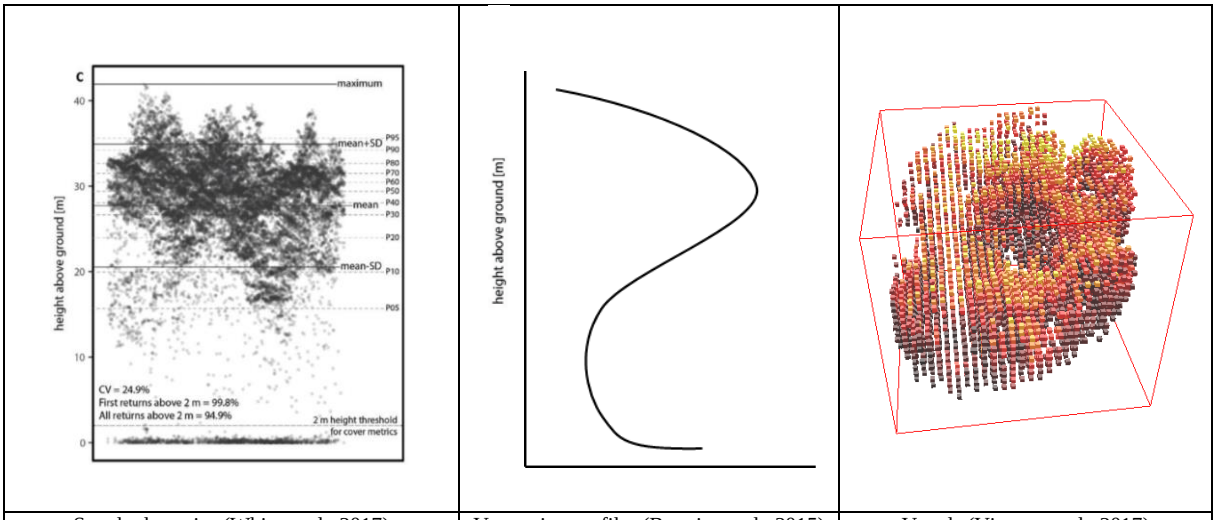

Standard metrics (White et al., 2017)	Vegetation profiles (Bouvier et al., 2015)	Voxels (Vincent et al., 2017)

Figure 5: Different ways to summarise lidar data into statistical descriptors

Lidar sensor development over the years now allows for scans at very high pulse repetition frequencies and with multiple echo detection capabilities. For ABA models, theoretically, there is no upper limit to the point/pulse densities, which are mainly governed by the field of study, operational considerations and storage capabilities. Studies have benchmarked the minimum pulse densities to be around one pulse per m² for ABA approaches to perform well. As regards the lidar scan angle, there are no well-defined upper limits.

1.4 Understanding the role of lidar scan angle in forestry applications

As it often happens that an invention or a technology goes on to serve a purpose for which it was not envisioned, lidar, or light detection and ranging, was never developed as a remote sensing tool to study forests. Nelson (2013) notes that the initial use of lidar remote sensing was driven by a need to accurately characterise terrain properties, sea ice roughness and thickness (Ketchum, 1971; Toomajr and Tucker, 1971) and bathymetric measurements (Hickman and Hogg, 1969). Lidar remote sensing was not used for forestry in the early years. However, studies attempted to employ lidar to penetrate the forest cover and extract the underlying surface (Krabill et al., 1980). Still, Rempel and Parker (1964) and Link (1969) were some of the early studies that acknowledged the possibility of using the lidar profile measurements for studying forests. However, these findings were also a by-product of using lidar to profile the terrain below forest cover. In profiling lidar, the sensor is generally locked in its position, pointing nearly vertically downwards, i.e. the scan angle is fixed at around 0° (Figure 6a).

Rempel and Parker (1964) acknowledged that vegetation heights could be directly estimated even if only "5 per cent of the forest cover permits an optical path to the ground". Krabill et al. (1980) noted the possibility of using lidar scanning to measure tree heights if part of the laser pulse was reflected from the canopy and the remaining from the forest floor.

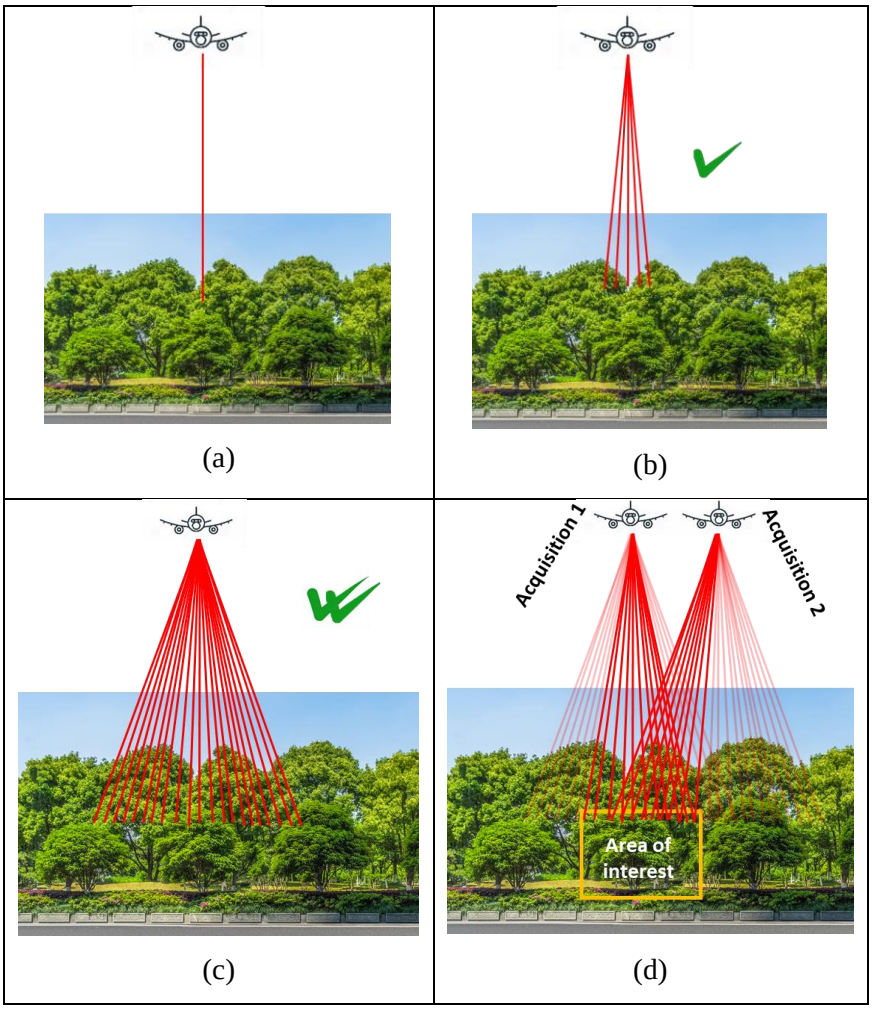

Figure 6: (a) Profiling lidar fixed at a scan angle of 0°, (b) rotating scanning mechanism that allows for scans of a larger area, (c) higher scan angles can cover an even greater surface area on the ground, (d) different acquisitions for the same area of interest with wider scans. Note: In reality, the pulses are diverging.

In the same decade, in a hydrography workshop aimed at developing a lidar system for detecting underlying terrain, it was established that a conical scan angle of 15°, expandable to 25°, would be suitable for the purpose (Nelson, 2013). The underlying principle was that tree height accuracy depends on how accurately the treetops and the ground below could be identified. This was a reasonable assumption since an increase in lidar scan angle means that it is more challenging to have an optical path to the ground due to an increase in the apparent density of the vegetation (Roussel et al., 2018). Besides, many early systems had a pulse repetition frequency (PRF) of a few hundred pulses per second (Nelson, 2013). Naturally, limiting the scan angle to a predominantly nadir configuration of 10°-15° ensured that laser pulses had low resistance on the way to the ground and back. Over the decades, this principle has been followed as a convention to extract tree heights and other forest attributes.

Extraction of accurate tree height measurements using lidar was the basis of lidar measurements during the 80s and 90s using profiling lidar configurations (Næsset, 1997b, 1997a). Tree height measurements were used to extract/model other forest attributes (Dubayah and Drake, 2000). However, profiling lidar does not offer the benefit of scaling up operations, which is the primary advantage of remote sensing. Eventually, a rotating mechanism was incorporated into lidar instruments, enabling a broader coverage to emit laser pulses at different angles in a sweeping or scanning fashion (Lefsky et al., 2002). In the 90s, studies began exploring the potential of increasing lidar scan angle up to 20° (Næsset, 1997b, 1997a). The scan angle was not found to be an influential parameter in predictions of tree heights (Næsset, 1997a) or timber volume (Næsset, 1997b) of boreal forests. However, the need to quantify the effects of "looking" through the canopy at different angles was emphasised.

Over the years, there has been some investigation into the influence of scan angle on various lidar metrics and forest attributes. Still, the datasets in most of the studies were cut-off at the 15°-20° threshold, keeping in line with some of the early conventions. Magnussen and Boudewyn (1998) observed that the lidar scan angle has minor effects on estimating stand heights. However, their study was on a dataset with a maximum scan angle of 12°. Morsdorf et al. (2008) observed fractional cover to be affected by scan angle despite using a lidar system with a maximum scan angle of 7.5°. Ahokas et al. (2005) found that the DTMs derived from lidar data were not significantly affected by scan angles of up to 15°. Chen et al. (2014) found that gap-fraction was stable up to 15°, which was the scan angle threshold in the study. Keränen et al. (2016) tested the effect of scan angle on the prediction of plot volume and mean height and found that a narrower scan angle range of $\pm$15° was more accurate than a scan angle range of $\pm$20°.

Even full-waveform data has been studied for the effect of scan angle. Crespo-Peremarch and Ruiz (2020) found that the return waveform energy (RWE), a metric derived from full-waveform lidar, had a lower radiometric error when computed for off-nadir pulses. RWE is sensitive to the energy loss along the trajectory. However, they limited the study to lidar pulses with a scan angle of less than 20°. They also found that predictions of forest fuel variables were marginally more accurate with inclined pulses. Interestingly, Kamoske et al. (2019) also recommended that higher scan angles would ensure a better sampling of the vegetation resulting in a more accurate understanding of the gaps in the canopy. Kellner et al. (2019) also suggest that point clouds acquired with wider scan angles can "resolve individual tree and branch structure and are similar to TLS".

Limited by cost considerations, lidar data acquisition does not allow for a comprehensive scanning of forest plots from multiple locations, making it difficult to understand the effect of scan angle for a range of acquisition geometries as most operational lidar acquisitions have been constrained to a scan angle of 15°-20°. On the one hand, acquisition costs could be brought down by increasing the scan angle to 30°, and on the other, data users prefer a 50% of overlap to minimise the error and make the data reliable.

The resulting tradeof, therefore, underlines a need for a comprehensive investigation of the effects of higher scan angles, which were also addressed from a data simulation point-of-view. Studies tried to overcome acquisition limitation on diversity in lidar scan angles in datasets by simulating lidar point clouds for different forest types (Disney et al., 2010; Holmgren et al., 2003; Qin et al., 2017). Simulation enabled generation of lidar data with different characteristics without the practical constraints. Holmgren et al. (2003) simulated lidar data with scan angles up to 30° in 5° intervals from computer models of pine and spruce trees. Similarly, Disney et al. (2010) also simulated lidar data with scan angles of up to 30°. Qin et al. (2017) simulated lidar datasets in intervals of 5° up to 30° and from different altitudes. They observed that foliage profiles from simulated vegetation models were similar to those retrieved from simulated lidar data with a scan angle of 20°, highlighting the benefits of inclined observations. Conversely, Roussel et al. (2018) proposed a mathematical framework to normalise effects of the scan angle on lidar metrics (classical lidar descriptors such as mean, standard deviation, percentiles, kurtosis and skewness and height distribution entropy) to result in metrics as if they were computed for nadir point clouds. When using voxelisation approaches, the path length is also considered to normalise information (Grau et al., 2017; Soma et al., 2018). Recently, van Lier et al. (2021) tested the effect of using lidar data with scan angles up to 30° on forest attribute predictions. They concluded that although lidar metrics were significantly affected, their impact on the predictions was not of great magnitude.

Over the years, there has been a gradual increase in the lidar scan angle marking a shift away from the traditional practice of limiting the scan angle to nadir or just off-nadir angles owing to practical considerations and the development of systems with high pulse repetition frequency capabilities. The flexibility of lidar allows for large-scale nationwide multipurpose acquisitions (IGN, n.d.). Recent innovations such as the Leica SPL100 have fixed FOV capabilities of up to 60° allowing wide-area acquisition at a lower cost per data point (Leica Geosystems). In recent years UAV acquisitions have been carried out at local levels, which involve scan angles higher than 20° (Cao et al., 2019; Liu et al., 2018; Lu et al., 2020; Ma et al., 2022). In the coming years, increasing the use of such low-flying platforms with high scan angles will entail the need for simultaneous knowledge building concerning the influence of lidar parameters.

There seem to be two schools of thought, a) one that prefers to limit the scan angle to nadir or just off-nadir and b) one that believes it is possible to obtain new insights by increasing the scan angle. Roussel et al. (2018) remarked that the effect of scan angle of forest predictions might vary from one forest type to another and may also depend on the chosen lidar metrics and subsequent ABA models. Sometimes contrasting observations in different studies evidence this. There is a lack of conclusive knowledge about the lower and upper thresholds for scan angle. Indeed, this further reinforces the need to improve our understanding of the problem.

Additionally, in any given scene, the acquisition geometry is defined by the lidar scanning parameters, the terrain and vegetation type physical characteristics. In steep environments, if the aircraft is relatively 'upslope' of the forest being scanned, the pulses must travel through some vegetation immediately next to the area of interest. Furthermore, the trees grow with some inclination in steep terrains with asymmetrical crowns due to competition for light (Breidenbach et al., 2008). Considering the acquisition geometry is thus essential to understanding lidar scan angle.

Although some of the research so far has attempted to study the influence of lidar scan angle on lidar metrics and, to a lesser extent, on attribute estimations using lidar data, there is certainly scope for more work to be done in this regard. On the one hand, as mentioned before, the general understanding is to limit lidar acquisition to 20° or filter out datasets acquired with high inclination (ICSM, 2010). Using 50% overlap is one way to ensure sufficient sampling of forest plots. However, ensuring a high degree of overlap can be costly. In NFI recommendations of some countries, there are specifications of overlap criteria of 30% (Ministry of Forests, Lands and GeoBC, 2020), while some other countries do not have an explicit consideration of the same (ACT, n.d.; IGN, n.d.; Swisstopo, n.d.).

1.5 Research questions and objectives

For sustainable forest management, accurate information about the forests is critical. With differing data acquisition practices across local, regional, national and global scales and different platforms, it is essential to move towards harmonisation of information while ensuring cost-effectiveness. While lidar scan angle has been acknowledged to impact ABA models, there is a lack of convergence among some of the studies. Even lesser attention has been given to strategies to deal with datasets comprising inclined scan angles while the incidence of such datasets is increasing either due to new technological developments or due to limitations in costs. Due to the complexity of vegetation, measuring its structure using lidar highly depends on the acquisition geometry. Studying these interactions and better evaluating their impact on forest attribute estimations from lidar data is essential to determine if more attention should be paid to this acquisition parameter.

Two main hypotheses were:

H1: ABA predictions will be unreliable if influences of scan angle are not considered when modelling relationships between forest attributes and lidar variables

The main research question based on the hypothesis is:

Q1: What are the impacts of lidar scan angle on lidar metrics and ABA predictions?

H2: The effect of scan angles on the accuracy of predictions can be reduced by normalising lidar metrics to changes in acquisition geometry or by incorporating this geometry in ABA models.

The main research question based on the hypothesis is:

Q2: How to manage the impact of lidar scan angle on ABA predictions?

In the context of the hypotheses, the main objective of this PhD study was to understand whether accounting for the impact of scan angles on lidar data could be helpful in the development of robust and accurate ABA models for the prediction forest attributes, and therefore fostering use of lidar for forestry application.

The sub-objectives of the study were:

1) To assess the impact of lidar scan angle on ABA models metrics on a diversity of complex forest environments
    a. By assessing the impact of scan angle on commonly used lidar metrics that are used in ABA models
    b. By assessing the impact of using metrics that are explanatory but sensitive to lidar scan angle on ABA predictions
2) To develop methods to manage the impacts of lidar scan angle on ABA models
    a. By considering different combinations of acquisition geometries (scan angle)
    b. By developing metrics using voxel-based approaches to normalise for effects of scan angle
    c. By modelling the effects of scan angles by considering overall acquisition geometry using deep learning approaches.
3) Draw perspectives and recommendations from our findings for the operational use of lidar data for forest applications

1.5.1 Impact of scan angle on ABA models

The impact of scan angle on ABA models was addressed via the sub-objectives 1a and b. The fundamental challenge, as illustrated in Figure 5, is that although increasing the scan angle will help improve the operational efficiency, we do not know the implications of doing so on lidar metrics and on subsequent forest attribute predictions using ABA models. The challenges arise from the fact that numerous lidar metrics used in ABA models are not assessed from the point of view of the impact of scan angle before the development of ABA models. Studies have documented the effect of various scan angles in different forest environments (Keränen et al., 2016; Montaghi, 2013; Roussel et al., 2018; van Lier et al., 2021). For example, Keränen et al. (2016) observed that a scan angle lower than 15° was preferable for the prediction of volume in pine-dominated managed forests, while van Lier et al. (2021) found marginal effects of lidar scan angle even up to 30° for forest attribute predictions in balsam-fir dominated stands. As forests are not homogenous environments, 'viewing' them from different locations can result in varying information. Furthermore, as forests have varying physical characteristics, it is

imperative to assess the impact of scan angle in various forest environments, especially in complex stands and mountainous areas.

This part of the study comprises two stages. In the first stage, it was hypothesised that lidar metrics would be influenced by changing acquisition geometry (scan angle), driven by the spatial heterogeneity of complex forest environments. The effect of lidar scan angle on a set of lidar metrics was studied for the riparian forests along the river Ciron in southwestern France. The riparian forests were relatively flat terrain with average slope of 8.9 degrees. The set of metrics comprised statistical descriptors of the distribution of point heights and forest structural characteristics. For the second stage of the study, it was hypothesised that ABA models calibrated based on a set of plots scanned with specific geometries (which depends on the flight plan) may be prone to prediction errors when applied to assess stand characteristics of similar stands scanned with different acquisition geometries. At this stage, three other types of forests were also considered, which consisted of broadleaf, coniferous and mixed stands in mountainous terrain with an average slope of 26 degrees.

The specific questions that were addressed in this part of the study were:

Q1) What is the impact of lidar scan angle on commonly used lidar metrics?

Q2) What is the effect of the inclusion of lidar metrics sensitive to scan angle on ABA models?

1.5.2 Strategies to deal with impacts of lidar scan angle

This part of the study concerns the second sub-objective. So far, most lidar acquisitions are planned based on the hypothesis that high scan angles (above 20°) must be avoided to ensure ground detection. As a strategy to manage lidar datasets with inclined scanning, studies have proposed the normalisation of lidar metrics for point clouds acquired from inclined scans to correspond to those acquired from vertical scans (Roussel et al., 2018).

Accurate characterisation of the canopy properties is an essential requirement for a better understanding of spatial and temporal properties of vegetation, and voxel-based metrics have been shown to perform well in these tasks (Carrasco et al., 2019; Kim et al., 2016; Pearse et al., 2019). Three strategies were proposed and evaluated to manage scan angle impacts and improve ABA model robustness.

The simplest method for reducing the impact of scan angle effects was investigated in the first strategy (S1), which involved mixing point clouds from several flight lines with various scan angles. The performance of ABA models was also studied when the data consisted of point clouds from single flight lines. As it can be costly to ensure overlaps, this technique is not feasible in an operational environment. Therefore, two different strategies were also investigated. The second strategy (S2) suggested a voxel-based approach to normalising lidar metrics. It was hypothesised that the impacts of the lidar scan angle could be normalised by voxel-based 3D reconstruction techniques based on the lidar pulse trajectory

retrace resulting in a calculation of voxel-level plant area density (PAD) with higher accuracies (Figure 7).

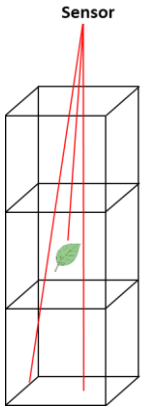

Figure 7: Ray-tracing

The third strategy (S3) hypothesised that any given acquisition geometry results from the unique interaction between lidar acquisition parameters, terrain properties and vegetation characteristics. Therefore, changes in lidar metrics, if any, due to varying scan angles provide some unique insights into the properties of the vegetation. The innovative aspect of this part of the study was to consider point clouds for the same plots but from different flight lines as independent and unique observations to augment standard lidar datasets for ABA models. The variables describing the acquisition geometry were thus considered critical explanatory variables to be included in the model.

The specific questions that were addressed in this part of the study were:

Q3) How does overlap in lidar data acquisition influence the quality of ABA models?

Q4) How to normalise lidar metrics sensitive to lidar scan angle?

Q5) How to model acquisition geometry in ABA models?

1.6 Overview of the thesis

This thesis is divided into three main chapters corresponding to three publications.

Chapter 2 mainly addresses Q1. The influence of lidar scan angle was assessed on commonly used lidar metrics that were computed for an entire forest. ABA approaches involve developing models for a given set of field plots followed by dividing the whole forest into a grid with a grid-cell area comparable to the area of field plots used. Similarly, the forest was divided into a grid and metrics were computed for different scan angles in a grid cell. The study site is a riparian area along the Ciron river and some of its tributaries in Southwestern France. It includes broadleaved and mixed stands with low levels of management intensity. Stands are characterised by a high diversity in species and by their structural complexity. The variability of the metrics was analysed by comparing metrics computed for point clouds

acquired with inclined scan angles to those computed for point clouds obtained with nadir acquisition. The study highlighted that metrics were differently sensitive to scan angle and that metrics such as gap fraction, commonly used in models, were amongst the most sensitive.

This chapter was published in the ISPRS Archives in 2020 as a part of the proceedings of the ISPRS Congress Nice 2020. Initially accepted as an oral presentation, it was also presented as a poster in the ISPRS Congress Nice 2020/2021/2022.

In Chapter 3, several questions are addressed using lidar datasets for varying types of forests and terrain properties. The first study area (riparian region) was studied along with three different forest types (coniferous, broadleaf and mixed) in the *Massif des Bauges* in eastern France. For both sites, lidar datasets were acquired with multiple overlaps, and different regions were scanned with different acquisition geometry or viewing characteristics. Lidar datasets were resampled from the existing data to datasets with constraints on the lidar scan angle. In other words, for the same area, different and independent lidar acquisitions were simulated. A predefined ABA model with metrics with varying sensitivities to scan angle was chosen to model forest attributes. Firstly, the impact of scan angle on the lidar metrics chosen or the ABA model was assessed at the level of the plots for three forest types at Bauges. Then the effect of using lidar metrics sensitive to scan angle on the forest attribute predictions was investigated (Q2). The lack of robustness was reflected in the ABA predictions for models built with metrics sensitive to scan angle for datasets with different acquisition geometries.

In this Chapter 3, questions Q3 and Q4 were also addressed to evaluate the potential of two suggested strategies, S1 (combining several flight lines) and S2 (using voxelisation to normalise metrics), to mitigate the effects of scan angles on ABA models. Based on S1, it was observed that the variation in ABA predictions was lower when datasets consisted of point clouds combined from multiple flight lines. Regarding S2, the resampled datasets were used to build ABA models with equivalent metrics derived from voxelisation. The benefit of using voxelisation as a strategy to manage the effects of scan angle was assessed. Voxel-based metrics had a positive contribution to the predictions on account of improving the average accuracy of predictions and reducing the variability in predictions for datasets with different acquisition geometries. This chapter has been submitted to the ISPRS Journal of Photogrammetry and Remote Sensing. It has been accepted with major revisions and was resubmitted.

Chapter 4 focuses on Q5. A different perspective was applied to understand the impact of scan angle on lidar metrics and ABA predictions. Forest vegetation is not evenly distributed, and the terrain is not always flat, as was the case for the study area at Bauges. In such complex terrains, the azimuth of acquisition also plays a role in the acquisition. Neural networks were used to model the interaction between factors such as the acquisition parameters, terrain and vegetation properties. A point cloud for any given plot resulting from the interactions of these factors was considered a unique observation. A related study investigating the fusion of lidar and optical data using deep learning-based approaches was

published in Lahssini et al. (2022). A part of that study using the multilayer perceptron (MLP) was adapted to the requirements of this study. This chapter has been written in the form of a publication for submission to peer-reviewed journals. The findings were also presented at the ForestSAT conference in Berlin in 2022

The findings are discussed in Chapter 5. Few recommendations and perspectives are provided to foster the operational use of lidar data for forest applications.

Chapter 2: **Scan angle impact on lidar-derived metrics used in ABA models for prediction of forest stand characteristics: a grid based analysis**

K. R. Dayal [1*], S. Durrieu [1], S. Alleaume [1], F. Revers [2], E. Larmanou [1], J-P Renaud [3], M. Bouvier[4]

[1] INRAE, TETIS, Université de Montpellier, AgroParisTech, CIRAD, CNRS, INRAE, Montpellier, France

[2] INRAE, UMR 1202 BIOGECO, Université de Bordeaux, Cestas, France

[3]Office National des Forêts, Nancy, France

[4] INFOGEO, Montpellier, France

* Corresponding author

Abstract: Lidar scan angle can affect estimation of lidar-derived forest metrics used in area-based approaches (ABAs). As commonly used first-order metrics and various user-developed metrics are computed in the form of a grid or a raster, their response to various scan angles needs to be investigated similarly. The objective of this study was to highlight the impact of scan angles on 11 metrics (9 height-based and 2 other commonly used metrics) at the level of the grid-cell. The study area was divided into a grid of cell size 30 m. In every grid-cell, the flight lines that sampled at least 90% area of the grid-cell were identified. The flight lines and the corresponding point clouds were then classified based on their mean scan angle into four classes 0°–10°, 10°–20°, 20°–30° and 30°–40°. Metrics were computed for one flight line per class for each grid-cell. This resulted in a maximum of four values for a metric in every grid-cell. Comparing these values revealed the evolving nature of the metrics with the scan angle. For the comparison we used a paired t-test and simple linear regression. We observed that most of the metrics were systematically under-estimated with increasing scan angle. Gap-fraction, rumple index were affected more than standard deviation of height while the maximum height was relatively stable. Among the height percentiles, the higher percentiles were relatively more stable compared to the lower percentiles. Scan angles can indeed have an impact on the estimation of lidar derived metrics. Although, many of the metrics studied showed statistically significant differences in their computation for different scan angles, their impact on the accuracies of ABA models needs to be studied further by accounting for the differences as shown in this study.

Keywords: lidar, scan-angle, area-based approach, forest metrics, forest inventory

2.1 Introduction

Lidar acquires an explicit three-dimensional representation of the forest structure. Such information is essential to model both ecological and resource management information, and there is a broad spectrum of methods, across various airborne LiDAR platforms, for improved characterisation of forest ecosystems and a better understanding of their functioning. It is possible to extract several forest inventory attributes with improved accuracies for better resource management (Bohn and Huth, 2017; Breidenbach et al., 2010; Côté et al., 2018; Næsset, 2007; Wallace et al., 2012). Lidar data can also be used to assess biophysical variables, such as above-ground biomass (AGB) and Leaf Area Index (Bouvier et al., 2015; Breidenbach and Astrup, 2012; Lefsky et al., 2002; Vincent et al., 2017)

In Area-based approaches (ABAs), a set of ALS variables (X_i) – derived from lidar data for a given area – is linked to a target variable (Y) measured at the same area on the ground (Dubayah and Drake, 2000). This is done for a handful of different plots to build a predictive model to predict the target variable for the entire forest. The fundamental unit of a predictive model is a small subset from the lidar point cloud, the area of which equals the area of a reference field plot (i.e., typically 0.025 to 0.07 ha). A model developed for representative plots is then applied to the whole forest area divided into grid cells, the area of which still equals the area of reference field plots. Any given target forest attribute is thus predicted at the cell level. Notwithstanding the trade-off between area coverage, the density, and the resolution of measurements between different platforms (i.e. aerial and un-manned aerial vehicles (UAV)), studies have recommended further investigation of variation in acquisition parameters for forest parameter assessment (Cao et al., 2016; Korhonen et al., 2011; Tompalski et al., 2019). Some studies focussed on the effect of point density on the accuracy of stand attribute predictions (Bouvier et al., 2019; Næsset, 2009; Singh et al., 2016). Relevant lidar metrics selected to build predictive models were found to differ significantly with pulse density in Næsset, (2009) but in Bouvier et al., (2019) there was no change in the four metrics used. However, in the range of explored pulse densities, i.e. from 0.06 to 12.7 pulses/m², in all the studies considered together, only minor or even no impact on stand attribute predictions was found.

Another critical acquisition parameter is the maximum off-nadir scan angle (Bater et al., 2011). Liu et al., (2018) demonstrated the effect of scan angle on gap fraction estimation which, in turn, affects the estimation of LAI. Tompalski et al., (2019) recommend the disentangling of various acquisition parameters, including scan angle, to develop robust transferable models. Studies utilising lidar-based metrics generally do not consider the influence of scan angles, and there may be unaccounted biases which may cancel each other in predictive models (Roussel et al., 2018). There can only be one, or a few flight-passes for a given area, and it is evident that the ‘viewing

configuration', or the scan angle with which each grid-cell is sampled will be different (Figure 1). Owing to these inconsistencies, metrics computed for an entire forest, in the form of a raster may possess inherent biases. For airborne acquisitions, Evans et al., (2009) recommend limiting the maximum scan angle to 15° to reduce measurement errors, despite a reduction in flight time and cost that would have enabled higher scan angles. In Montaghi, (2013), several metrics were found to be relatively stable up to an angle of 20 degrees. However, with the increasing popularity of light systems embedded on low altitude platform – such as ULM or UAVs – it is imperative to understand the response of various commonly used metrics to varying scan angles as limiting the scan angle to 15-20 degrees is hardly feasible in an operational mode for reasons of time and data volume optimisation. This would allow for better management of the biases and result in more informed mission planning for efficient data acquisition.

In the present study, with the objective to contribute to the understanding of how scan angles modify metrics that are commonly used in ABA approaches, we analysed the impact of scan angles on a set of metrics that can be used to describe the horizontal and vertical vegetation structure of a riparian forest located in the Landes area, in south-west France.

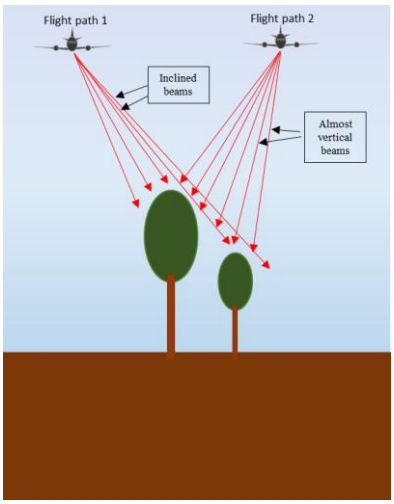

Figure 1: Acquisition geometry from different flight lines

2.2 Materials

2.2.1 Study area

The study area is a riparian zone bordered by pine forests in the Ciron valley in the southeast of the Gironde and the northwest of the Lot-et-Garonne departments, in the Aquitaine region of south-western France. As a result of related projects, field plot information was available for 30

circular sites (15 m radius) along the river Ciron (flowing in SE-NW direction) and its tributaries, covering a total length of approximately 45 km. The plots are representative of the riparian ecosystem. The field measurements are indicative of structurally diverse vegetation in the region, with as many as 33 different species of trees and a diameter at breast height (DBH) varying from 7.5 cm to 87 cm (Figure **2**). The riparian region includes the active floodplains. It is highly biodiverse because of sparse forest management activities. In contrast, periodic management practices are carried out in the pine forests located beyond the riparian region.

Figure 2: Example of the riparian environment in the study area

2.2.2 Lidar data

In early October 2019, INFOGEO (France) acquired lidar data using a VQ580 laser scanner (RIEGL, Austria) on an ultralight aircraft platform. The flying altitude was approximately 250 m, which enabled data-acquisition at an overall point density of around 68 pts/m². Overlap of 35%-40% and several passes over any given area (Figure 3) ensured that several locations across the region were sampled with multiple 'viewing' configurations (Figure 1). However, it was not possible to obtain all the configurations for all the areas. Additional sensor specifications are available in Table1. Data pre-processing was carried out by INFOGEO, which involved classification of ground points using TerraScan (Terrasolid Ltd., Finland).

Date of acquisition	Early October 2019
Sensor	RIEGL VQ580
Wavelength	Near-infrared
Field of view	60° (+30°/-30°)
Beam divergence	0.2 mrad
Footprint diameter	52 mm @ 250m
Ground speed	25 m/s
Point density	68 pts/m²
Flight altitude AGL	250 m

Table 1: Technical specifications of the sensor

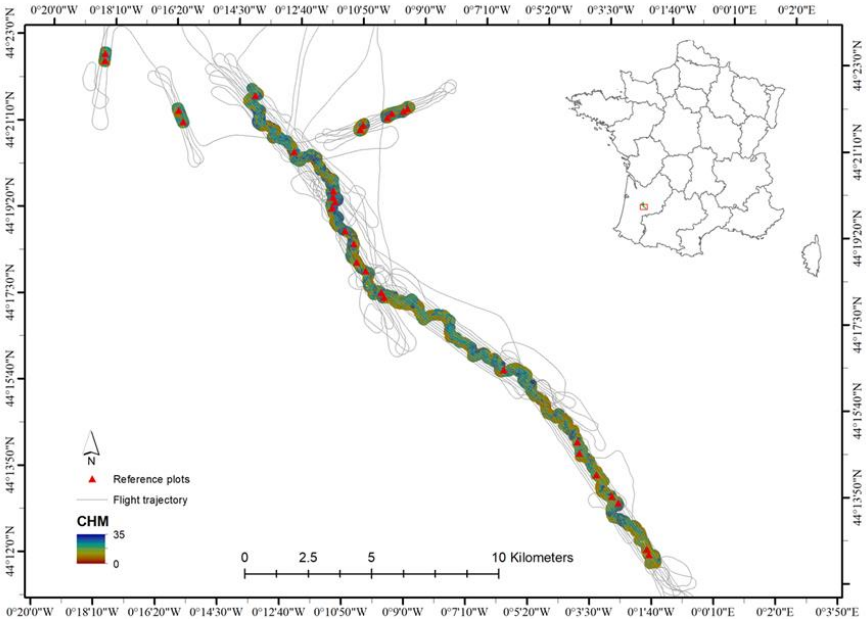

Figure 3: Canopy height model of the Ciron valley area with field plot locations and data acquisition flight lines

2.3 Methods

2.3.1 Metrics selection

While new metrics are continually being developed to improve prediction of forest attributes (Almeida et al., 2019; Bouvier et al., 2015; Véga et al., 2016), first order derivatives such as height-based and density-based metrics are commonly utilised in ABA approaches (Mitchell et al., 2012). We thus considered height-based metrics such as mean, maximum, standard deviation, coefficient of variation of heights, and height percentiles (10^{th}, 30^{th}, 50^{th}, 70^{th} and 90^{th}). When computing these metrics, the understory vegetation and ground points were not considered by filtering out all points below a height threshold of 1m. Besides typically describing distributions (Roussel et al., 2018), these also considered to be descriptors of forest structural conditions.

We also included two other widely studied metrics in our study: gap fraction and rumple index. The distribution of foliage determines the proportion of open areas in forest vegetation, which, in turn, determines the amount of energy from the sun and the sky that travels through the canopy (Nilson, 1971). Gap frequency or gap fraction is a good indicator of the structural characteristics of the vegetation and can be assessed from lidar data (Bouvier et al., 2015). Gap fraction was calculated as described by Bouvier et al., (2015) by dividing the number of first returns below a specific reference height (2m) by the total number of first returns. Rumple index is the ratio of the outer surface area of the canopy to the ground surface (Parker and Russ, 2004). It is a measure of the structural complexity of the stand. It characterises the outer-canopy, which is related to the development of the forest stand.

2.3.2 Data preparation to analyse effects of scan angle

As stated in the introduction, the grid-cell is the unit area used to apply an ABA model. The dimensions of the grid-cell are similar to those of field reference plots, which are 30 m diameter circular plots in this study. Hence, we attempted to discretise the scan angles according to a grid containing cells of 30 m x 30 m and analysed the point cloud in every cell to understand the impact of variations in scan angle on pre-defined metrics. Due to the acquisition geometry illustrated in Figure 1, not every grid-cell is sampled with all the possible scan angles. In other words, the data with continuous scan angles, i.e. 1°, 2°, 3°…10°, 11° etc. is not available for every grid-cell. Five classes of scan angle (absolute value) were thus defined based on the scan angle rank of the LAS dataset, namely 0°- 10° as class 1, 10°- 20° as class 2, 20°- 30° as class 3, 30°- 40° as class 4 and >40° as class 5. The scan angle is based on 0 degrees for nadir and -90° and +90° to the left and right sides of the aircraft respectively (ASPRS, 2013). We hypothesised that, for each pair of scan-angle classes (class 1-class 2, class 1-class 3 etc.), the number of common grid-cells sampled from the five different classes of angle would be sufficiently high and representative of the diversity of the stand types present across the site.

The steps of the process followed are: (i) for each grid-cell, we identified all the flight lines from which the lidar sensor sampled it either entirely or partially, and divided the point cloud in the grid-cell into subsets based on the flight lines. We did not consider any flight lines and, by extension, point clouds that partially sampled a grid-cell if they covered less than 90% of its area to avoid including in the analysis metrics that are not representative of the whole forest plot within the grid-cell; (ii) we then computed the mean scan angle for each of the remaining point clouds. We assumed that from a particular flight line and at a flight height of 250 m, the sensor samples a given grid-cell largely homogeneously and that the mean scan angle could be considered representative of the acquisition characteristics. This assumption was necessary for the sake of simplification, as it is not possible to analyse the influence of scan angle continuously. In practical applications, all regions are not sampled equally with all scan angles, i.e. the laser beams are never parallel. When a grid-cell was viewed with the same scan-angle class from more than one flight line, we considered the flight line that had mean scan angles closest to the respective class median values (0° for -10° to +10°, 15° for 10° to 20° etc.); (iii) the metrics were computed for the point clouds from each of the remaining flight lines. After considering the area threshold of 90%, there were instances where some classes had no flight lines/point clouds and in such cases, the metrics were not calculated.

The result comprised a stack of five rasters in which every grid-cell had a vector of five values for the metrics, one for each class of scan angle (including NA values for empty classes). During the data acquisition, a certain buffer area was considered on either side of the riparian forests. These areas contained urban settlements and agricultural fields. We used a 95^{th} height percentile

raster to conditionally filter out all the pixels in the five layers corresponding to a 95th percentile value of 7 m or less. The number of grid-cells with points belonging to class 5 (40°-50°) were significantly lower compared to other classes. We also observed that these grid-cells were in regions where the aircraft was making a turn during data acquisition. Therefore, we did not consider class 5 and conducted further analysis of the other four classes. After dropping class 5 and retaining only grid-cells corresponding to forests (95th height percentile > 7 m) we first analysed the diversity of viewing configurations that could be found on the area by counting the number of scan angle classes per grid-cell. Then, metrics were compared for grid-cells viewed concurrently from the first four classes of scan angles. 2000 common grid-cells distributed across the entire study area were available.

2.3.3 Analysis of scan angle effects on the selected metrics

For a statistical understanding of the influence of scan angle on metrics, we compared the distribution of metrics using mean and standard deviation. We used the paired sample t-test or dependent sample t-test to determine whether the mean difference between two sets of observations is zero. In a paired sample t-test, each subject or entity is measured twice, resulting in pairs of observations. We compared the metric values for class 2, class 3 and class 4 to class 1 values. The null hypothesis (H_0) being that the true mean difference (μ_d) between the classes is equal to zero. The two tailed alternative hypothesis (H_1) assumes that the true mean difference (μ_d) is not zero. The level of significance was 0.05. The dispersions of differences between class 1 and class i (i= {2,3,4}) were also assessed by computing the standard deviations of the cell by cell differences for each pair of scan-angle classes considered.

Furthermore, we also compared the metric values for each of classes 2, 3 and 4 to class 1 using simple linear regression to assess the impact of scan angle as we move away from a predominantly vertical 'viewing conditions' (class 1). The linear relationships were tested for statistical significance in two aspects, namely, slope and intercept. The equation for the linear regression model that can be used to explain the relation between Y (class i, where i = {2,3,4}) and x (class 1) is as follows:

$$Y = \beta_0 + \beta_1 x + \epsilon \qquad (1)$$

β_0 is the coefficient for intercept and β_1 is the coefficient for the slope. Using the linearHypothesis() function in R, we jointly tested for the significance of $\beta_0 = 0$ and $\beta_1 = 1$, at a level of significance of 0.05. For P-values<0.05, the null hypotheses were rejected, thereby indicating that there was a bias in the estimation of the metrics for higher scan angles, either due to the slope or the intercept.

2.4 Results

2.4.1 Summary of the grid-cells

There were 16758 grid-cells with a 95th height percentile value of 7 m or more considered as forest. Among these, 2446 grid-cells did not return any class of scan angles; 906 grid-cells contained *any* one class; 4549 grid-cells contained *any* two classes; 6857 grid-cells contained *any* three classes; and 2000 grid-cells contained four classes.

2.4.2 Mean differences and standard deviation

The results of the paired t-tests for the sample of 2000 grid-cells containing the four scan-angle classes are presented in Table 2. As per the mean differences, for almost every metric there was an underestimation for the inclined classes, which led to statistically significant differences as shown in the table. The max (maximum) metric was not significantly affected across class 1, class 2 and class 3; however, class1-class 4 was statistically significant with a mean difference of 0.183 m. For the mean metric, the mean differences for class 1-class 2 and class 1-class 3 are statistically significant at 0.113 m and 0.130 m respectively. In the case of coefficient of variation of height and rumple index, the metrics for class 2 seem to have been overestimated compared to the reference class (class 2>class 1). There was no difference between class 1 and class 3 and a significant underestimation for class 4 compared to class 1.

For coefficient of variation, the mean difference for class 1-class 4 was approximately 0.869 m. The mean differences for the percentiles were mostly positive (ranging from 0.09 to 0.18) for class 1-class 2 and class 1-class 3. The lower percentiles had no significant mean difference for class 1-class 4, with the exception of p30 (30th percentile), which had a p-value of around 0.02. Within the percentiles, for class 1-class 2 and class 1-class 3, p10 had the highest mean difference and the p90 (90th percentile) had the lowest mean difference. For any given metric, the standard deviations of the differences had an increasing trend from class 1-class 2 to class 1-class 4. This was observed for all metrics with no exception.

2.4.3 Simple linear regression (cli~cl1)

A visual analysis of the scatterplots for class i vs class 1 showed that class 1 metrics are linearly related to the metrics of the other scan-angles. Figure 4 depicts the scatterplots for a subset of six metrics. Some metrics such as gap fraction and rumple index were clearly affected by the scan angle, while some such as p10 (10th percentile) were affected to a lesser extent. The effect of scan angle on mean, max (maximum), and p90 is relatively lesser. Testing how different the regression lines are from the y=x line can reveal the existence of systematic (intercept) and variable (slope) biases (Table 2). We observed that for almost every metric, the slopes of the respective regressions lines were less than one. For the height percentiles, between p10 to p90 there was a gradual shift

of the regression lines towards the y=x. Lower percentiles were more affected by a change in scan-angle than higher percentiles. The null hypothesis, that slope = 1 and intercept = 0, was not rejected for the max metric for class 2~class 1. Although the slope values for class 3~class 1 and class 4~class 1 are close to 1, under the joint hypothesis test, the null hypothesis was not rejected due to a significant effect of the intercept. This was also the case for other metrics as shown in Table 2. Coefficient of variation, gap fraction, and rumple index appear to be considerably influenced by the scan angle either due to the existence of a significant systematic bias (CV and rumple index), or due to variable bias (gap fraction and rumple index).

Metric	Mean differences			Standard deviation of differences			(Intercept, Slope)		
	cl1 - cl2	*cl1 - cl3*	*cl1 - cl4*	*cl1 - cl2*	*cl1 - cl3*	*cl1 - cl4*	*cl2 ~ cl1*	*cl3 ~ cl1*	*cl4 ~ cl1*
Max (m)	-0.001	0.014	0.183 ***	0.563	0.575 (+2.1%)	0.903 (+60.4%)	(0.1,1)	(0.19,0.99) **	(0.21,0.98) ***
Mean (m)	0.113 ***	0.130 ***	0.030	0.453	0.547 (+20.8%)	0.864 (+90.7%)	(0.02,0.99) ***	(0.13,0.98) ***	(0.33,0.97) ***
sd (m)	0.010	0.035 ***	0.103 ***	0.258	0.326 (+26.4%)	0.447 (+73.3%)	(0.25,0.95) ***	(0.3,0.94) ***	(0.38,0.91) ***
cv (m)	-0.187 **	0.008	0.869 ***	2.625	3.418 (+30.2%)	4.919 (+87.4%)	(3.61,0.92) ***	(4.59,0.9) ***	(5.24,0.86) ***
p10 (m)	0.176 ***	0.147 ***	-0.025	0.971	1.198 (+23.4%)	1.628 (+67.7%)	(0.37,0.89) ***	(0.57,0.85) ***	(0.96,0.81) ***
p30 (m)	0.104 ***	0.090 **	-0.121 *	0.993	1.347 (+35.6%)	2.113 (+112.8%)	(0.34,0.96) ***	(0.74,0.92) ***	(1.56,0.86) ***
p50 (m)	0.130 ***	0.159 ***	0.051	0.620	0.879 (+41.8%)	1.217 (+96.3%)	(0.07,0.99) ***	(0.2,0.97) ***	(0.5,0.96) ***
p70 (m)	0.123 ***	0.153 ***	0.102 ***	0.541	0.715 (+32.2%)	0.813 (+50.3%)	(0.01,0.99) ***	(0.11,0.98) ***	(0.18,0.98) ***
p90 (m)	0.089 ***	0.122 ***	0.132 ***	0.518	0.663 (+28.0%)	0.827 (+59.7%)	(-0.01,1) ***	(0.08,0.99) ***	(0.2,0.98) ***
rumple#	-2.269 ***	-0.206	5.394 ***	4.757	5.143 (+8.1%)	7.102 (+49.3%)	(3.94,0.93) ***	(5.13,0.8) ***	(5.86,0.54) ***
gap-fraction#	0.029 ***	0.050 ***	0.079 ***	0.038	0.051 (+34.2%)	0.079 (+107.9%)	(-0.01,0.94) ***	(-0.02,0.89) ***	(-0.03,0.82) ***

Table 2: Tabulation of the paired t-tests, standard deviation of differences (with the increase relative to cl1-cl2 in % in parenthesis) and joint hypothesis tests for the intercept = 0 and slope = 1 scenario; cl1, cl2, cl3, cl4 are short for classes 1, 2, 3 and 4 respectively.

*(#= unit less, *** = <0.001, ** = <0.01, *=<0.05, . = <0.1, ' '= >0.1)*

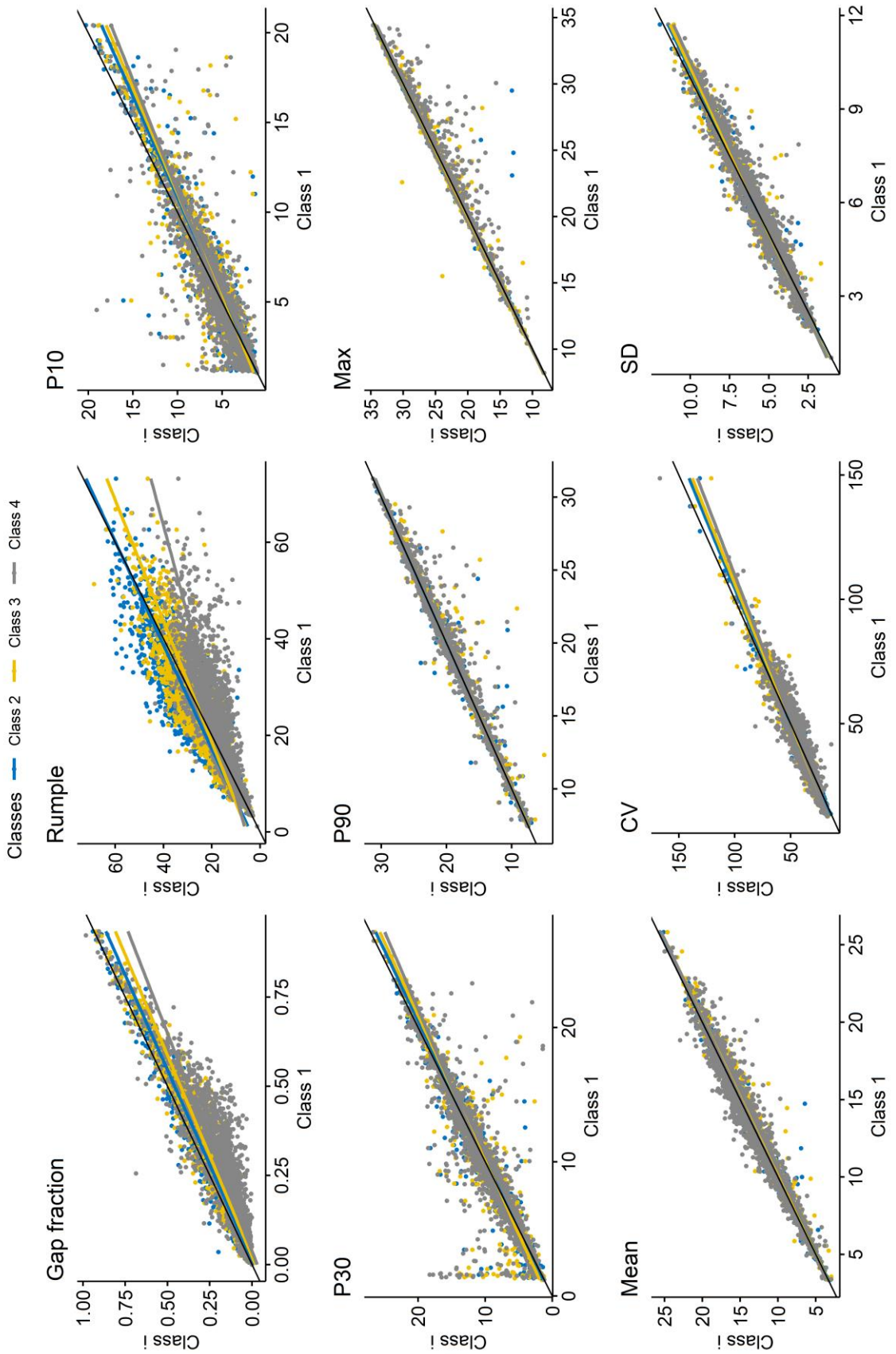

Figure 4: Scatter plots for selected metrics that depict the evolution of the metric under the influence of scan angle.

2.5 Discussion

The mean differences revealed the variations in metrics for different classes, but it could not adequately convey some of the biases (sometimes means are equal but can hide the existence of biases). On the other hand, simple linear regression was able to add to this information in two aspects. Firstly, as a visual diagnostic, it presented linear relationships between the classes for all the metrics. It also showed an increasing spread of the data as class 1 was compared with classes 2, 3, and 4. This spread is responsible for the increase in the standard deviations of the differences as shown in Table 2. The rate of increase of the standard deviations are very high for the metrics (except max and rumple when comparing class 1-class 2 to class 1-class 3), with a percentage increase ranging between +2% and +42% and +50% and +112% when comparing class 1-class 2 to class 1-class 3 and to class 1-class 4, respectively. Secondly, the different slope and intercepts revealed the inherent biases in the estimation of these metrics from different scan angles. Rumple index and gap fraction were considerably affected which is significant as studies (Bouvier et al., 2015; Véga et al., 2016) have reported that these metrics were useful to improve models to predict forest parameters. Liu et al. (2018) observed that the scan angle affected the gap fraction differently in different forests (and different structural conditions). However, they did conclude that the estimation is maximum for vertical observation, i.e. nadir, which was also observed in this study.

The height based metrics were affected to a lesser extent. The max metric showed the least variation. The higher percentiles appeared to be relatively stable compared to the lower percentiles. Montaghi (2013) reported that the higher percentiles, in particular, remained relatively stable compared to density metrics (not explored in this study). They also said that the Understory ratio, defined as “the ratio between all returns below a given height (e.g., 2 m) and the number of these returns plus returns classified as ground”, was also affected by the scan angle. The computation of the understory ratio is similar to the calculation of the gap fraction in this study.

The variation in the estimation of metrics could potentially impact the quality of ABA models that utilise these metrics. Practical limitations in flight planning cause the grid-cells in an area to be sampled with different “viewing conditions”. When several classes of angles are used together, changes in the metrics

will also be due to differences in scan-angle and not only in stand characteristics. This effect could perhaps be systematically addressed by taking into account classes of scan angle when building models. For example, building one model for one class of scan angles which would necessitate

more field plot measurements; or using regression analysis to model the effect of scan angle, with the possibility to partially correct for these effects before developing the model.

The limitations of the study are related to the generalisation of scan angles with mean scan angles in a range of 10° to one class value. Within-class variations could not be addressed systematically. Moreover, even the mean scan angle for a flight line is a generalisation of range of scan angles. It is not possible to overcome these acquisition limitations. Furthermore, the characteristics of the stands could also have a significant role to play. This was however not addressed in the present study. It is pertinent that the intermingling of the effects of stand characteristics and scan angle be decoupled for a systematic appraisal. Radiative transfer based simulation of forest point clouds could open up potential avenues to address these issues.

2.6 Conclusions

In this study, we analysed metrics that are frequently used in ABA methods to understand their response to varying scan angles. Metrics were computed in the form of a grid for each class of 'viewing configuration,' i.e. scan angle. There was a noticeable impact on the metrics with gap fraction, rumple index, and CV of height being affected significantly. Higher height percentiles were affected to a lesser extent than lower height percentiles and the maximum height metric was relatively stable. The key advantage of ABA methods is the ability to characterise within-stand variability. This has been a proven development over the conventional stand-level based inventory (Dubayah and Drake, 2000). However, practical data acquisition constraints may eventually lead to biases in metrics as demonstrated in this study. These biases can vary depending on the locations of the grid-cell and how they are sampled. The capacity to handle these biases could significantly contribute in improving the accuracy of the ABA models.

2.7 Acknowledgement

This research was supported by CNES, the French Space Agency, within the framework of the FRISBEE TOSCA project (convention n° 190337/00) and by the GRAINE program of ADEME (Agence de l'Environnement et de la Maîtrise de l'Énergie) (PROTEST project, convention n° 1703C0069). We also wish to acknowledge the financial support of Région Occitanie for the co-funding of K. Dayal's PhD grant (subvention n° 2018001466/ALDOCT-000520).

Chapter 3: **An investigation into lidar scan angle impacts on stand attribute predictions in different forest environments**

Karun R. Dayal[a], Sylvie Durrieu[a], Kamel Lahssini[a], Samuel Alleaume[a], Marc Bouvier[b], Jean-Matthieu Monnet[c], Jean-Pierre Renaud[d], Frédéric Revers[e]

[a] UMR TETIS, INRAE, Montpellier

[b] IRD, Montpellier

[c] LESSEM, INRAE, Université Grenoble Alpes,

[d] Office National des Forêts, Nancy, France

[e] INRAE, UMR 1202 BIOGECO, Université de Bordeaux, Cestas, France

Abstract: As studies have underlined the sensitivity of lidar metrics to scan angles, the objective of this study was twofold. Firstly, we further investigated the influence of lidar scan angle on the ABA predictions of stand attributes of riparian (29 field plots), broadleaf (42 field plots), coniferous (31 field plots) and mixed (45 field plots) forest types in France. Secondly, we evaluated the potential of voxelisation approaches to normalise scan angle effects in lidar metrics and mitigate scan angle effects in ABA models. To achieve these objectives, we first selected a model based on four lidar metrics with different sensitivities to lidar scan angle, i.e. mean and variance of canopy height values, gap-fraction, and coefficient of variation of plant area density (PAD) profile. For each plot, we considered the point cloud scanned from one flight line independently and characterised each resulting point cloud by the mean scan angle (*MSA*) and classified them into one of three classes: *A* (0° <=*MSA* < 10°), *B* (10°<=*MSA* < 20°) or *C* (20°<=*MSA* < 30°). An experimental setup involving nine scenarios was conceived to study the impact of the number of flight lines (scenarios *fl1, fl2* and *fl3*) and predominant scan angle (scenarios *A, B* or *C*) or combination of scan angle directions (scenarios *A* and *B*, or *A* and *C*, or *B* and *C*), on area-based approach (ABA) models. We built ABA models for the same forest plots for 5000 resampled datasets in each scenario to predict three forest attributes, i.e., stem and total volume (V_{st} and V_{tot}) and basal area (*BA*). Three goodness-of-fit criteria were computed for each model (coefficient of determination (R^2), relative root mean square error (rRMSE) and mean percentage error (MPE). We compared the distributions of the goodness-of-fit criteria between scenarios to assess the behaviour of the predictive models when: 1) the number of flight lines (i.e., scan angles) increases (*fl1, fl2 or fl3*); 2) lidar datasets comprise specific scan angle (*A, B or C*) or combination of scan angles (*AB, AC or BC*); 3) voxelisation is used to compute P_f and CV_{PAD}. The results show that models built with point clouds scanned from multiple flight lines were more robust, with a lower standard deviation of their goodness-of-fit criteria. On average, across all forest types, compared to *fl1*, the standard deviations of R^2 distributions were lower for *fl2* and *fl3* by 42 % and 77 %, respectively. We also observed that a dataset with a predominantly nadir configuration (i.e., scenario *A)* did not always result in better predictions (mean R^2 higher by 0.08, 0.07, 0.04 for scenario *B* for broadleaf, coniferous and mixed, respectively). For a set of calibration plots, the resulting forest attribute models depend on the acquisition geometry over the plots, as observed in this study, which could result in unreliable wall-to-wall predictions. The risk is particularly high in acquisitions with low overlapping rates, with many areas covered by only one flight line. Using voxel-based P_f and CV_{PAD} together with the mean and variance of heights helped to mitigate the impacts of changes in scan angles by a) increasing the means of the distributions, thereby improving the accuracy of predictions, or b) reducing the standard deviations, thereby increasing prediction precision, or c) both of the above.

Keywords: lidar, scan angle, forest structure, voxelisation, vegetation profile, leaf area index, forest inventory, ABA models

3.1 Introduction

Lidar scanning was initially developed for topographical surveys by taking advantage of its ability to penetrate the forest canopy (Krabill et al., 1984). However, lidar can also probe forest canopies with high accuracy, thus making it suitable for deriving forest attributes for large areas (Nelson, 2013). Over the years, the data collected by lidar in forest environments, which generally take the form of 3D point clouds with signal-related attributes, have been used to directly and accurately measure forest attributes such as the treetop height, canopy height, and also model forest attributes such as above-ground biomass (AGB), basal area (BA), wood volume (stem and total volume), canopy volume and vegetation profiles (Bouvier et al., 2015; Drake et al., 2003; He et al., 2013; Ioki et al., 2014; Kankare et al., 2013; Næsset, 2002, 1997a; Tompalski et al., 2019; Vincent et al., 2017). These attributes are essential from resource management and biodiversity perspectives.

Forest attributes are commonly estimated via area-based approaches(ABA), which involve establishing statistical relationships between forest attributes, computed from manual measurements of trees in sample plots and a set of lidar metrics for the same areas (Næsset, 1997a, 1997b; White et al., 2016; Wulder et al., 2012). Plot-level classical lidar metrics are computed by measuring the vertical distribution of the 3D points in terms of the mean, variance, percentiles and many other standard statistical descriptors of distribution (White et al., 2017). Voxelisation is an alternative method to summarise the point clouds while retaining more detailed structural information. It can be used to characterise the 3D distribution of leaf or plant area density within a 3D grid of localised regular volumes, i.e., the voxels (Grau et al., 2017; Popescu and Zhao, 2008; Soma et al., 2018). Studies have also tried to derive new plot-level metrics by summarising the information in profiles and voxels (Bouvier et al., 2015; Carrasco et al., 2019; Fischer et al., 2019; Zhang et al., 2017). The possibilities are endless, and there is a continuous effort to identify robust metrics that could contribute to accurate predictions of forest attributes. However, the use of classical lidar metrics and new metrics should take into consideration the potential variations that arise due to lidar data acquisition factors.

There are differences in the point clouds inherent to data acquisition processes, which need further investigation to comprehend their influences better when assessing tree or stand characteristics. The lidar pulse density, for example, can vary from under one pulse per m2 in airborne data to several pulses per m2 in unmanned aerial vehicle (UAV) data. Some studies have investigated the influence of pulse density and found that the prediction accuracies in ABA approaches relying on classical lidar metrics were largely unaffected until pulse densities were as low as one pulse per m2 (Bouvier et al., 2019; Jakubowski et al., 2013; Magnussen et al., 2010; Silva et al., 2017). On the other hand, studies using voxel-based approaches to estimate gap-fraction studies have demonstrated the potential biases that can arise due to poorly sampled voxels (Pimont et al., 2018; Soma et al., 2018).

Lidar scan angle is another parameter that can significantly affect lidar metrics and the prediction of forest attributes (J. Liu et al., 2018; Montaghi, 2013; Tompalski et al., 2019). A scan angle of 15–20 degrees is the often-recommended upper threshold in airborne lidar acquisitions for forestry applications (Wulder et al., 2012). Some early studies, such as Rempel and Parker (1964), observed that tree heights could be measured with sufficient accuracy if the signal reached some part of the ground. The chance of detecting ground surface is higher for vertically incident beams. Consequently, a convention of sorts has been followed over the years with regard to inclined lidar scanning. It is still followed in current recommendations (see, for example, Mitchell et al., 2018). However, systems have evolved considerably with an increased capacity to detect multiple echoes, including echoes of lower intensity (Li et al., 2020). Conversely, it is also believed that with higher scan angles, lidar pulses cover a larger area, thus increasing their chance of encountering gaps within the canopy and penetrating deeper into dense forest canopies (Kamoske et al., 2019).

A narrow scan angle range limits the swath width, and increasing the scan angle range could help optimise costs. Some studies have experimented with scan angles greater than 20° (Bolton et al., 2020; Cartus et al., 2012; J. Liu et al., 2018; van Lier et al., 2021). Therefore, it is of practical interest to explore the extent to which scan angle can be increased with negligible effects on lidar-derived forest metrics and forest attributes and make the most out of the diversity of existing and future data sets.

Several studies have analysed the influence of lidar scan angle on lidar metrics (Chen et al., 2014; Dayal et al., 2020; Disney et al., 2010; J. Liu et al., 2018; Montaghi, 2013; Soudarissanane et al., 2009). Differing forest types, sensors, and the metrics studied have certainly influenced the findings in different studies. However, there were also points of convergence among these studies, such as the fact that some metrics were not significantly affected by scan angle (e.g., maximum of height values) and some others, which depend on the returns from lower parts of the forests (understory ratio metrics), were indeed influenced by scan angle.

Regarding implications for forest attribute prediction, in a study by Næsset (1997), scan angles of up to 20° were found not significantly to impact the prediction of mean heights. Recently, van Lier et al. (2021) examined the impact of scan angle on predictive models, and their data was acquired with scan angles up to 30°. Their study indicated that attribute predictions were indeed affected by the use of lidar metrics impacted by scan angle, but not very significantly. Moreover, Lorey's mean height predictions were stable up to 30°. Interestingly, they also found that predictions of forest attributes (Lorey's mean height, gross merchantable volume and total volume) were more accurate when lidar data comprised scans from a single flight line instead of a combination of flight lines. However, the difference was marginal (difference in mean absolute percentage error < 1.3 %)

To our knowledge, the strategies to manage the likely influence of lidar scan angle on metrics and ABA predictions have been little explored. Roussel et al. (2018) proposed a correction for the biases caused by scan angle based on the hypothesis that an increase in lidar pulse inclination increases the chances of it being intercepted due to the increased distance covered. It is crucial to underline the need for further study on the influence of scan angle due to virtually countless lidar metrics, different modelling methods, various scanner properties, flight planning considerations, different forest types and varying terrain properties, which would enable the development of robust lidar-based models.

In this context, the main objective of this study was twofold. First, to assess the influence of the inclusion of lidar metrics sensitive to scan angle on ABA models for different kinds of complex forests, i.e., riparian forests and mountainous forests with coniferous, broadleaf and mixed stands. Second, to propose means to manage the impact of unavoidable and continuous changes in scanning conditions of forest environments that characterise lidar acquisitions. The study is a natural follow-up to our previous study investigating the effect of lidar scan angle on lidar metrics (Dayal et al., 2020). We worked with two hypotheses. Firstly, we assumed that the established impact of scan angle on metrics would eventually affect both the quality and the robustness of predictive models. Secondly, we assumed that using plant area density (PAD) profiles, rather than point clouds, would allow us to normalise lidar information for impact of changes in scan angles, and would make both metrics and models more robust to changes in scan angles. We firstly demonstrated the effects of using metrics sensitive to lidar scan angle in ABA models. We chose four metrics with a proven capacity to predict forest attributes, each with different sensitivities to scan angle. Secondly, we conceived an experimental setup wherein standard lidar datasets were resampled to create multiple datasets made up of lidar observations corresponding to different scanning scenarios to build ABA models. The resampling was done at the level of the flight lines by randomly picking flight lines to make different combinations. The experimental setup comprises lidar scanning scenarios with different inclinations (scan angle), with (multiple flight lines), and without (single flight line) overlap. Finally, we used voxel-based metrics to demonstrate their potential to normalise the effects of scan angle and improve predictions. We proposed these new metrics based on the underlying hypothesis that voxel-based tracking of the extinction of a laser pulse can improve the accuracy of forest variables such as LAD/PAD (used in this study) (Vincent et al., 2017).

3.2 Materials and methods

3.2.1 Study sites and field plot measurements

We used two sites representative of complex forest environments for this study. The first study site in southwest France is a riparian zone along the river Ciron, a tributary of the Garonne, and three of its sub-tributaries. It is rich in biodiversity and not subject to intense forest management. Field data

were collected at 29 locations along the river Ciron and its tributaries. These sites were chosen to represent a gradient in width and density of the riparian forest. The species present on this site include the common oak (*Quercus robur*), Pyrenean oak (*Quercus Pyrenaica*), common alder (*Alnus glutinosa*), and maritime pine (*Pinus pinaster*). Several locations are also characterised by shrub species such as common hawthorn (*Crataegus monogyna*) and alder buckthorn (*Frangula alnus*). At each of the 29 sites, plots of radius 15 m were established, and differential GNSS (DGNSS, Trimble, USA) was used to measure the plot centre coordinates. For all the trees with a diameter at breast height (DBH) above 7.5 cm, trunk circumferences at breast height were measured with a tape and tree heights were measured using a hypsometer Vertex (Haglöf, Sweden). All the measurements were carried out between June and August 2019. The basal area (BA) computations were made from the circumference measurements, and the stem volume (V_{st}) and total volume (V_{tot}) were estimated using robust allometric equations developed for French metropolitan species (Deleuze et al., 2013).

The second study site is located in the French department of Haute-Savoie in eastern France, in the French Alps. It is a part of the Massif des Bauges Natural Regional Park, covering an area of approximately 373.5 km2. The terrain is hilly (plot altitudes range from 420 m to 1760 m). The most common tree species comprise silver fir (*Abies alba*), Norway spruce (*Picea abies*) and common beech (*Fagus sylvatica*). Field inventory was carried out for 118 15 m radius plots during spring and fall 2018. Plot centre locations were measured using differential GNSS (DGNSS, Trimble, USA). Field inventory protocol involved measuring tree DBH of trees with DBH greater than 17.5 cm. Small trees (7.5 cm $\leq$ DBH < 17.5 cm) were counted within a plot radius of 10 m and classified as either coniferous or broadleaf.

Since DBH and height measurements were unavailable for all the trees with DBH greater than 7.5 cm, computation of basal area, stem and total volumes at plot level required estimations for the unmeasured trees. Firstly, the number of small trees was extrapolated from 10 m radius plots. Secondly, the nationwide tree inventory database (NFI) generated by IGN (Institut National de l'Information Géographique et Forestière), containing measurements of trees with DBHs in the 7.5 cm to 17.5 cm range, was used to extrapolate DBH and height values for non-measured trees. All NFI plots located in the ecoregion that includes the study site were selected to have forest plots with similar climatic and growing conditions to those measured on the study site. For trees with DBH ranging from 7.5 cm to 17.5 cm, the median DBH value in the NFI database is around 11.1 cm. This value was used to compute the basal area of the trees with DBHs lower than 17.5 cm. Using NFI measurements, allometric relationships were established for each species (or group of species when the number of trees was not high enough) to estimate the heights of all the trees when there were no available height measurements. Volumes were then computed using the allometric equations available in Deleuze et al. (2013). Plots were classified into three main forest types, i.e., broadleaf, coniferous and mixed. Plots with the BA of coniferous trees greater than 75 % and lower than or

equal to 25 % of the total BA were labelled as coniferous (31 plots) and broadleaf (42 plots), respectively. The 45 remaining plots were labelled as mixed stands.

Table 1 summarises the main characteristics of the forest types under study, i.e., riparian stands and coniferous, broadleaf and mixed mountainous stands. The distribution of the plots at both study sites is shown in Figure1.

	Ciron			Bauges								
	Riparian (29 plots)			Coniferous (31 plots)			Broadleaf (42 plots)			Mixed (45 plots)		
	Min	Mean	Max	Min	Mean	Max	Min	Mean	Max	Min	Mean	Max
Slope (degrees)	4.9	8.9	21.0	12.9	28.7	40.6	11.4	29.8	45.1	8.5	24.8	40.2
Basal area (m^2/ha)	17.2	28.5	47.6	10.7	36.8	89.7	3.4	28.0	57.0	4.5	29.7	63.3
Stem volume (m3/ha)	118.7	272.7	475.5	101.2	401.6	1148.2	23.8	269.9	617.2	40.6	298.2	759.5
Total volume (m3/ha)	135.9	296.2	552.9	102.4	410.3	1171.9	25.2	294.8	683.9	42.3	311.7	788.4

Table 1: Summary of average slope and field plot measurements for Basal area, Stem volume and Total volume for all the forest types

3.2.2 Lidar data acquisition and processing

At the Ciron study area, INFOGEO (France) acquired lidar data using a VQ580 laser scanner (Riegl, Austria) on an ultralight aircraft platform in early October 2019. The flying height was approximately 250 m, which enabled data acquisition at an overall point density of around 68 pts/m2. Overlap of 35 % - 40 % and several passes over any given area ensured that most of the area was sampled using multiple scanning configurations. Data pre-processing was carried out by INFOGEO, which involved the classification of ground points using TerraScan (Terrasolid ltd., Finland).

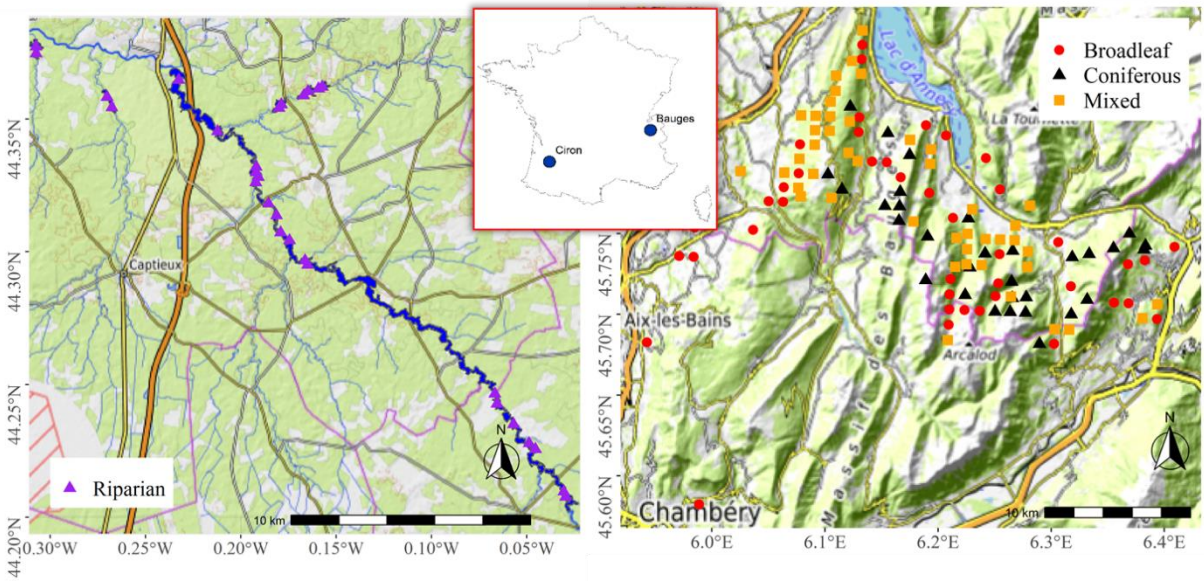

Figure 1: Location of study sites and distribution of plots. In the left image, the riparian plots (purple) are distributed in the riparian region (blue) along the river Ciron and its tributaries. In the right image, the broadleaf (red), coniferous (black) and mixed (orange) plots are distributed across the northern part of Massif des Bauges Natural Regional Park .

For the Bauges site, the company Opsia (France) carried out airborne lidar data acquisition and processing in September 2018. The flying height was around 1050 m with several passes of flight lines to ensure most of the area was scanned using multiple scanning configurations. Due to a higher flying altitude, the point density of this dataset was lower at approximately 13 pts/m2. Trajectory information, essential for voxelisation (used in this study), was also known for both sites. Additional specifications are given in Table 2.

	Ciron	Bauges
Date of acquisition	October 2019	September 2018
Sensor	Riegl VQ580	Riegl LMSQ780
Wavelength (nm)	1064	1064
Scan angle (deg)	60° (+30°/-30°)	60° (+30°/-30°)
Beam divergence (mrad)	0.2	<=0.25
Ground speed (m/s)	25	45
Point density (pts/m²)	68	13
Flight height (AGL) (m)	250	1050

Table 2: Technical specifications for the lidar sensor and data that were acquired for the two sites

3.2.3 Data processing and experimental setup

3.2.3.1 Splitting of point clouds based on flight lines

Point clouds corresponding to the field plots were clipped from the lidar data using coordinates of the plot centres and plot diameters (30 m). Due to flight line overlaps, the point cloud for a given plot is typically a composite of point clouds acquired with different scanning configurations. We split the point clouds for each plot based on the constituent flight lines. Each resulting constituent point cloud was represented by the mean of the scan angles (*MSA*) with which it was scanned. We categorised these point clouds within three classes based on their absolute *MSA* values: class *A* (0° ≤

MSA < 10°), class *B* (10°≤ *MSA* < 20°), class *C* (20° ≤ *MSA* < 30°). We did not consider those point clouds acquired with *MSA* greater than 30° as they were most likely acquired when the aircraft made turns, and there were few such instances. The fundamental 'unit' in our experiments is the point cloud for a plot acquired from only one flight line. We assessed pulse densities for each of the point clouds. For the Bauges dataset, 99 % of the constituent point clouds had a pulse density greater than 1 pulse per m², and for the Ciron dataset, all the point clouds had a pulse density greater than 14 pulse m². These values were higher than the thresholds below which pulse densities are known to influence lidar metrics and forest attribute predictions. (Bouvier et al., 2019, Jakubowski et al., 2013, Magnussen et al., 2010, Pearse et al., 2019).

3.2.3.2 Partially sampled point clouds per plot

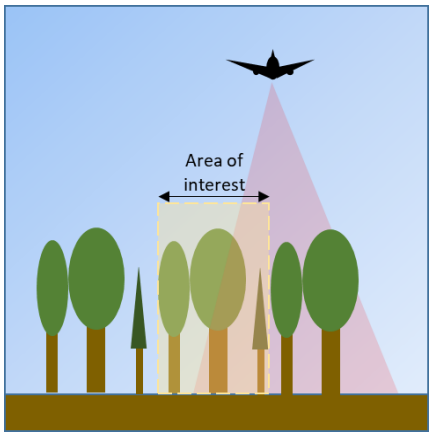

Figure 2: Flight lines that partially cover a plot .

We computed the area covered by each constituent point cloud by fitting a two-dimensional hull to the points projected onto a horizontal plane. Then, an area threshold was used to drop any point cloud that covered<90 % of the total plot area (Figure 2), resulting in a final dataset set of 93, 110, 144 and 149 point clouds for riparian (29 plots), coniferous (31 plots), broadleaf (42 plots) and mixed plots (45 plots), respectively. Figure 3 shows the number of flight lines per plot and class for different forest types.

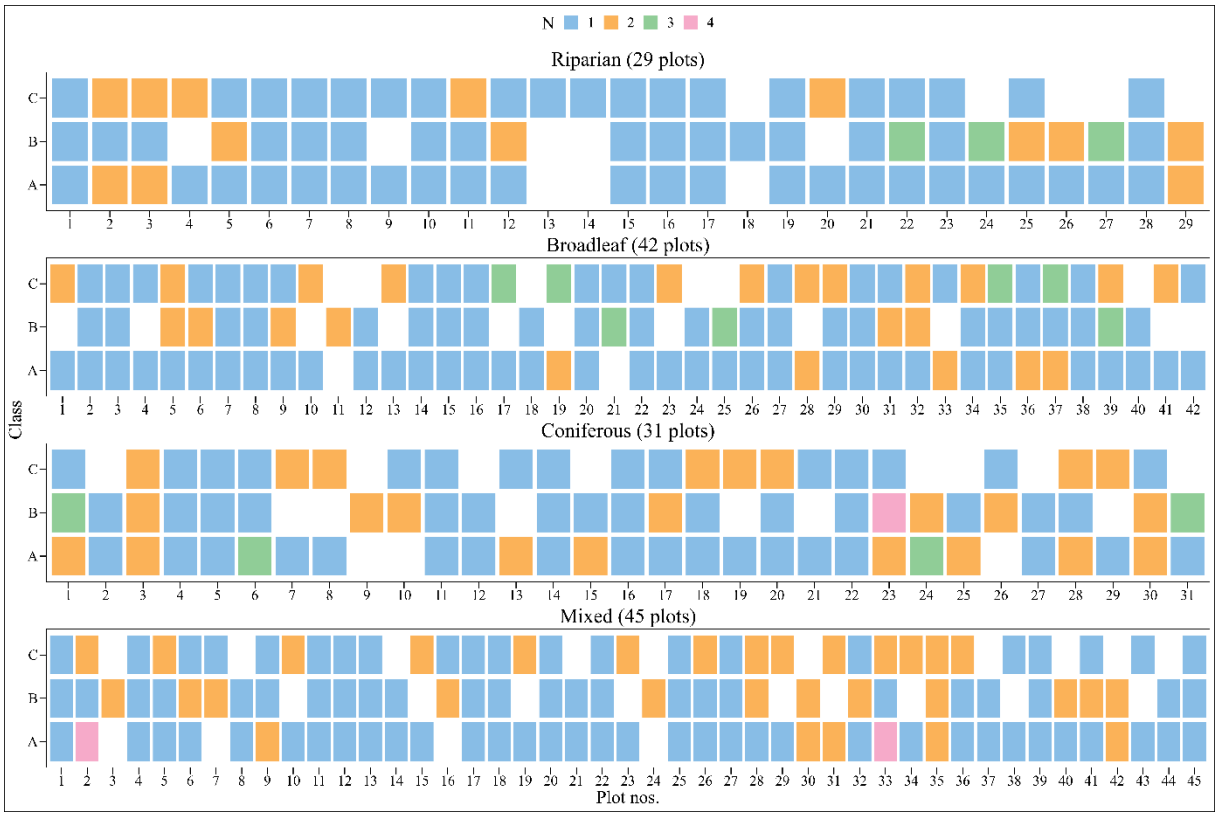

Figure 3: Heatmap depicting the number of flight lines (N) belonging to each MSA class (A, B, C) in a plot in different forest types. Each sub-division along the horizontal axis represents a plot. The blank tiles (white) are cases where no flight lines belong to that particular class for the given plot

The 'expansion' of the dataset made it possible to pick any one or a combination of point clouds per plot. In other words, it was possible to recreate datasets with different scanning configurations. With multiple possibilities for each plot, there were thousands of unique combinations in which the point clouds could be picked under different experimental scenarios (explained in the following sections). We use the two terms 'point cloud' and 'flight line' interchangeably, and they essentially refer to the same data.

3.2.3.3 Description of experiments

From the available flight lines per plot, we simulated different scenarios for scan-angle configurations based on (1) the number of flight lines, (2) homogeneity in scanning configurations and (3) with conventional point-cloud subsets, i.e., merging all flight lines. The three main kinds of scenarios are described in detail.

3.2.3.3.1 General scenarios based on the number of flight lines per plot

These scenarios were divided into three categories *fl1*, *fl2* and *fl3* (Figure 4). In the first scenario, *fl1*, we picked any one flight line and its corresponding point cloud per plot. This scenario represents the

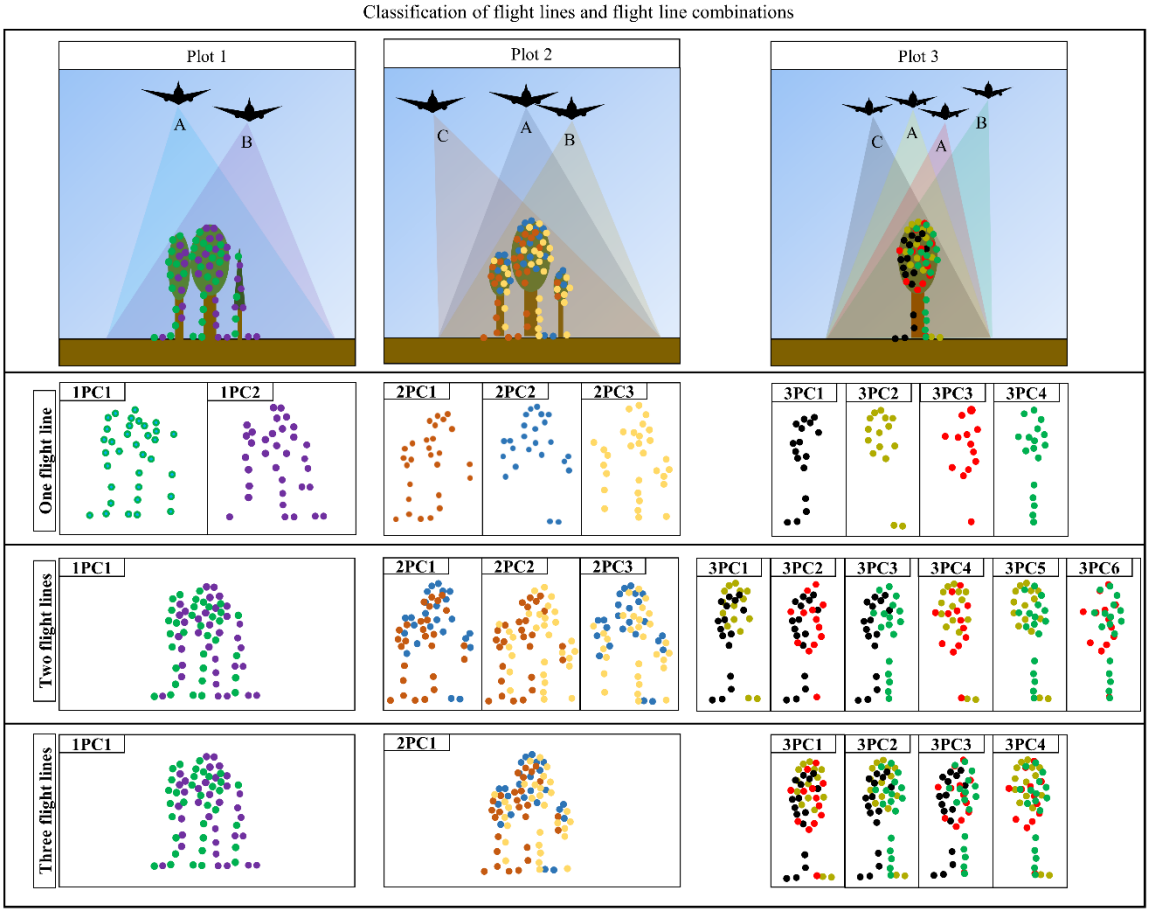

Figure 4 : Splitting of the point clouds based on the flight lines to obtain point clouds from single flight lines. The resulting datasets for three general scenarios (fl1, fl2 and fl3) are illustrated.

worst-case scenario or the most basic scenario wherein each plot was scanned only once. This scenario corresponds to an acquisition with no overlap between flight lines. In the second scenario, *fl2*, we picked any two flight lines per plot and merged the respective point clouds to build a composite point cloud. In the third scenario, *fl3*, we picked any three flight lines per plot to build the corresponding composite point cloud. In the second and third scenarios (*fl2 and fl3*), we automatically considered all the available flight lines for the plots that were scanned based on either less than or equal to two or three flight lines, respectively (Figure 4).

When a plot was scanned from three different flight lines, there were $C_3^1 = 3$ possibilities of picking any one flight line, $C_3^2 = 3$ possibilities of picking two flight lines and $C_3^3 = 1$ possibility of picking three flight lines each time (Figure 5). For each forest type, the total number of all possible combinations in each scenario is given by $\prod \mathrm{n_i}$, where n_i is the total number of flight lines (for *fl1*) or combinations of flight lines (for *fl2* and *fl3*) in plot i. Each combination represents a unique way in which all the plots were collectively scanned.

3.2.3.3.2 Weighting for unequal distribution of flight lines

Due to uneven distribution of flight lines across the classes for any given plot (Figure 3), randomly sampling a flight line (or flight line combination) could result in over-representation of some classes (or class combination). Over several iterations, unequal probabilities may lead to sample induced biases and, therefore, some of the information may be incorrectly utilised (Nahorniak et al., 2015). We computed the probability of picking a class (or class combination) as a consequence of randomly picking a flight line (or flight line combination) for a plot. The probabilities were assigned to the corresponding flight line (or flight line combination) and inverse probability weights (wt_i) were computed using the following equation:

$$\mathrm{wt_i} = \frac{\frac{1}{p_\mathrm{i}}}{\frac{1}{\sum_1^n p_i}} \quad (1)$$

where p_i is the assigned probability of a flight line (or flight line combination) i, n is the number of flight lines (or flight line combinations) available for the plot. The weights were scaled between 0-1. The weighting ensured that the flight lines (or flight line combinations) were picked in such a way that over several iterations, all the available classes (or class combinations) for the plot are picked almost equally. Scenario *fl1* and the corresponding weighting step is illustrated in Figure 5 left in the panel 'weights'.

3.2.3.3.3 Special cases within general scenarios based on homogeneity in scanning configurations

These scenarios were divided into six categories *A, B, C, AB, AC* and *BC*. In scenarios *A, B* and *C*, we picked any one flight line per plot, as in scenario *fl1*, but with a constraint on the flight-line *MSA*. For example, we considered only flight lines with *MSA* belonging to class *A* in scenario *A* (0° <=*MSA*< 10°). Similarly, we considered only those flight lines with *MSAs* belonging to classes *B* and *C* for scenarios *B* and *C*, respectively. Scenarios *A, B* and *C* are special cases of scenario *fl1*. Scenario *A* is illustrated in the panel on the right labelled 'weights' in Figure 5.

Furthermore, for scenario *AB*, for example, we picked any two flight lines per plot such that one of them belonged to class *A* and the other to class *B*. Similar constraints were applied to scenarios *AC* and *BC*. Scenarios *AB, AC* and *BC* are special cases of scenario *fl2*. We did not consider other scenarios, such as *AA, BB*, etc., as such cases were not numerous.

In Figure 3, the distribution of flight lines across different classes and across all the plots is clearly not even. In addition, some plots do not have any flight lines belonging to one or more classes. For example, riparian plots 13 and 14 do not have any flight lines in classes *A* and *B*, and such plots cannot be a part of experiments for scenarios *A* and *B*. Therefore, we identified the common plots with at least one flight line in classes *A, B* and *C* each to make the results across different scenarios comparable. There were 19 plots (out of 29) with at least one flight line in each class among the

riparian plots. We picked the flight lines (or combinations of flight lines) for scenarios *A, B, C, AB, AC* and *BC* only in these plots. For those special cases within general scenarios based on homogeneity in scanning configurations, the weighting step was adapted accordingly. For the remaining plots, i.e., plots that were not a part of the common plots, weightings ensured that all available classes (or class combinations) were picked roughly equally. The same process was followed for the other three forest types.

All the possible experimental scenarios can be listed as *fl1, A, B, C, fl2, AB, AC, BC,* and *fl3*. Based on the sampling framework described above, we were able to create 5000 unique lidar datasets for each scenario.

3.2.3.3.4 Scenario with conventional point cloud subsets

We also built models in the conventional way, which is the standard procedure followed when building models with ABA approaches. The point clouds from different flight lines were considered together and metrics were computed for the composite point clouds.

The detailed workflow followed in this study is illustrated in Figure 5 for scenarios *fl1, A, B,* and *C.* Figure 4 illustrates how flight lines in each plot were combined in *fl2, AB, AC, BC,* and *fl3*. The remainder of the process was identical.

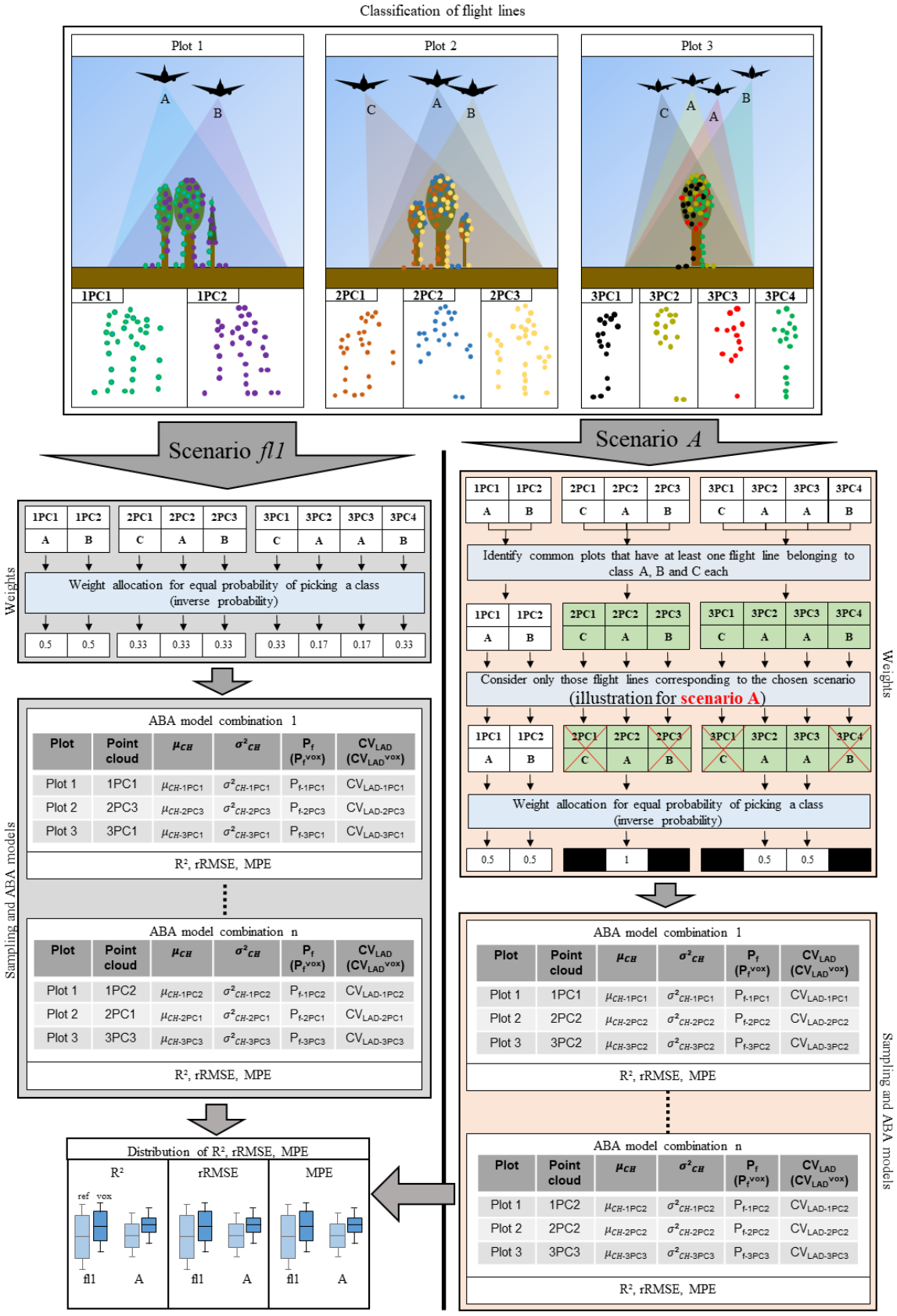

Figure 5: Illustration of the experimental setup for scenarios fl1, A, B and C. n=5000 for all experiments. The illustration is for an example set of three plots each scanned with different number of flight lines. In the left panel, scenario fl1 is illustrated and in the right panel, scenario A is illustrated.

3.2.4 Lidar metrics and regression models

3.2.4.1 Selection of metrics

While lidar-derived metrics can be sensitive to lidar scan-angle, they are not all sensitive to the same degree (Dayal et al., 2020; Holmgren et al., 2003; Montaghi, 2013). In our preceding study (Dayal et al., 2020), we observed that the mean of the lidar point heights was not sensitive to scan angle. Moreover, the lower percentiles appeared to be more sensitive than the higher percentiles. Gap-fraction, computed as the ratio of the number of first returns below a height threshold of 2 m to the total number of points, was also very sensitive to changes in scan angle. As a result, the computation of metrics that depend on the sampling of the lower strata is affected. The scan angle could affect many of the metrics mentioned above (and several others not mentioned here).

We opted to restrict the analysis of the effect of scan angle on ABA models built with four metrics that proved relevant to predicting *Basal Area (BA)*, *Stem Volume (V_{st})* and *Total Volume (V_{tot})* in various forest types, as demonstrated in Bouvier et al. (2015). The ABA models proposed in this study were developed to generalise and simplify the model selection process, thus making it easier to compare models (Véga et al., 2016). The metrics used in the models were selected while considering the spatial heterogeneity in the forest structure. These metrics are a) average value of canopy height values, μ_{CH}, b) variance of canopy height values, σ^2_{CH}, c) gap-fraction P_f, and d) coefficient of variation of PAD profile, CV_{PAD}. These metrics are generally stable even at low pulse densities (Bouvier et al., 2019). For the Bauges site, we computed these metrics at the level of the plots for the Bauges site for classes *A*, *B* and *C*. We compared the metrics for classes *B* and *C* to metrics for class A (considering class A as reference as in Dayal et al., 2020) and found that class *B* and class *C* P_f metrics and only the class *C* σ^2_{CH} metrics were most sensitive to scan angle. μ_{CH} and CV_{LAD} were relatively stable. These results are in Appendix A

3.2.4.2 Computation of lidar metrics

During the field measurements along the river Ciron, we observed that the bushes, considered a part of the lower vegetation, grew to a height of approximately 5 metres. Therefore, the threshold for computation of the metrics was set at 5 metres and applied to all study areas. μ_{CH} and σ^2_{CH}, were computed after normalising point elevations by removing the influence of terrain on above ground measurements using a digital terrain model (DTM). P_f and CV_{PAD}, were computed in two ways, i.e., by traditional computation and voxel-based computation.

3.2.4.2.1 Traditional computation

The ground returns show that corresponding laser pulses were not fully intercepted in their round trip path through the canopy, which represent gaps in the canopy (Hopkinson and Chasmer, 2009). In the ratio method of computation of gap-fraction, P_f, when computed as a fraction of the total first returns,

may be considered equivalent to the transmittance. The transmittance is related to the LAI as per the Beer-Lambert law (Nilson, 1971)as shown below:

$$P_f(\theta) = e^{\frac{-G(\theta,\alpha)LAI}{cos\theta}} \quad 2)$$

$P_f(\theta)$ is the gap-fraction in direction θ; LAI is the leaf area index, and G(θ,α) is the ratio of foliage area projected in direction θ to the actual area. G(θ,α)/$cos\theta$ is generally assumed to be 0.5, considering the spherical leaf angle distribution. The canopy-return ratio assumes that the laser pulses are incident vertically. This assumption may be considered a reasonable generalisation for lidar data when the scan angle is not very high (Almeida et al., 2019; MacArthur and Horn, 1969), which is generally not the case for platforms flown at lower altitudes. PAD profiles were generated by applying the same principle to 1 m point-cloud layers and by computing the per layer P_f (Bouvier et al., 2015). It is implied that each layer is assumed to be homogeneous. This assumption tends to simplify the structural distribution of the vegetation. PAD is the plant area density, which includes leaves and other woody material, while LAD is the leaf area density, which does not consider the woody material. However, as originally done in earlier studies, we considered PAD profiles for the computation of P_f and CV_{PAD}.

3.2.4.2.2 Voxel-based computation

Metrics were also computed using voxel-based approaches to generate plant area density (PAD) profiles. These approaches are better at characterising uneven forest canopy due to improved space discretisation (gaps and non-gaps) (Pearse et al., 2019; Soma et al., 2021; Wang et al., 2020). When combined with path distribution methods, they provide refined estimates of PAD. It is thus expected that changes in scan angles will be better managed with voxel-based approaches, and that the PAD profile will be at least partly normalised from scanning conditions.

This study used the voxel-based 3D reconstruction method implemented in the software AMAPVox version 1.6.2 (Vincent et al., 2017). The software recreates the acquisition geometry using the trajectory information (position and orientation) as well as retracing each laser pulse path and its subsequent interaction with elements of the forest, i.e., point cloud. It then computes the local transmittance in each voxel which is then converted to the PAD using the Beer-Lambert law. For voxelisation, we used point clouds before height normalisation, i.e., with the Z coordinates being elevations instead of height above the ground, to avoid distortion of the geometry. The voxel size was set to 1 m. The DTM for each point cloud was resampled to 1 m to align it with the overlaying voxels, and the columns of voxels were normalised accordingly. We then computed the mean of the local PAD values per layer to obtain the PAD profiles and then summed up the profile values to calculate the plant area index (PAI) for the plot (Lovell et al., 2003). The PAI can be linked to the P_f based on the following equation:

$$P_f = e^{-kPAI} \quad (3)$$

where k is 0.5 for spherical leaf angle distribution. P_f is computed in this way as P_f^{vox}. The CV_{LAD}^{vox} was computed as the coefficient of variation of the profile. The comparison of vegetation profiles for all the plots can be found in Appendix C.

To summarise, two sets of metrics were used. The first set is called *reference metrics*, which is comprised of μ_{CH} , σ_{CH}^2 , P_f and CV_{PAD} The second set is called *voxel metrics*, and it comprises μ_{CH} , σ_{CH}^2 , P_f^{vox} and CV_{PAD}^{vox}. Metrics were computed for each point cloud (fl_1) and composite point clouds (fl_2 or fl_3).

3.2.4.3 Regression models

We used a multiplicative power model (Bouvier et al., 2015; Gobakken and Næsset, 2005; Kangas et al., 2018) to estimate forest attributes. A log-log transformation was used to achieve linearity. The model is as follows:

$$log\ y = b_0 + \sum_{i=1}^{n} b_i \log x_i + \varepsilon \quad (4)$$

Where b_i are model coefficients, y is the forest attribute ($V_{st,}$ V_{tot} or BA) and x_i are the ith retained lidar metrics (n = 2 or 4)

This relationship is suitable for estimating forest attributes (Næsset, 2002, 1997).

3.2.4.4 Model validation and performance assessment

Leave-one-out cross-validation is most suitable for smaller datasets (Picard and Cook, 1984). Thus, it was employed in this study to analyse the predictive capabilities of the models. A model is built for all but one of the plots at a given instance. The model is used to predict a value for the disregarded plot. This process is repeated until predictions are made for each of the plots.

Log-transformation of variables introduces a systematic bias. The bias was corrected using a correction factor as per Sprugel (1983). The standard error of estimate (SEE) of regression was computed, as given by:

$$SEE = \sqrt{\sum \frac{(\log y_i - \log \hat{y}_i)^2}{(n-p)}} \quad (5)$$

y_i and $\hat{y}_i$ are the i$_{th}$ observed and predicted values, respectively, in log-scale, n is the number of observations, and p is the number of parameters in the model. The correction factor (CF) was computed using SEE as per:

$$CF = exp^{(\frac{SEE^2}{2})} \quad (6)$$

The observed and predicted values in the log scale were back-transformed to the arithmetic scale, and the back-transformed predicted values were multiplied by the correction factor. The goodness-of-fit of the models was assessed using the determination coefficient (R^2), the Root Mean Squared Error (RMSE), the relative Root Mean Squared Error (rRMSE) and the Mean Percentage Error (MPE). The formulae for these measures are as follows:

$$R^2 = 1 - \frac{\sum_1^n (y_i - \hat{y}_i)^2}{\sum_1^n (y_i - \bar{y})^2} \quad (7)$$

$$RMSE = \sqrt{\frac{\sum_1^n (\hat{y}_i - y_i)^2}{n}} \quad (8)$$

$$rRMSE = \frac{RMSE}{\bar{y}} * 100 \quad (9)$$

$$MPE = \frac{100}{n} \sum_1^n \frac{(y_i - \hat{y}_i)}{y_i} \quad (10)$$

3.2.5 Statistical analysis for comparison of scenarios

We expected each experimental scenario to result in a distribution of the goodness-of-fit criteria (R^2, rRMSE, MPE), as illustrated in Figure 5. Distribution spreads (or variances) indicate the prediction precision, and distribution means indicate accuracies across different experimental scenarios. To compare distributions of R^2, rRMSE, MPE of different scenarios, different statistical tests were used: a) Welch's ANOVA to compare the means, b) Games-Howell posthoc tests for pairwise comparisons (R package *rstatix* Kassambara, 2021), and c) pairwise F-tests with Bonferroni correction for multiple comparisons (Hervé, 2021) to compare the variances. Games-Howell posthoc test maintains the significance level for multiple comparisons and does not require any adjustments to the significance level (Lee and Lee, 2018).

To summarise, all the results and analyses were presented as follows:

Firstly, to demonstrate the effect of inclusion of metrics with different sensitivities to scan angle, we built ABA models with only, μ_{CH} and σ^2_{CH}, and compared the goodness-of-fit criteria to those of ABA models built with *reference metrics* (μ_{CH}, σ^2_{CH}, P_f and CV_{PAD}), to predict V_{st} for scenarios *fl1* and *fl2*. We computed the percentage changes in the means and standard deviations.

Secondly, we analysed the distributions of goodness-of-fit criteria for predictions of the three forest attributes using *reference metrics*, for all the experimental scenarios and all forest types. We compared the means and variances of the general *fl1*, *fl2* and *fl3* scenarios. Furthermore, we also compared the means and variances of homogenous scanning scenarios *A, B, C, AB, AC, BC* and *AC* in pairs. To quantify the inter-scenario variations, we computed the mean of the absolute pairwise

differences (or mean absolute differences, MAD) resulting from the posthoc tests. MAD measures the average magnitude of differences without considering the directions.

Thirdly, we analysed the distributions of goodness-of-fit criteria for the prediction of the three forest attributes with *reference metrics* (μ_{CH}, σ^2_{CH}, P_f and CV_{PAD}), in comparison to the distributions obtained with *voxel metrics* (μ_{CH}, σ^2_{CH}, P_f^{vox} and CV_{PAD}^{vox}). We reported the percentage changes in means and standard deviations when *voxel metrics* were used, per scenario. We also demonstrated the performance of *voxel metrics* when ABA models were built conventionally, i.e., all available flight lines per plot are considered together, in terms of the goodness-of-fit criteria.

3.3 Results

In what follows only results concerning stem volume (V_{st}) will be presented as the results for *BA* and V_{tot} exhibited similar trends. They are presented in the Appendix B.

3.3.1 Effect of inclusion of metrics sensitive to scan angle

For the riparian, broadleaf and mixed plots, the inclusion of P_f and CV_{LAD} improved the means of the R^2 by 6.3%, 10.3% and 9.1% for scenario *fl1* and by 7.4%, 7.7% and 8.6% for scenario *fl2*, respectively. For the coniferous plots, there were reductions in the mean R^2 values by 11% and 31% for *fl1* and *fl2*, respectively. The standard deviations of R^2 distributions increased by 222.7%, 292.8%, 159.4% and 33.4% for *fl1* and 158.8%, 171%, 217.2 and 119.2% for *fl2*, for riparian, broadleaf, coniferous and mixed plots. Similarly, the standard deviations of the error distributions (*rRMSE* and *MPE*) were higher for all the forest types (Table 3). The distributions are shown in Figure 6.

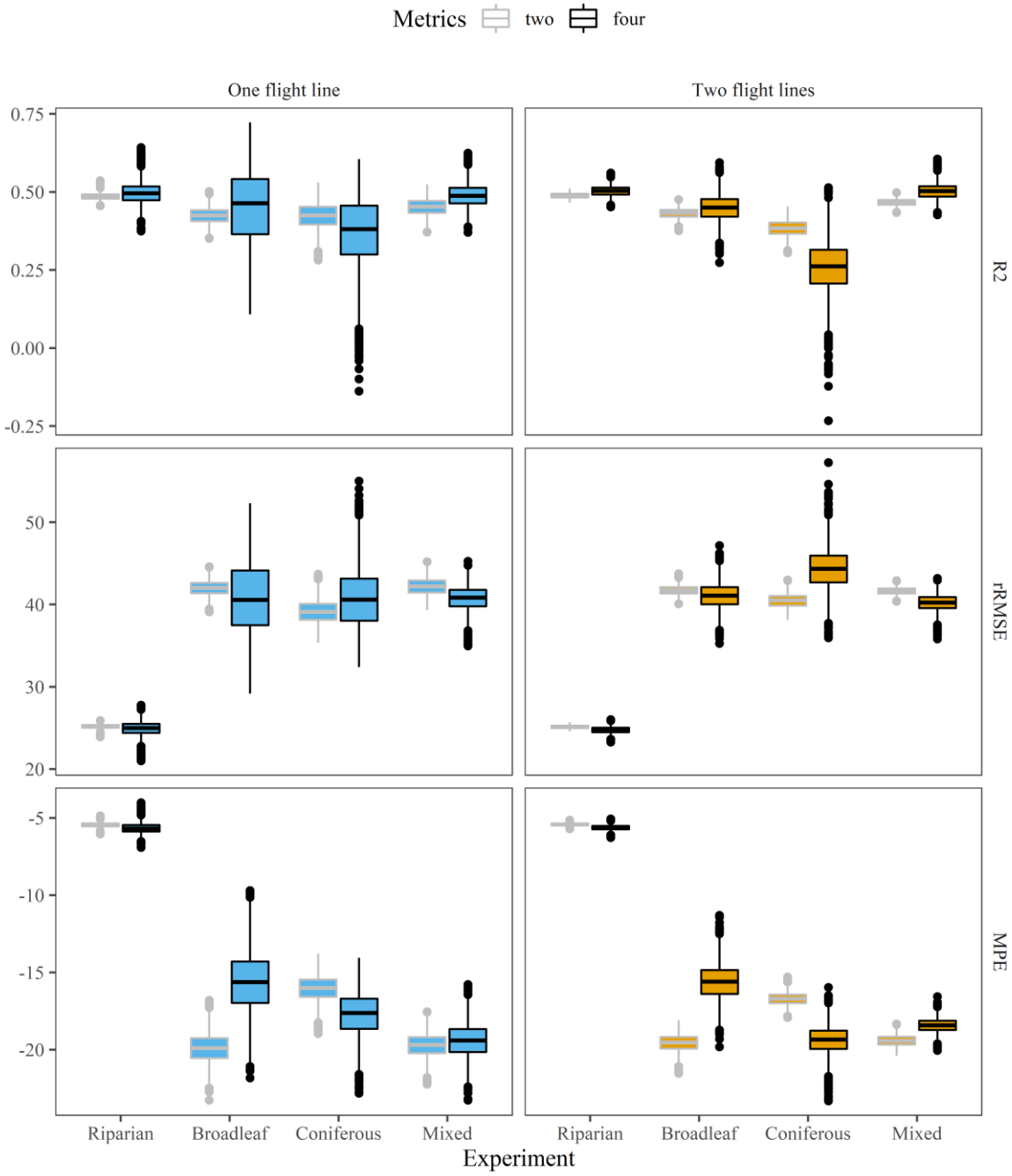

Figure 6: Distributions of the goodness-of-fit criteria for the models with (black) and without (grey) P_f *and* CV_{LAD}*; top panel:* R^2*; middle panel: rRMSE; bottom panel: MPE .*

		R2				rRMSE				MPE			
	Flight lines	Riparian	Broadleaf	Coniferous	M i x e d	Riparian	Broadleaf	Coniferous	M i x e d	Riparian	Broadleaf	Coniferous	M i x e d
% change Mean	One	6.3	10.3	-11.0	9.1	-3.7	-4.3	3.6	-3.7	-0.4	-23.0	10.0	-0.9
	Two	7.4	7.7	-30.9	8.6	-4.3	-3.1	8.9	-3.8	-1.0	-22.0	15.7	-4.3
% change in SD	One	222.7	292.8	159.4	33.9	237.5	307.3	147.1	39.9	96.2	98.1	74.6	41.7
	Two	158.8	171.0	217.2	119.2	170.2	180.2	190.2	128.3	71.4	110.3	126.0	26.5

Table 3: Percentage changes in the means and standard deviations of the distributions of the goodness-of-fit criteria for models with and without P_f *and* CV_{LAD}

3.3.2 Comparison of performance measures for different scenarios with randomly chosen scan angles (fl1, fl2, fl3) and of homogenous scanning scenarios

For the scenario-wise comparisons, we included the results for stem volume V_{st} for the four forest types (results for BA and V_{tot} can be found in Appendix B). The distributions of goodness-of-fit criteria for predicting V_{st} for each experimental scenario are shown in Figure 7. For scenarios fl1, fl2, fl3, percentage changes in the means and SD of the distributions are given in Table 4. For the riparian and mixed plots, the means of the R2 values show an upward trend with an increase in the number of flight lines per plot. For the broadleaf and coniferous plots, we observed an opposite trend for R2 distributions. For the coniferous plots, there was a considerable reduction (approximately 30 %) in the mean R2 values for scenarios fl2 and fl3 compared to scenario fl1. The reduction was marginal for broadleaf plots. The spreads, or standard deviations, for all the distributions for all forest types and all goodness-of-fit criteria successively reduced with an increase in the number of flight lines (i.e. fl2 and fl3 compared to fl1). The reductions ranged from 23 % to 85.9 %, and all pairwise F-test comparisons were statistically significant.

Among the homogenous scenarios, i.e., *A, B, C, AB, AC* or *BC*, the distribution means were mainly stable on the riparian plots except for scenario *C*, which deviated considerably. We also observed that scenario *A* (predominantly nadir) was not always better than scenarios *B* or *C* (Figure 7) for all forest types. The variability among scenarios *A, B* and *C* was the highest for the mixed plots (MAD of 0.07) and the lowest for the riparian plots (MAD of 0.03). The mean absolute difference (MAD) of the pairwise differences of mean R^2 values among scenarios *AB, AC* and *BC* were generally lower than those among scenarios *A, B* and *C*, for all forest types (Table 5). This indicates an overall stabilisation in the means due to point clouds acquired from at least two flight lines, each belonging to different *MSA* classes.

The third part of Table 5 shows that the MAD of comparisons between single (A, B or C) and double flight line (AB, AC or BC) scenarios are similar to those of comparisons among single and double flight line scenarios, respectively except for the coniferous plots. The MAD of the goodness-of-fit criteria for the coniferous plots were highest than those for riparian, broadleaf and mixed plots, respectively, highlighting a greater difference between single and double flight line scenarios. The same pattern was observed for the overall MAD with the lowest values for the riparian plots followed by broadleaf, mixed and coniferous (0.02, 0.04, 0.05 and 0.08 for R2 and 0.6, 1.3, 2.0 and 2.5 percentage points for rRMSE), except for mixed plots that had a higher MPE MAD value (1.5 percentage points) than coniferous plots (1.2 percentage points) (Figure 7).

Regarding the pairwise F tests in (Table 6), comparisons among scenarios A, B and C revealed that scenario A had lower standard deviations than scenarios B and C only for the mixed plots. We observed that scenario B had lower standard deviations for the other forest types than scenario A (reductions in SD of R2 in the 9 % to 18 % range). Similarly, scenario C had lower standard deviations compared to scenario A for broadleaf and coniferous (reductions of 14 % and 6 %, respectively). However, scenario C systematically resulted in higher standard deviations than scenario B.

The comparisons among AB, AC and BC revealed that the presence of nadir acquisition, i.e. scenario A, in combination with scenarios B or C (AB or AC), is beneficial compared to scenario BC. For scenario BC, the R2 standard deviations increased in the 4.8 % to 224 % range for riparian, broadleaf and mixed plots except coniferous, for which there was no significant change. However, comparisons between scenarios AB and AC revealed different trends according to forest types (Table 6).

The spreads of the distributions for double flight scenarios lines (AB, AC or BC) were significantly lower than those for single flight line scenarios (A, B or C), with reductions in the standard deviations in the range of 31.2 % to 65.2 % across all forest types and goodness-of-fit criteria, with a single exception of the pair A-BC (Mixed, R2 and rRMSE) wherein the standard deviation increased by 31.4 % and 46.4 % for R2 and rRMSE respectively (third part of Table 6).

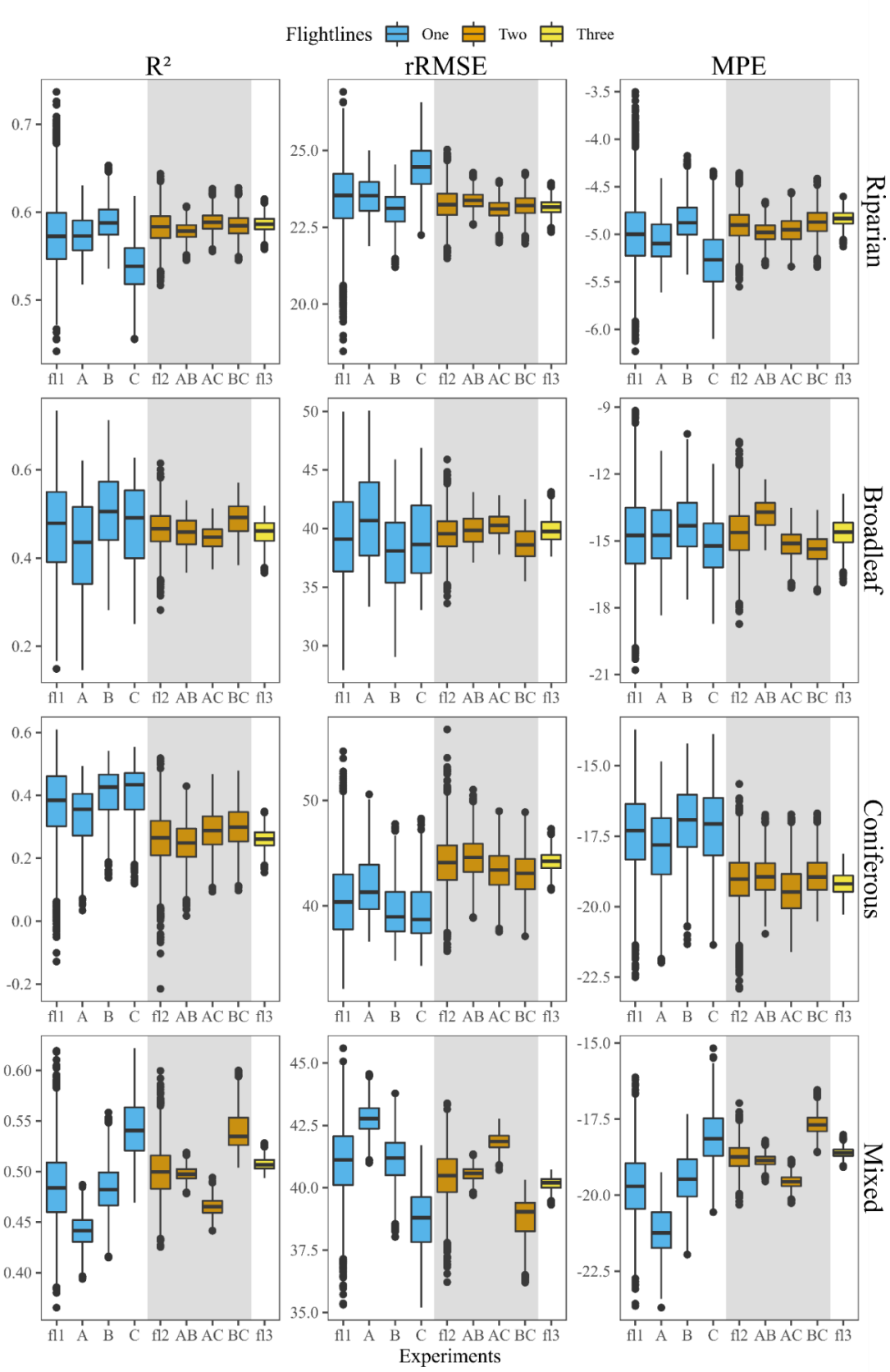

Figure 7: Distribution of the goodness-of-fit criteria of predictions of stem volume (V_{st}) models (R^2, rRMSE, MPE) for different scenarios and for the different forest types (Riparian, Coniferous, Broadleaf and Mixed). The single (fl1, A, B and C), double (fl2, AB, AC and BC) and triple (fl3) flight lines scenarios are depicted in blue, orange and yellow, respectively

		R^2				rRMSE				MPE			
		Riparian	Broadleaf	Coniferous	Mixed	Riparian	Broadleaf	Coniferous	Mixed	Riparian	Broadleaf	Coniferous	Mixed
% change in mean	*fl1-fl2*	1.4*	**-0.6**	-29.8*	3.0*	-0.9*	0.6*	8.8*	-1.4*	-1.8*	-0.6*	9.8*	-4.9*
	fl1-fl3	2.0*	-2.2*	-30.3*	4.6*	-1.3*	1.4*	9.1*	-2.1*	-3.2*	-0.7*	10.5*	-5.6*
	fl2-fl3	0.6*	-1.7*	**-0.6**	1.6*	-0.4*	0.8*	0.2*	-0.8*	-1.4*	**-0.1**	0.6*	-0.7*
% change in SD	*fl1-fl2*	-52.8*	-58.2*	-23.0*	-33.7*	-53.0*	-58.1*	-28.3*	-33.0*	-54.6*	-39.0*	-35.8*	-58.6*
	fl1-fl3	-78.5*	-73.7*	-72.4*	-81.7*	-78.4*	-74.0*	-74.3*	-81.4*	-77.5*	-65.1*	-74.0*	-85.9*
	fl2-fl3	-54.3*	-37.1*	-64.2*	-72.5*	-54.1*	-37.9*	-64.2*	-72.3*	-50.4*	-42.8*	-59.6*	-65.8*

Table 4: Pairwise comparisons of means and standard deviations of distributions of goodness-of-fit criteria in terms of percentage changes for scenarios fl1, fl2 and fl3. Values in bold indicate comparisons that were not statistically significant (p>0.05) (Games-Howell test for means and pairwise F tests for variances)

		R^2				rRMSE				MPE			
Group 1	Group 2	Riparian	Broadleaf	Coniferous	Mixed	Riparian	Broadleaf	Coniferous	Mixed	Riparian	Broadleaf	Coniferous	Mixed
A	B	0.02*	0.08*	0.07*	0.04*	-0.4*	-2.9*	-2.3*	-1.6*	0.2*	0.4*	0.9*	1.7*
A	C	-0.03*	0.05*	0.07*	0.10*	0.9*	-1.7*	-2.4*	-4.1*	-0.2*	-0.5*	0.7*	3.1*
B	C	-0.05*	-0.03*	**0.00**	0.06*	1.4*	1.2*	**-0.1**	-2.5*	-0.4*	-0.9*	-0.2*	1.4*
MAD		*0.03*	*0.05*	*0.05*	*0.07*	*0.9*	*1.9*	*1.6*	*2.7*	*0.3*	*0.6*	*0.6*	*2.1*
AB	AC	0.01*	-0.01*	0.04*	-0.03*	-0.3*	0.5*	-1.2*	1.3*	0.0*	-1.4*	-0.5*	-0.7*
AB	BC	0.01*	0.03*	0.05*	0.04*	-0.2*	-1.1*	-1.5*	-1.8*	0.1*	-1.6*	**0.0**	1.2*
AC	BC	0.00*	0.04*	0.01*	0.08*	0.1*	-1.6*	-0.4*	-3.1*	0.1*	-0.2*	0.5*	1.9*
MAD		*0.01*	*0.03*	*0.03*	*0.05*	*0.2*	*1.1*	*1.0*	*2.1*	*0.1*	*1.0*	*0.4*	*1.3*
A	AB	0.01*	0.03*	-0.09*	0.06*	-0.1*	-0.9*	2.7*	-2.2*	0.1*	0.9*	-1.0*	2.3*
A	AC	0.02*	0.02*	-0.05*	0.02*	-0.4*	-0.4*	1.5*	-0.9*	0.1*	-0.5*	-1.6*	1.6*
A	BC	0.01*	0.06*	-0.04*	0.10*	-0.3*	-2.1*	1.2*	-4.0*	0.2*	-0.7*	-1.0*	3.5*
B	AB	-0.01*	-0.05*	-0.16*	-0.01*	0.3*	2.0*	5.0*	0.6*	-0.1*	0.5*	-1.9*	-0.6*
B	AC	**0.00**	-0.06*	-0.12*	0.02*	**0.0**	2.5*	3.8*	-0.7*	-0.1*	-0.9*	-2.4*	0.1*
B	BC	0.00*	-0.02*	-0.11*	0.06*	0.1*	0.8*	3.5*	-2.4*	**0.0**	-1.1*	-1.9*	1.8*
C	AB	0.04*	-0.02*	-0.16*	0.05*	-1.1*	0.8*	5.1*	-1.9*	0.3*	1.4*	-1.7*	0.8*
C	AC	0.05*	-0.03*	-0.12*	0.08*	-1.4*	1.3*	3.9*	-3.2*	0.3*	**0.0**	-2.3*	1.5*
C	BC	0.05*	0.01*	-0.11*	**0.00**	-1.2*	-0.3*	3.6*	-0.1*	0.4*	-0.2*	-1.7*	-0.4*
MAD		*0.02*	*0.03*	*0.10*	*0.04*	*0.6*	*1.2*	*3.4*	*1.8*	*0.2*	*0.7*	*1.7*	*1.4*
Overall MAD		*0.02*	*0.04*	*0.08*	*0.05*	*0.6*	*1.3*	*2.5*	*2.0*	*0.2*	*0.7*	*1.2*	*1.5*

*Table 5: Pairwise differences of comparisons of means between different scenarios. The comparisons are grouped into three types, i.e., among A, B and C, among AB, AC and BC and between A, B, C and AB, AC and BC. Mean absolute differences per type and overall mean absolute differences are also provided. * p<0.05 and non-significant differences are in bold.*

		R^2				rRMSE				MPE			
Group 1	Group 2	Riparian	Broadleaf	Coniferous	Mixed	Riparian	Broadleaf	Coniferous	Mixed	Riparian	Broadleaf	Coniferous	Mixed
A	B	-8.9*	-18.4*	-14.8*	50.1*	-7.1*	-11.3*	-10.0*	56.5*	-9.1*	-4.1*	-7.3*	7.5*
A	C	32.9*	-13.5*	-6.1*	87.1*	27.9*	-10.2*	**-1.2**	107.9*	38.4*	-8.5*	**2.3**	12.0*
B	C	46.0*	6.0*	10.3*	24.7*	37.7*	**1.3**	9.8*	32.9*	52.3*	-4.6*	10.3*	4.2*
AB	AC	8.2*	-23.3*	**-1.1**	21.9*	9.9*	-24.3	**1.8**	18.1*	26.0*	-6.8*	23.9*	10.3*
AB	BC	28.1*	4.8*	**0.0**	223.9*	29.3*	7.4*	**3.8**	242.4*	29.9*	-4.6*	**-2.1**	70.6*
AC	BC	18.4*	36.6*	**1.0**	165.6*	17.6*	42.0*	**1.9**	189.9*	**3.1**	**2.3**	-20.9*	54.7*
A	AB	-53.9*	-64.0*	-27.0*	-59.4*	-53.7*	-63.2*	-30.2*	-57.3*	-51.9*	-54.2*	-49.7*	-75.6*
A	AC	-50.1*	-72.4*	-27.7*	-50.5*	-49.1*	-72.2*	-28.9*	-49.5*	-39.3*	-57.3*	-37.6*	-73.1*
A	BC	-41.0*	-62.3*	-27.0*	31.4*	-40.2*	-60.5*	-27.5*	46.4*	-37.5*	-56.3*	-50.7*	-58.4*
B	AB	-49.4*	-55.9*	-14.2*	-73.0*	-50.2*	-58.5*	-22.4*	-72.7*	-47.0*	-52.2*	-45.7*	-77.3*
B	AC	-45.2*	-66.2*	-15.1*	-67.0*	-45.3*	-68.6*	-21.0*	-67.7*	-33.2*	-55.4*	-32.8*	-75.0*
B	BC	-35.2*	-53.8*	-14.3*	-12.4*	-35.6*	-55.5*	-19.5*	-6.5*	-31.2*	-54.4*	-46.8*	-61.3*
C	AB	-65.3*	-58.4*	-22.3*	-78.3*	-63.8*	-59.0*	-29.3*	-79.4*	-65.2*	-49.9*	-50.8*	-78.2*
C	AC	-62.5*	-68.1*	-23.1*	-73.6*	-60.2*	-69.0*	-28.1*	-75.7*	-56.2*	-53.3*	-39.0*	-76.0*
C	BC	-55.6*	-56.4*	-22.3*	-29.8*	-53.2*	-56.0*	-26.7*	-29.6*	-54.8*	-52.2*	-51.8*	-62.8*

*Table 6. Pairwise F tests quantified by the percentage changes in standard deviations of different scenarios. The values are changes in standard deviation of group 2 relative to group 1. * $p<0.05$ and non-significant comparisons are in bold.*

3.3.3 Inclusion of voxel metrics

3.3.3.1 Analysis of impact of voxel metrics considering the scenarios together

The distribution of the goodness-of-fit criteria for models built with reference and voxel metrics for all scenarios considered together is shown in Figure 8 for V_{st}. The overall percentage changes in means and standard deviation of the distributions are given in Table 7, in which deteriorations are highlighted in red. Voxel metrics had an overall positive impact on the R2 distribution (riparian (+22.2 %), broadleaf (+8.3 %), coniferous (+0.1 %), mixed (+23.1 %)). The mean rRMSE values were reduced by 16.6 %, 3.6 % and 12.2 % for riparian, broadleaf and mixed plots. The mean rRMSE value increased by 0.1 % for coniferous plots. For broadleaf and coniferous plots, the MPE values did not improve with voxel metrics for predictions of all three attributes (an increase of 12.6 % and 8.1 %, respectively). In contrast, mean MPE values improved for both riparian and mixed plots (a decrease of 25.2 % and 18.7 %, respectively). For coniferous, broadleaf plots and mixed plots, the standard deviations of distributions of R2, rRMSE and MPE improved with voxel metrics with reductions in the range of 0.8 % to 42.6 %. For riparian plots, the standard deviations increased by 29.6 %, 60.3 % and 42.1 % for R2, rRMSE and MPE, respectively. The scenario-wise percentage changes in means and standard deviations are given in Table 8 and Table 9, respectively.

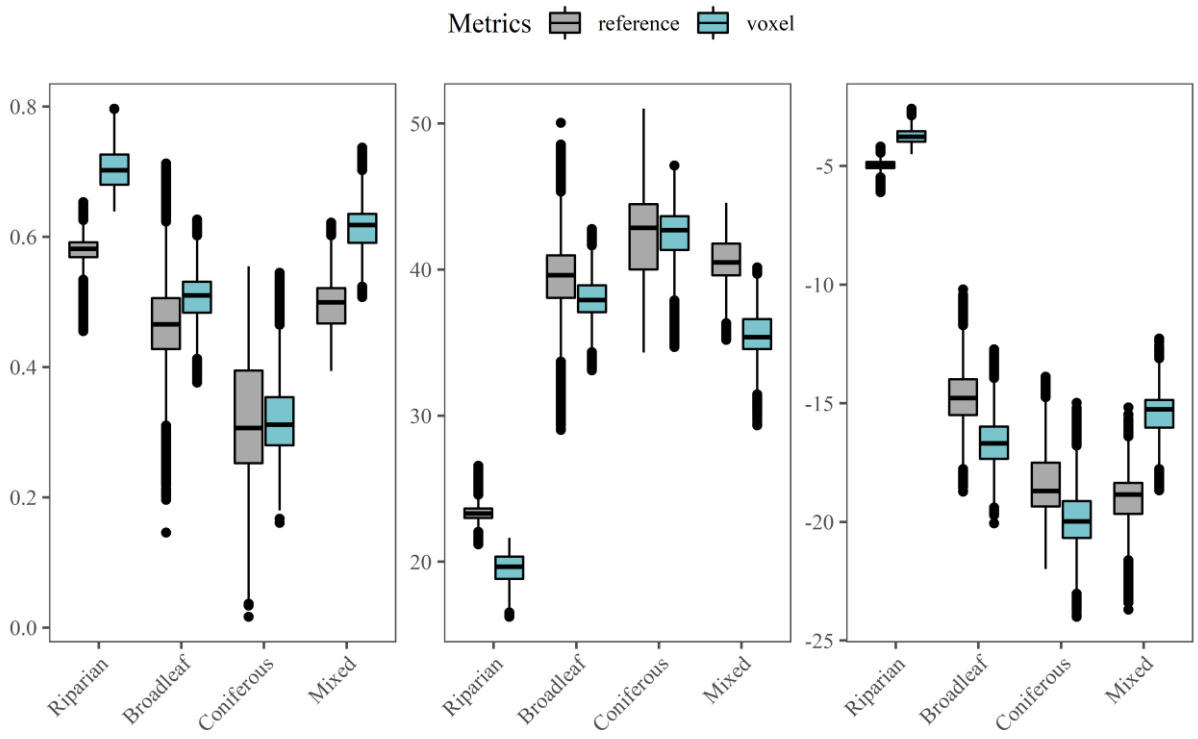

Figure 8: Comparison of the distribution of goodness-of-fit criteria (R², rRMSE, MPE) between models for the prediction of V_{st} with reference (grey box-plots) and voxel (blue box-plots) metrics, respectively, for different scenarios combined and for different forests types (Riparian, Broadleaf, Coniferous and Mixed)

	R²				rRMSE				MPE			
	Riparian	Broadleaf	Coniferous	Mixed	Riparian	Broadleaf	Coniferous	Mixed	Riparian	Broadleaf	Coniferous	Mixed
% change in mean	22.2*	8.3*	**0.1**	23.1*	-16.6*	-3.6*	0.1*	-12.2*	-25.2*	12.6*	8.1*	-18.7*
% change in SD	29.6*	-42.6*	-38.5*	-15.0*	60.3*	-41.1*	-38.1*	-4.7*	42.1*	-0.8*	-10.1*	-24.3*

Table 7: Overall (scenarios A, B, C, AB, AC, BC considered together) percentage change in the means and standard deviations of distributions using voxel metrics in ABA predictions of V_{st}. Values in red indicate deterioration. All comparisons were significant (*) except for those in bold.

3.3.3.2 Scenario-wise impact of voxel metrics

3.3.3.2.1 Effect on the median and mean values of the distributions for the different scenarios

The scenario-wise percentage changes in the means are given in Table 8. R2 and rRMSE means improved in the range of 2.3 %-144 % and 0.9 %-24.2 %, respectively, except for some scenarios in coniferous plots (scenarios fl1, B, C, AC and BC) where voxel metrics did not perform well. There were contrasting results for MPE, with reductions in the 5.7 %-34.6 % range across all the scenarios for the riparian and mixed plots and increases in the 3 % to 21.8 % range for the coniferous and broadleaf plots. Comparisons across one, two and three flight lines scenarios revealed no systematic trend in the magnitude of the changes for both improvement and deterioration cases.

	Forest type	One flight line				Two flight lines				Three flight lines
		fl1	A	B	C	fl2	AB	AC	BC	fl3
R^2	Riparian	27.0*	28.1*	22.6*	36.3*	18.9*	21.2*	18.9*	15.9*	13.7*
	Broadleaf	4.1*	6.7*	2.3*	3.1*	10.7*	10.7*	10.5*	10.3*	15.1*
	Coniferous	-3.8*	6.0*	-2.8*	-20.1*	9.3*	35.1*	-1.8*	-10.8*	9.7*
	Mixed	20.0*	39.9*	29.1*	2.2*	24.0*	19.2*	33.8*	18.2*	24.1*
rRMSE	Riparian	-20.3*	-21.1*	-17.8*	-24.2*	-14.2*	-15.8*	-14.6*	-11.9*	-10.2*
	Broadleaf	-1.5*	-2.3*	-0.9*	-1.2*	-4.7*	-4.6*	-4.3*	-5.0*	-6.6*
	Coniferous	1.4*	-1.4*	1.0*	6.9*	-1.6*	-5.9*	0.4*	2.4*	-1.7*
	Mixed	-10.1*	-17.3*	-14.8*	-1.3*	-12.8*	-10.0*	-16.0*	-11.4*	-13.3*
MPE	Riparian	-30.0	-30.3*	-26.7*	-34.6*	-22.1*	-24.3*	-24.8*	-18.6*	-15.8*
	Broadleaf	11.9*	21.7*	3.1*	10.4*	13.5*	21.8*	15.6*	3.9*	12.6*
	Coniferous	9.6*	5.6*	8.7*	16.8*	6.2*	3.0*	5.8*	12.0*	5.5*
	Mixed	-17.5*	-24.4*	-23.3*	-5.7*	-18.8*	-16.4*	-23.1*	-16.0*	-20.1*

Table 8: Scenario-wise percentage changes in the means of distributions of goodness-of-fit criteria when using voxel metrics for the predictions of V_{st}. Values in red indicate a deterioration. All comparisons were significant (*) except for those in bold, all comparisons were significant (*) except for those in bold

3.3.3.2.2 Effect on the distribution spread for the different scenarios

Voxel metrics also positively impacted the distributions by reducing the spread, or the standard deviations, of all three goodness-of-fit criteria for all the scenarios for broadleaf and coniferous forest types (Table 9). The standard deviations of the distributions for broadleaf and coniferous plots decreased by 23.3 % to 70 %, 22.5 % to 68.2 % and 2.1 % to 55.8 % for R2, rRMSE and MPE, respectively. The only exception was a slight increase of 2.1 % in the standard deviations of MPE values for scenario C for coniferous plots.

For the riparian and the mixed plots, at least one of the three goodness-of-fit criteria was negatively impacted due to voxelisation (except scenarios C and BC for mixed plots).

	Forest type	One flight line				Two flight lines				Three flight lines
		fl1	A	B	C	fl2	AB	AC	BC	fl3
R^2	Riparian	-29.0*	-1.6*	25.7*	-4.1*	-7.9*	54.9*	31.1*	13.7*	-0.3*
	Broadleaf	-54.0*	-61.1*	-57.8*	-42.2*	-52.9*	-59.9*	-42.1*	-48.5*	-60.1*
	Coniferous	-44.4*	-45.6*	-23.3*	-41.7*	-52.0*	-70.0*	-63.9*	-59.3*	-31.1*
	Mixed	56.9*	94.8*	27.0*	-38.7*	16.0*	68.0*	11.1*	-30.5*	81.9*
rRMSE	Riparian	-11.8*	24.9*	53.2*	27.1*	8.0*	84.9*	54.2*	29.6*	11.1*
	Broadleaf	-52.9*	-59.9*	-57.7*	-40.3*	-50.5*	-58.0*	-39.4*	-45.5*	-57.1*
	Coniferous	-44.0*	-43.8*	-22.5*	-43.9*	-51.2*	-68.2*	-64.2*	-60.3*	-29.9*
	Mixed	75.7*	137.0*	49.5*	-38.0*	33.5*	87.3*	32.9*	-22.4*	109.6*
MPE	Riparian	10.6*	24.2*	68.0*	24.8*	33.1*	67.2*	29.3*	28.6*	22.8*
	Broadleaf	-41.7*	-54.3*	-55.8*	-33.4*	-48.7	-55.0*	-21.0*	-20.0*	-35.9*
	Coniferous	-13.9*	-22.7*	-15.9*	2.1*	-11.2*	-35.1*	-40.2*	-14.2*	-1.3*
	Mixed	22.1*	0.9*	-9.6*	-41.2*	34.9*	63.6*	32.0*	-3.9*	90.6*

Table 9: Scenario-wise percentage changes in the standard deviations of distributions of goodness-of-fit criteria using voxel metrics for the predictions of V_{st}. Values in red indicate a deterioration. All comparisons were significant (*) except for those in bold

3.3.3.2.3 Effect of voxel-based metrics on conventional models

We observed a general improvement in the goodness-of-fit criteria for all the three forest attributes (Table 10) when using voxel metrics in conventional models, i.e., considering all the flight lines

together. The R2 improved for all forest types (9.1 % for riparian, 3.8 % for coniferous, 8.5 % for broadleaf and 25.3 % for mixed plots), respectively. The rRMSE values decreased by 9.5 %, 0.5 %, 4 %, and 14 % for riparian, broadleaf, coniferous, and mixed plots, respectively. There were only marginal changes in all goodness-of-fit criteria for the coniferous plots, with minor improvements in the R2 and rRMSE values, while the MPE increased by 8.5 %. The MPE for broadleaf plots was also higher by 13.1 %. Results for BA and V_{tot} are presented in Appendix B.

Goodness-of-fit criteria	Forest type	reference metrics	voxel metrics	% change
R^2	Riparian	0.66	0.72	9.1
	Coniferous	0.26	0.27	3.8
	Broadleaf	0.47	0.51	8.5
	Mixed	0.51	0.64	25.3
rRMSE	Riparian	21.1	19.1	-9.5
	Coniferous	44.2	44	-0.5
	Broadleaf	40.2	38.6	-4.0
	Mixed	40.2	34.4	-14
MPE	Riparian	-4.3	-3.6	-16.3
	Coniferous	-20	-21.7	8.5
	Broadleaf	-15.3	-17.3	13.1
	Mixed	-18.3	-14.7	-20.4

Table 10: Goodness-of-fit criteria for predictions of V_{st} for conventional models built with reference and voxel metrics

3.4 Discussion

The overall objective of this study was to evaluate the impact of different scanning configurations on ABA predictions. Our results showed that including lidar metrics sensitive to scan angle could result in highly variable ABA model performances. We also proposed alternate methods to compute lidar metrics based on voxelisation to mitigate scan angle effects.

3.4.1 Impact of scan angle on models of different scanning scenarios

The percentage changes in the means and standard deviations of goodness-of-fit criteria for models built using lidar data for the same plots, based on different scanning configurations, reflect the variability of ABA models and the resulting predictions. The standard deviations (spread) of all three goodness-of-fit criteria (R2, rRMSE and MPE) for all the forests decreased when the dataset was comprised of multiple flight lines per plot. However, the distribution means were different according to forest types, and there was no definite pattern. For example, for the riparian plots at Ciron, the distribution means appeared to be broadly stable for all scenarios except for scenario C (20°<=*MSA* < 30°), which decreased considerably. For the three forest types at Bauges, the goodness-of-fit criteria means of the models generally improved in conjunction with an inclination increase, i.e., *A* to *C* (class *A* (0° <=*MSA* < 10°), class *B* (10°<=*MSA* < 20°), class *C* (20°<=*MSA* < 30°), except for

broadleaf plots, where there was a marginal decrease for scenario *C* relative to scenario *B*. Overall, the distribution means for scenario *B* were relatively stable compared to scenarios *A* and *C*. It is worth noting that the predominantly nadir configuration, i.e., scenario A, was not clearly better than scenarios fl1, *B*, or *C*. Scenario *A* distributions were marginally lower than those of fl1 broadleaf, coniferous and mixed plots. There were significant differences between the distribution means, but their magnitude varied across the different types of forests. We observed that the variations among scenarios *A*, *B*, and *C* tended to be higher than those among scenarios *AB, AC,* and *BC*. For the coniferous plots, the means for scenarios fl2 and fl3 were considerably lower than those for scenario fl1 by almost 30 % in each case. We observed the same phenomenon for broadleaf plots, but the differences were lower (fl2-fl1: −0.6 %, fl3-fl1: −2.2 %*). Van Lier et al. (2021) also observed marginally higher errors for models built with multiple flight line data. On the other hand, we observed an opposite trend for riparian plots.

Let us consider the goodness-of-fit distribution as unexpected 'risk' when using a dataset acquired with a particular configuration to build ABA models. The risk of having highly variable predictions is reduced when at least two flight lines are used to scan each plot. The reduction in the goodness-of-fit criteria spreads (or variance), thanks to the inclusion of more flight lines, is thus highly significant because it indicates an improvement in the precision of the goodness-of-fit criteria. Although this implies that the chance of having an apparently 'great' model is reduced, it also means that the possibility of having a poorly defined model is also diminished. Suppose the model was extrapolated to provide a map of the targeted forest attributes, then, in that case, the goodness-of-fit criteria might not be valid for areas scanned with configurations other than those of the plots used to build the model. These results underline the importance of having a large number of field plots, which should be representative of the diversity of both forest stands and scanning conditions. Future studies need to assess the prediction variability when ABA models, based on a specific scanning configuration dataset, are used to generate wall-to-wall predictions.

The metrics commonly used in ABA approaches are certainly affected by scan angle, as demonstrated by several studies (Holmgren et al., 2003; Liu et al., 2018; Montaghi, 2013). To our knowledge, few studies have explored the effect of the inclusion of metrics sensitive to scan angle in ABA models (Holmgren et al., 2003; van Lier et al., 2021). Van Lier et al. (2021) recently investigated the effect of scan angle on both lidar metrics and ABA models to predict different forest attributes. In their study, which addresses scan angle effects on area-based models, they found relatively stable goodness-of-fit (R2, rRMSE and MPE), with minor differences between models built with and applied to datasets acquired from near-nadir, off-nadir as well as combinations of flight lines. These findings are similar to those we obtained on the riparian plots at Ciron. The mean R2 values ranged between 0.57 and 0.59 for V_{st}, without considering scenario C, which had lower R2 and higher errors. For the other three forest types, the inter-scenario variations were higher.

Interestingly, Van Lier et al. (2021) observed that the accuracy of the models was marginally lower when built with point clouds scanned from multiple flight lines (aggregate of flight lines). Their observations were for balsam fir stands, a coniferous forest type. We observed similar patterns for coniferous plots but with substantial differences (30 % lower mean R2 values) between fl1 and fl2, and fl1 and fl3 scenarios. Although we observed variations between scenarios at the Bauges site, more flight lines did not necessarily lead to better predictions (higher R2 and lower errors) but rather to more precise predictions, which is essential from a practical point of view. Moreover, it is interesting to note the better performances with point clouds acquired from single flight lines.

For the Bauges site, scenario *C* (20°<=*MSA*< 30°) does not have the same negative impact it had on the riparian plots, which could be related to the differences in data acquisition properties. *MSA* classes for both sites are not fully comparable due to the differences in flying altitudes (250 m over Ciron sites and 1050 m over Bauges sites). In addition, depending on the slope of the plots, the lidar pulse-canopy interactions may be different for flight lines with similar mean scan angles but with different azimuths, as illustrated in Figure 9. In a related study, we found that the inclusion of terrain parameters positively impacted the forest attribute predictions (Lahssini et al., 2022). Nevertheless, using two flight lines for a predominantly inclined scenario, i.e., scenario BC, seems to have ensured that the distributions are more stable for both sites and all stand types. Furthermore, if a 50 % overlap is ensured during data acquisition, single flight line scenarios (fl1, A, B and C) are generally not observed everywhere (typically scenarios B and C). Our results will provide a useful reference for subsequent analyses, and it is always beneficial to be aware of potential risks associated with specific data properties.

An acquisition configuration with a maximum of 30° scanning angle and ensuring a 2/3 overlapping between successive flight lines would limit scan angle impacts on ABA prediction quality over a forest area. However, this high level of overlapping comes at a prohibitive cost for many operational campaigns. In practice, different specifications for forestry applications can be found, such as, those provided by the USDA (Mitchell et al., 2018), with scan angle ≤ 13° and swath overlap of possibly 50 %, by Natural Resources Canada (NRC, 2017), with scan angle ≤ 20° and at least 20 % swath overlap increased to 30 % in British Columbia (Ministry of Forests, Lands and GeoBC, 2020). Several countries have undertaken multipurpose acquisitions. The specifications provided for New Zealand and Australia include a maximum scan angle of 20° and a minimum swath overlap of 10 % (ICSM, 2010). Specifications are not always easy to find. However, we picked a few las tiles in several European countries' open source national lidar data sets. We found that scan angles could reach at least 30° for France (IGN, n.d.), Luxembourg (ACT, n.d.) and Switzerland (Swisstopo, n.d.) and even 36° for Slovenia ("AGENCIJA RS ZA OKOLJE," n.d.).

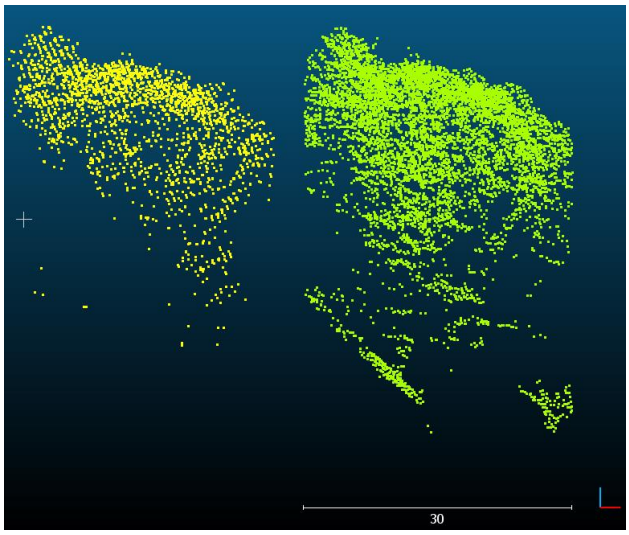

Figure 9: Two point clouds from the same plot on a steep slope with the same scan angle class (class C) of mean scan angles, 26° (yellow) and 22° (green)

In addition, local-scale forest applications based on light lidar systems are likely to develop in the near future (Jaakkola et al., 2017; Lei et al., 2019; K. Liu et al., 2018; Torresan et al., 2017). Such acquisitions are characterised by higher scan angle ranges than traditional airborne acquisitions. In these cases, the impact of the scanning condition differences over the forest must be effectively managed to ensure ABA model quality and robustness for operational applications. Normalising lidar metrics concerning scan angle changes could help achieve this goal.

3.4.2 The potential of normalised metrics

Inclusion of carefully considered metrics such as Pf certainly contribute to more accurate predictions, but the return-ratio-based computation is highly variable due to its dependence on the ground returns. However, metrics such as P_f and vegetation profiles based metrics such as CV_{PAD} are helpful for better characterisation of structural characteristics and prediction of wood volume (Bouvier et al., 2015; Næsset, 2002). The spreads of the distributions with μ_{CH}, σ^2_{CH} were higher for Bauges plots compared to Ciron (Figure 6) which could be due to class C σ^2_{CH} which was found to be more sensitive (see Appendix A). However, the effects due to inclusion of P_f and CV_{PAD} were much higher (Figure 6) with average increase in standard deviations of 143% across all forest types and goodness-of-fit criteria (Table 3).

Voxel-based methods were applied to derive normalised vegetation profiles, which were in turn used to compute P_f^{vox} and CV_{PAD}^{vox}. Substituting these metrics positively impacted mean R^2 values with an average increase of 38 %, barring some mainly concerning coniferous plots. Similarly, the rRMSE values were reduced by an average of 10 %. This method of estimating gap fraction did not depend on ground returns but rather on estimating PAD values as a function of the interaction between the laser pulses/canopy interactions. In some of the attribute-scenario combinations (riparian and mixed

type), distribution variation of the goodness-of-fit criteria was higher for voxel metrics. However, distribution mean increases underline the benefit of using P_f^{vox} and CV_{PAD}^{vox}, and other profile-based metrics in general that can more accurately characterise canopy structural properties. Indeed, when comparing with reference PAD profiles, which are based on the number of points per layer, for most plots, we observed a normalisation of the profiles regarding scan angle effects. In Appendix C, vegetation profiles obtained using layers of points (Bouvier et al., 2015) and voxelisation, as described in this study, are shown for two cases: (a) where appears to reduce the variation, and (b) where it seems to add some noise to profiles. The profiles obtained from both methods show similar patterns, but the areas under the curves are different. However, we have no reference data to conclude that one type of profiles is better than the others. Based on the results of this study, we can conclude that voxel-based profiles and metrics have the potential to better characterise the distribution of the vegetation.

Voxel-based PAD estimations are, however, sensitive to the number of beams passing through a voxel and voxel size (Pimont et al., 2018; Soma et al., 2021). These factors were beyond the scope of the present study. However, biases arising from poorly sampled voxels, which is generally the case in the lower strata when airborne lidar is used, could ultimately affect the ABA models. On the one hand, studies have reported that low pulse densities do not affect ABA predictions; on the other hand, the low sampling density has been shown to affect voxel-based estimation of PAD.

Additionally, voxel size was also influential in generating the profiles as the voxels were normalised using a resampled DTM of length 1 m (same as the size of the voxel). In each voxel column, the lowest voxel containing points (ground and lower vegetation) was identified as the ground or the 0th voxel, followed by successive labelling of voxels in each column. The profiles were computed as the mean of all the voxels with the same label. This ensured we generated the PAD profiles by following the terrain by considering layers of voxels at a uniform distance from the ground. The way in which columns of voxels were aggregated to compute the profile added some noise because ground position accuracy based on the voxel resolution. For very steep slopes, if the ground is located in both the bottom of a voxel and the top of the neighbouring voxel, the PAD in the resulting profile will combine information from nearly-two metres of vegetation instead of one. In addition, any error in identifying the correct ground voxel could incorrectly shift an entire column of voxels by a metre. Finally, there is also scope for refining the method of vegetation profile conversions to Pvoxf or any other metric that could contribute to ABA models.

Nonetheless, voxel metrics had a generally positive impact by either improving the means of the distributions, or by reducing the standard deviations, or both. Metrics derived from PAD profiles obtained using voxelisation approaches are an option to manage the effect of scan angles on ABA models if point densities are high enough to ensure a good sampling of lower layers. However,

voxelisation approaches need to be improved, and tools for easy computation of such PAD profiles need to be developed. This will facilitate the computation of PAD profiles at various resolutions and in hilly environments at the level of the field plots (model development) and the whole area (model implementation).

3.4.3 Characterisation of plots and interactions between topography and scanning conditions in complex stands

Riparian models seemed to perform better than the three other plot types located at Massif des Bauges. The goodness-of-fit criteria for predictions of all forest attributes on the riparian plots had R2 values 0.67–0.74 and rRMSE values in the range of 18 %-20 %, which were within the range of values reported in several studies (Coops et al., 2021). However, the model quality deteriorated for the broadleaf, mixed and coniferous plots (Table 10 for V_{st} and Table 15 for BA and V_{tot}). Measuring DBHs of small trees contributing to the lidar signal would have enabled an improved classification and an improved estimation of the reference BA and wood volumes, limiting additional sources of noise in the model. Nonetheless, the improvements with voxel metrics were notable.

In the Bauges plots, the high slopes of many plots could have affected the interaction of the lidar with the canopy. Due to limited datasets, the azimuth of the lidar acquisition was not considered. In some plots, the tree sizes heterogeneity was very high, with many instances of large trees found near the periphery of the plots. Many such trees were found beyond the plot while a significant part of the canopy was still present in the plot subsets, thereby occluding acquisition from flight lines with certain azimuths. The occlusion was especially prominent for inclined scanning.

3.4.4 Perspectives for improved models

The distributions of the goodness-of-fit indicate that there may indeed be a ’risk’ linked to how data is acquired. Each data acquisition for any given area may be different and the associated higher risk may cause discrepancies in forest attribute modelling and in forest environment monitoring. Our findings showed that greater the number of flight lines (high overlap), the lower the risk. However, increasing the overlap is not a cost-effective solution. Another solution may be to strike a better balance between acquisition characteristics and the identification or development of metrics that capture the structure of the forest effectively (vegetation profiles, for example). Therefore, lidar metrics need to be studied or developed from the perspective of different lidar scanning characteristics. Furthermore, in case of coniferous forests, the distribution means were better with only two metrics. Upon investigation, we found that some of the metrics were correlated and P_f and CV_{PAD} were not useful for the coniferous plots resulting in lower (adjusted) R2 and higher errors.

These metrics ought to be tested further to better understand their behaviours when dealing with different canopies various other modelling methods could also be considered. The plots were in very steep terrain and variables related to the terrain properties could be a useful input for ABA models (Lahssini et al., 2022). Integration of terrain properties along with scan angle information could be approached from a deep learning perspective, as these factors are complex to model. However, evaluating the potential of such approaches would require more than the 118 plots studied on the Bauges site.

3.5 Conclusion

In this study, we studied the influence of lidar scan angle on forest attribute prediction for four different forest types: riparian, broadleaf, coniferous, and mixed. We opted for a predefined model using four metrics based on different behaviours under changing lidar scan angles. These metrics were a) average value of canopy height values μ_{CH}, b) variance of canopy height values σ^2_{CH}, c) gap-fraction P_f, and d) coefficient of variation of PAD profile, CV_{PAD}. Although P_f and CV_{PAD} helped improving accuracies of ABA models, their sensitivity to lidar scan angle transferred to ABA model accuracies and resulted in highly variable predictions. However, the presence of multiple flight lines tended to reduce the variability, thus increasing the probability of developing models that are more robust. Furthermore, we proposed alternative computations of P_f and CV_{PAD} from vegetation profiles generated using voxelisation. These metrics either improved overall prediction accuracy, or reduced the variation in predictions or both, thereby highlighting two key points: a) lidar metrics sensitivity to scan angle must be assessed, especially when developing general ABA models, and b) voxel-based metrics have the potential to better characterise forest structural characteristics, which in turn contribute to more accurate predictions. Developing models that are unaffected by changing scan angle would result in accurate and reliable wall-to-wall predictions. Many countries and regions plan multipurpose lidar acquisitions based on different specifications. Concurrently, local surveys based on with light lidar systems are likely to develop in the near future for forest applications. In both cases, homogenous scanning configuration over a whole forest area is not achievable in practice and different parts of the forest will be observed using different scan angles or combinations of scan angles. Our study emphasises the necessity to develop new approaches that are better at mitigating scan angle impacts on ABA models to enable the further development of operational forest applications.

3.6 Acknowledgements

This study was carried out in the framework of the PROTEST project, supported by the French Agency for Ecological Transition (ADEME) (grant 1703C0069, GRAINE program) and the FRISBEE project, supported by the TOSCA Continental Surface program of the Centre National

d'Etudes Spatiales (CNES) (order N° 4500070632). It also benefited from the support of the French region of Occitanie with the funding of part of PhD scholarship of K.R. Dayal. The authors would also like to thank the team comprising Jennifer Dudit, Yannick Mellerin, Alexis Ducousso, Gilles Saint-Jean, and Inge van Halder, Harri Evers, Charly Feppon and Éric Mermin for field measurements. The authors also thank the reviewers for their valuable criticisms and suggestions.

Chapter 4: Improving ABA models for forest attribute prediction using neural networks by considering effects of terrain and scan angles on 3D lidar point clouds

Karun R. Dayal[a], Sylvie Durrieu[a], Kamel Lahssini[a], Dino Ienco[a], Jean-Matthieu Monnet[b]

[a] UMR TETIS, INRAE, Montpellier

[b] LESSEM, INRAE, Université Grenoble Alpes,

Abstract

Lidar metrics are differently sensitive to lidar scan angle, which can eventually affect the robustness of area-based approach (ABA) models and modelling the interplay of scan angle, azimuth of acquisition, and terrain properties can be complex. The study hypothesises that neural networks can manage the interplay of lidar acquisition parameters, terrain properties, and vegetation characteristics to improve ABA models. The study area is in *Massif des Bauges* Natural Regional Park, eastern France comprising 291 field plots in mountainous environment with broadleaf, coniferous, and mixed forest types. Lidar data was acquired with high overlap to scan field plots from multiple flight lines. The point cloud data for each field plot was expanded based on the flight lines resulting in 1095 independent observations. Standard lidar metrics, terrain metrics and scan metrics were also defined. A multilayer perceptron (MLP) was used to model basal area (*BA*) and total volume (V_{tot}), while considering the interactions between the 3D lidar point cloud metrics, terrain metrics and scan metrics of the expanded dataset. With expanded datasets, the MLP R^2 for the median predictions per plot were higher (R^2 of 0.83 and 0.85 for *BA* and V_{tot}) than predictions with standard datasets (291 observations) (R^2 of 0.77 for both *BA* and V_{tot}). It also outperformed an MLP model that neither accounted for the terrain properties nor the scanning geometry (R^2 of 0.66 and 0.71 for *BA* and V_{tot}, respectively). The MLP also outperformed RF regression, which was unable to exploit additional terrain and scan information effectively.

Keywords: ABA, ANN, forest attribute, lidar, RF, terrain

4.1 Introduction

The ability of lidar technology to create dense three-dimensional representations of vegetation has been widely used to extract useful information characterising forest properties (Dubayah and Drake, 2000). With airborne lidar systems (ALS), it is possible to cover large areas to generate accurately measured three-dimensional point clouds. An essential requirement in lidar remote sensing of forests is detecting the ground surface beneath the canopy, enabling accurate measurement of vegetation heights. As a result, the lidar scan angle, or the (half) field of view, has been limited to 20° to ensure most lidar pulses reach the ground (Nelson, 2013). So far, most studies involving lidar remote sensing for forestry applications have followed this convention (Fekety et al., 2018; Gobakken and Næsset, 2008, 2005; Leiterer et al., 2015; Mitchell et al., 2018; Næsset, 1997a; Ørka et al., 2018). Recently, some studies (Fedrigo et al., 2018; Lopatin et al., 2016; van Lier et al., 2021) have tried to assess the impact of scan angles greater than 20°, and many studies involving UAV-based lidar data routinely used much higher scan angles (Corte et al., 2020; Ma et al., 2022).

It may be difficult for highly inclined lidar pulses to reach the ground surface owing to the increased occlusions. Nonetheless, it is also true that probing lidar canopies with inclined pulses may also lend newer insights or different perspectives (Kamoske et al., 2019). A related study (Dayal et al., 2022) observed that datasets comprising nadir point clouds did not always result in better ABA models. Forest canopies are not a homogenous medium, and the lidar-derived information (lidar metrics) depends on how the lidar pulses sample the canopy. In addition, two lidar acquisitions may not have identical properties. The lidar metrics could be affected by the overall acquisition geometry as characterised by the acquisition properties (sensor properties, scan angle, scan azimuth, flying height), terrain properties, and vegetation structural characteristics.

In area-based approaches (ABA), there are numerous lidar metrics to choose from, and new metrics are constantly being developed to summarise the vegetation structural information comprehensively. Standard metrics used over the years include statistical descriptors such as the mean, standard deviation, variance, entropy, percentiles of the height or intensity values or cover rate metrics, density metrics, and gap-fraction. A stepwise selection procedure is often employed to identify metrics useful in predicting forest attributes using multiple linear regression (Næsset, 2002). However, the final set of metrics may vary depending on the forest type or lidar acquisition parameters. Another approach is to use expert knowledge to define and select a short list of metrics that could explain most, if not all, of the variance of the dependent variables (Bouvier et al., 2015). Still, assessing the influence of scan angle on selected metrics and, subsequently, on the forest attribute predictions may not always be practical. Furthermore, the influence of lidar metrics may be site-specific, and it is advisable to assess the effects of scan angle before further analysis on a case-by-case basis (Coops et al., 2021; Roussel et al., 2018).

Traditionally, the modelling of forest attributes is done using parametric and non-parametric models. Due to their simplicity, parametric methods such as ordinary least squares (OLS) regression have been widely used by studies to model forest attributes (Næsset, 2002; Tompalski et al., 2019; White et al., 2017). Non-parametric methods such as KNN or random forest (RF) do not depend on any assumptions regarding the data. They can accommodate nonlinear relationships between the dependent and independent variables (Cosenza et al., 2022). Both KNN and RF are among the most commonly used non-parametric approaches in ABA (Fassnacht et al., 2014). However, RF was found to have a higher level of transferability to new areas than KNN (Tompalski et al., 2019). Artificial neural networks (ANN) have also become a popular non-parametric method to address inherent non-linearity in datasets (Atkinson and Tatnall, 1997; Gopal and Woodcock, 1996). Neural networks are also known for their capacity to generalise (Özçelik et al., 2013). The feed-forward back-propagation multi-layered perceptron (MLP) is often used with remote sensing data. It consists of a network of several interconnected layers of neurons designed to mimic the capabilities of the human brain, such as generalisation and understanding complex patterns. In parametric methods such as OLS, only a few metrics can be used to avoid the problem of overfitting and the use of correlated variables. In non-parametric methods, there are no such limitations. Therefore, they are suited to understanding complex interactions between several lidar variables, acquisition geometry, and vegetation properties. Among the various non-parametric methods, the MLP has been demonstrated to have better generalisation capabilities (Liu et al., 2021; Özçelik et al., 2013).

However, MLP methods depend on the volume of data, which generally comprises large datasets with several thousand samples. In ABA approaches, which involve collecting labour-intensive field measurements in often-complex terrains, it is impossible to measure many field plots (samples) as field measurements make up a significant part of the costs. The field plots in ABA models typically range from a few tens to a few hundred. In addition, only a few field plots describe particular stand types. Generally, lidar acquisitions for forests are planned with multiple overlaps such that each forest area (or field plot) is thoroughly sampled from multiple locations. Point clouds acquired from each location may be considered independent observations. In addition, owing to the heterogeneous nature of the vegetation, the point clouds for any field plot may, in most cases, certainly retain differences and, therefore, may be used as they are for data expansion. Therefore, each point cloud results from the real-world interaction of the physical lidar signal with the natural vegetation.

A point cloud obtained from a flight line results from the interaction of acquisition parameters, terrain properties, and vegetation characteristics. Thus, it can be considered a unique and independent observation in ABA models. The objective of this study was to use individual point clouds obtained from multiple flight lines independently to improve ABA predictions by increasing the number of observations in lidar datasets. We demonstrated: i) the capacity of multilayer perceptron to model

complex interactions between lidar signal and both acquisition and terrain properties and ii) the benefits of expanding lidar datasets based on flight lines to build ABA models.

4.2 Materials and methods

4.2.1 Study area and field measurements

The study site is the Massif des Bauges Natural Regional Park in the French Alps. It is located between the two administrative departments of Savoie and Haute-Savoie and covers an area of approximately 850 km². The terrain is hilly (plot altitudes range from 420 m to 1760 m). The most common tree species comprise silver fir (Abies alba), Norway spruce (Picea abies), and common beech (Fagus sylvatica). Field inventory was carried out for 291 15 m radius circular plots during spring and fall 2018. Plot centre locations were measured using differential GNSS (DGNSS, Trimble, USA). Field inventory protocol involved measuring tree Diameter at Breast Height (DBH, measure 1.3 m above ground) of trees with DBH greater than 17.5 cm. Small trees (7.5 cm ≤DBH<17.5 cm) were counted within a plot radius of 10 m and classified as either coniferous or broadleaf.

Since DBH and height measurements were unavailable for all the trees with DBH greater than 7.5 cm, computation of basal area, stem, and total volumes at plot level required estimations for unmeasured trees. Firstly, the number of small trees was extrapolated from the number of trees in 10 m radius plots to 15 m radius plots. Secondly, the nationwide tree inventory database (NFI) generated by IGN (Institut National de l'Information Géographique et Forestière) containing measurements of trees with DBHs in the 7.5 cm to 17.5 cm range was used to extrapolate DBH and height values for non-measured trees. All NFI plots in the ecoregion that includes the study site were selected to have forest plots with similar climatic and growing conditions to those measured on the study site. For trees with DBH ranging from 7.5 cm to 17.5 cm, the median DBH value in the NFI database is around 11.1 cm. This value was used to compute the basal area of the trees with DBHs lower than 17.5 cm. Using NFI measurements, allometric relationships were established for each species (or group of species when the number of trees was not high enough) to estimate the heights of all the trees when there were no available height measurements. Volumes were then computed using the allometric equations available in Deleuze et al. (2013). The same protocol was followed in Lahssini et al. 2022 and Dayal et al. 2022.

Basal area (m²/ha)			Total volume (m^3/ha)		
Min	Mean	Max	Min	Mean	Max
0.36	30.2	89.7	2.52	312.1	1172

Table 1: Summary for Basal area (BA) and Total volume (V_{tot}) for the 291 inventory plots

4.2.2 Lidar data

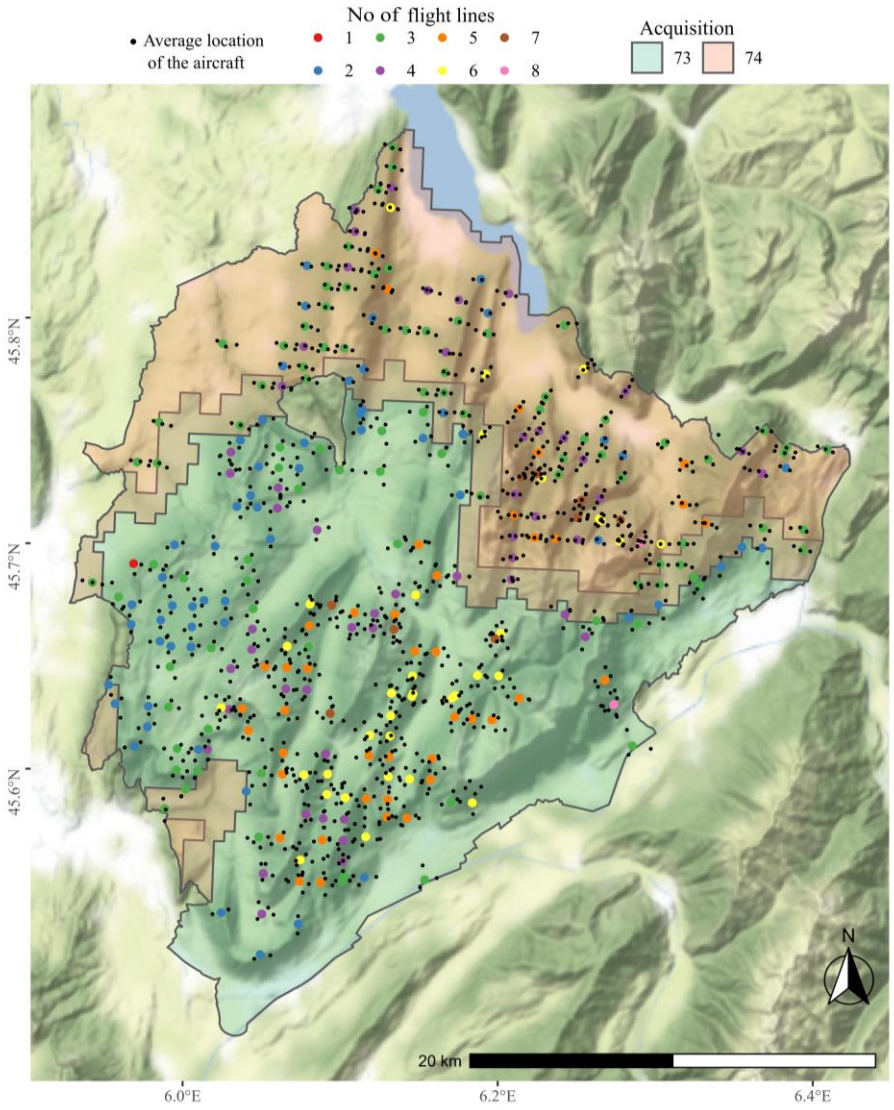

Figure 1: Location of the study site, distribution of field plots and coverage of lidar missions. The small dots in black depict the approximate (average) location of the aircraft when it scanned a field plot.

Lidar data acquisition was carried out in two missions. The first mission (summer 2016) covering areas of department 73 resulted in a dataset of 4-5 points/m² point density on average and the second mission (summer 2018) covering areas in department 74 resulted in a dataset of approximately 14 points/m² point density on average. Lidar acquisitions were carried out with multiple overlaps such that each field plot was scanned from several locations with different azimuths and scan angles. Figure 1 shows the locations of the field plots in the study area along with (average) aircraft locations while scanning respective field plots.

	73	74
Date of acquisition	September 2016	September 2018
Sensor	Leica ALS70-HP	Riegl LMSQ780
Wavelength (nm)	1064	1064
Scan angle (deg)	46° (+23°/-23°)	60° (+30°/-30°)

Beam divergence (mrad)	0.15	<=0.25
Ground speed (m/s)	85	45
Point density (pts/m²)	4	14
Flight height (AGL) (m)	1500*	1050

*Table 2: Acquisition parameters for the two flights (*calculated from data)*

4.2.3 Splitting of point clouds based on flight lines

Point clouds corresponding to the field plots were clipped from the lidar data using coordinates of the plot centres and plot radius (15 m). Due to flight line overlaps, the point cloud for a given plot is typically a composite of point clouds acquired with different scanning configurations. We split the point clouds for each plot based on the constituent flight lines. Each resulting constituent point cloud was represented by the mean of the scan angles (*MSA*) with which it was scanned. We did not consider those point clouds acquired with MSA greater than 30° as they were most likely acquired when the aircraft made turns, and there were few such instances. The fundamental 'unit' in our experiments is the point cloud for a plot acquired from only one flight line. We assessed pulse densities for each point cloud, and 90% of the constituent point clouds had a pulse density greater than one pulse per m². We computed the area covered by each constituent point cloud by fitting a two-dimensional hull to the points projected onto a horizontal plane. Then, an area threshold was used to drop any point cloud that covered less than 90% of the total plot area (Figure 2).

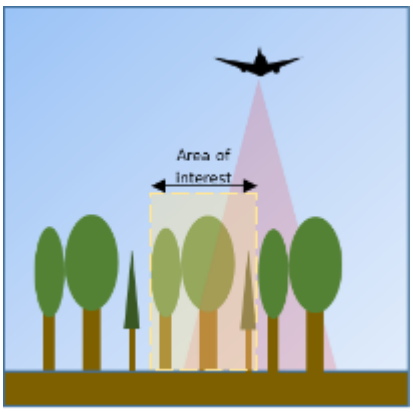

Figure 2: Flight lines that partially cover a plot

The flight trajectory data was used to extract the locations of the aircraft while scanning respective field plots, and the average location of the aircraft was computed. The azimuth of the scan was calculated as the angle with respect to geographic north between the average location of the aircraft and the respective field plot centre. Each point cloud results from unique scan geometry that is characterised by the mean scan angle, scanning azimuth, and scanning distance.

Two kinds of datasets were considered. In the first kind of dataset, point clouds were not separated based on the flight lines. This dataset was called the *standard* dataset and contained as many point clouds as field plots in the study (291). Point clouds were separated based on the flight line information for the second dataset, called the *expanded* dataset. In the *expanded* dataset, there were

from one to eight point clouds per field plot resulting in 1095 point clouds and corresponding to a mean number of 3.8 point clouds per plot.

4.2.4 Lidar metrics

Lidar metrics were computed for each point cloud in both datasets after normalising the point clouds in height, i.e., transforming the point elevation into height above the ground using the lidar-derived DTM. All points below a height threshold of five meters were considered lower vegetation and filtered out. Fifty-five metrics related to heights, intensities, canopy and terrain properties and scan geometry were computed. The height-based metrics are the statistical distributions computed for the Z values of the point cloud. The intensity metrics comprise statistical descriptors of the intensity values. Canopy metrics consist of gap fraction (Hopkinson et al., 2004) and rumple index (Jenness, 2004). The gap fraction was computed as the ratio of the number of returns below the 5m threshold to the total number of returns. Rumple index is the ratio of the 3D surface area of the canopy to the surface area of the ground. Gap-fraction and rumple index were found to be very sensitive to the scan angle (Dayal et al., 2020). The summary of these metrics is given in Table 3.

Type of metric	Metrics
Height based	max, mean, standard deviation of heights percentiles of heights, skewness of heights (first and last returns), kurtosis of heights (first and last), entropy, percentage of echoes above mean, layer wise cumulative percentage of echoes
Intensity-based	total, mean, max, standard deviation, skewness, kurtosis, layer-wise cumulative percentage of echoes, percentage of total intensity below percentiles (10, 30, 50, 70, 90)
Echoes	Percentage of n^{th} echoes
Canopy properties	gap fraction, rumple index
Terrain properties	slope, aspect, elevation
Scan geometry	mean scan angle, scan azimuth and distance from the plane

Table 3: Summary of the metrics obtained from lidar data, terrain properties and scan geometry

Point clouds can change according to the local topography and viewing configuration for a given forest plot. Depending on the slope, orientation, elevation, scan angle, and aircraft position, there could be several cases. In Figure 3, the illustrations depict two possibilities of lidar scanning a plot on a slope with similar scan angles, a) scanning *along* the slope and b) scanning *against* the slope.

An example of a point cloud scanned from different directions is shown in 3c, wherein two point clouds with similar mean scan angles can have different properties due to the interaction between terrain properties and scanning parameters. Information on terrain properties and scan geometry were thus added as additional variables (Table 3). Terrain information was computed by generating digital terrain models (DTM) of a resolution of 1m. The DTM of each plot was used to generate slope and aspect maps. The average slope, aspect, and elevation values were computed from the slope and aspect maps and DTMs, respectively.

The values of the dependent variables, i.e., *BA* and V_{tot} and terrain properties (slope, azimuth, and elevation), were replicated for each plot depending on the corresponding number of flight lines or point clouds. All the values were scaled between 0 and 1. All lidar metrics were computed using the lidR package in R (Roussel et al., 2020).

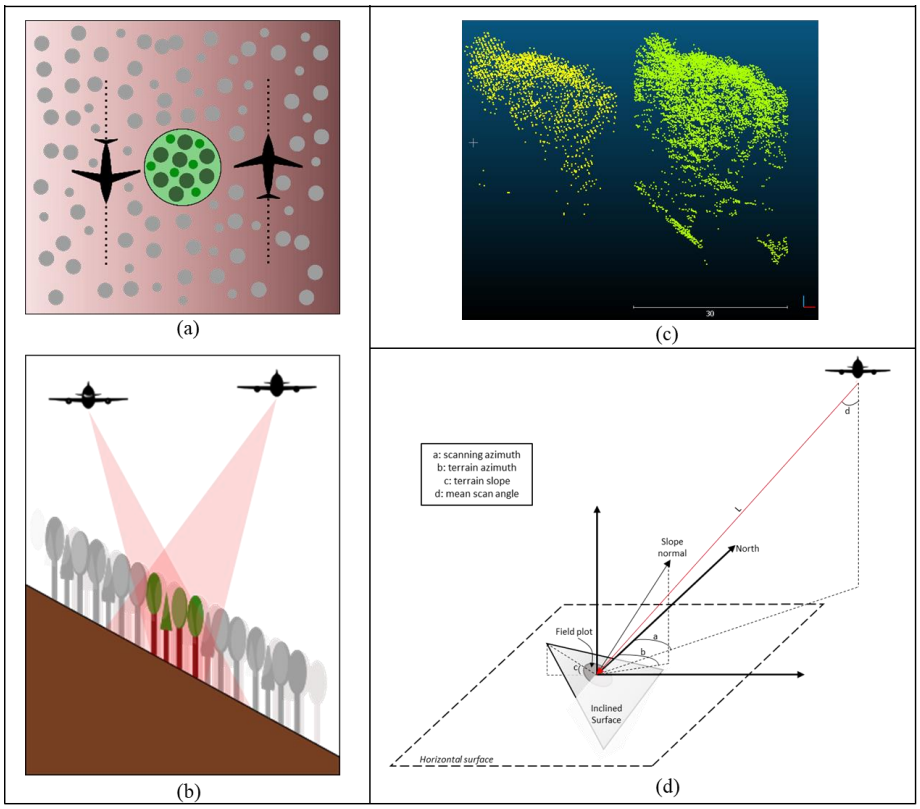

Figure 3: Illustration of lidar scanning along the slope and against the slope. (a) top view; (b) side view; (c) example point clouds with similar mean scan angle 26° (yellow) and 22° (green) ; (d) example scan geometry with relevant parameters

4.2.5 Experiments and cross-validation scheme

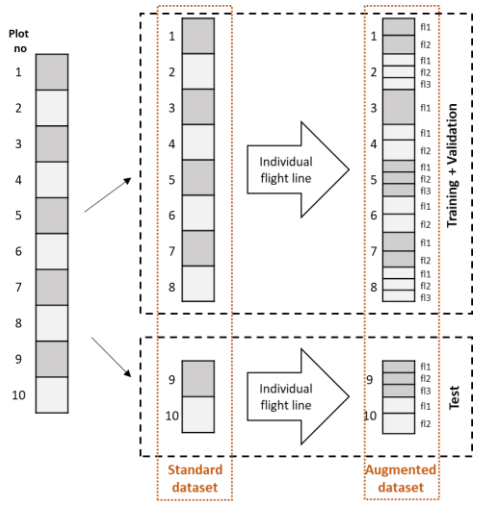

Figure 4: Illustration of the cross-validation scheme for standard and augmented datasets. The process was repeated 30 times (30 splits).

We used the same splits of data as those used for cross-validation of the models in Lahssini et al. (2022) to enable a direct comparison to results from our study. The field plot measurements and corresponding lidar metrics were split in the standard dataset into training and test sets. The training set was further subdivided into training (191 field plots or samples) and validation set (50 field plots or samples), with roughly an 80: 20 ratio. The test set (50 field plots or samples) was completely blind to the training and validation sets. The dataset generated in this way is referred to as the *standard* dataset. When the point clouds were considered per flight line, there were 1095 samples total, while the number of field plots was still the same (291). This dataset is referred to as the *expanded* dataset on account of the higher number of point clouds based on flight lines. We used the field plot ids from the test set of the *standard* dataset to create the corresponding test (and training) set(s) of the *expanded* datasets. This ensured that point clouds for the sample field were not present in both the test and training sets (data leakage). However, the training set was randomly divided into an 80: 20 ratio, which ensured that there were chances of some point clouds for the same plots being present in both training and validation sets to aid the model fitting process. The cross-validation scheme is illustrated in Figure 4. Thirty splits containing training, validation, and test data were generated for all the datasets.

The benefit of the data expansion strategy was tested via three experiments.

1. The *standard* dataset (*std)* comprising only the lidar metrics was used to build a model and then compared with a model built with the *expanded* dataset (*exp)* comprising only the lidar metrics.

2. The *standard* dataset was appended with terrain variables (slope, azimuth, and elevation) ($std_{terrain}$) to build a model and compared to a model built with the *expanded* dataset also appended with terrain variables ($exp_{terrain}$).
3. The *expanded* dataset was appended with both terrain and scan geometry variables ($exp_{terrain+scan}$).

Indeed, scan geometry features are not available along with standard lidar metrics as, in this case, the point cloud results from a mixture of scanning configurations. The workflow used in the study is illustrated in Figure 5.

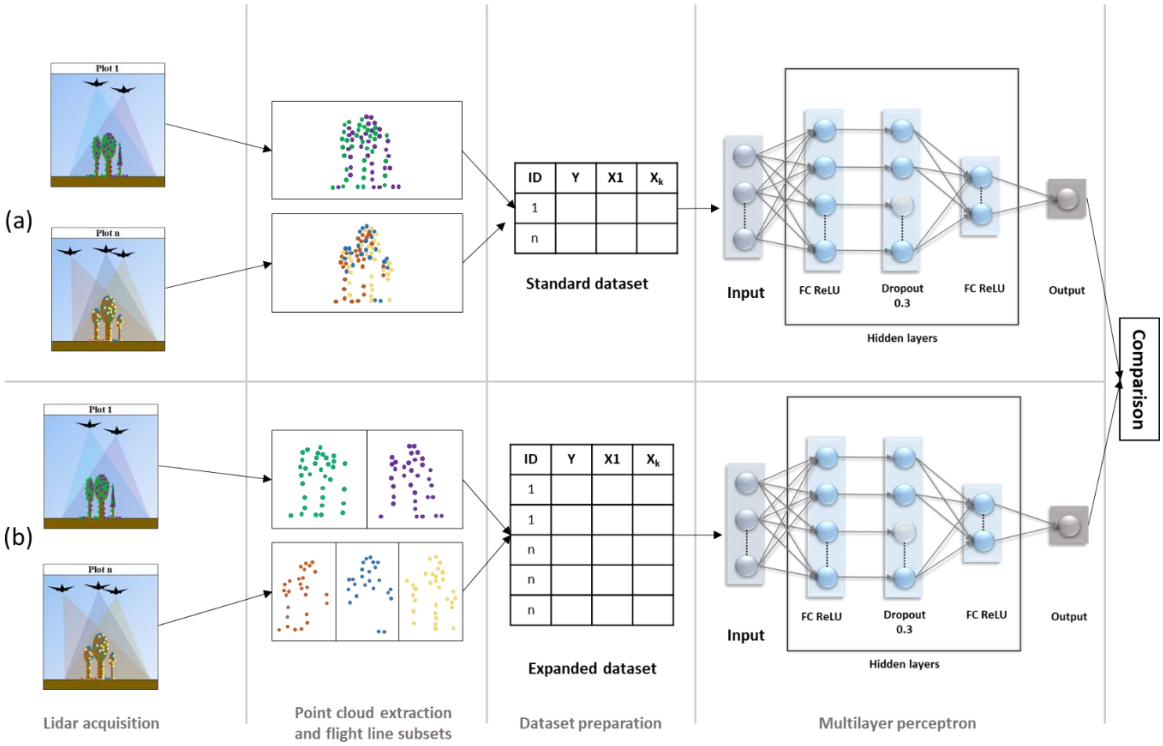

Figure 5: Illustration of the workflow employed in the study using a multi-layer perceptron

4.2.6 Regression models

We used the TensorFlow (2.6.0) library in Python (3.9.7) for the fully connected multilayer perceptron (MLP) (Martín Abadi et al., 2015). The MLP network consisted of two hidden layers. Each neuron in a layer is fully connected (FC) to all the neurons in the following layer. The components of the designed MLP include the input layer, two hidden layers, and an output layer. The rectified linear units (ReLU) function was used as the activation function. It defines how the input values it receives are output to the next neuron. A dropout rate of 0.3 was used to regularise the network to prevent overfitting. The adaptive moment estimation (ADAM) optimiser was used for the optimisation of the network. The network is illustrated in Figure 5. The KerasTuner (O'Malley et al.,

2019) was used for the hyperparameter optimisation to obtain three hyperparameters: a) the number of neurons in the first hidden layer, b) the number of neurons in the second hidden layer, and c) the learning rate of the Adam optimiser. The tuned hyperparameters are given in the results section (Table 3). Random forests (RF) models were also built for all the datasets to compare the performances with the MLP network. The number of trees built were 500 and mtry value was set to default, i.e. number of independent variables divided by 3. The model was implemented using the randomForest package in R (Liaw and Wiener, 2002).

4.2.7 Model accuracy assessment

The goodness-of-fit of the MLP and RF models was assessed using the determination coefficient (R^2), the Root Mean Squared Error (RMSE), the relative Root Mean Squared Error (rRMSE), and the Mean Percentage Error (MPE). The formulae for these measures are as follows:

$$R^2 = 1 - \frac{\sum_1^n (y_i - \hat{y}_i)^2}{\sum_1^n (y_i - \bar{y})^2} \quad (1)$$

$$RMSE = \sqrt{\frac{\sum_1^n (\hat{y}_i - y_i)^2}{n}} \quad (2)$$

$$rRMSE = \frac{RMSE}{\bar{y}} * 100 \quad (3)$$

$$MAE = \frac{\sum_1^n |(y_i - \hat{y}_i)|}{n} \quad (4)$$

Depending on the number of flight lines that scanned a given plot, there could be multiple predictions per plot for models built with the three kinds of expanded datasets (*exp*, $exp_{terrain,}$ and $exp_{terrain+scan}$). The median value was considered for computing the goodness-of-fit criteria.

4.3 Results

4.3.1 Hyperparameter tuning

Dataset	Basal area	Total volume
Standard (metrics) or *std*	(256, 32, 0.01)	(256, 64, 0.01)
Standard (metrics + terrain) or $std_{terrain}$	(256, 64, 0.01)	(256, 32, 0.01)
Expanded (metrics) or *exp*	(1024, 32, 0.001)	(1024, 64, 0.001)
Expanded (metrics + terrain) or $exp_{terrain}$	(1024, 128, 0.001)	(1024, 128, 0.001)
Expanded (metrics + terrain + scan geometry) or $exp_{terrain+scan}$	(1024, 128, 0.001)	(1024, 128, 0.001)

Table 4: Summary of the tuned hyperparameters for different experiments (neurons in the first hidden layer, neurons in the second hidden layer, learning rate)

Tuning for each dataset resulted in different hyperparameters. The tuned hyperparameters are given in Table 4 [Table 4 near here]. Tuning for the standard and expanded datasets resulted in two options

for the number of neurons in the first hidden layer. For the standard datasets, there were 256 neurons, while for the expanded datasets, the tuning resulted in 1024 neurons. For the second hidden layer, the number of neurons varied between 32, 64, and 128. The learning rate was either 0.01 (*std*) or 0.001(*exp*).

4.3.2 Model performances

Forest attribute	Dataset	R^2		MPE		RMSE		rRMSE%	
		MLP	RF	MLP	RF	MLP	RF	MLP	RF
Basal area	*std*	0.66	0.53	6.7	7.9	8.9	10.4	30.5	35.8
	$std_{terrain}$	0.77	0.58	5.4	7.4	7.3	9.8	25	33.6
	exp	0.76	0.54	5.7	7.8	7.5	10.4	26	35.7
	$exp_{terrain}$	0.81	0.61	5	7.2	6.7	**9.5**	21.3	**32.6**
	$exp_{terrain+scan}$	**0.83**	**0.60**	**4.7**	**7.2**	**6.2**	**9.5**	**19.9**	**32.6**
Total volume	*std*	0.71	0.57	78.2	95.0	103	126.2	34.4	42.2
	$std_{terrain}$	0.77	0.62	71.7	89.2	96.2	117.5	32.2	39.3
	exp	0.78	0.55	68.2	96.8	91.3	129.7	30.5	43.2
	$exp_{terrain}$	0.83	0.64	57.6	86.5	77.9	115.1	26	38.3
	$exp_{terrain+scan}$	**0.85**	**0.64**	**54.6**	**86.2**	**71.8**	**114.6**	**24**	**38.1**

Table 5: Compilation of the goodness-of-fit criteria for all the experiments. Best results for each models, i.e. for MLP and RF, respectively, are underlined in bold. Results of the best model are framed in red.

The R^2, MAE, RMSE, and rRMSE are presented in Table 5 [Table 5 near here] for both MLP and RF models. The observed and predicted values for *BA* and V_{tot} are shown in Figure 6 and Figure 7, comparing the results of the MLP ABA models built with a) *std* and *exp* datasets, b) $std_{terrain,}$ and both $exp_{terrain}$ and $exp_{terrain+scan}$, respectively. We rebuilt the models with *std* and $std_{terrain}$ and observed that the goodness-of-fit criteria were higher for models with both *std* and $std_{terrain}$ (*BA*: R^2 of 0.66 and 0.71; V_{tot}: 0.71 and 0.77) compared to Lahssini et al., (2022) (*BA*: R^2 of 0.61 and 0.69; V_{tot}: 0.67 and 0.74).

The regression lines in Figure 6 reveal a bias in the predictions for MLP. The plots with higher values of *BA* and V_{tot} have underestimated predictions, and those with lower values have slight overestimations, especially for BA.

MLP systematically outperformed RF. The RF R^2 was lower by 19% (*BA and* V_{tot}, *std*). The differences in R^2 between MLP and RF increased across the datasets highest differences for the $exp_{terrain+scan}$ datasets for *BA* and V_{tot}. The rRMSE values with $exp_{terrain+scan}$ datasets were higher for RF by approximately 60% for both *BA* and V_{tot}.

Regarding the data sets used, the trends were similar for MLP and RF. The lowest model accuracies were observed for the model built with the *std* datasets (*BA*: R^2=0.66 and 0.53, rRMSE=30.5% and

35.8%; V_{tot}: R^2=0.71 and 0.57, rRMSE=34.4% and 35,8%, for MLP and RF, respectively). The *exp* datasets demonstrated relative improvements for the MLP (*BA*: R^2=0.76; rRMSE=26%; V_{tot}: R^2=0.78, rRMSE=30.5%) with 15% and 10% increase in R^2 and 15% and 11% percentage points reduction in the rRMSE for *BA* and V_{tot}, respectively. Incorporating terrain properties ($std_{terrain}$) resulted in better models with both MLP and RF.

However, in contrast to the MLP, RF models did not benefit from the data expansion (datasets *exp*). *BA* predictions improved marginally (R^2:0.54 for *exp* vs 0.53 for *std*) while V_{tot} predictions deteriorated (R^2:0.55 for *exp* vs 0.57 for *std*). RF models with $exp_{terrain}$ were better than those with $std_{terrain}$ for both *BA* (R^2:0.58 for $std_{terrain}$ vs 0.61 for $exp_{terrain}$) and V_{tot} (R^2:0.62 for $std_{terrain}$ vs 0.64 for $exp_{terrain}$) with increases of 5% and 3% in R^2 values, respectively. There errors reduced in the range of 3%-5%. [Figure 6 near here] [Figure 7 near here]

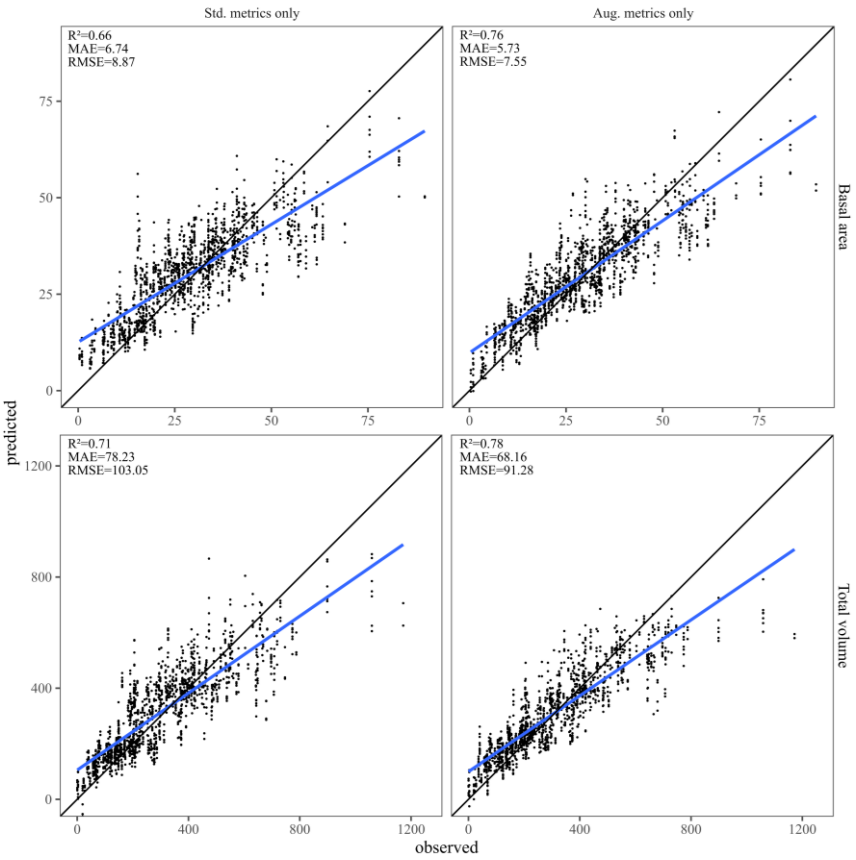

Figure 6: Scatterplots of predicted and observed values for models built with std and aug datasets

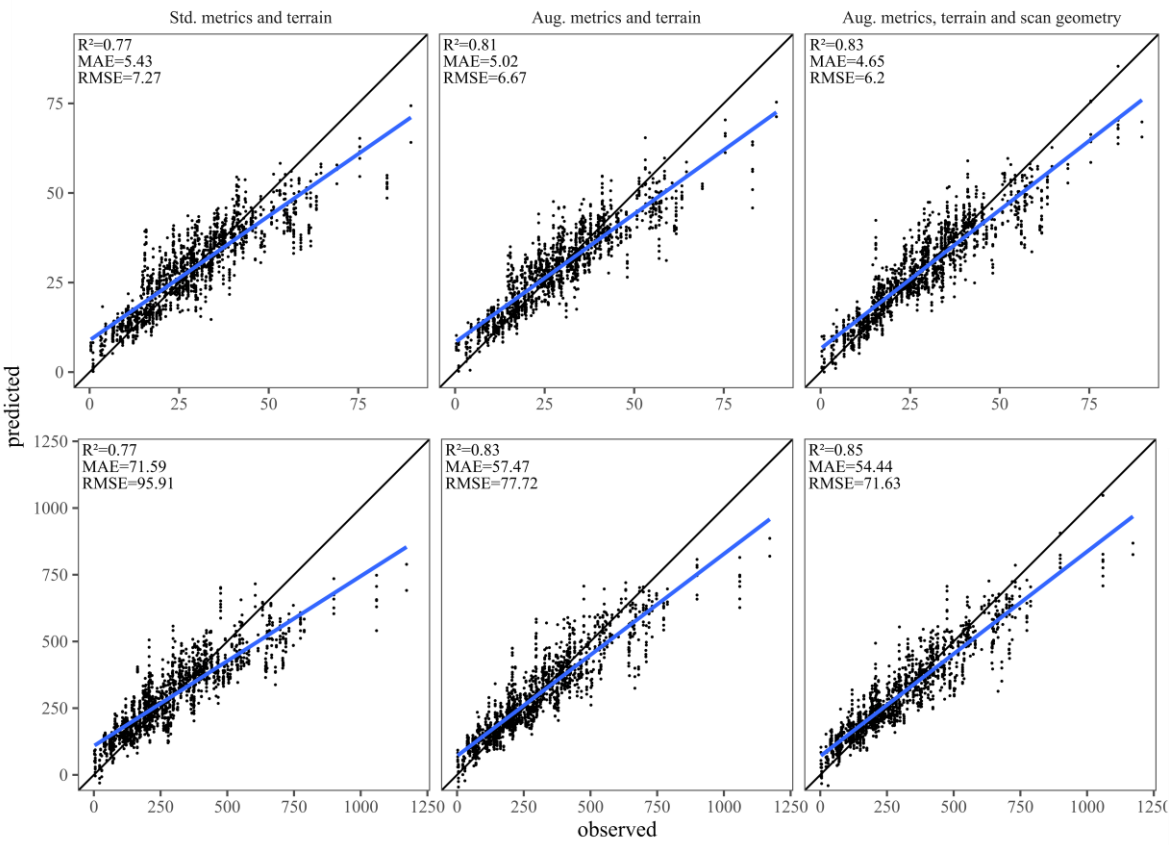

Figure 7: Scatterplots of predicted and observed values for models built with $std_{terrain}$, $aug_{terrain}$ and $aug_{terrain+scan}$ datasets.

The MLP models built with $std_{terrain}$ resulted in better goodness-of-fit values (*BA*: R^2=0.77, rRMSE=25%; V_{tot}: R^2=0.77, rRMSE=32.2%) than those built with *std* datasets (*BA*: R^2=0.66, rRMSE=30.5%; V_{tot}: R^2=0.71, rRMSE=42.2%). The goodness-of-fit of models built with $exp_{terrain}$ datasets were better for both *BA* and V_{tot} (*BA*: R^2=0.81, rRMSE=25%; V_{tot}: R^2=0.83, rRMSE=32.2%) with increases of 5% and 8% respectively. The three error goodness-of-fit criteria (MAE, RMSE, and rRMSE) reduced in the 7% to 15% range and around 19% for *BA* and V_{tot}, respectively. Incorporating additional information about the scan geometry ($exp_{terrain+scan}$) resulted in slightly better MLP models with 3% higher R^2 values and lower errors in the 5%-8% range for both *BA* and V_{tot}. The RF models with $exp_{terrain+scan}$ datasets did not result in any improvements (less than a 1% reduction in errors).

In addition, in Figure 6, the saturation problem of underestimating large values is evident. It appears to be well-handled by the MLPs when combined with terrain information and scan information.

4.4 Discussion

Hyparameter tuning was a crucial step in this study. The models built with *std* and $std_{terrain}$ datasets for both *BA* and V_{tot} were better than those observed in Lahssini et al. (2022). This could be due to variations in hyperparameter tuning resulting in better models and underlining the importance of the

tuning process to obtain better models. The random initialisations of the algorithms used in the models may yield varying hyperparameters. In our experiments, we observed the learning rate as an essential parameter and often tuned to 0.001 for the expanded datasets.

A prevalent problem regarding saturation was also observed in this study with *std* datasets for both basal area (*BA*) and total volume (V_{tot}). The saturation issue was handled well by a deep-learning-based fusion strategy using lidar and optical (Sentinel-2) datasets (Lahssini et al., 2022). In this study, however, the saturation effects appear less apparent for models built with expanded datasets consisting of terrain properties ($exp_{terrain}$ and $exp_{terrain+scan}$ datasets). The changes in lidar point cloud geometry may convey information on species composition at the plot level, as done by the Sentinel-2 time series study by Lahssini et al. (2022).

The models with expanded datasets consistently outperformed those with corresponding standard datasets. However, between $exp_{terrain}$ and $exp_{terrain+scan}$, the R^2 values improved for MLP models from 0.81 to 0.83 and 0.83 to 0.85 for *BA* and V_{tot}, respectively. It appears that the improvement was not of a large magnitude. The goodness of fit criteria for RF was stable when comparing the two data sets. This could be attributable to the fact that there may be some redundancy in the information offered by the point clouds that were considered independent observations. Figures 3a and 3b illustrate the differences in point clouds due to slope, even if the scan parameters are nearly similar due to the steep slope. Irrespective of the variations due to differences in scan angle, the slope directly affects the point cloud and the resulting lidar metrics (see Figure 3c). The MLP is perhaps able to learn this relationship in this instance. There is, however, scope to better model the relationship between the scan properties and terrain properties analogous to the concept of topographic normalisation of optical images (Gu and Gillespie, 1998).

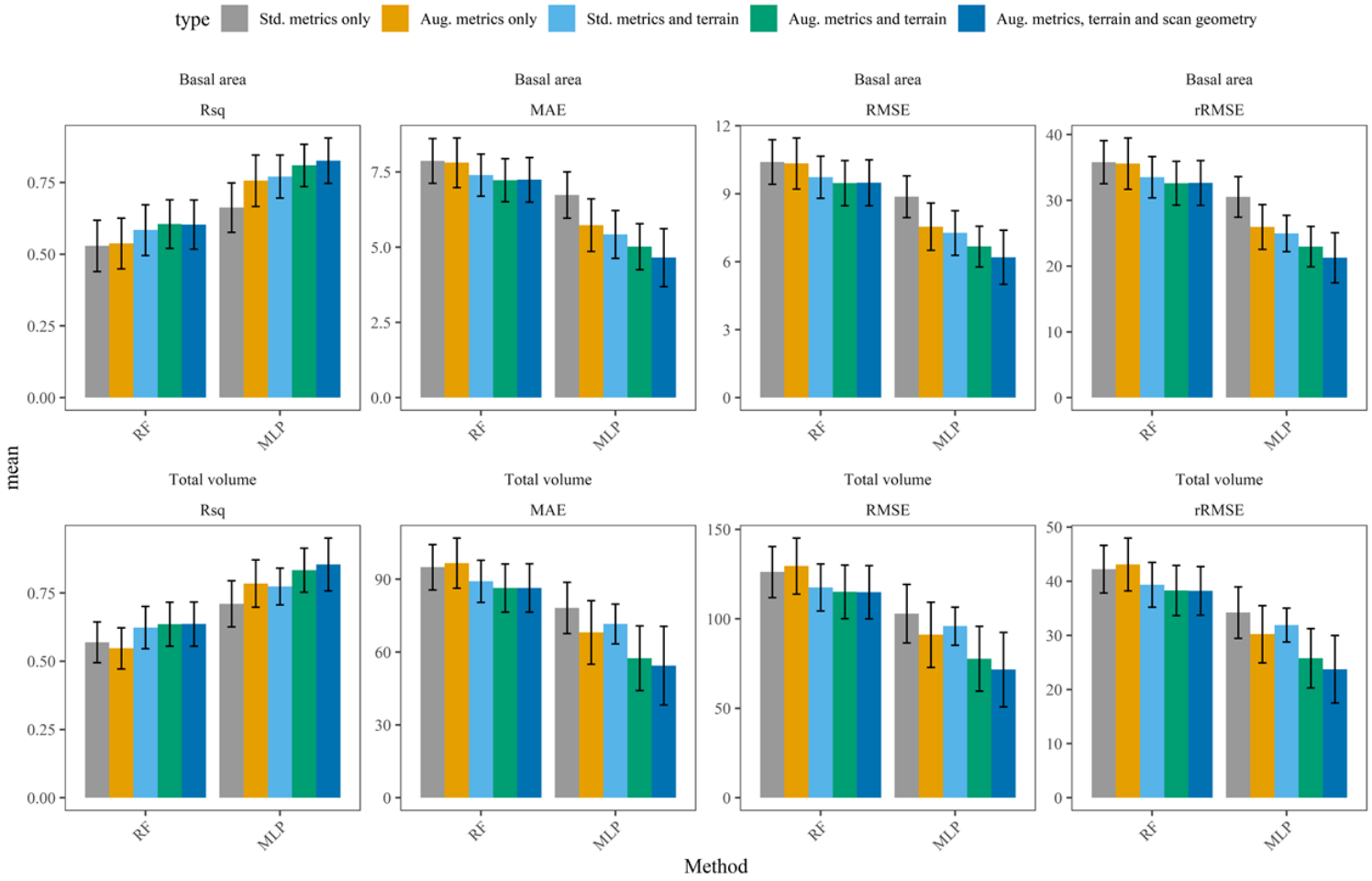

Figure 8: Graphical illustration of the goodness-of-fit criteria. The bars represent the standard deviations of the results obtained for 30 splits of data

Nonetheless, the addition of scan geometry demonstrated improvements with the MLP. A qualitative assessment of the scatterplots in Figure 7 reveals that a model built with $exp_{terrain+scan}$ dataset was indeed capable of dealing with the issue of saturation that is commonly observed with large values. The scatterplots are comparable to those obtained in Lahssini et al. (2022) after implementing a fusion of lidar and optical information, and this creates interesting possibilities for future studies. Furthermore, while the MLP outperformed the RF models, some of the relative improvements across the datasets, though marginal, were apparent even in the RF models.

Modelling strategies certainly influence the results. A few studies have explored different deep-learning methods to predict forest attributes from lidar data. Martins-neto et al., (2021) used an MLP architecture with the principal components of a set of metrics similar to our study. They observed an rRMSE of 22.5% for the predictions of BA in heterogeneous tropical forests. In our study, the best performing model was the $exp_{terrain+scan}$ dataset with an rRMSE of 19.9%. However, they did not consider metrics such as the gap-fraction with proven explanatory power for forest structure characterisation.

Additionally, gap-fraction and the rumple index (used in this study) are metrics that are sensitive to lidar scan angle (Dayal et al., 2020; Montaghi, 2013). The data expansion strategy may have benefited from additional information from these two metrics, among other sensitive metrics. On the other hand, Liu et al. (2021) observed lower rRMSE values of 14.5% in volume predictions in predominantly Eucalyptus, and Chinese-fir-dominated stands. In comparison, an rRMSE of 24% was observed in this study. Even if they used a more advanced modelling framework that combines a fully-connected neural network and an optimised radial basis neural network, the result difference is also likely to be linked to relatively simpler forest stands under study. In addition, studies using other modelling methods, such as OLS or RF, reported rRMSE values of basal area (BA) and volume (V_{tot}) predictions were in the range of 23% to 29% and 22% to 34%, respectively (Coops et al., 2021). In this study, we observed an rRMSE for BA and V_{tot} of 19.9% and 24% for a model built with $exp_{terrain+scan}$ datasets.

We used the intensity information provided by the data provider without implementing a normalisation step to enhance it, as demonstrated in different studies (Gatziolis, 2011; Hopkinson, 2007; Martins-neto et al., 2021). Shi et al. (2018) demonstrated that intensity information is more effective than other height-based metrics in discriminating tree species. The forests in PNR Bauges comprise forest plots of broadleaved, coniferous, and mixed types of forests with different species of vegetation. Calibrated intensity information could further help in improving the accuracies of the models. In addition, the intensity information is also known to be affected by the scan angle (Martins-neto et al., 2021).

The distribution of *BA* and V_{tot} across different test sets reveals that the dataset was not balanced as there are very few plot measurements with very high values. Many of the cross-validation splits used in this study (and in Lahssini et al., (2022)) also suffered from a lack of balanced training and testing samples. We believe that field plot measurement representing diverse forest stands will further help build robust models. The sampling strategy used to collect field measurements followed a systematic sampling scheme to establish sites for periodic monitoring. A stratified sampling scheme would be more suitable for building models. Moreover, some differences may arise because small trees (DBH<7.5cm) were not measured as per the field measurements protocol. The contribution of such trees in estimating the signal could be higher.

Dayal et. al. (2022) demonstrated the benefits of using voxel-based metrics. Voxel-based metrics contributed by reducing rRMSE values for ordinary least squares regression (OLS) ABA models based on forest type (riparian, broadleaf, coniferous, and mixed). For OLS ABA models, using voxel-based metrics improved the predictions by reducing the rRMSE by 10%, 4%, and 14% for riparian, broadleaf, and mixed types, respectively. The rRMSE values for different forest types and with only four lidar metrics (including voxel-based metrics) ranged between 30%-40%, comparable to those observed with MLP models built with *std*, $std_{terrain,}$ and *exp* datasets in this study. However, including normalised intensity information along with stand type characteristics and voxel-based metrics could be beneficial for building better models using deep-learning approaches and a possible future area of exploration.

In this study, we opted to describe our datasets based on the flight lines as 'expanded datasets.' The common practice combines all these observations in lidar ABA models to generate the 'standard' datasets. Essentially, each observation in the dataset represents an independent physical observation (or lidar scanning) of a given field plot. As the vegetation in the field plots is rarely identical when viewed from multiple directions, it may be argued that the resulting differences from different scans are comparable to the data augmentation procedure that is commonly used to increase the number of samples when dealing with images (Mikolajczyk and Grochowski, 2018; Shorten and Khoshgoftaar, 2019; Taylor and Nitschke, 2019; Wang et al., 2017). In order to avoid confusion with commonly practised data augmentation strategies, we referred to our modified datasets as 'expanded' datasets. Nonetheless, we would like to emphasise the similarities.

4.5 Conclusion

This study demonstrated that considering point clouds from different flight lines as independent observations in non-parametric models can improve ABA predictions for forest attributes. By considering the point clouds as independent observations, we retained the heterogeneity in the lidar metrics due to variations in the acquisition geometry in the form of an expanded dataset with a

significantly higher number of observations than a standard dataset. A multilayer perceptron (MLP) could harness the expanded information to predict forest attributes with higher accuracies than a Random Forest model, commonly used in ABA approaches. The present MLP model also demonstrated the potential to result in predictions comparable to methods involving the fusion of optical and lidar data (Lahssini et al., 2022). Optical data may be incorporated to improve further the results observed in this study.

Considering point clouds from different flight lines could be used to revisit existing lidar datasets to improve the ABA predictions by harnessing both the homogeneity and heterogeneity alike of lidar metrics (Dayal et al., 2020) when field plots are scanned from multiple locations. The different perspectives of the same field plots could help develop robust models.

Furthermore, the point clouds from different flight lines were considered independent observations for simplicity. In reality, they are observations of the same field plot and can be grouped based on field plots, resulting in a longitudinal dataset. A longitudinal dataset contains repeated observations of the same entity over different periods, which, in this case, happens to be the scan geometry. Longitudinal datasets are dealt with differently with methods such as pooled OLS or fixed-effects model, among others, or deep learning methods such as recurrent neural networks and their variations. Such methods could be possible alternatives that may be employed to extract the maximum amount of information from such lidar data.

Acknowledgements

This study was carried out in the framework of the PROTEST project, supported by the French Agency for Ecological Transition (ADEME) (grant 1703C0069, GRAINE program), and the FRISBEE project, supported by the TOSCA Continental Surface program of the Centre National d'Etudes Spatiales (CNES) (order N° 4500070632). It also benefited from the support of the French region of Occitanie with funding a part of the PhD scholarship of K.R. Dayal. The authors would also like to thank the team comprising Harri Evers, Charly Feppon, and Éric Mermin for field measurements.

Chapter 5: Conclusion

5.1 Synthesis of the thesis

The ability to exercise the accurate measurement capabilities of lidar over vast areas of vegetation makes it the most suitable remote sensing technique for forest management purposes. The increasing use of lidar globally is evidence of its potential. Its use has been incredibly beneficial for forest inventories by making it possible to obtain information at a very high level of detail. Linking field plot measurements with accurately measured lidar data for the same, also known as area-based approaches (ABA), is the most common way to arrive at predictions of forest attributes at a fine scale. However, the lidar scanning mechanism and its scan parameters make it challenging to have uniformly dense point clouds everywhere. One of the parameters, the lidar scan angle, has been insufficiently studied, and in recent years understanding its influence on lidar metrics and ABA models has assumed importance. As a convention, scan angle has been limited to less than 15-20 degrees for most studies using lidar for scanning forests. A low scan angle poses challenges to many national-level lidar acquisitions seeking operational efficiency. Even local-level lidar acquisitions benefit from a wider scan angle, reducing operation costs. Furthermore, data acquisition using UAV lidar often employ high scan angles. Therefore, it is imperative to understand and study further the effect of using such.

Lidar scan angle is integral to the acquisition geometry defined by the scanning parameters, terrain, and vegetation properties. This PhD thesis studied the effect of different acquisition geometries on lidar-based ABA models in different complex forest environments. The study was conducted in two broad parts covered in three main chapters of the thesis. In the first part of the study, the effect of lidar scan angle on lidar metrics and ABA models was assessed. In the second part of the study, different strategies to manage the impacts of scan angle were explored. The study had five specific questions; the main findings per question are summarised below. Finally, the limitation of the study and future perspectives will be discussed at the end.

5.1.1 Assessing the impact of lidar scan angle on ABA models in diverse, complex forest environments.

Q1) What is the impact of lidar scan angle on commonly used lidar metrics?

This study objective demonstrated that different lidar metrics are differently sensitive to the scan angle. 11 lidar metrics (9 height metrics and two canopy metrics) were analysed to understand their behaviour under changing scan angle. The scan angle impacted some metrics, such as gap fraction and rumple index, while impacting others, like p10 (10th percentile), to a lesser extent. Mean, max (maximum), and p90 are substantially less affected by scan angle. Similar findings were observed in Montaghi (2013), who studied boreal forests. Contrastingly, Yang et al. (2011) found that the higher percentiles (100^{th} percentile) were more sensitive to scan angle for simulated deciduous forest

environments with full waveform data. Irrespective of the differences in the study areas, it is clear that it is impossible to have universal assumptions regarding the effect of scan angle on lidar metrics. Although conceptual ideas may guide hypotheses, it is recommended to be mindful of the sensitivity of lidar metrics to scan angle while planning lidar acquisitions. For example, it is a reasonable hypothesis that a metric such as gap-fraction, which has proven capabilities to characterise vegetation structure, will undoubtedly be biased when assessed from the point cloud distribution since the path length increases with increasing scan angle. This behaviour may be emphasised further when the acquisition geometry changes with higher slopes in mountainous terrain. Based on the observations in this chapter, a predefined model was selected consisting of metrics with different sensitivities to scan angle to study the inclusion of these metrics in the same.

Q2) What is the impact of including lidar metrics sensitive to scan angle on ABA models?

An attempt was made to answer this question by simulating different acquisition geometries by resampling existing lidar datasets. The simulated sets of data broadly were of two kinds a) composed only of point clouds scanned from only one flight line (single flight line set, *fl1*) and b) composed only of point clouds scanned from any two flight lines (double flight line set, *fl2*). The idea was to evaluate and compare the behaviour of ABA models built with the same lidar metrics for the single flight line set for the same area and when using two sets of metrics more or less sensitive to scan angle. Models to predict wood volume (stem and total volumes) and basal area were evaluated for three different and complex stands (riparian area and broadleaved, mixed and coniferous stands in a mountainous area) through a leave-one-out cross-validation approach. In an ideal scenario where lidar metrics are not affected by the acquisition geometry (scan angle), the models should result in similar predictions. In other words, there will be no variations in the goodness-of-fit criteria. However, as demonstrated in Chapter 2, different lidar metrics are affected differently. Firstly, models were built using two highly explanatory metrics (mean and variance of heights) that were found to be relatively less sensitive to scan angle. Secondly, models were built using two additional explanatory metrics, gap fraction (P_f) and coefficient of variation of LAD profile (CV_{LAD}) (Bouvier et al., 2015), which were more sensitive to scan angle. With models built with the mean and variance of heights as references, using the simulated datasets, the inclusion of P_f and CV_{LAD} increased the variations in the accuracy (R^2) of the predictions across experimental scenarios (see Chapter 3) by an average of 171%. However, it does not mean they are not beneficial. Inclusion of the metrics, while increasing the standard deviation (SD) of the predictions, also increased the average accuracy by 8% (except for coniferous forests). Results were relatively more stable when models were built with the second data set (*fl2*), i.e. two flight lines scanning each forest plot. Different acquisition geometries may not be well represented when few field plots exist. Building a model for such lidar acquisitions will undermine the accuracy of predictions of attributes in datasets (or areas) scanned with different geometries. If lidar data is acquired from single flight lines, the risk of a poorly

specified model will increase, resulting in unreliable forest attribute maps. It may be the case that even a few plots that are not scanned well may impact ABA models. Therefore, it is essential to develop approaches to manage scan angle effects when developing ABA models.

5.1.2 Methods to manage the impacts of lidar scan angle on ABA models

Q3) How does overlap in lidar data acquisition influence the quality of ABA models?

Overlapping of flight line swaths is mainly done to ensure areas on the ground are sampled from multiple locations to create a dense point cloud representation of the vegetation. The data acquisition in both the study areas was carried out with sufficient overlap to ensure that many, if not all, field plots were scanned from multiple locations. Some field plots in the Bauges dataset were scanned from as many as eight flight lines enabling eight different point clouds from individual flight lines and 28 different point clouds from any two flight lines. The average number of flight lines from which scanned a plot was approximately four (3.8). There was sufficient variability in the combinations of point clouds in both study sites to investigate to what extent the combination of different 'points of view' could help manage the impact of scan angle. The first set of simulated datasets corresponds to absolutely zero overlaps (single flight line set), and the second set corresponds to 50% overlap (double flight line set). Datasets resampled in terms of any three flight lines were also included for comparison despite the lack of variability of point clouds due to an insufficient number of flight lines (triple flight line set). The standard deviations of the goodness-of-fit criteria distribution were reduced by an average of 42% for double flight line sets compared to the single flight line sets.

Constraints were also applied to the single and double flight line sets to simulate specific acquisition geometries. There were six acquisition geometries obtained by filtering flight lines belonging to: only nadir (*A*), slightly off-nadir (*B*) and off-nadir (*C*) from single flight line sets, and their combinations (*AB, AC* and *BC*) from double flight line sets. There was a reduction in the SDs of the R^2 distribution by an average of 45% for all comparisons of *AB, AC* and *BC* with *A, B* and *C*. At the level of the forest types, these reductions were 51%, 62%, 21% and 46% for riparian, broadleaf, coniferous and mixed forest types. Therefore, ensuring at least a 50% overlap to scan any given area from two different locations could curtail the variability in predictions due to varying acquisition properties.

On the other hand, the means of the goodness-of-fit criteria distributions revealed an interesting phenomenon. The means represent the average accuracies of the models in each set (*fl1, A, B, C, fl2, AB, AC* and *BC*). It would seem intuitive to ensure overlaps will result in dense point clouds and more accurate models. Based on the results observed in this study, it may only be partially true. The mean R^2 values predictions for *fl1* datasets were lower than those for *fl2* datasets only for the riparian and mixed plots. For the broadleaf and coniferous plots, the opposite, i.e. the predictions were better

with individual flight line datasets (*fl1*) than with double flight line datasets (*fl2*). There was a considerable difference for coniferous plots. The fl2 dataset mean R^2 was almost 30% lower than that for the *fl1* dataset. The trend was more apparent in comparison with the results for *fl3*. The trend was reinforced when compared to the single point goodness-of-fit values for models built with all the point clouds from different flight lines considered together, i.e. the traditional ABA models. The trend of better models with single flight line point clouds was also observed by van Lier et al. (2021) for balsam fir-dominated stands. Across *fl1*, *fl2* and *fl3* datasets, there was a tendency to converge at the goodness-of-fit criteria of the traditional models. The results underline that, even with lower values for the goodness of fit criteria, models built with datasets acquired from multiple flight lines in every forest location will be more robust and reliable. However, our results also open up questions regarding such contrasting trends, with mean trends better with a single flight line than with two or three for some of the stands.

Furthermore, despite the changes in the acquisition geometry between the two study areas, i.e. Ciron and Bauges, the goodness-of-fit distributions for different acquisition geometries (*f1, A, B, C fl2, AB, AC, BC* and *fl3*) indicate that some inclination (*B*) is desirable. In addition, as acquiring data with high overlap between flight lines is costly and could hinder the use of lidar for forestry applications, it is worthwhile to develop strategies to better deal with the influence of scan angles on metrics and models. Some approaches in that regard have been addressed through the two last questions.

Q4) How to normalise lidar metrics sensitive to lidar scan angle?

With datasets corresponding to different acquisition geometries (*f1, A, B, C, fl2, AB, AC, BC* and *fl3*), ABA models were built for each set by including metrics computed from a voxel-based estimation of plant area density (PAD) profiles. It was assumed that voxelisation could normalise information due to its capacity to estimate PAD values from the point clouds at the voxel level (better discretisation of space) while mitigating occlusion effects and taking into account the path length of the laser pulse in the vegetation. The resulting pot level PAD profiles were used in place of ground returns for gap fraction and CV_{LAD} estimation. Besides a few exceptions that mostly involved coniferous plots, using voxel-based metrics positively impacted mean R^2 values, increasing them on average by 38%. The rRMSE values were also decreased by an average of 10%. The advantage of voxel-based metrics, as well as other profile-based metrics generally, is that they more accurately characterise canopy structural properties, highlighted by increased accuracy. Moreover, the goodness-of-fit of the traditional ABA models improved when voxel-based metrics were used for riparian, broadleaf and mixed plots. Voxel-based metrics also reduced the SD of the distributions of the goodness-of-fit criteria for all resampled datasets (*f1, A, B, C fl2, AB, AC, BC* and *fl3*) of broadleaf and coniferous plots.

There are two aspects to the PAD profiles obtained from voxelisation and layer-based method. The first is the shape of the profile, and the second is the similarity between the profiles for different point clouds on the same plots. The improvement in R^2 values when voxel-based metrics were used indicates that the profiles (and subsequent metrics) based on voxelisation were better at characterising the vegetation. Moreover, the similarity of the voxel-based profiles was considered indicative of the normalisation tendency with voxelisation. Therefore, with voxelisation, it is possible to increase the accurate characterisation of the vegetation from multiple 'points of view'. However, it did not work perfectly in all the cases (for all field plots). There were some instances wherein voxel-based profiles were more dissimilar than the layer-based profiles. Nonetheless, the shape of the profiles was also different, and it may be assumed that voxelisation generally performed better

Moreover, voxelisation was done without height normalisation as the geometry needs to remain intact for the ray tracing. The height normalisation is done at the level of the voxels, which is coarser and could lead to some artefacts. Also, implementation of voxel-based methods at the level of the entire forest is not easily possible right now, and it requires greater computation efforts.

Q5) How to model acquisition geometry in ABA models?

So far, only the lidar scan angle was studied. A given lidar scan is a part of the acquisition geometry, which also includes the terrain and vegetation properties, especially in areas with steep slopes. Therefore, the lidar acquisition geometry is not only defined by the scan angle but also by the azimuth. In terrain with a slope, the impact of azimuth can be prominent when interacting with the topography: a point cloud over a forest scene with the same scan angle can be highly different when the sensor is scanning along or against the slope. Hence, the relationship between the lidar scanner and the local topography becomes an important consideration. Yang et al. (2011) observed that full-waveform shapes are affected by vegetation structure and terrain parameters. Previous work also demonstrated that considering local topography when developing ABA models based on point clouds is beneficial (Lahssini et al., 2022). Therefore, it was attempted to incorporate the overall acquisition geometry in ABA models using neural networks. A multilayer perceptron (MLP) was used in an attempt to disentangle the complex non-linear interactions between various lidar variables, terrain and scan properties

In this chapter, the slope was characterised by the degree of slope, the azimuth of the slope and the elevation, and the acquisition parameters were characterised by the mean scan angle, azimuth of scanning and the distance of the scanner from the plot. For each plot, acquisition from each flight line results in a unique point cloud and a unique set of corresponding metrics describing the local stand, impacted by the interplay of terrain and acquisition parameters besides the vegetation properties.

Comparing MLP models with and without geometric information highlighted the importance of adding information on geometry in the model to improve the prediction of forest attributes. The R^2 values increased to 0.83 from 0.77 for basal area predictions and to 0.85 from 0.77 for total volume predictions. Furthermore, the augmentation of datasets also demonstrated an overall improvement in the predictions.

The multi-linear regression (MLR) for different stand types demonstrated the limitations of some of the metrics. To a great extent, this limitation was overcome by using voxel-based metrics. However, MLR regressions are generally built by stratifying for the forest types to obtain good results. The MLP does not have this limitation. The results for MLP models with terrain and scan informations were nearly similar to those obtained with the deep learning-based fusion of lidar and optical data by Lahssini et al. (2022). Optical data is known for discriminating between well between different species. It may be hypothesised that when the MLP was trained with different views of the same forest plots, it could learn to discriminate between the three forest types well and result in improvements similar to those obtained by the fusion strategy.

Finally, explicit consideration of factors that explain the interaction of acquisition parameters, terrain and vegetation properties can improve ABA models. As these factors may be challenging to model, methods such as Artificial Neural networks (and more advanced deep learning-based methods) can be harnessed for their capabilities to learn complex relationships.

5.2 Limitations and Perspectives

Most lidar acquisitions are carried out with a lidar scan angle rarely greater than 20°. In that context, it was pretty challenging to identify datasets that could be adapted to the experimentation scheme in this study. The two datasets that were used were considerably different in terms of the acquisition parameters. The Bauges dataset was acquired in two standard airborne lidar acquisitions that resulted in datasets with point densities of 14 points/m² and 4 points/m². In contrast, the Ciron dataset was acquired from a light aircraft resulting in a dataset with a point density of 69 points/m².

Some limitations with the datasets influenced the experiments for the two first parts of the study. In the first part involving the assessment of lidar scan angle on metrics, the various flight lines had to be grouped based on their mean scan angles (MSA) in 10° intervals. A near-continuous change of scan angle is not practical in real datasets. Flight lines with MSAs closest to respective class medians were chosen from each class, thereby losing information from some of the other flight lines in the same classes. In the second part of the study, the datasets were resampled such that the point clouds for each plot corresponded to particular acquisition geometries. However, it was not possible to have the same acquisition conditions for all the plots (e.g. nadir (A) and moderate (class B) scan angle for all the plots). The comparison was instead of models built with “predominantly” nadir or off-nadir

datasets as opposed to a pure nadir or off-nadir. Nearly 50% of the plots in some forest types did not correspond to the main scanning scenario in consideration. It may be the case that there may be noise from such situations, but, on the contrary, it may also be argued that this leant some sense of realistic data acquisition characteristics to the datasets.

In the fourth chapter, a data augmentation procedure contributed positively to the ABA predictions. In that case, the unbalanced number of flight lines among the plots was less detrimental.

The experimental setup was devised to cover many possible scanning configurations. More possibilities exist that could refine the experiments to reflect many real-life acquisition scenarios. Furthermore, the increasing use of drones and multipurpose lidar acquisitions will bring scan angle into focus over the next few years and bringing down costs has always been an important consideration. Optimisation of lidar data acquisition in light of new technologies, platforms and practical considerations such as cost and time, therefore, sustain the need to study the effects of lidar scan angle in more detail. UAVs are low-cost alternatives that can be used to acquire experimental datasets with very high scan angles and degrees of overlap. They also provide high-density point clouds that can be used to resolve various vegetation elements.

Using simulated lidar datasets could also be a valuable solution to extend this work. Radiative transfer models such as DART could be used simulate lidar data in forest environments (Gastellu-Etchegorry et al., 2015). Simulations could be used to answer several questions raised in this thesis as they could provide lidar data sets (i) acquired from a continuously changing scan angle, (ii) acquired with specific acquisition geometry, and (iii) to generate additional samples to augment datasets for deep-learning based models. In recent years, simulated datasets have become increasingly realistic. They have the potential to fill in the gaps in real datasets.

Although the number of field measurements is critical to building ABA models, their quality also matters. The protocol followed during the field plot measurements in the Bauges site did not allow for measuring trees with diameters below 17.5 cm. Some plots had tree measurements for only a handful of trees with diameters greater than 17.5 cm. The other vegetation (small trees and lower vegetation), however, was sensed by the lidar sensor. Although the diameters of the smaller trees were estimated for this work, more accurate information about them will relate better to the lidar signal. Furthermore, the stratification of measurements to have plots with diverse field plot measurements will result in better-calibrated models. This was mainly a problem with the Bauges dataset because there were only a handful of plots with very high basal area and total volume values.

In the riparian field plots, one plot had the largest tree among those measured in the field plot measurements. However, while clipping the datasets using the plot centre coordinates, the tree trunk was not a part of the clipped subset, but a significant part of its canopy was a part of the subset. Such problems are known as the border or edge effects, and they have been known to affect ABA

predictions (Knapp et al., 2021). These effects can be more pronounced with higher scan angles, especially when dealing with single flight line datasets. For the example mentioned above, edge effects could have a role to play when dealing with very heterogeneous forest environments. In this study, however, it was not addressed, and plots with severe edge effects were not considered.

The most straightforward strategy to mitigate the impact of scan angles on ABA models would be to ensure that each part of the forest is "seen" from a diversity of scan angles and azimuths. This is not possible in practice. Voxel-based metrics were demonstrated to have great potential to normalise lidar metrics before building ABA models, thus improving model robustness. They are extremely useful for converting an unordered set of vegetation points into an ordered three-dimensional representation of the vegetation. Nevertheless, the voxel-level PAD estimation is known to be biased at low point densities (Pimont et al., 2018; Soma et al., 2018). Furthermore, the voxel size was set at 1m in this study. Voxel size is also an important parameter to consider as smaller voxels can better discretise the distribution of the vegetation. A balance must be achieved between the point densities and the voxel size. The bias-corrected estimators proposed by Soma et al. (2018) and Pimont et al. (2018) and the LAD kriging method by Soma et al. (2020) have the potential to increase the accuracy of PAD (or LAD) estimation. In this study, the vegetation profiles were derived from the voxelised scene to compute voxel-based gap-fraction to have comparable metrics to the original model containing gap-fraction as one of the metrics. Alternate metrics from the voxels and vegetation profiles are also a possibility. 3D convolutional neural networks called VoxNet (Maturana and Scherer, 2015) for object detection offer interesting possibilities for using the explicit 3D spatial structure of the information.

Accuracy of forest attribute prediction needs to be accompanied by precision in prediction accuracy. The precision is possible when forests are scanned uniformly from all directions. As that is not possible in real life, strategies have to be developed to manage the potential variations that could arise. The simplest way to manage the variations due to lidar scan angle is to ensure lidar data acquisition is made so that areas are scanned from at least two or three flight lines to ensure a comprehensive vegetation sampling. From a practical perspective, adopting more efficient and cost-effective practices is desirable. In such cases, metrics will have to be carefully chosen to be stable under changing scan angles. Voxelisation using ray-tracing can be an option to normalise the metrics at the field plots and the whole forest level to generate reliable wall-to-wall maps. Voxel-based methods also have the potential to characterise vegetation better. These methods must be developed further to incorporate them into operational lidar-based enhanced forest inventories (EFIs). Finally, acquisition geometries should be given due consideration while modelling forest attributes. Research in this regard, with various acquisition geometries, will enrich our understanding of the mechanism with which lidar pulses sample canopies from different viewpoints, in different terrains and different types of forests.

Appendix A: Effect of scan angle on metrics at plot level for Bagues site

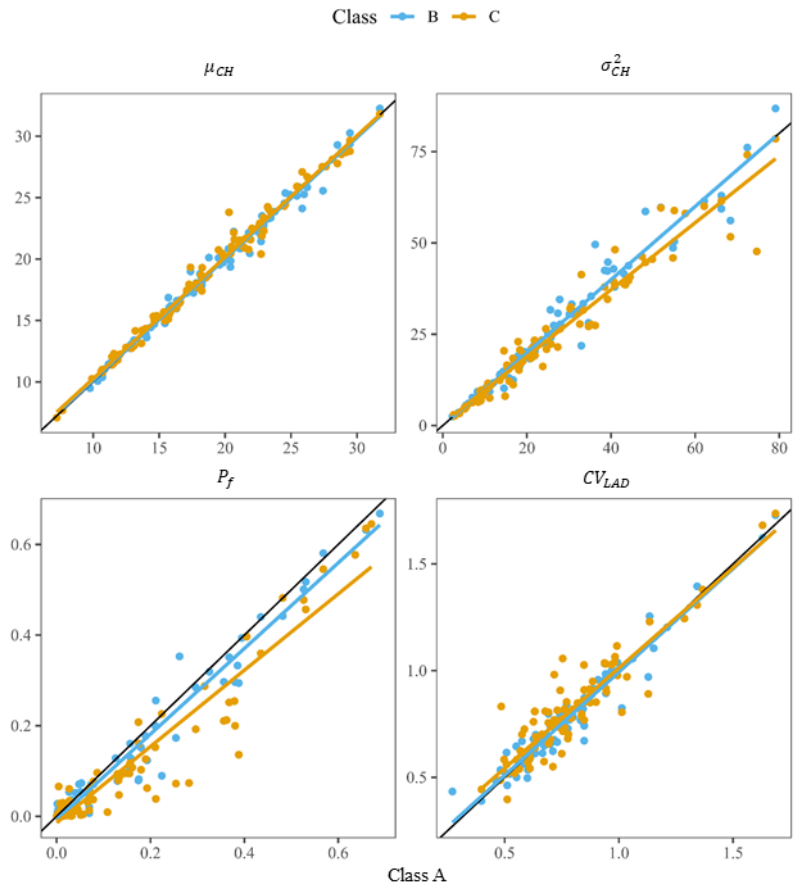

Figure 10: Comparison of metrics computed for classes B and C with class A, for all the three forest types at Bauges considered together. The methodology used was similar the one used in Dayal et al., (2020) but only at the level of the field plots available. The metrics were affected differently by changing scan angle with P_f being the most sensitive.

Appendix B: Results of Basal area and Total Volume

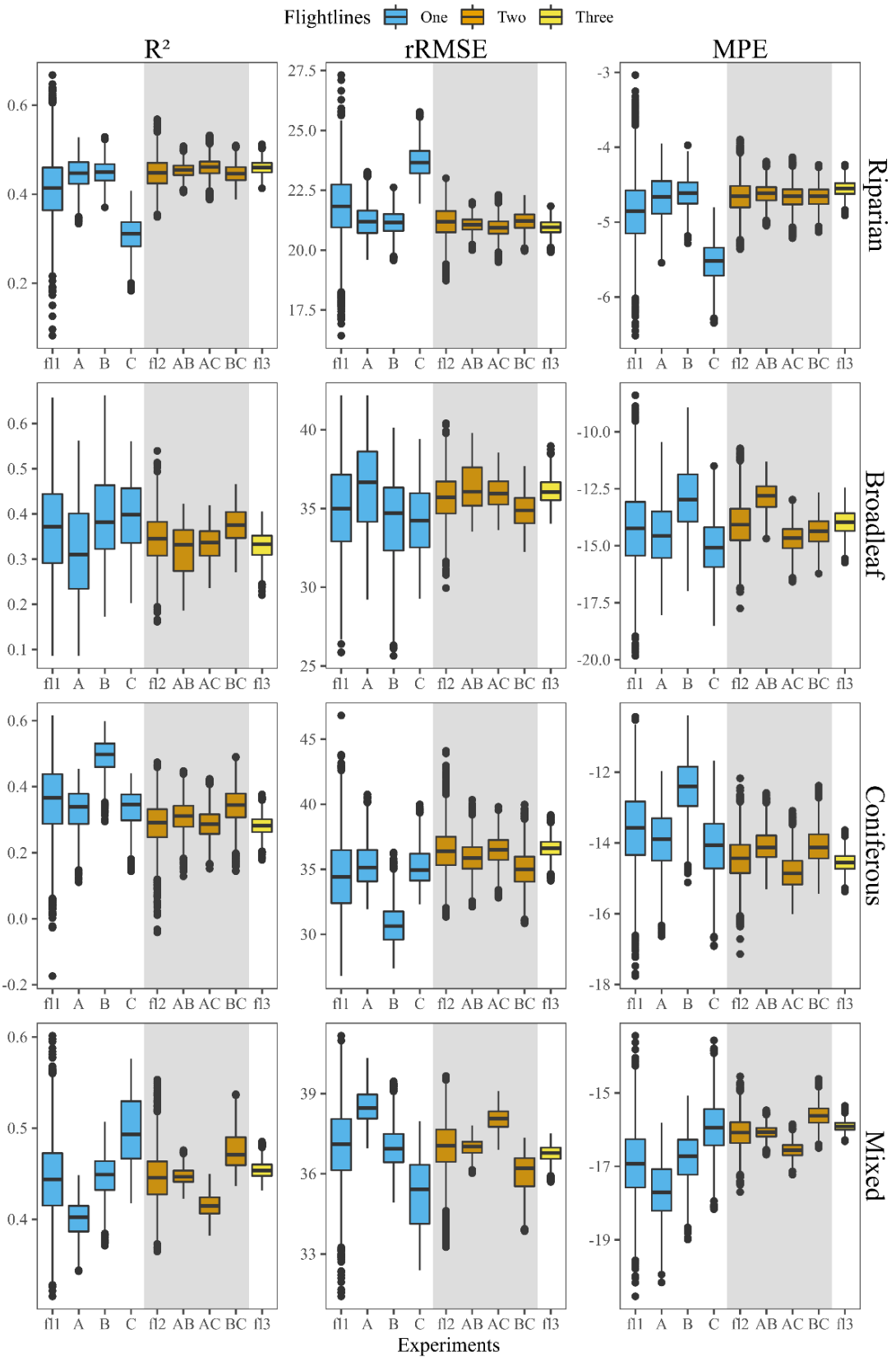

Figure 11: Distribution of the performance measures of basal area (BA) models (R^2, rRMSE, MPE) for different scenarios and for the different forest types (Riparian, Broadleaf, Coniferous and Mixed). The single (fl1, A, B, C), double (fl2, AB, AC, BC) and triple (fl3) flight lines scenarios are depicted in blue, orange and yellow respectively **(colour)**

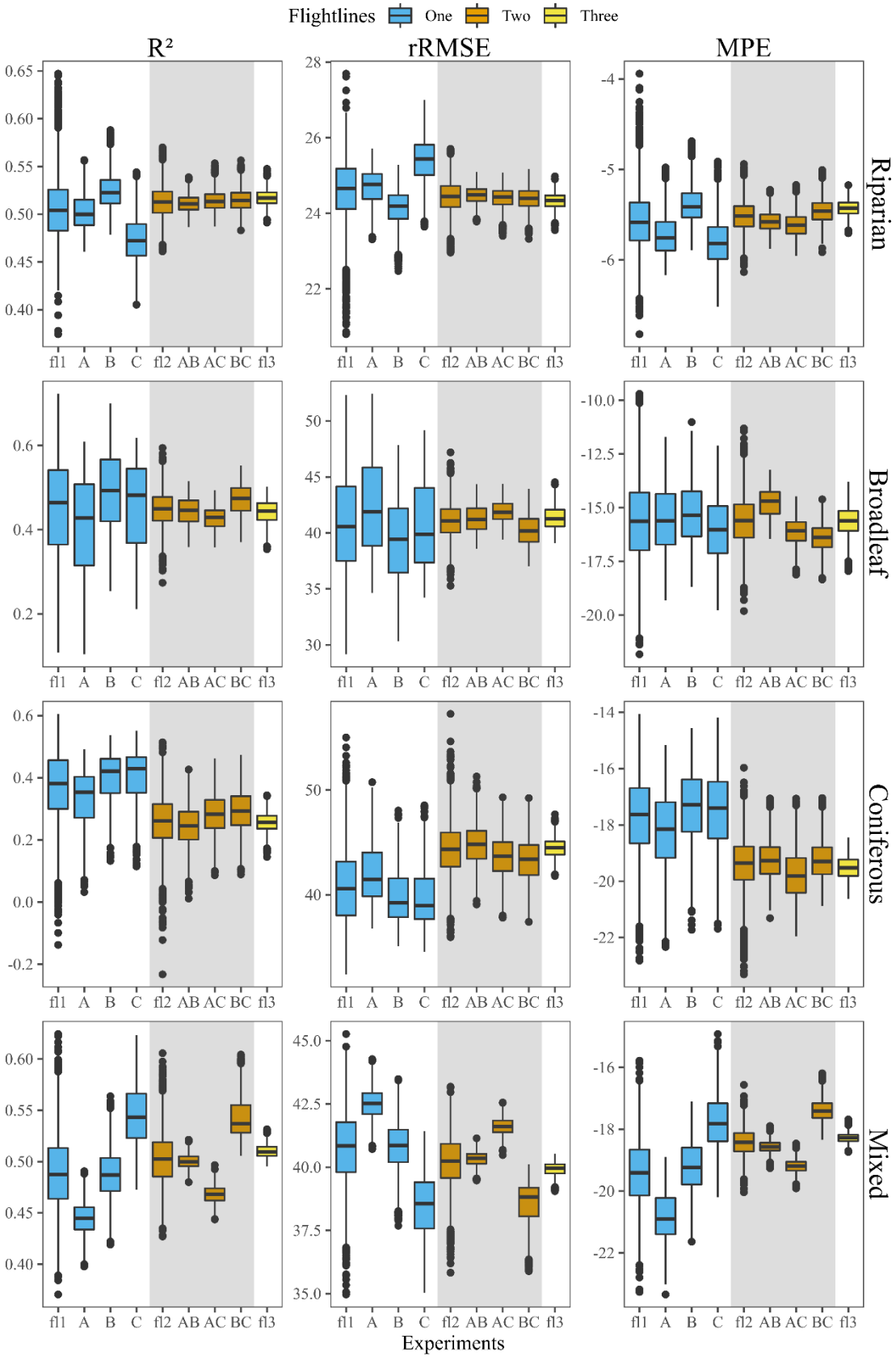

Figure 12: Distribution of the performance measures of total volume (Vtot) models (R^2, rRMSE, MPE) for different scenarios and for the different forest types (Riparian, Broadleaf, Coniferous and Mixed). The single (fl1, A, B, C), double (fl2, AB, AC, BC) and triple (fl3) flight lines scenarios are depicted in blue, orange and yellow respectively **(colour)**

B.1 Scenario wise comparison of distributions for reference and voxel metrics

	Forest type	One flight line				Two flight lines				Three flight lines
		fl1	A	B	C	fl2	AB	AC	BC	fl3
R^2	Riparian	40.2*	33.5*	26.6*	88.3*	27.0*	29.3*	27.0*	21.7*	19.9*
	Broadleaf	5.1*	11.2*	8.9*	-4.5*	20.1*	25.0*	16.3*	17.6*	31.3*
	Coniferous	10.1*	18.8*	2.1*	-8.3*	22.9*	37.0*	14.5*	**0.3**	24.8*
	Mixed	24.1*	42.3*	28.4*	10.5*	29.4*	21.3*	41.7*	24.9*	28.3*
rRMSE	Riparian	-15.3*	-14.5*	-11.6*	-22.3*	-11.6*	-13.0*	-12.2*	-9.2*	-8.9*
	Broadleaf	-1.3*	-2.4*	-2.7*	1.6*	-5.4*	-6.0*	-4.2*	-5.4*	-8.0*
	Coniferous	-2.7*	-4.7*	-1.0*	2.1*	-4.7*	-8.6*	-2.9*	**0.0**	-5.0*
	Mixed	-10.3*	-15.4*	-12.3*	-5.3*	-12.6*	-9.0*	-16.1*	-12.2*	-12.6*
MPE	Riparian	-23.6*	-25.9*	-17.1*	-30.5*	-17.9*	-21.2*	-21.2*	-11.5*	-12.3*
	Broadleaf	19.8*	25.7*	17.7*	18.0*	19.8*	32.0*	20.6*	13.4*	18.0*
	Coniferous	4.7*	2.2*	7.3*	8.8*	3.7*	1.4*	3.3*	9.3*	2.7*
	Mixed	-14.6*	-19.0*	-21.5*	-4.6*	-14.9*	-12.5*	-17.4*	-14.4*	-15.0*

Table 11: Scenario-wise percentage changes in the means of distributions of goodness-of-fit criteria using voxel metrics for the predictions of *BA*. Values in red indicate a deterioration All comparisons were significant (*) except for those in bold All comparisons were significant (*) except for those in bold **(colour)**

	Forest type	One flight line				Two flight lines				Three flight lines
		fl1	A	B	C	fl2	AB	AC	BC	fl3
R^2	Riparian	31.2*	34.5*	25.1*	39.6*	23.9*	25.6*	25.1*	20.2*	18.1*
	Broadleaf	5.0*	7.7*	2.3*	4.7*	11.9*	11.1*	12.2*	11.6*	16.2*
	Coniferous	-3.2*	6.4*	-2.7*	-19.1*	10.8*	36.3*	**0.0**	-9.0*	11.8*
	Mixed	19.1*	38.7*	27.6*	2.1*	23.1*	18.2*	33.0*	17.5*	23.4*
rRMSE	Riparian	-17.6*	-19.3*	-15.0*	-19.8*	-13.5*	-14.5*	-14.3*	-11.4*	-10.2*
	Broadleaf	-1.7*	-2.4*	-0.8*	-1.8*	-4.9*	-4.5*	-4.6*	-5.3*	-6.6*
	Coniferous	1.2*	-1.5*	1.0*	6.5*	-1.8*	-6.0*	**0.1**	1.9*	-2.0*
	Mixed	-9.7*	-17.0*	-14.3*	-1.3*	-12.5*	-9.6*	-15.7*	-11.1*	-13.0*
MPE	Riparian	-24.7*	-27.4*	-22.2*	-26.3*	-19.5*	-21.3*	-22.1*	-16.6*	-13.9*
	Broadleaf	10.1*	20.3*	0.6*	8.7*	11.3*	19.0*	13.6*	1.6*	10.5*
	Coniferous	9.5*	5.5*	8.6*	16.5*	6.1*	3.0*	5.7*	11.7*	5.4*
	Mixed	-17.6*	-24.5*	-23.6*	-5.7*	-18.8*	-16.4*	-23.0*	-15.9*	-20.0*

Table 12: Scenario-wise percentage changes in the means of distributions of goodness-of-fit criteria using voxel metrics for the predictions of V_{tot}. Values in red indicate a deterioration All comparisons were significant (*) except for those in bold All comparisons were significant (*) except for those in bold **(colour)**

	Forest type	One flight line				Two flight lines				Three flight lines
		fl1	A	B	C	fl2	AB	AC	BC	fl3
R^2	Riparian	-30.5*	-2.5*	58.3*	14.0*	-20.1*	35.0*	-12.1*	-4.1*	-17.0*
	Broadleaf	-52.4*	-59.4*	-61.7*	-35.0*	-60.7*	-72.5*	-54.6*	-48.3*	-62.9*
	Coniferous	-35.9*	-19.8*	-16.2*	-16.7*	-35.8*	-60.2*	-58.0*	-57.6*	-32.2*
	Mixed	21.2*	69.9*	30.9*	-40.3*	-6.2*	60.2*	-1.8*	-26.8*	39.9*
rRMSE	Riparian	-17.7*	15.3*	80.1*	48.5*	-9.5*	55.9*	0.8*	5.9*	-8.9*
	Broadleaf	-51.8*	-58.5*	-61.3*	-35.3*	-58.6*	-70.6*	-52.7*	-45.4*	-59.6*
	Coniferous	-33.5*	-15.6*	-13.9*	-17.4*	-32.1*	-56.4*	-56.8*	-57.5*	-28.7*
	Mixed	35.7*	102.6*	50.7*	-36.9*	7.3*	76.4*	17.3*	-17.6*	59.8*
M	Riparian	3.6*	6.3*	101.8*	63.9*	11.4*	33.3*	-1.7*	26.2*	-3.4*
	Broadleaf	-37.3*	-58.6*	-62.2*	-27.8*	-39.8*	-60.6*	-11.0*	-15.0*	-16.1*

	Coniferous	-17.4*	-7.9*	-12.2*	-6.5*	-7.4*	-21.9*	-28.5*	-27.5*	-5.1*
	Mixed	23.3*	-16.4*	-8.8*	-33.9*	17.0*	60.4*	39.1*	4.1*	90.9*

Table 13: Scenario-wise percentage changes in the standard deviations of distributions of goodness-of-fit criteria using voxel metrics for the predictions of *BA*. Values in red indicate a deterioration. All comparisons were significant (*) except for those in bold All comparisons were significant (*) except for those in bold **(colour)**

	Forest type	**One flight line**				**Two flight lines**				**Three flight lines**
		fl1	**A**	**B**	**C**	**fl2**	**AB**	**AC**	**BC**	**fl3**
R^2	Riparian	-4.5*	49.7*	63.6*	35.7*	5.4*	82.3*	45.1*	35.9*	-1.7*
	Broadleaf	-56.3*	-63.3*	-58.9*	-46.9*	-51.0*	-58.0*	-39.7*	-46.7*	-59.0*
	Coniferous	-44.1*	-45.7*	-22.4*	-41.5*	-52.5*	-70.1*	-63.9*	-59.3*	-32.3*
	Mixed	56.9*	96.2*	28.1*	-38.5*	15.0*	70.5*	14.2*	-30.8*	83.0*
rRMSE	Riparian	14.9*	85.0*	92.6*	69.6*	22.3*	114.0*	70.0*	53.9*	9.6*
	Broadleaf	-55.0*	-62.1*	-58.8*	-44.8*	-48.4*	-56.0*	-36.7*	-43.6*	-55.9*
	Coniferous	-43.6*	-43.9*	-21.7*	-43.5*	-51.5*	-68.2*	-64.0*	-60.2*	-30.9*
	Mixed	75.0*	137.8*	49.8*	-37.9*	31.8*	89.1*	36.2*	-23.2*	110.1*
MPE	Riparian	42.9*	64.5*	122.1*	64.9*	41.5*	70.5*	32.0*	36.5*	17.5*
	Broadleaf	-42.4*	-54.6*	-54.4*	-36.6*	-49.3*	-54.5*	-22.9*	-18.8*	-38.2*
	Coniferous	-13.3*	-23.0*	-16.2*	4.0*	-11.0*	-34.9*	-40.0*	-13.1*	-1.3*
	Mixed	22.7*	-0.3*	-8.8*	-42.5*	34.7*	62.0*	28.1*	-11.1*	96.3*

Table 14: Scenario-wise percentage changes in the standard deviations of distributions of goodness-of-fit criteria using voxel metrics for the predictions of V_{tot}. Values in red indicate a deterioration. All comparisons were significant (*) except for those in bold All comparisons were significant (*) except for those in bold **(colour)**

B.2 BA and Vtot predictions for conventional using voxel metrics

Goodness-of-fit	Forest type	Basal area		Total volume	
		W/ reference metrics	W/ voxel metrics	W/ reference metrics	W/ voxel metrics
R^2	Riparian	0.51	0.6	0.58	0.66
	Broadleaf	0.35	0.43	0.49	0.53
	Coniferous	0.29	0.34	0.27	0.27
	Mixed	0.44	0.6	0.51	0.64
rRMSE	Riparian	20	18.04	22.72	20.50
	Broadleaf	35.46	33.18	38.85	37.17
	Coniferous	36.33	35.24	43.95	43.90
	Mixed	37	32	40.3	34.5
MPE	Riparian	-4.24	-3.64	-4.91	-4.14
	Broadleaf	-13.38	-16.43	-14.33	-16.47
	Coniferous	-14.89	-15.85	-19.66	-21.40
	Mixed	-16	-13.5	-18.6	-14.7

Table 15: Goodness-of-fit criteria for predictions of *BA and* V_{tot} for conventional models built with reference and voxel metrics

Appendix C: Vegetation profiles

Plot: 1

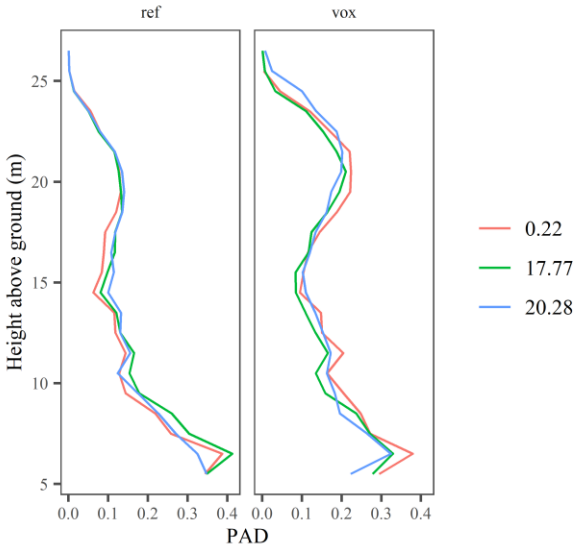

Plot: 10

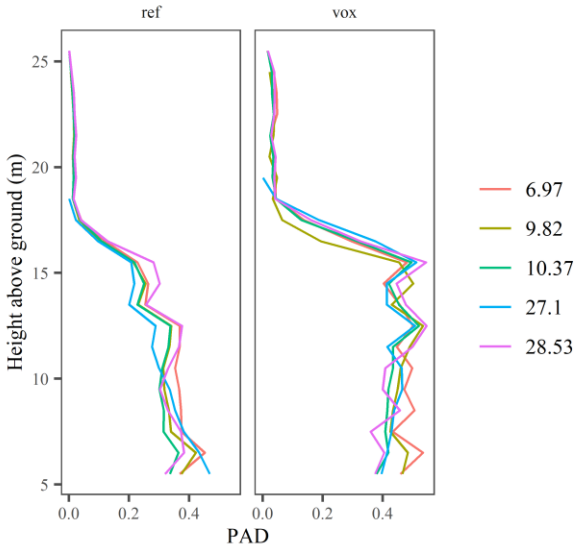

Plot: 11

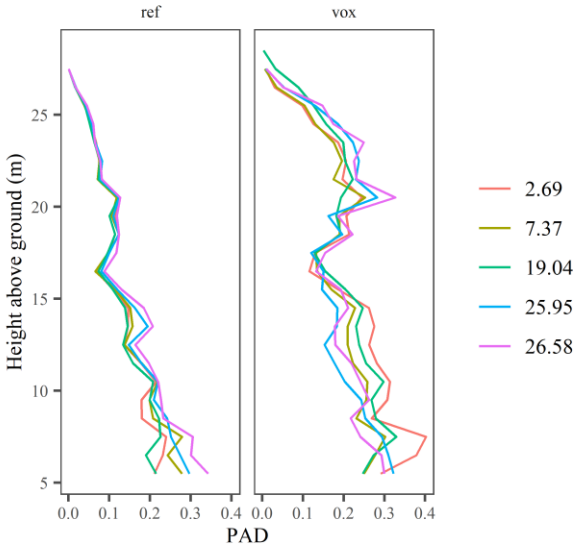

Plot: 12

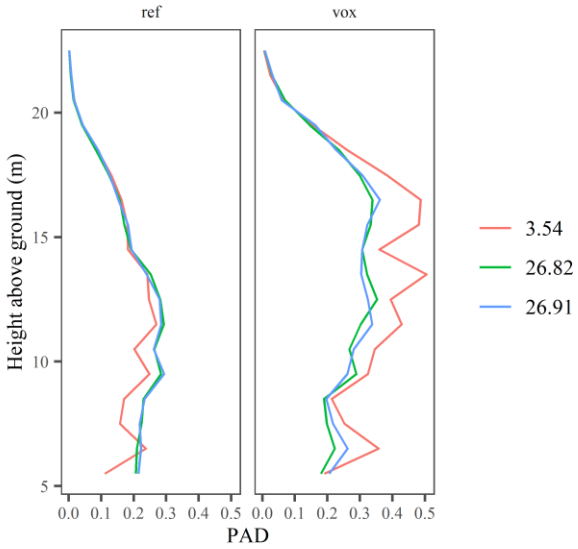

Plot: 13

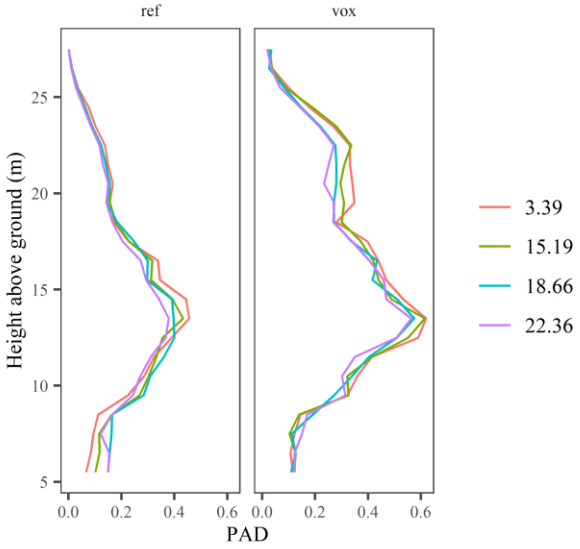

Plot: 15

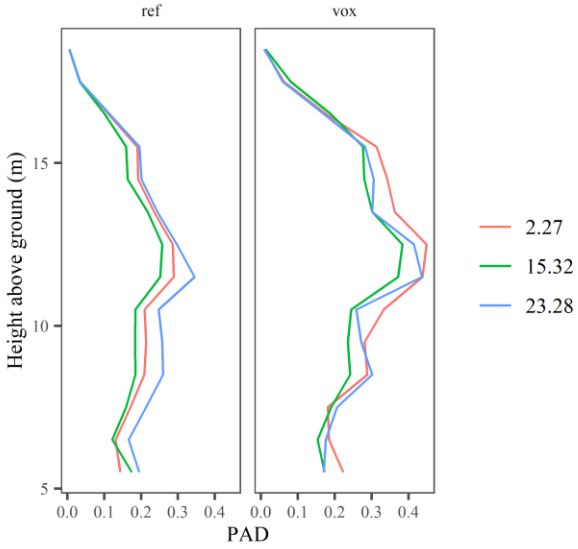

Plot: 16

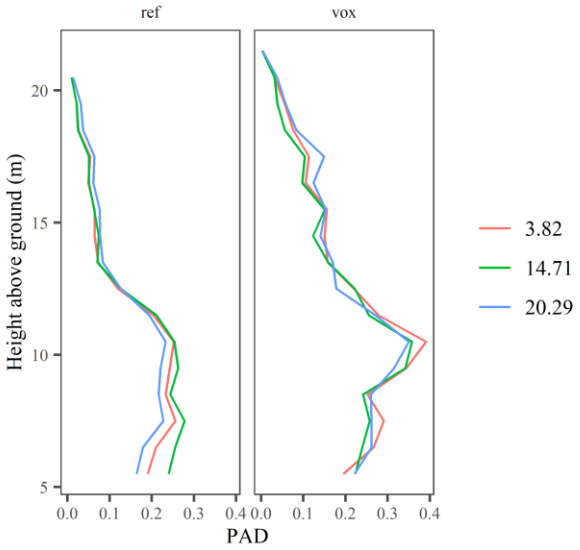

Plot: 17

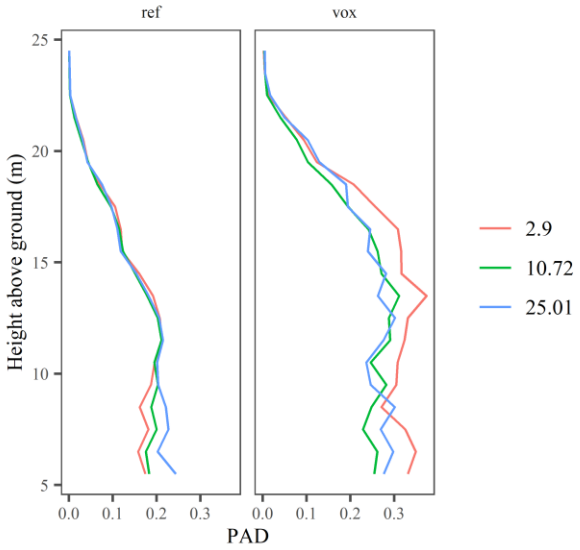

Plot: 18

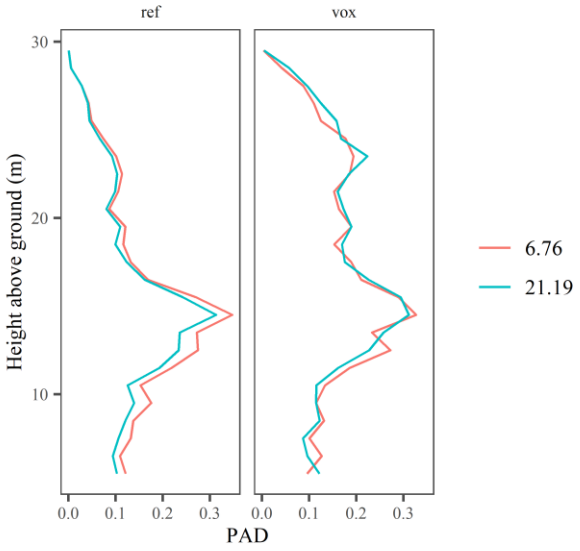

Plot: 19

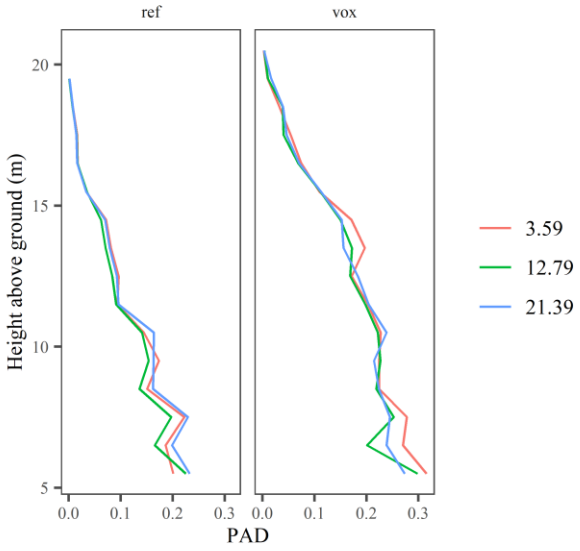

Plot: 2

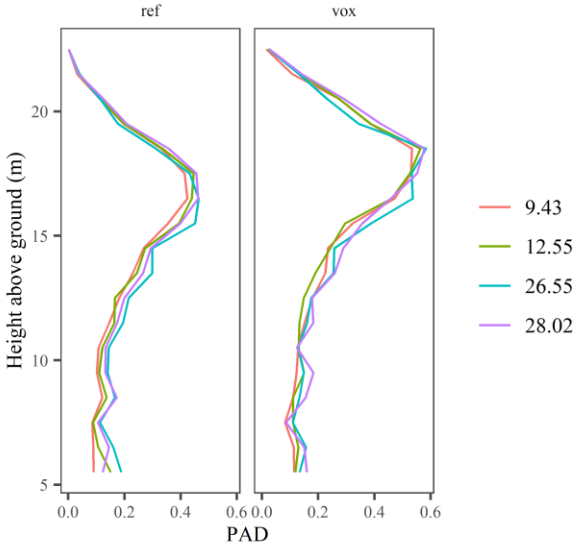

Plot: 20

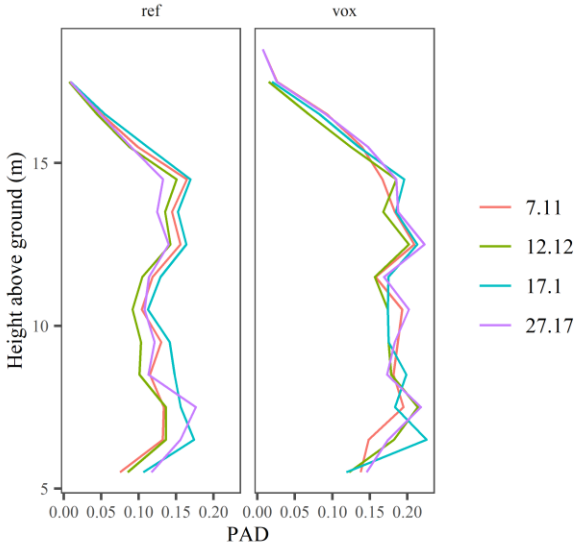

Plot: 21

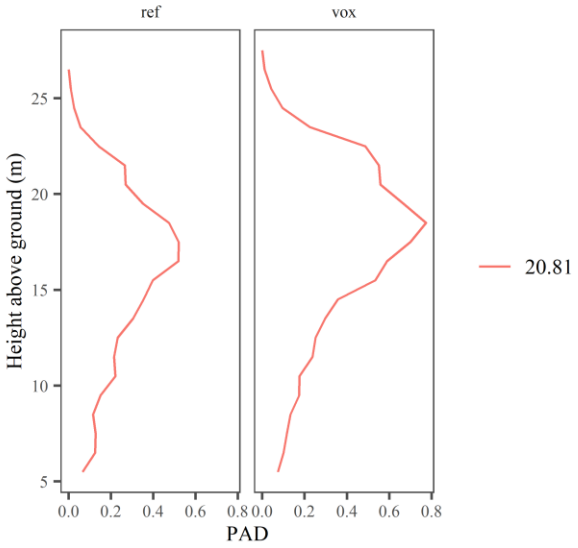

Plot: 22

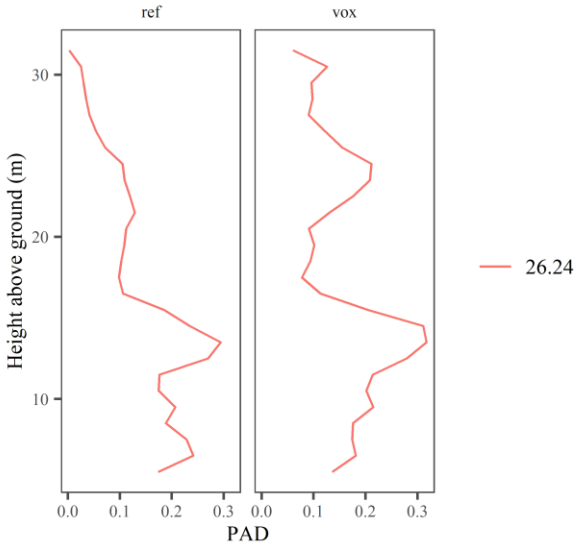

Plot: 23

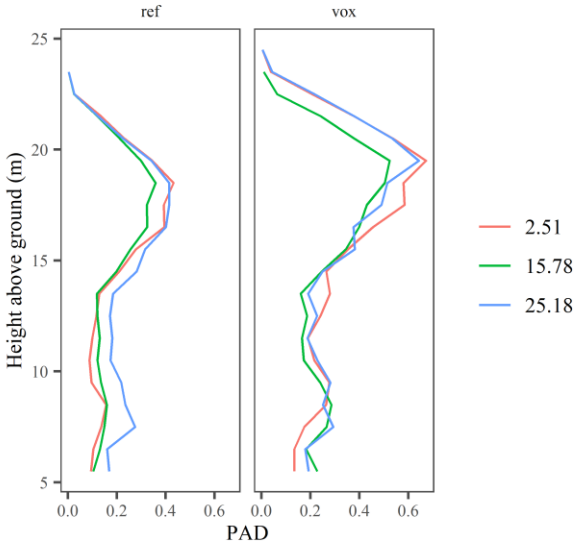

Plot: 24

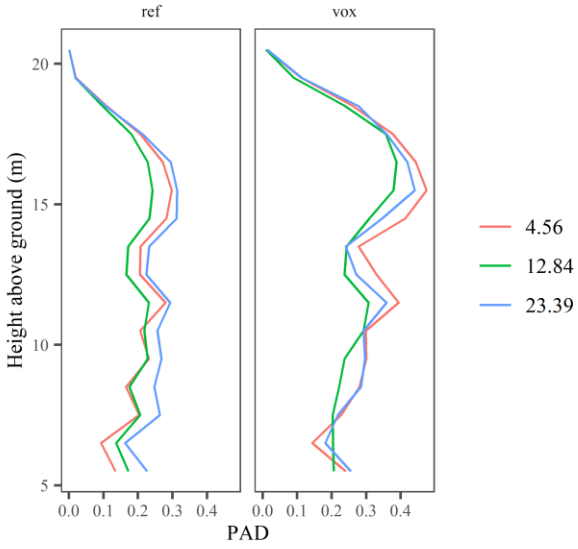

Plot: 25

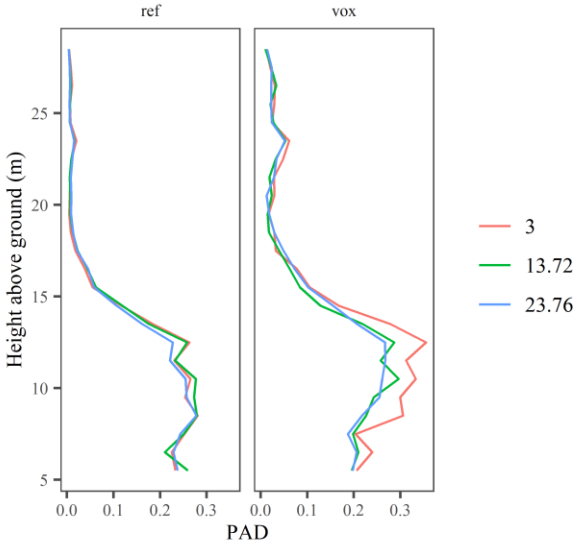

Plot: 26

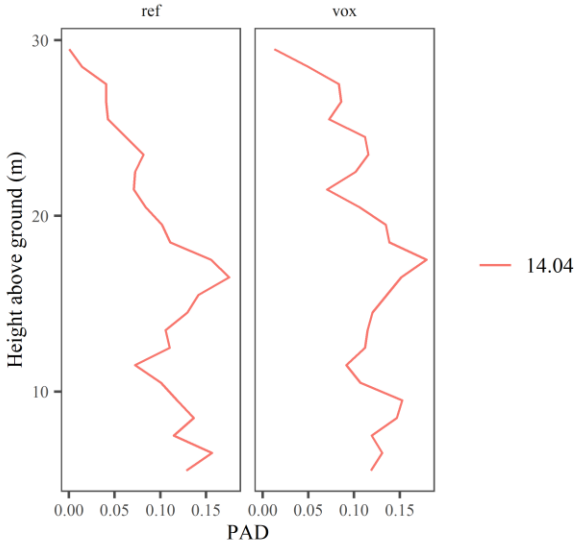

Plot: 27

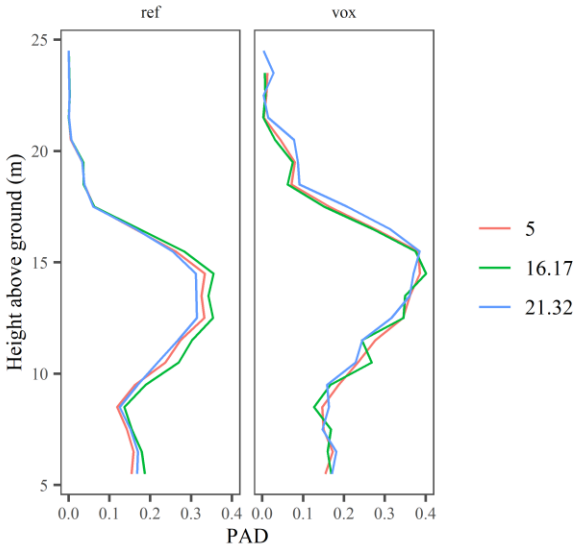

Plot: 28

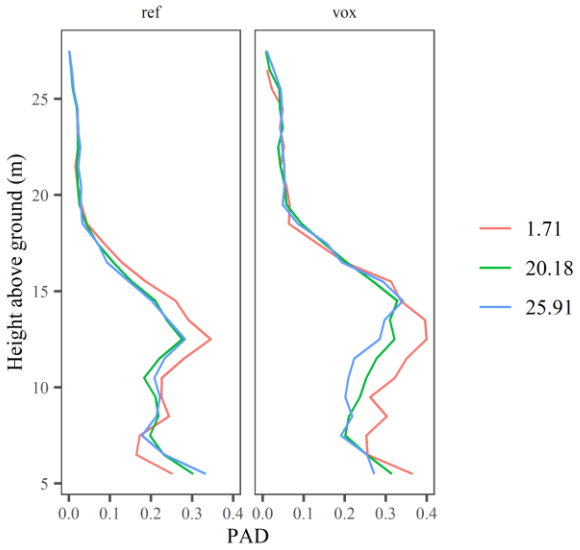

Plot: 29

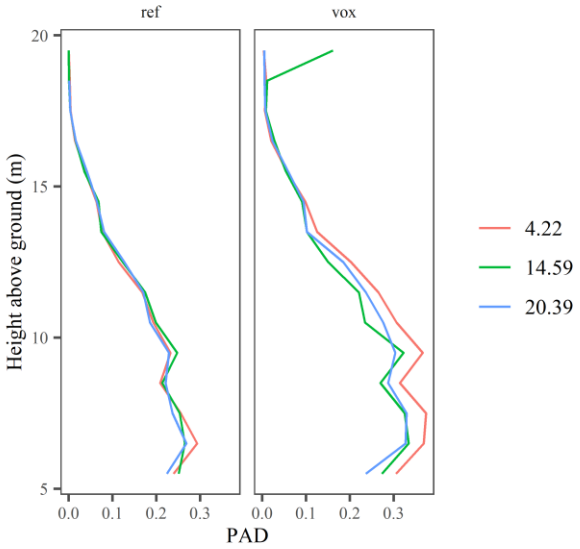

Plot: 3

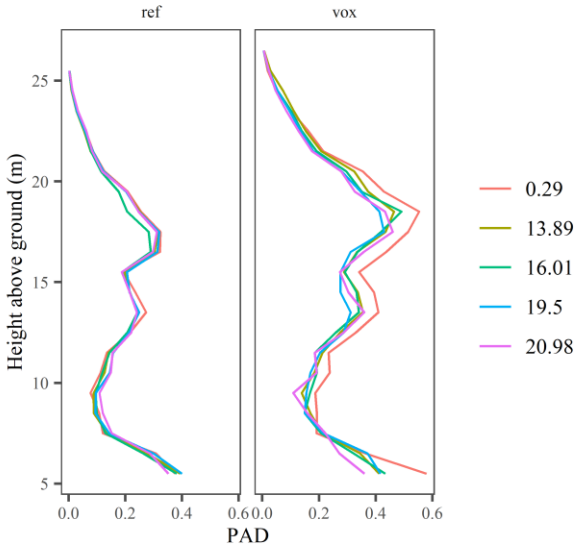

Plot: 30

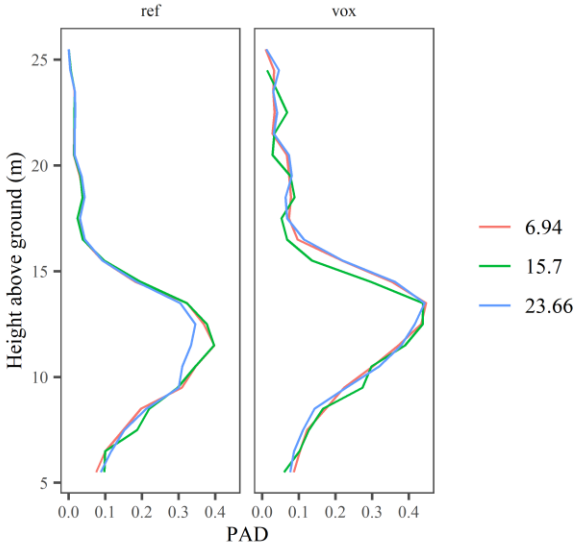

Plot: 4

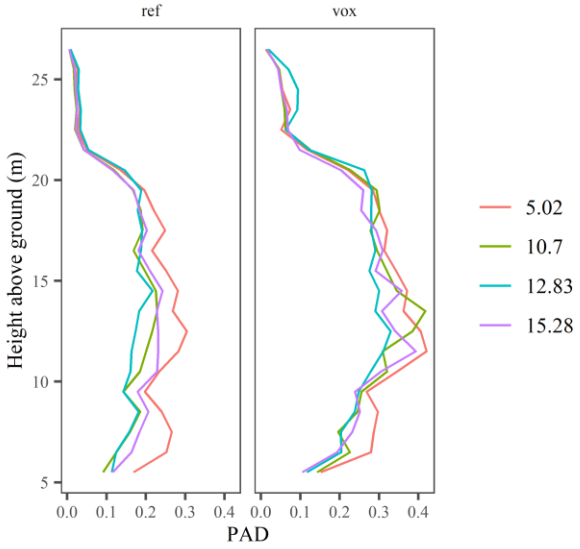

Plot: 5

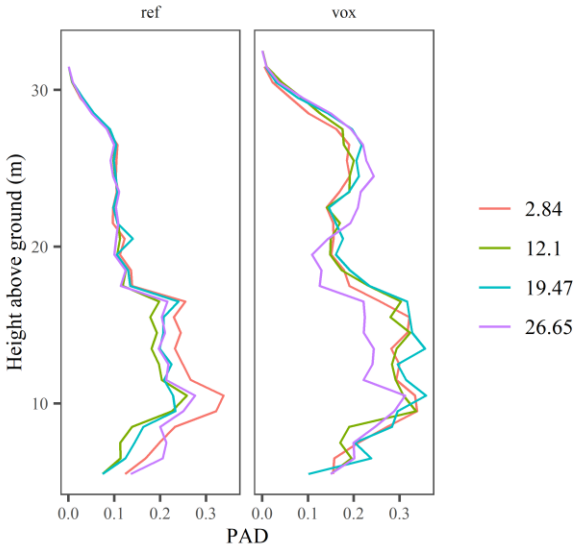

Plot: 6

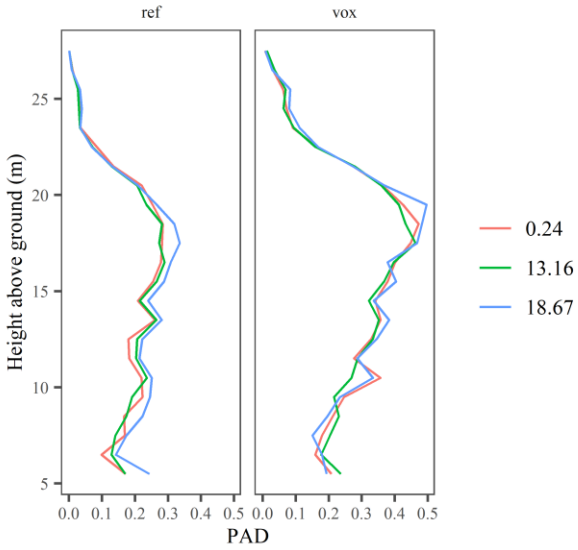

Plot: 7

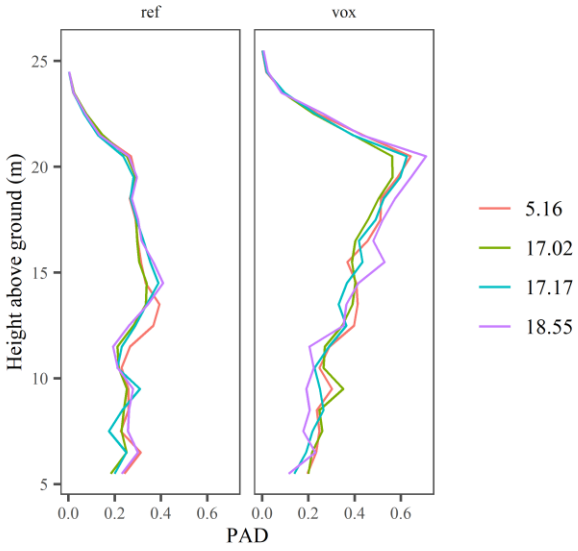

Plot: 8

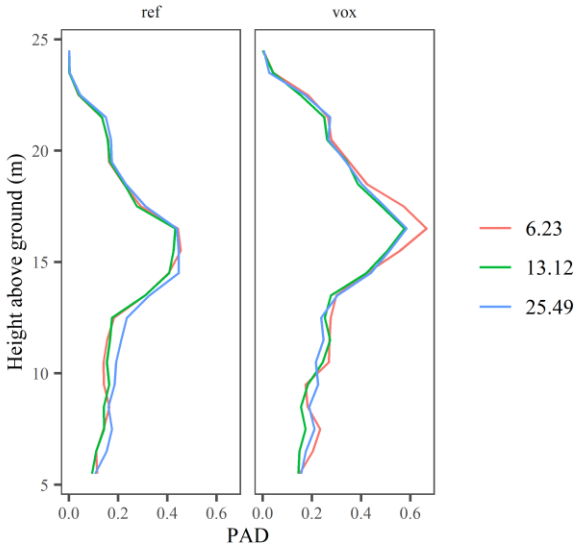

Plot: 9

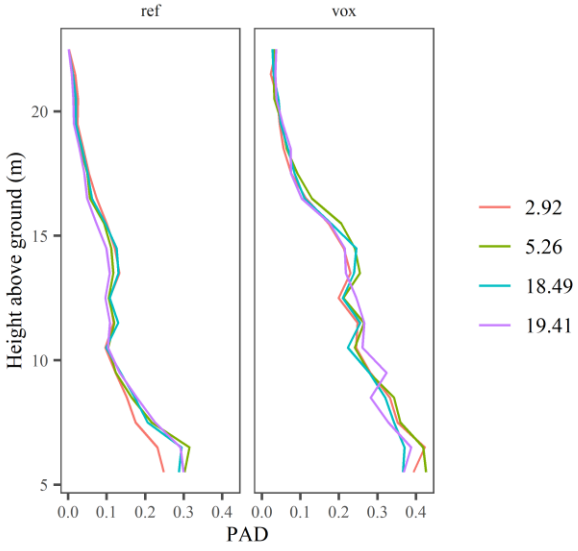

Plot: 100_IRSTEA

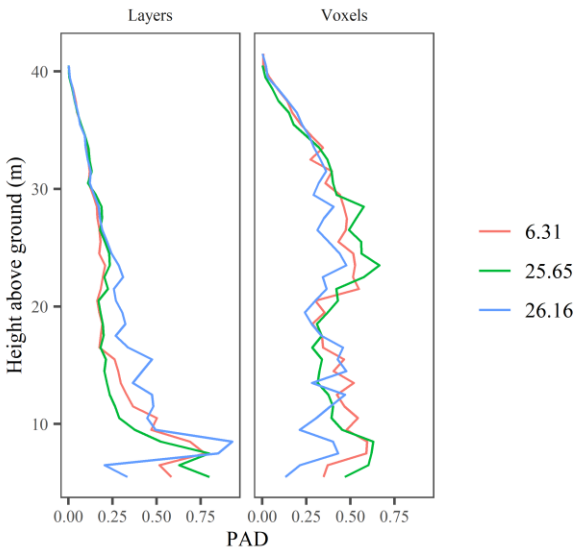

Plot: 107_IRSTEA

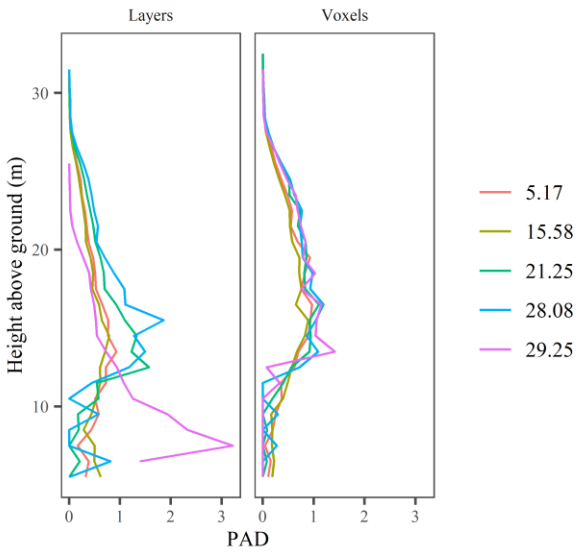

Plot: 108_IRSTEA

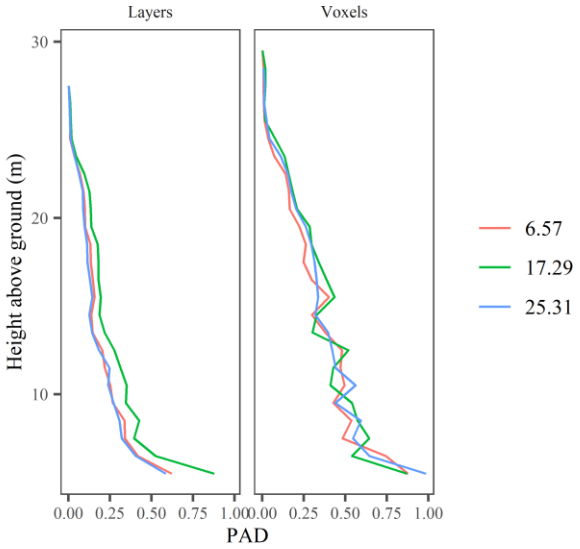

Plot: 10_74_ONF

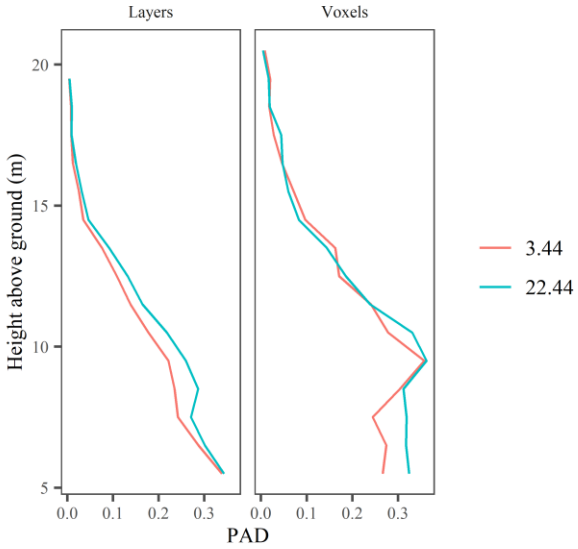

Plot: 116_IRSTEA

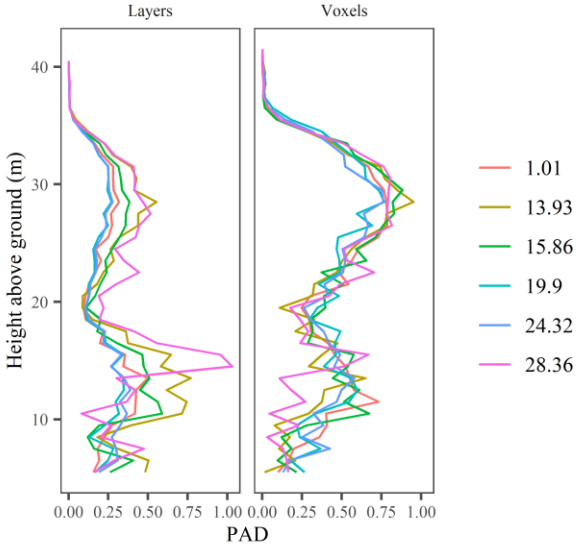

Plot: 117_IRSTEA

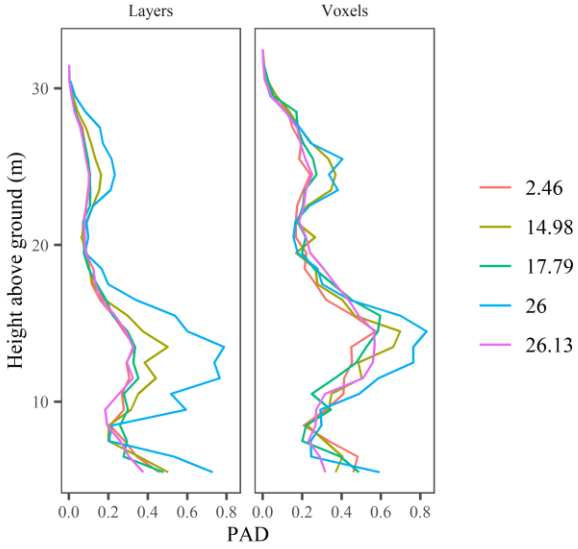

Plot: 118_IRSTEA

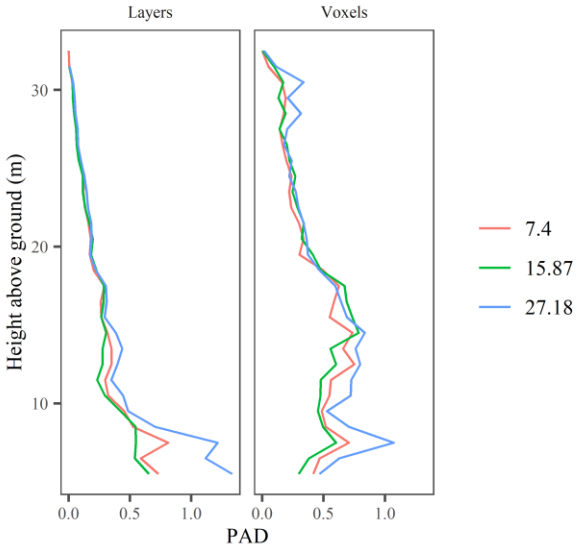

Plot: 119_IRSTEA

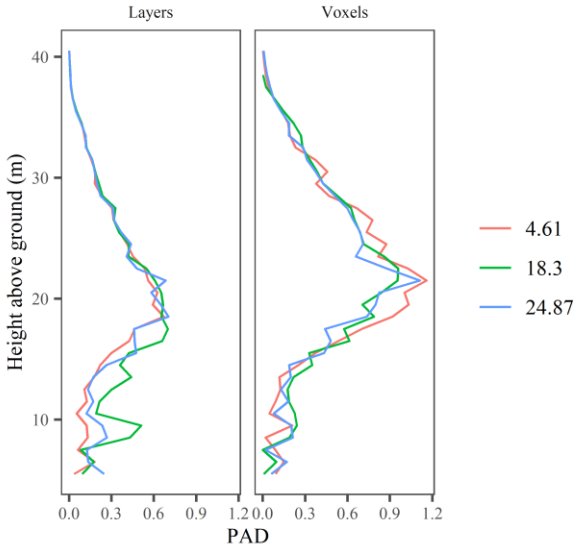

Plot: 139_IRSTEA

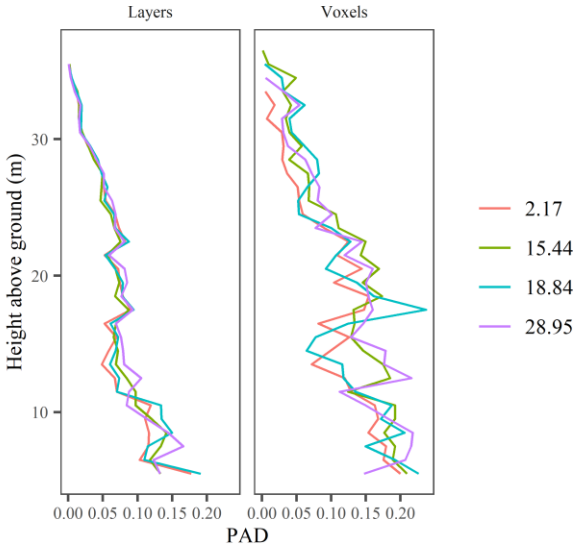

Plot: 13_IRSTEA

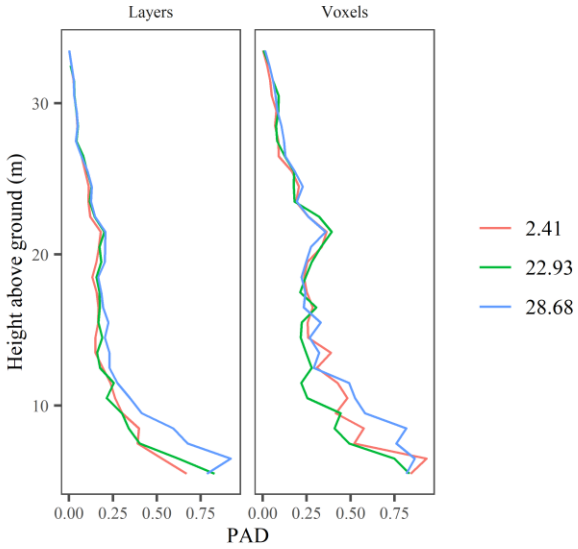

Plot: 141_IRSTEA

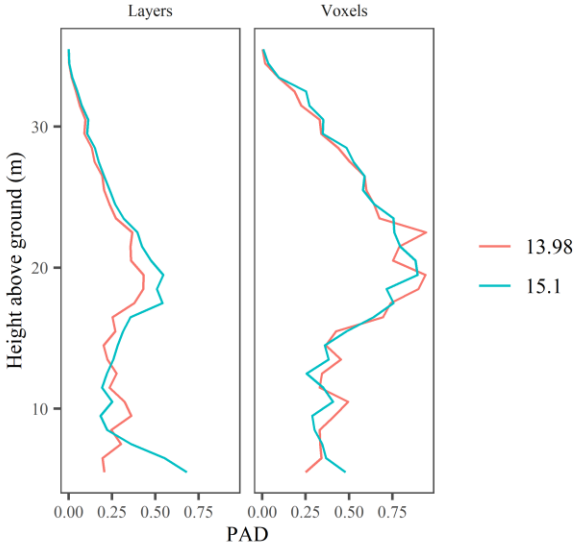

Plot: 142_IRSTEA

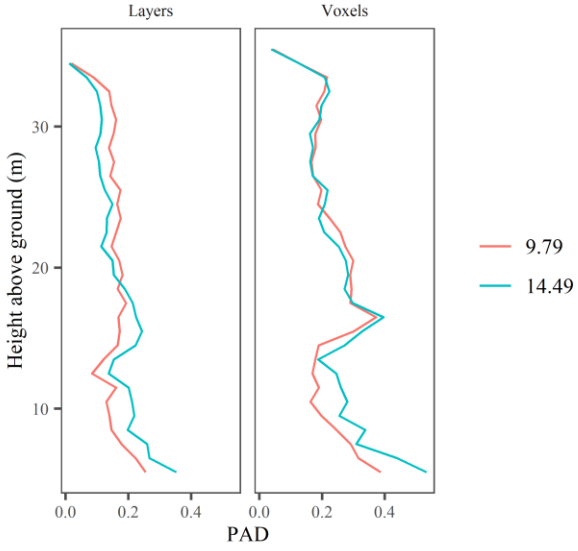

Plot: 143_IRSTEA

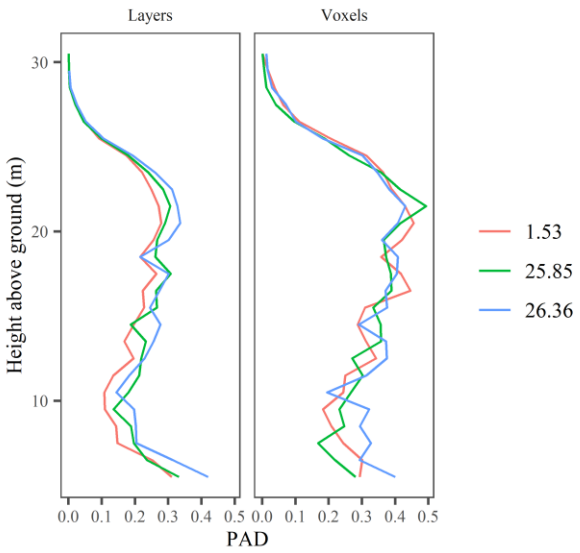

Plot: 153_IRSTEA

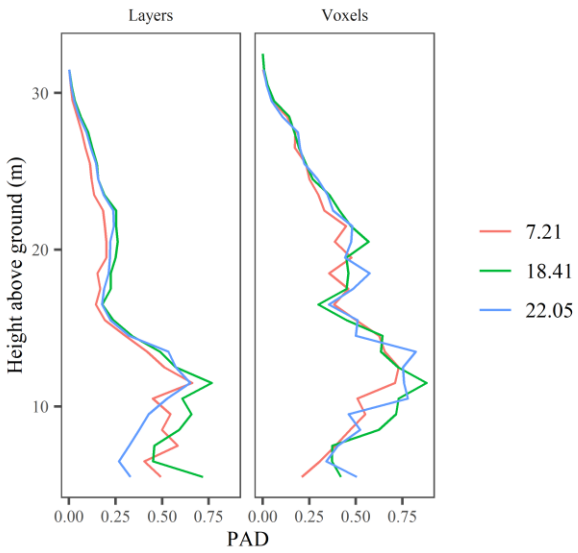

Plot: 156_IRSTEA

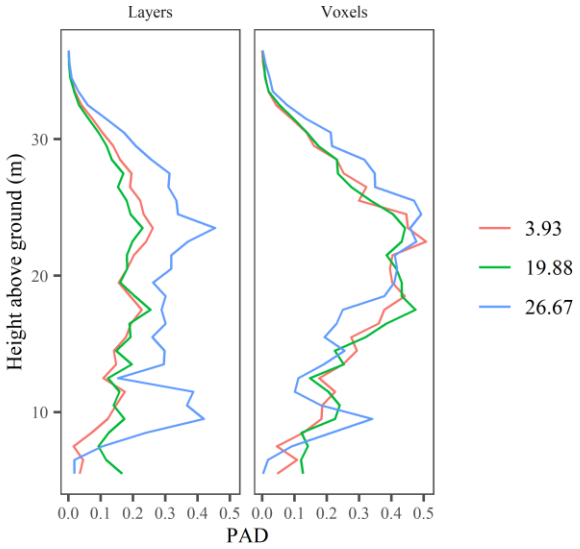

Plot: 165_IRSTEA

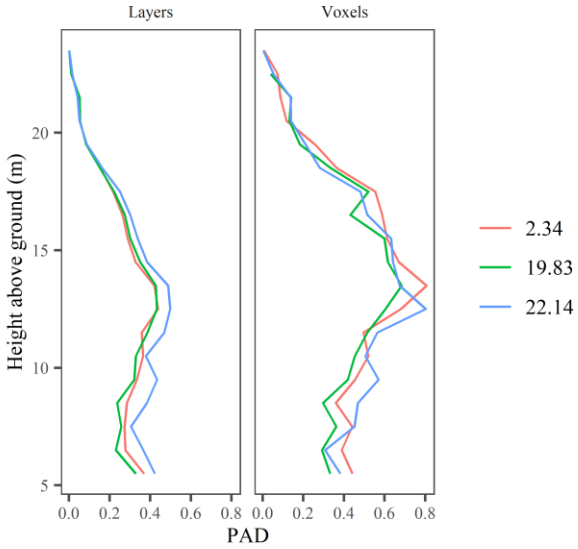

Plot: 166_IRSTEA

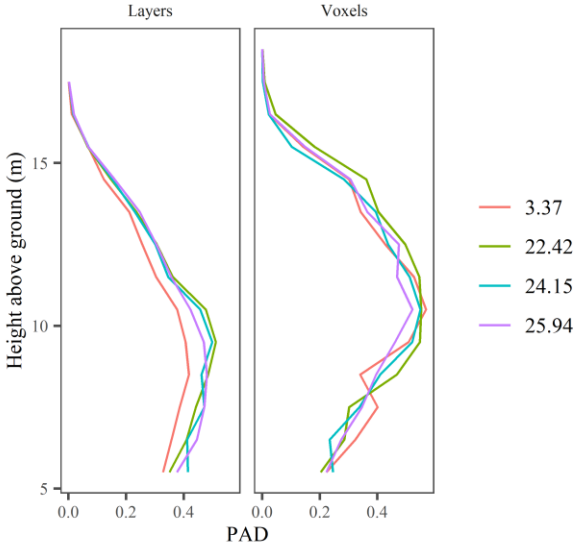

Plot: 174_IRSTEA

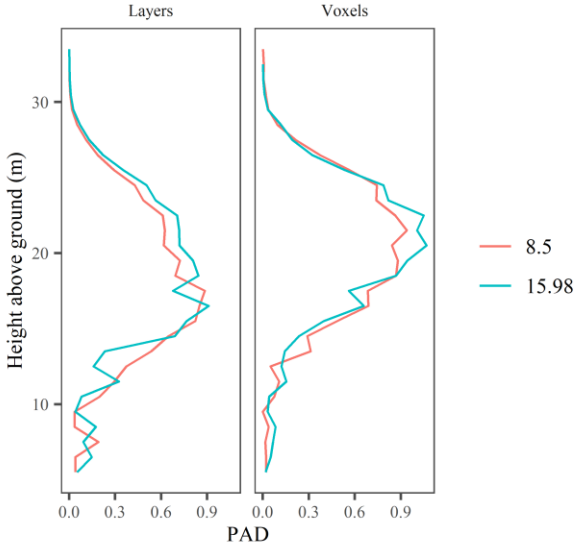

Plot: 178_IRSTEA

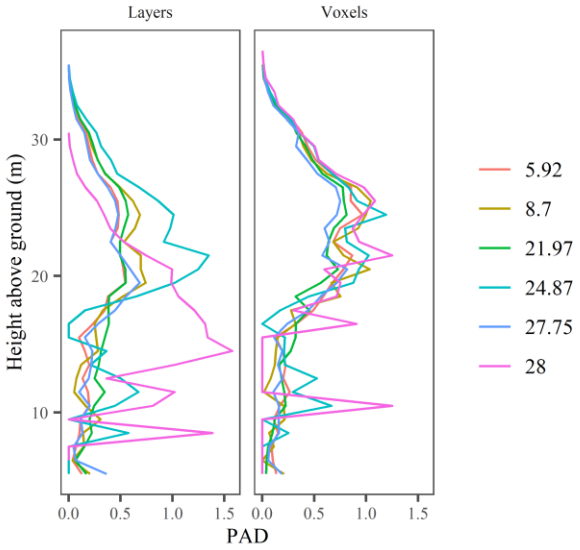

Plot: 182_IRSTEA

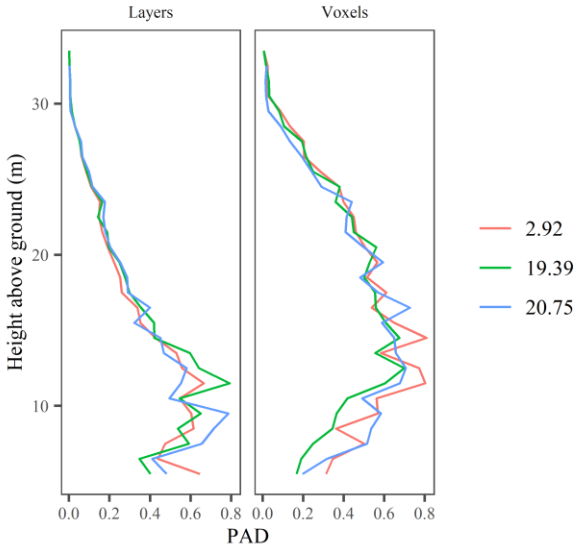

Plot: 185_IRSTEA

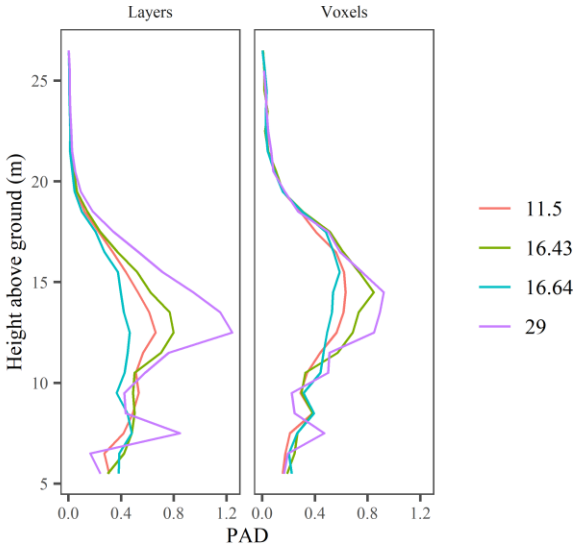

Plot: 189_IRSTEA

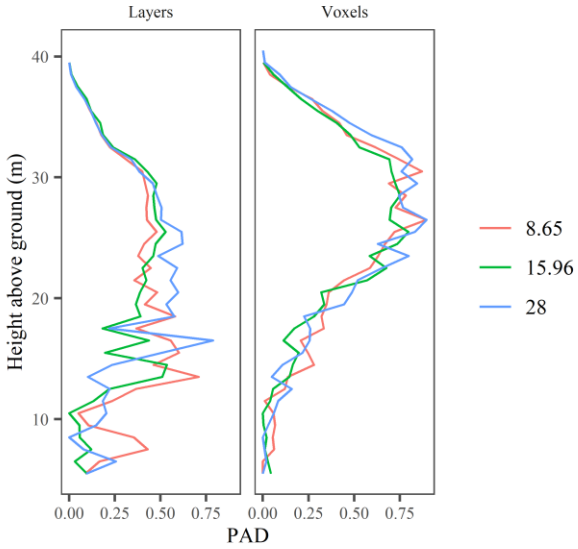

Plot: 190_IRSTEA

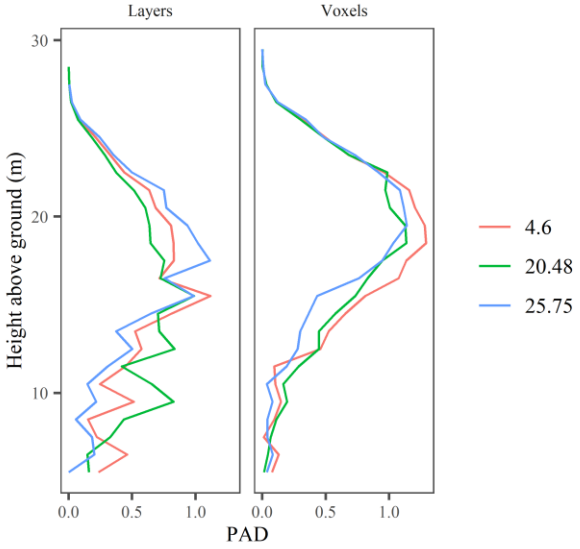

Plot: 192_IRSTEA

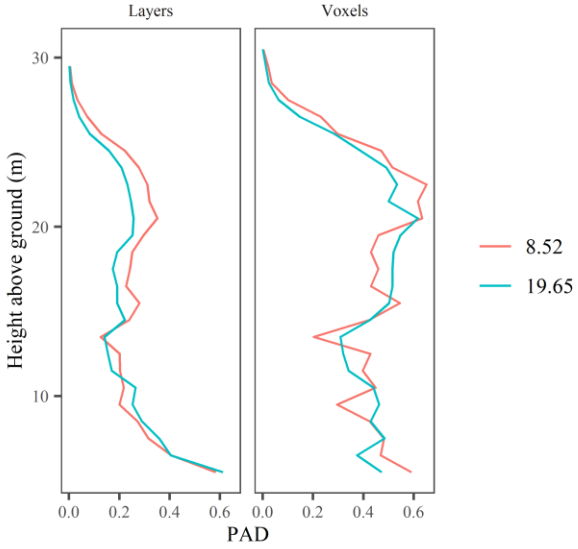

Plot: 197_IRSTEA

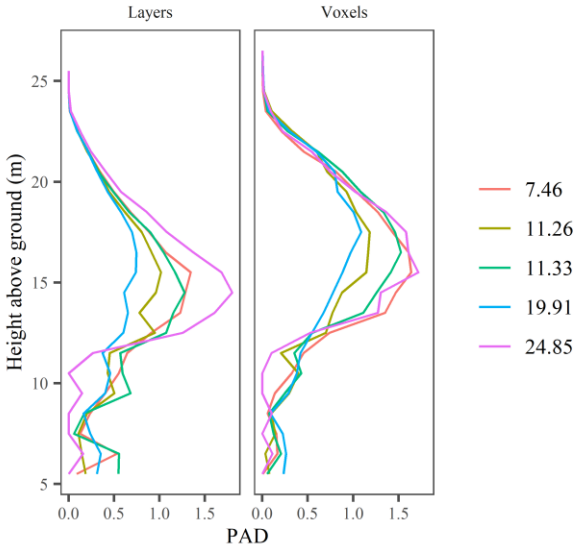

Plot: 199_IRSTEA

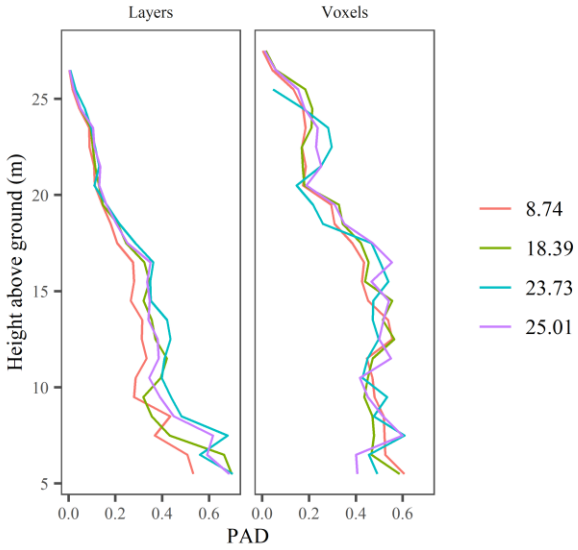

Plot: 203_IRSTEA

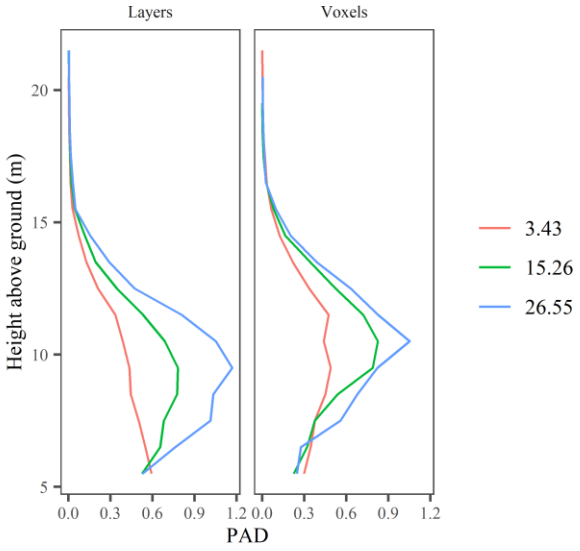

Plot: 205_74_ONF

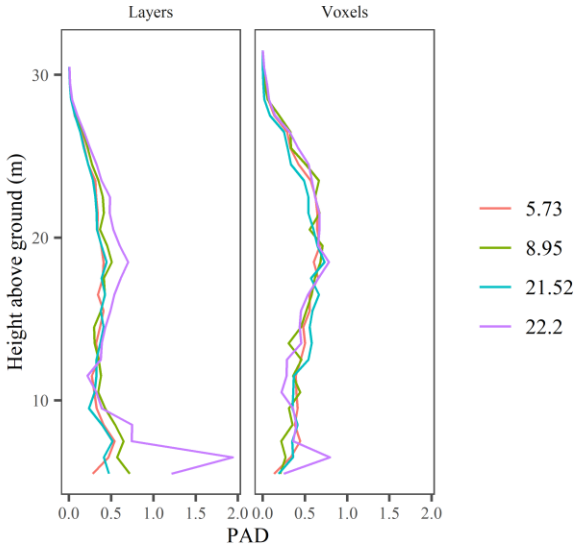

Plot: 207_IRSTEA

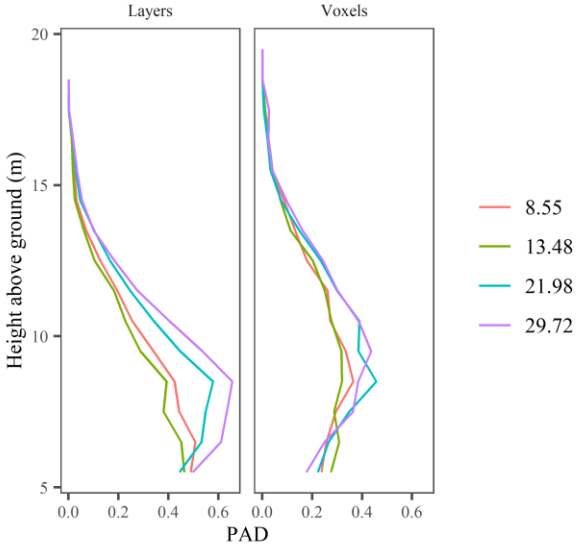

Plot: 208_IRSTEA

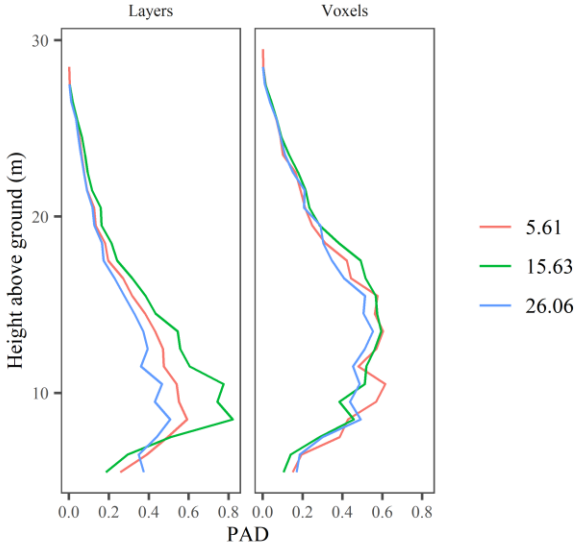

Plot: 209_74_ONF

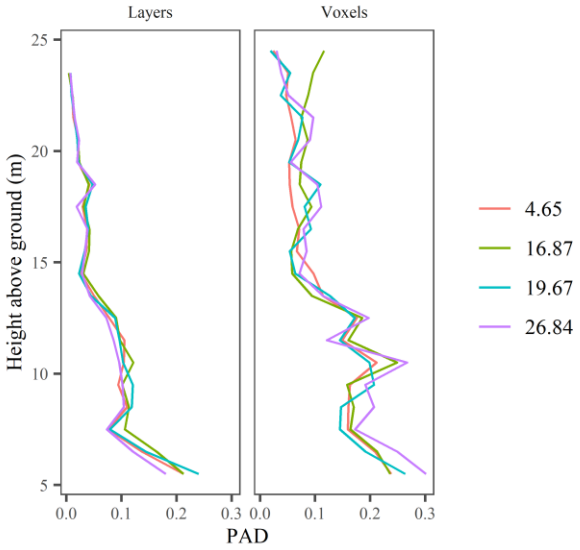

Plot: 210_74_ONF

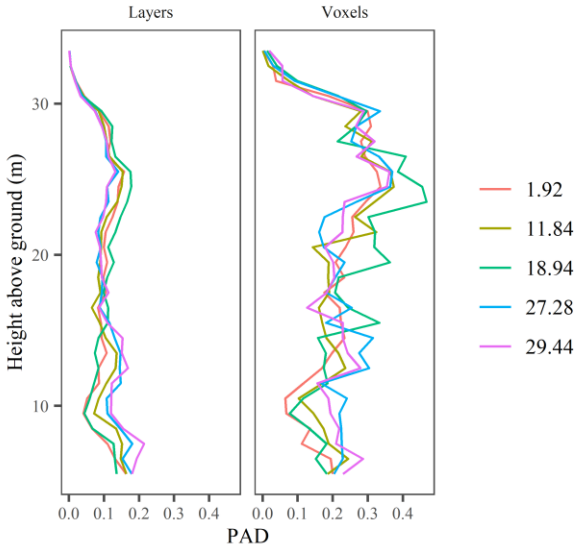

Plot: 211_74_ONF

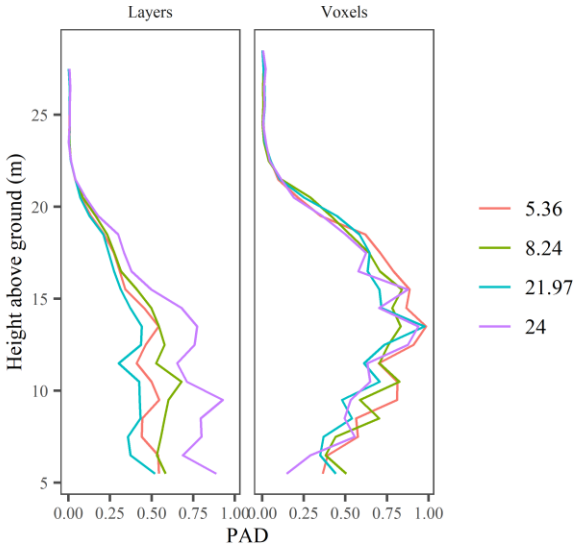

Plot: 212_74_ONF

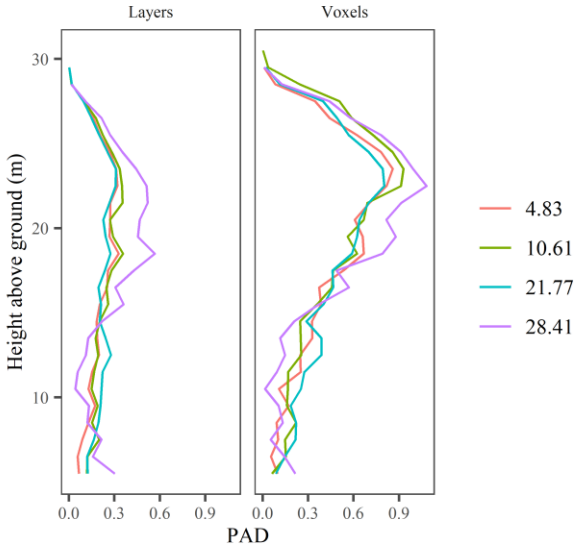

Plot: 223_74_ONF

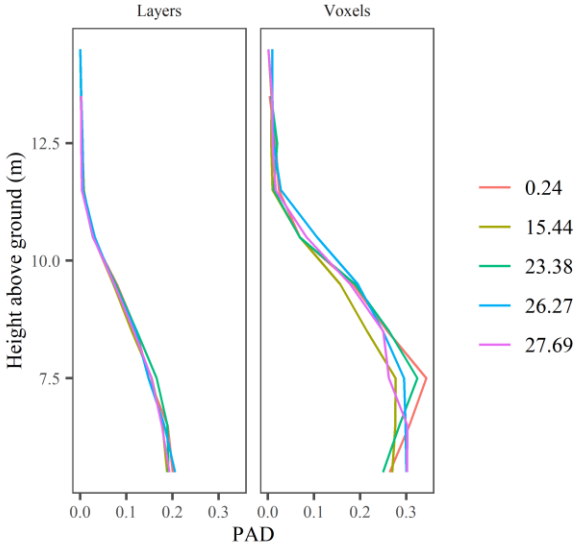

Plot: 235_74_ONF

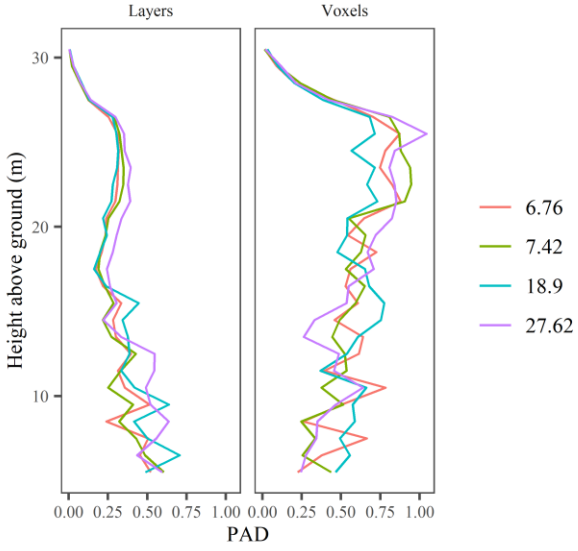

Plot: 239_74_ONF

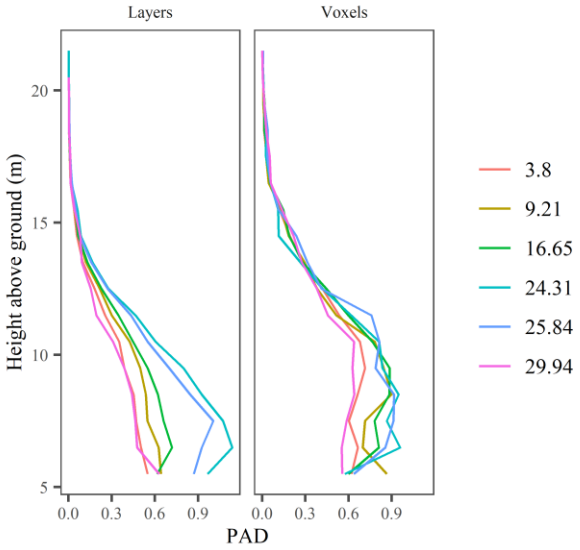

Plot: 23_73_ONF

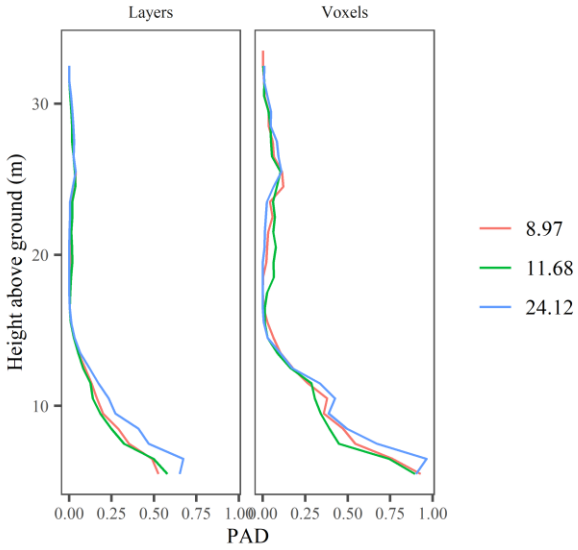

Plot: 246_74_ONF

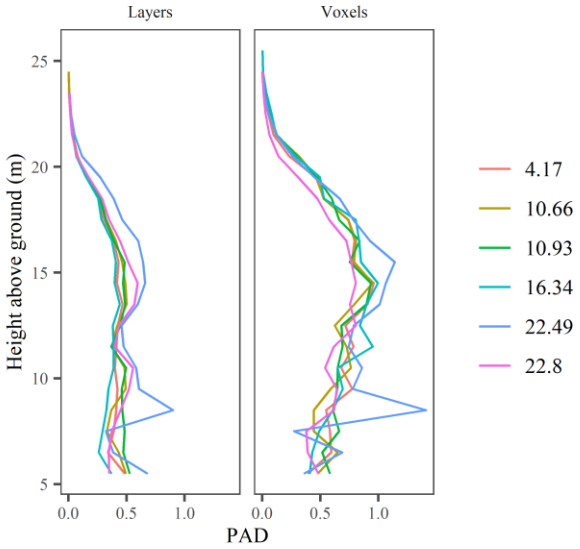

Plot: 364_74_ONF

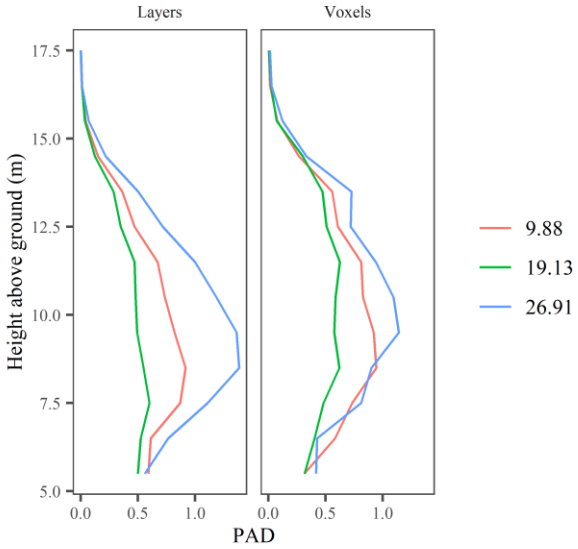

Plot: 73_IRSTEA

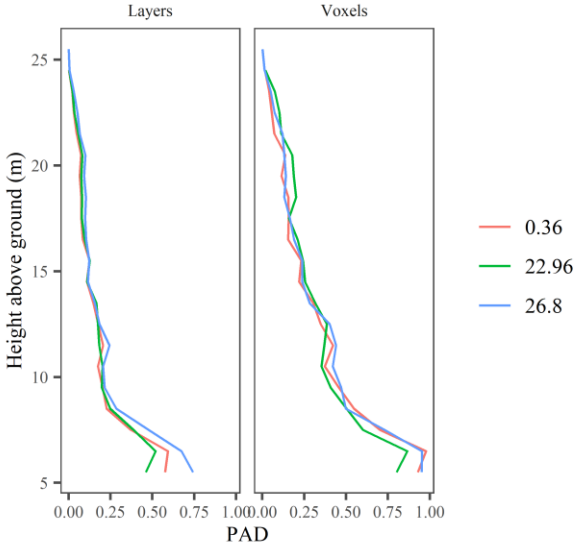

Plot: 85_IRSTEA

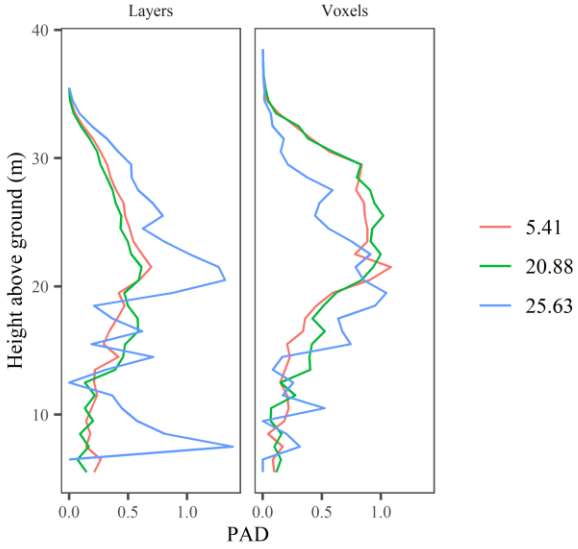

Plot: 105_IRSTEA

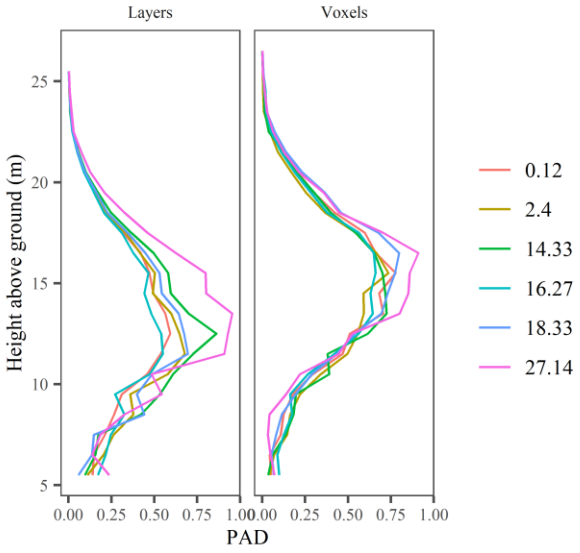

Plot: 114_IRSTEA

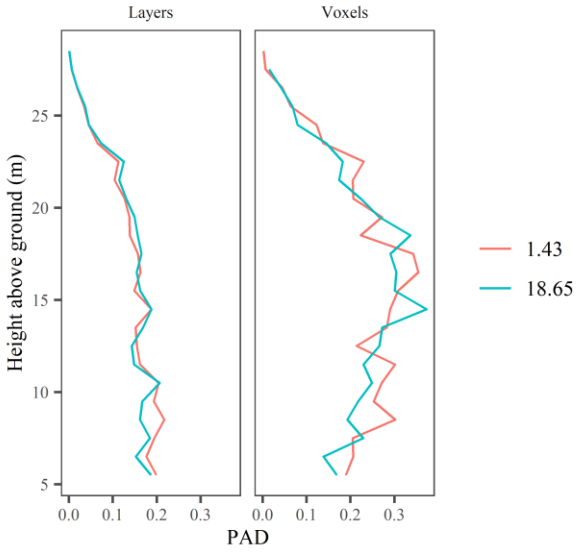

Plot: 127_IRSTEA

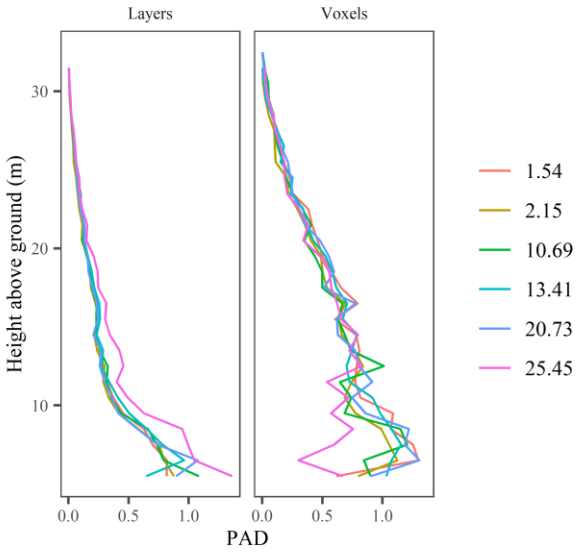

Plot: 138_IRSTEA

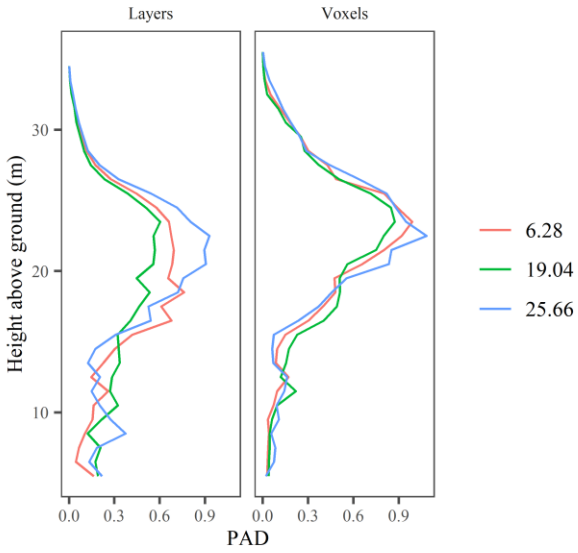

Plot: 140_IRSTEA

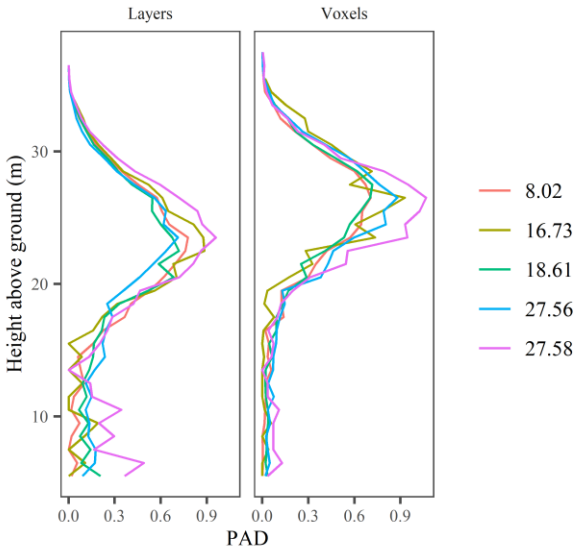

Plot: 148_IRSTEA

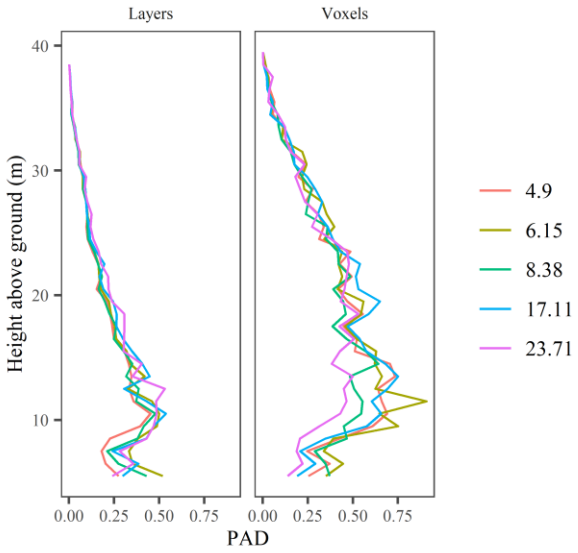

Plot: 14_74_ONF

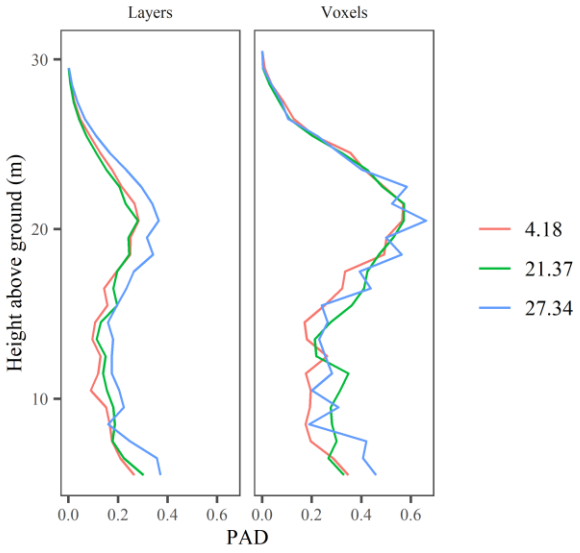

Plot: 155_IRSTEA

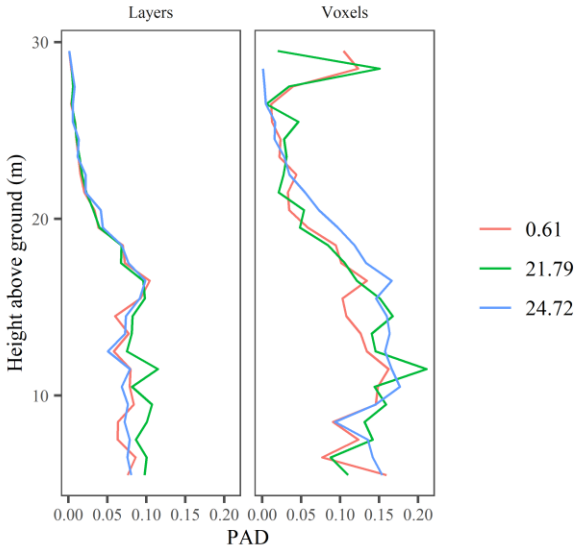

Plot: 162_IRSTEA

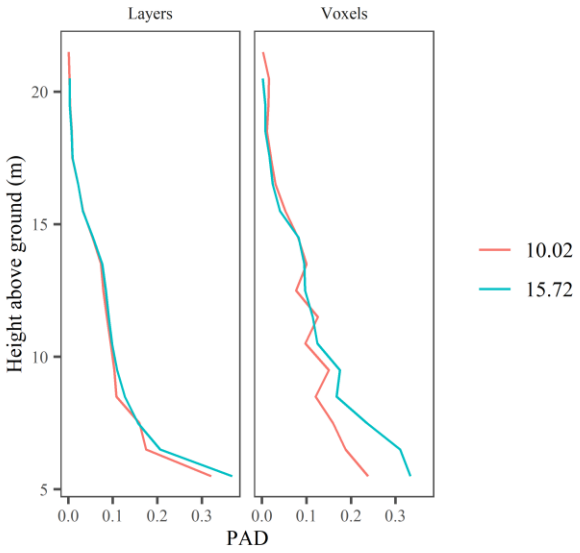

Plot: 170_IRSTEA

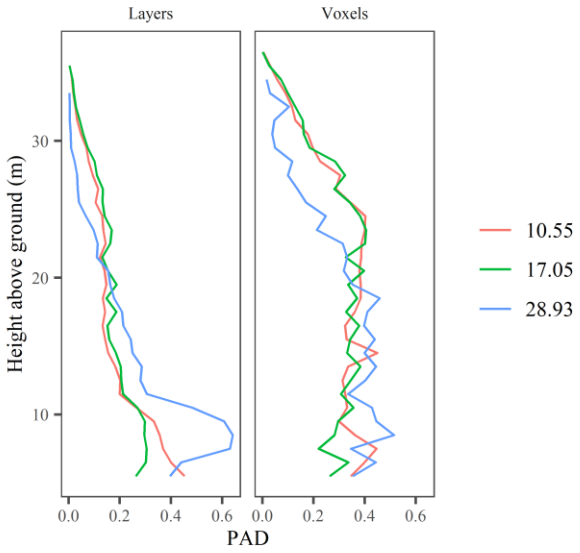

Plot: 171_IRSTEA

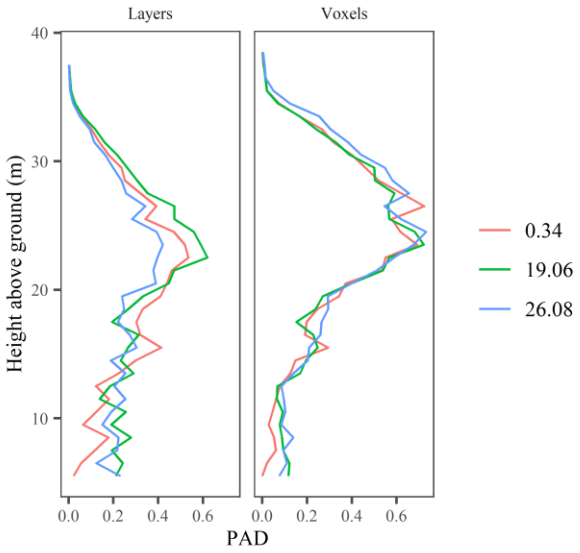

Plot: 176_IRSTEA

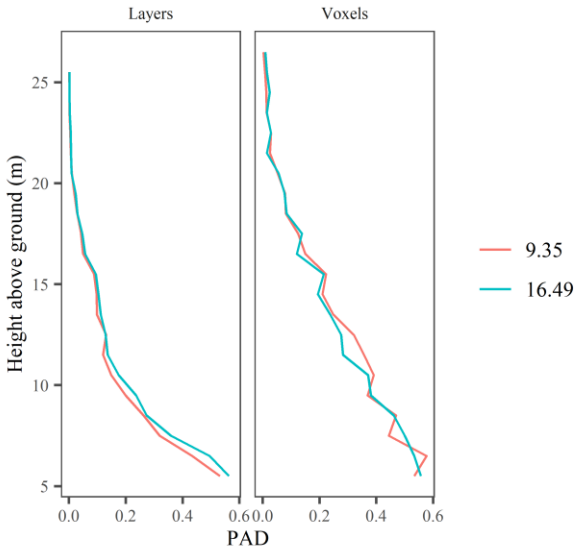

Plot: 177_IRSTEA

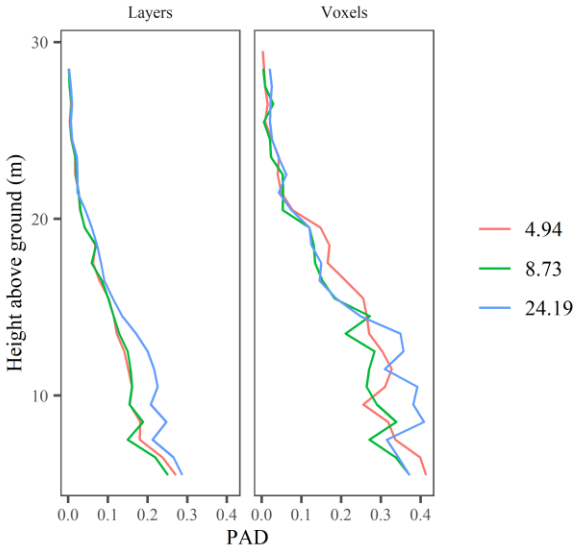

Plot: 184_IRSTEA

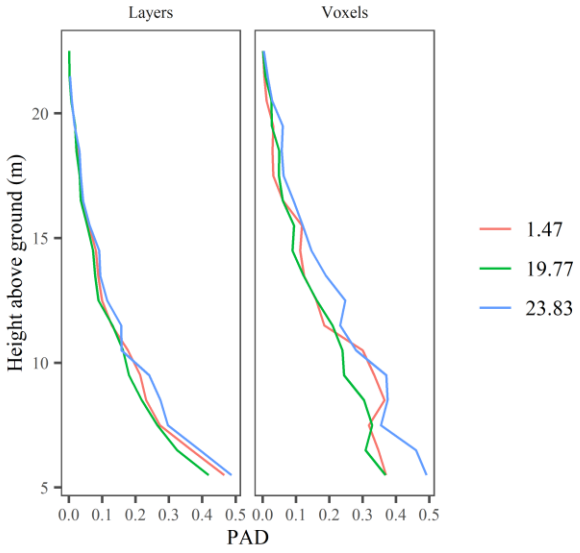

Plot: 198_IRSTEA

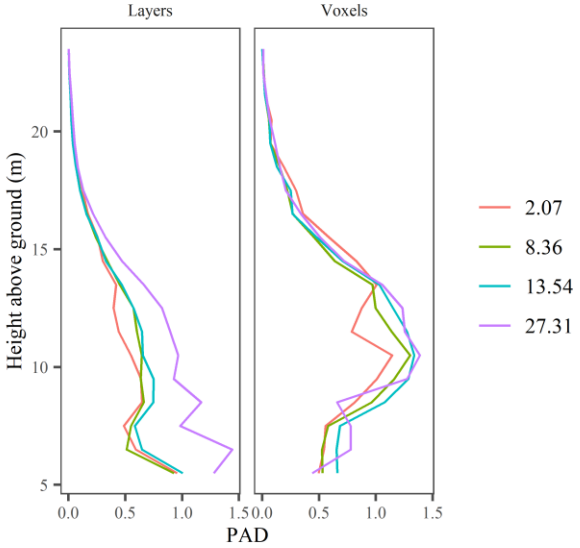

Plot: 217_74_ONF

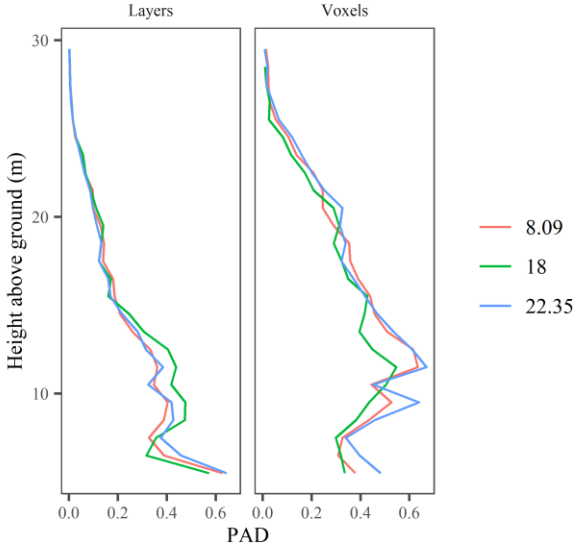

Plot: 222_74_ONF

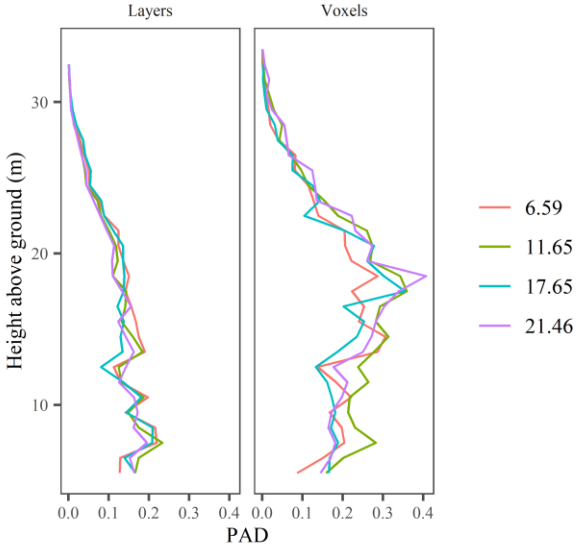

Plot: 247_74_ONF

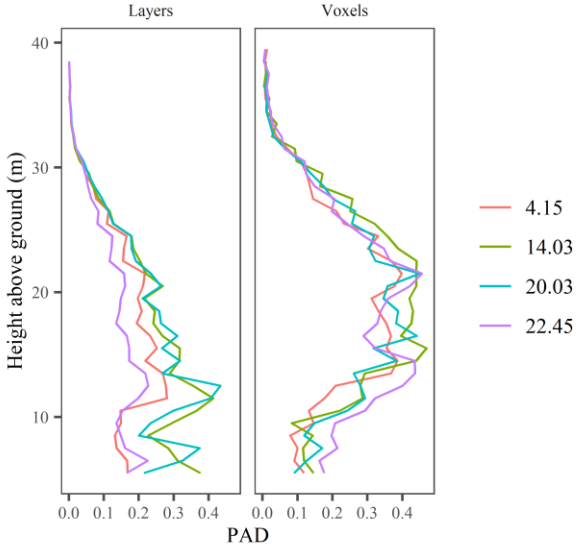

Plot: 255_74_ONF

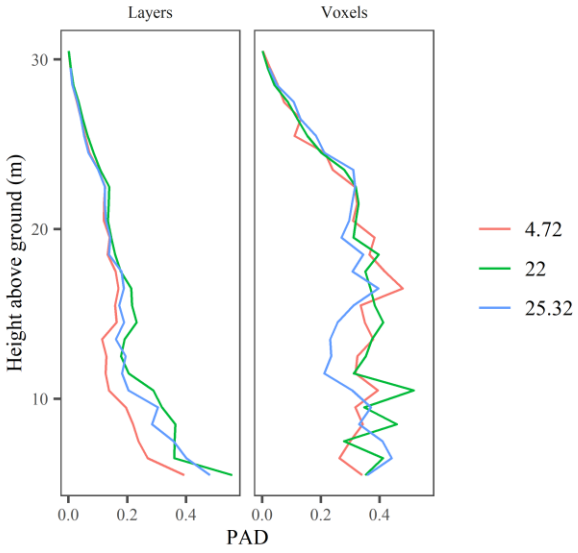

Plot: 257_74_ONF

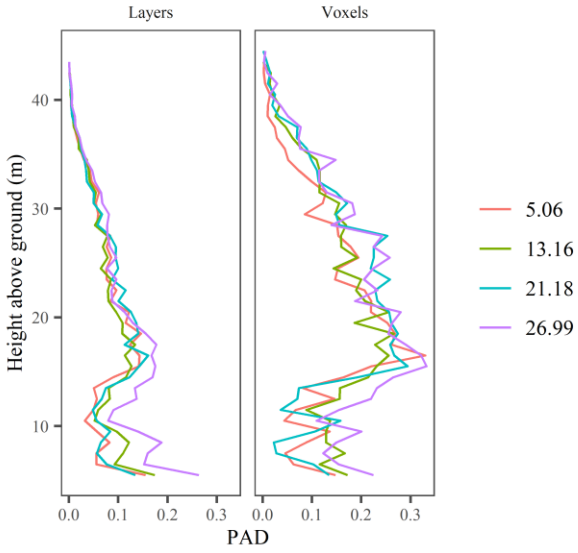

Plot: 259_74_ONF

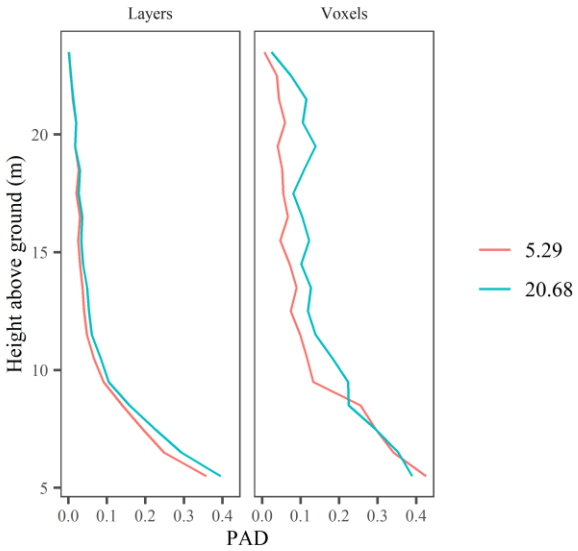

Plot: 25_73_ONF

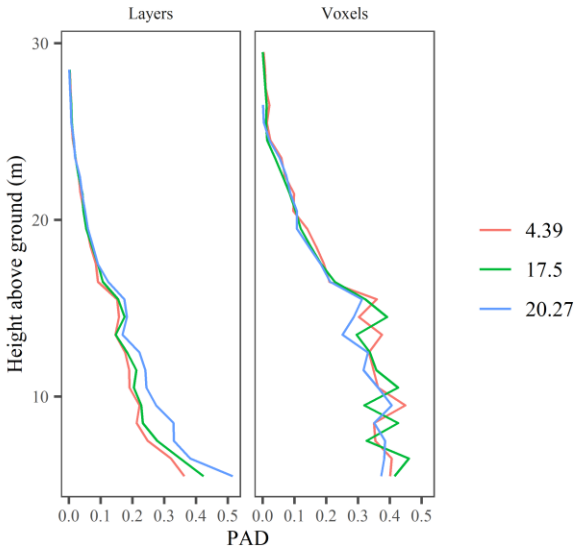

Plot: 270_74_ONF

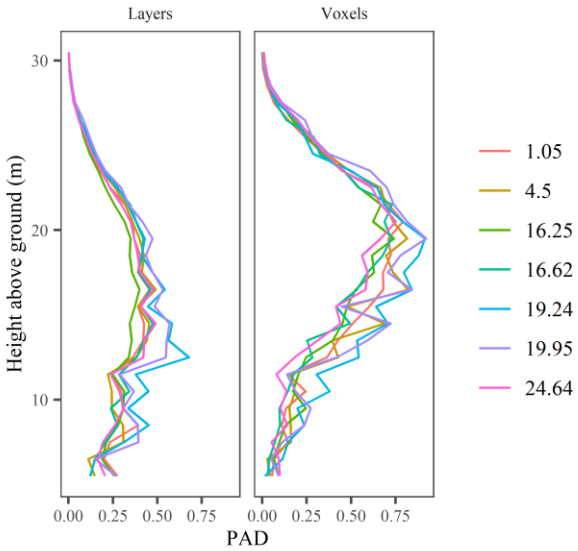

Plot: 271_74_ONF

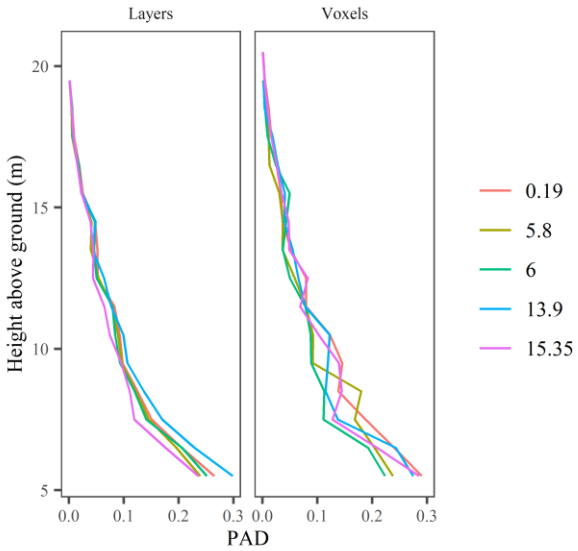

Plot: 285_74_ONF

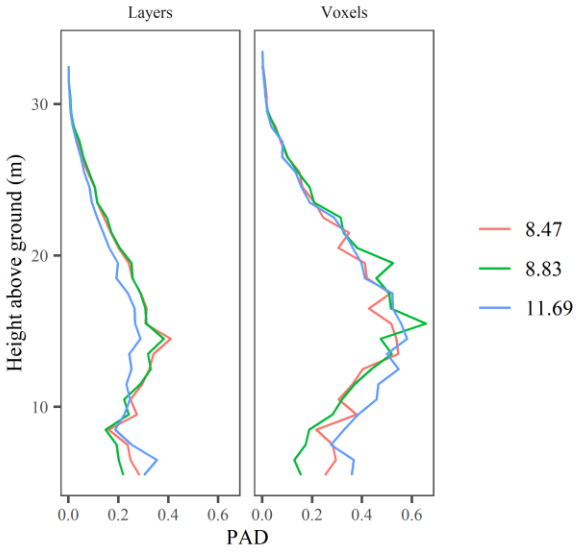

Plot: 307_74_ONF

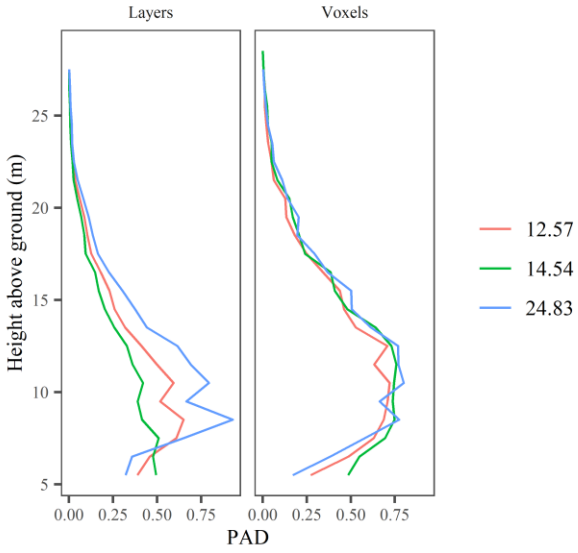

Plot: 314_74_ONF

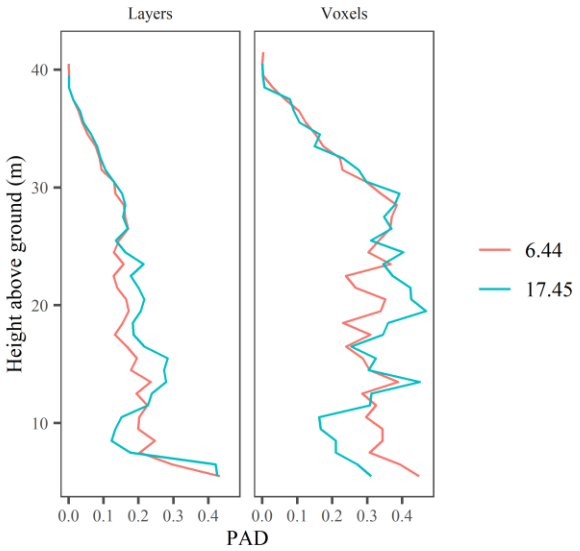

Plot: 317_74_ONF

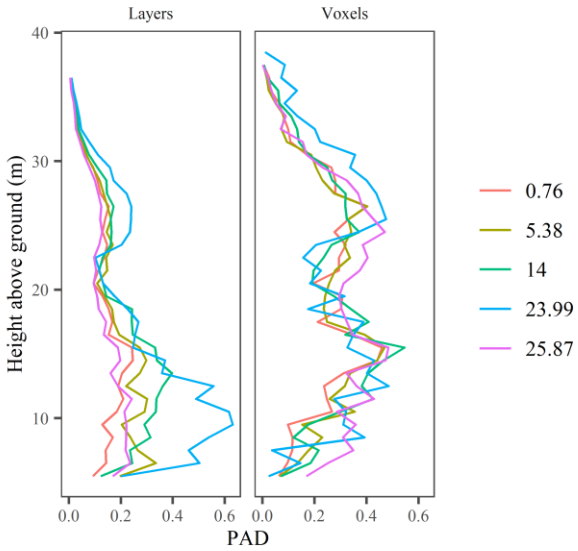

Plot: 3341_73_ONF

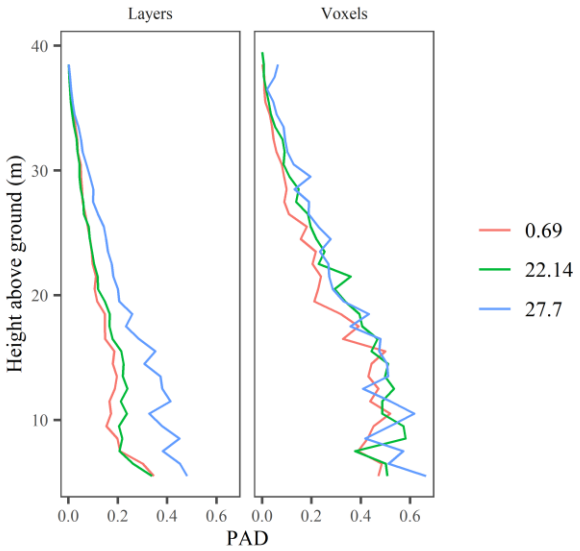

Plot: 49_74_ONF

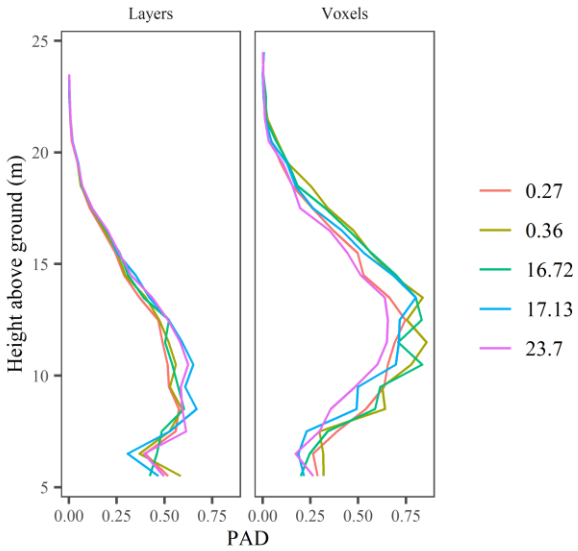

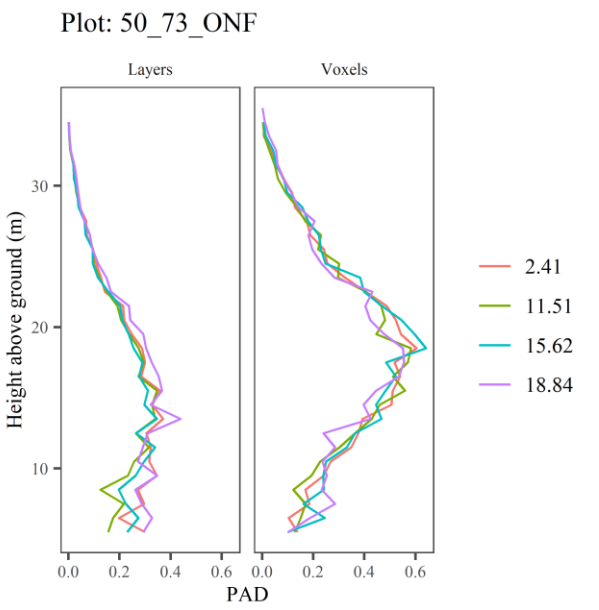
Plot: 50_73_ONF
Layers
Voxels
Height above ground (m)
30
20
10
0.0
0.2
0.4
0.6
PAD
2.41
11.51
15.62
18.84

Plot: 109_IRSTEA

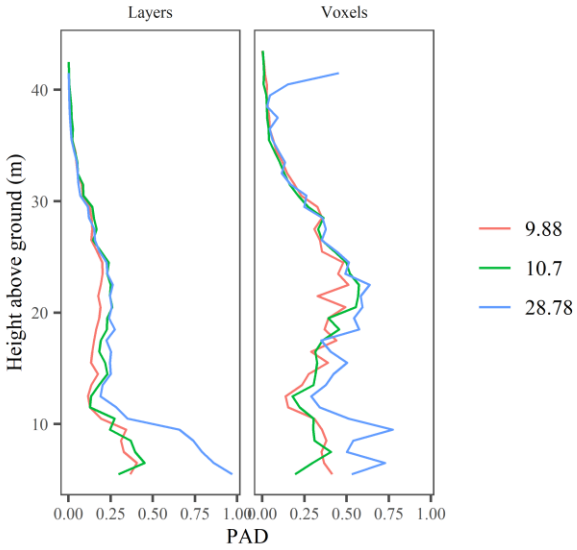

Plot: 126_IRSTEA

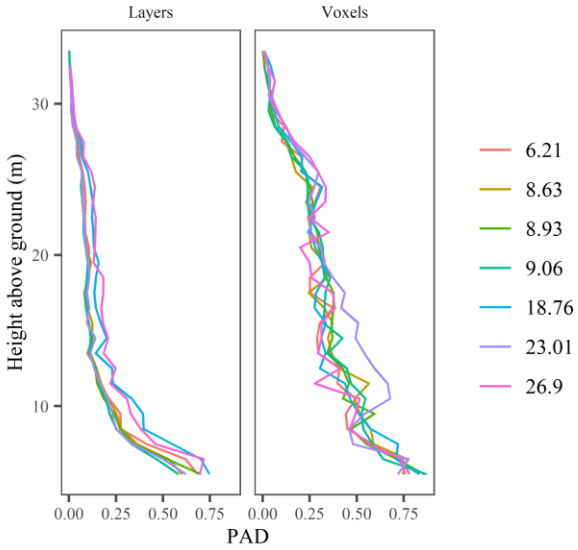

Plot: 137_74_ONF

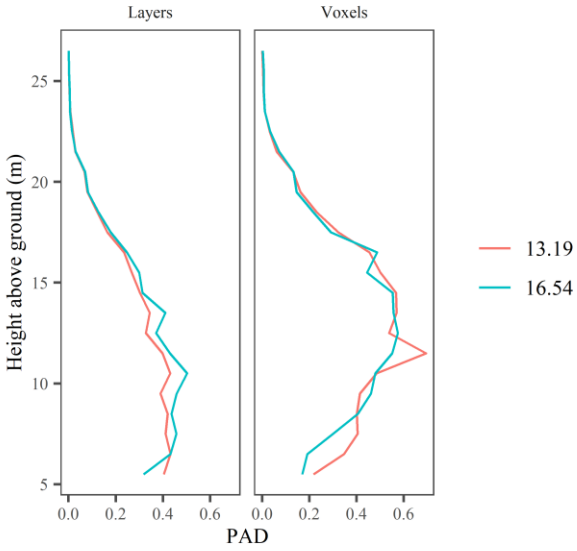

Plot: 139_74_ONF

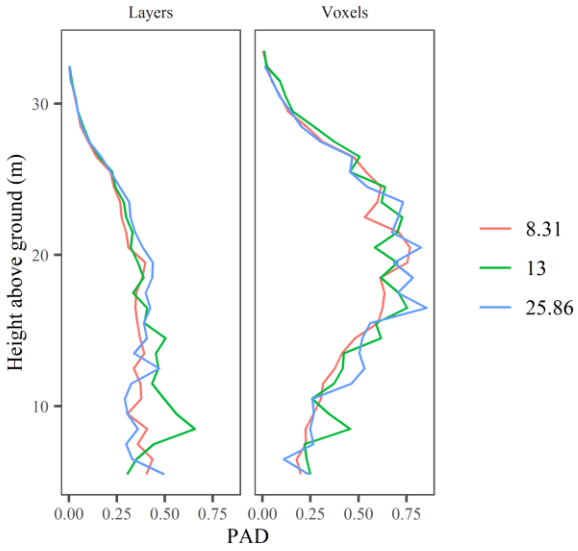

Plot: 149_IRSTEA

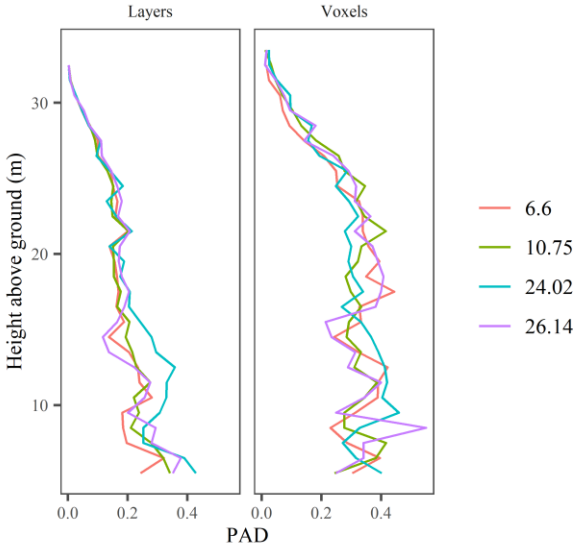

Plot: 150_IRSTEA

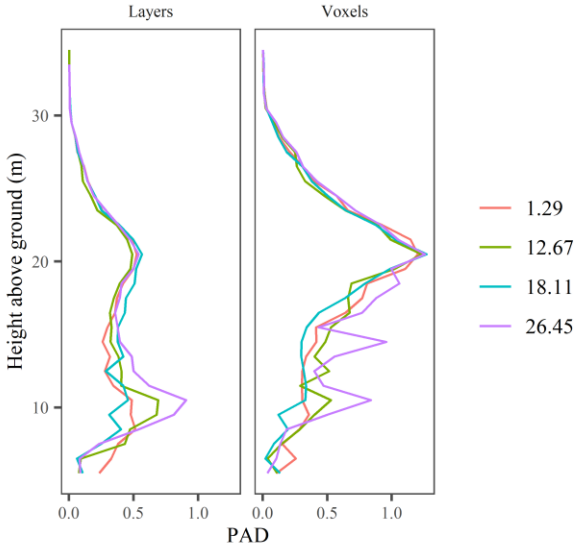

Plot: 151_IRSTEA

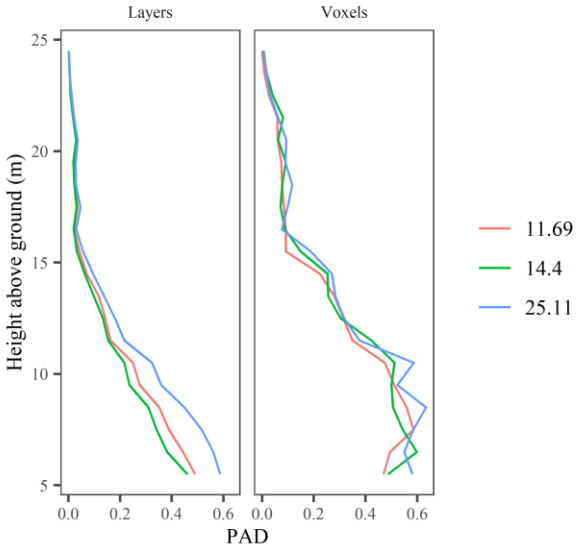

Plot: 152_IRSTEA

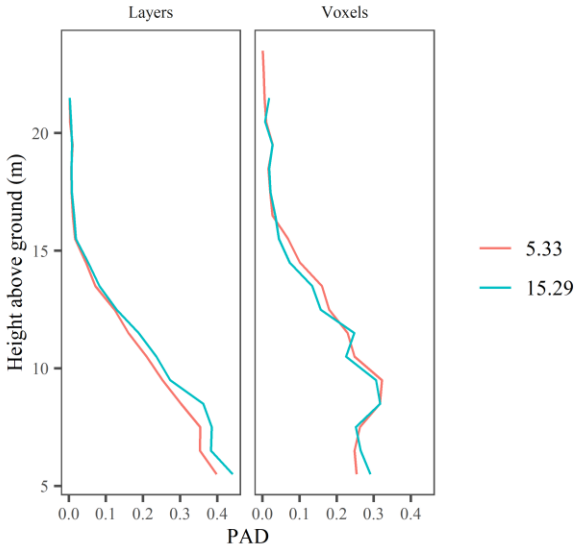

Plot: 15_74_ONF

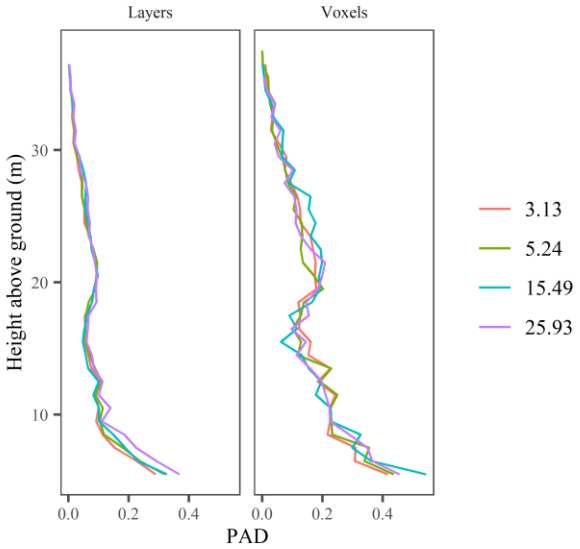

Plot: 163_IRSTEA

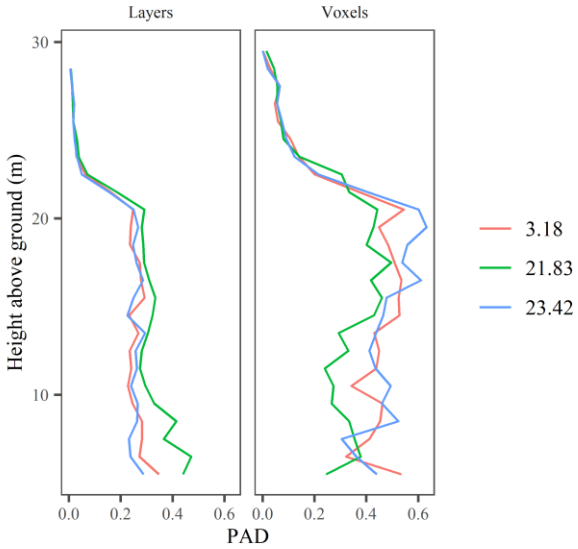

Plot: 164_IRSTEA

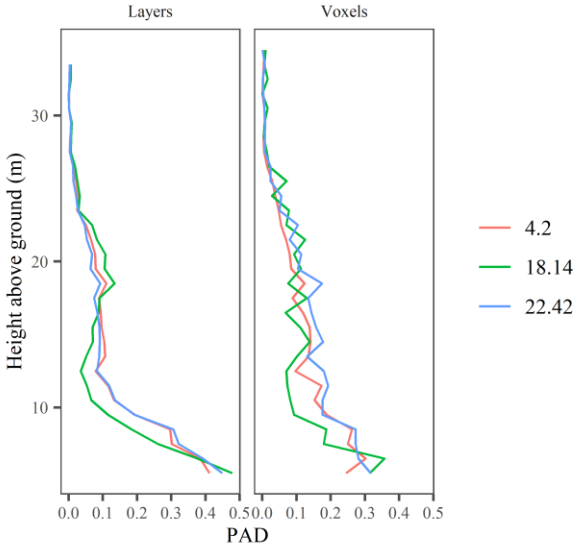

Plot: 172_IRSTEA

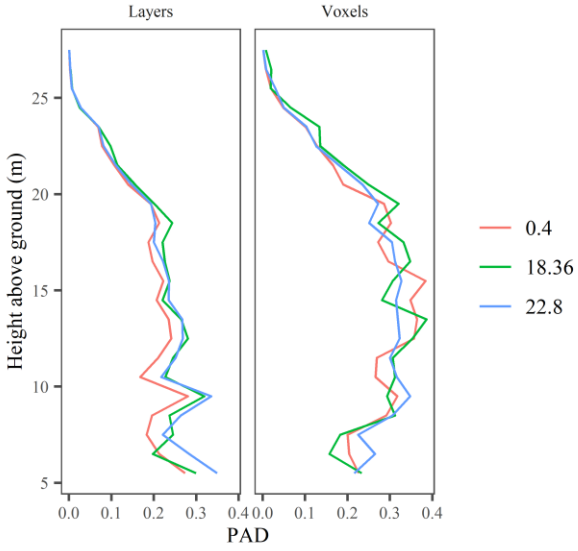

Plot: 175_IRSTEA

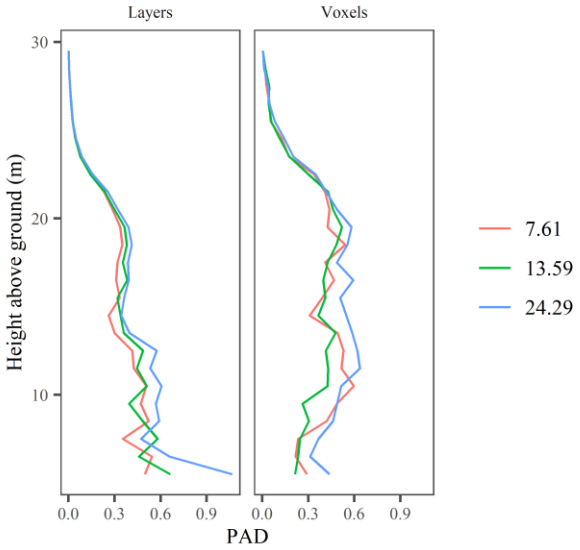

Plot: 180_IRSTEA

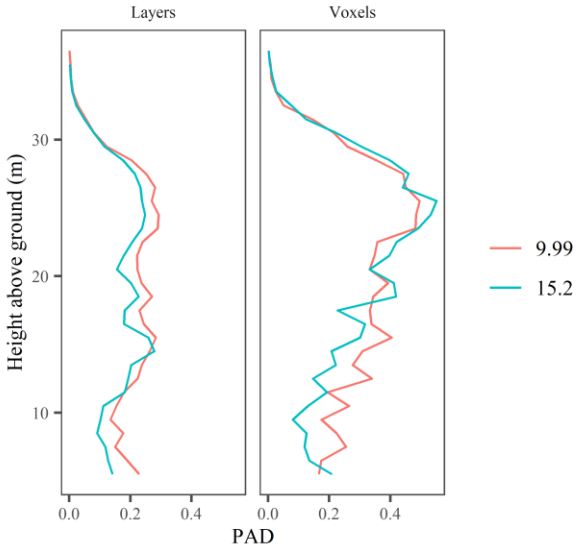

Plot: 181_IRSTEA

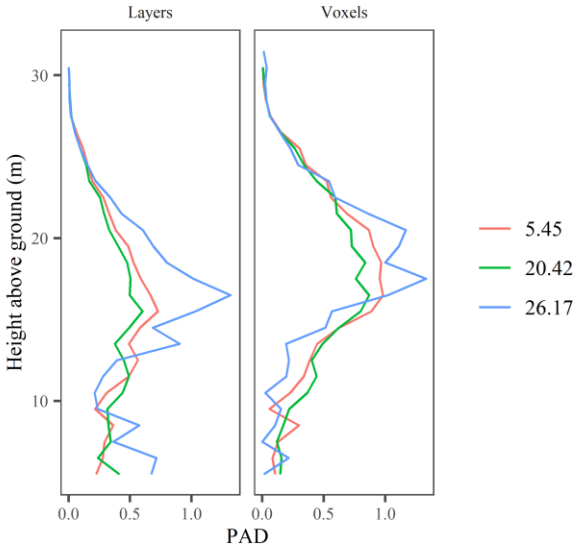

Plot: 183_IRSTEA

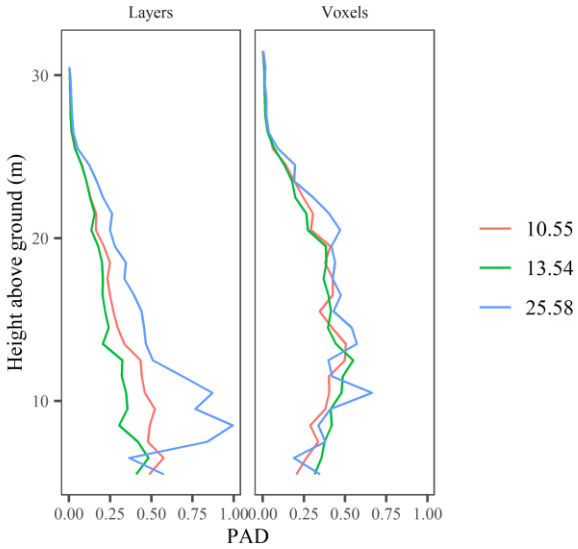

Plot: 186_IRSTEA

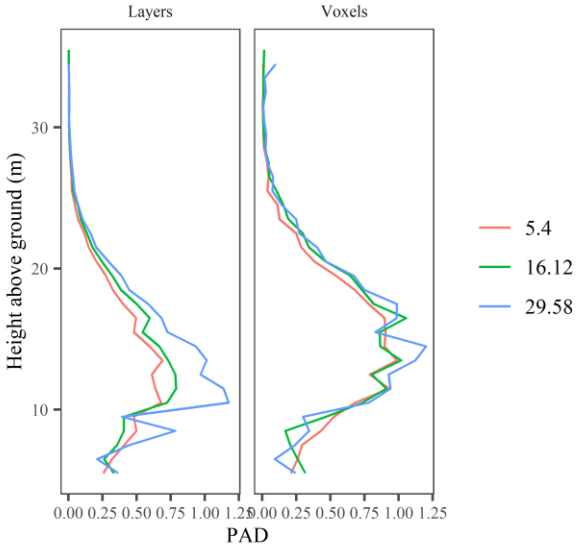

Plot: 188_IRSTEA

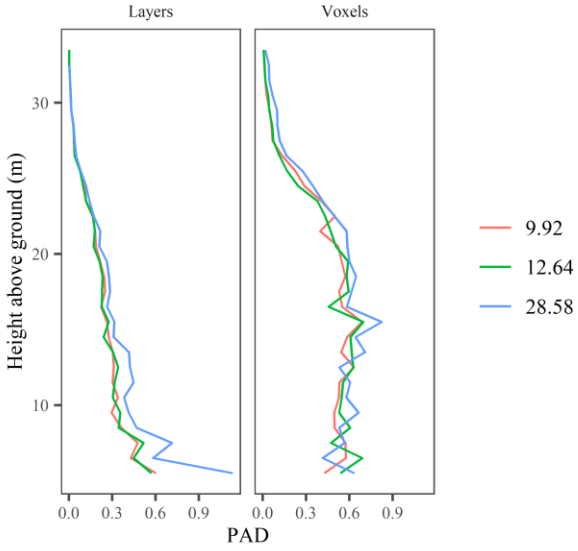

Plot: 191_IRSTEA

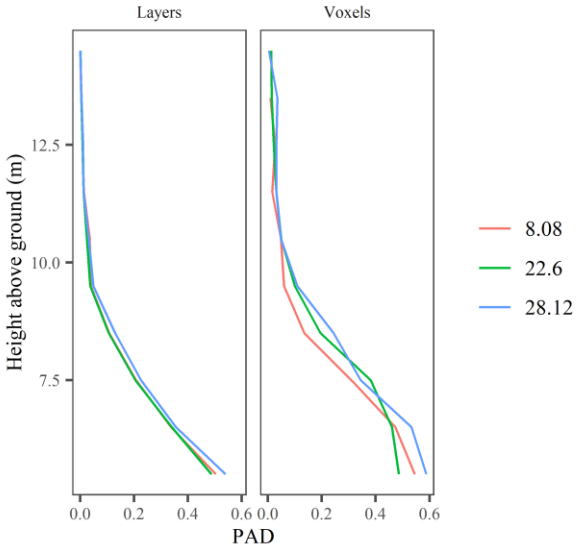

Plot: 193_IRSTEA

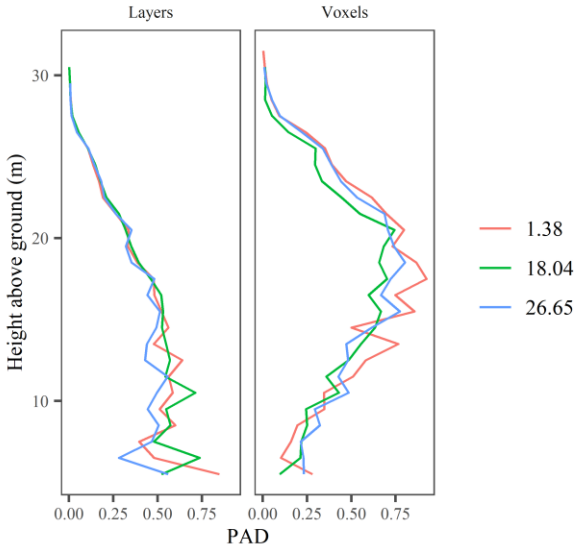

Plot: 194_IRSTEA

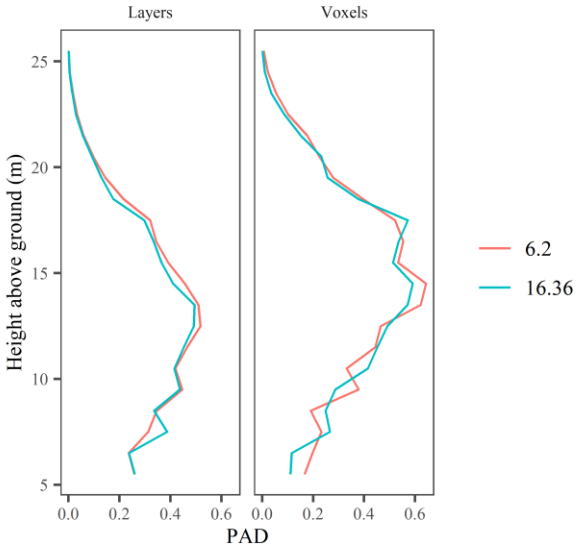

Plot: 195_IRSTEA

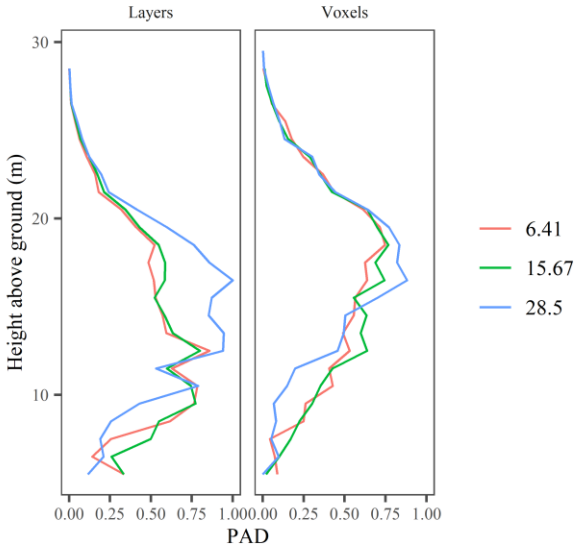

Plot: 196_IRSTEA

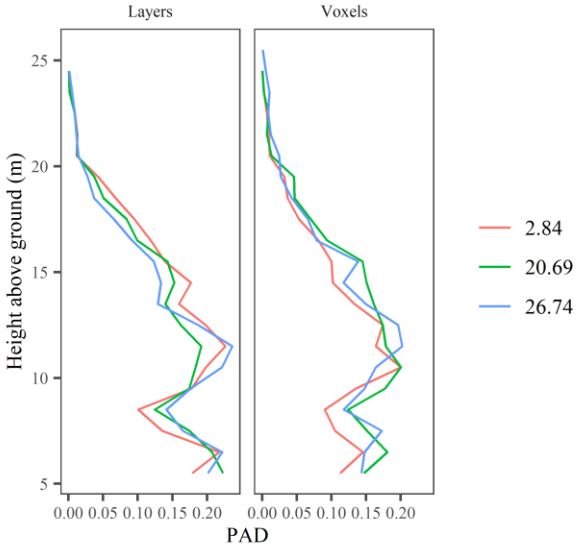

Plot: 200_IRSTEA

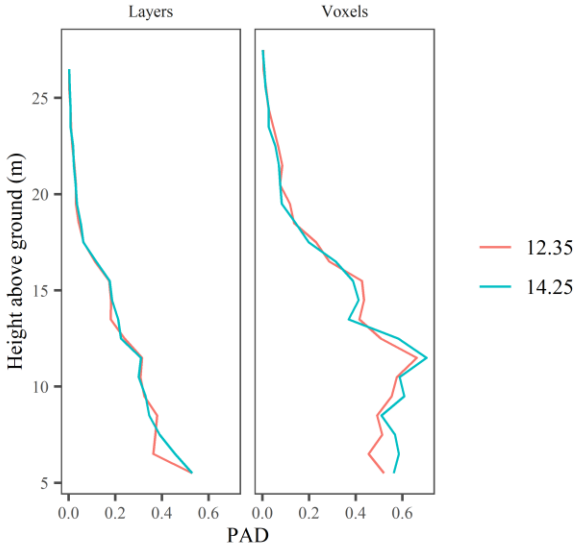

Plot: 201_IRSTEA

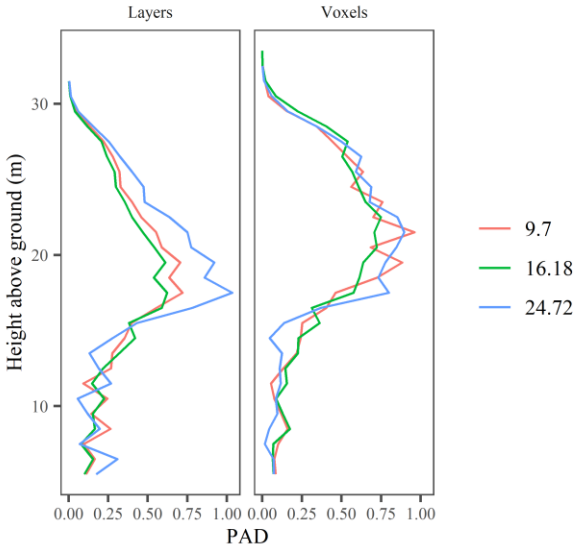

Plot: 202_IRSTEA

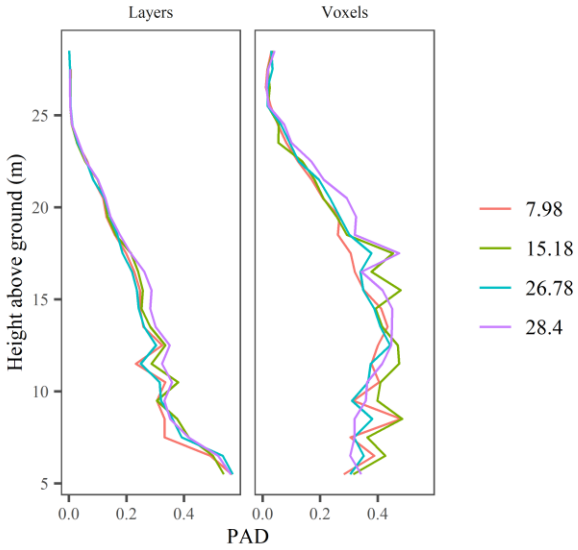

Plot: 204_IRSTEA

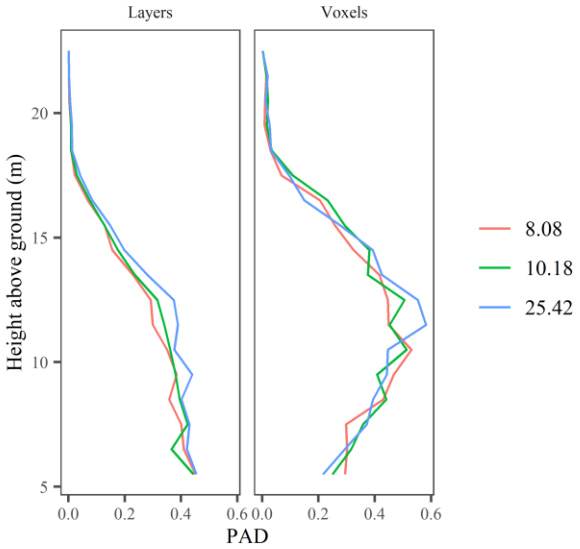

Plot: 206_IRSTEA

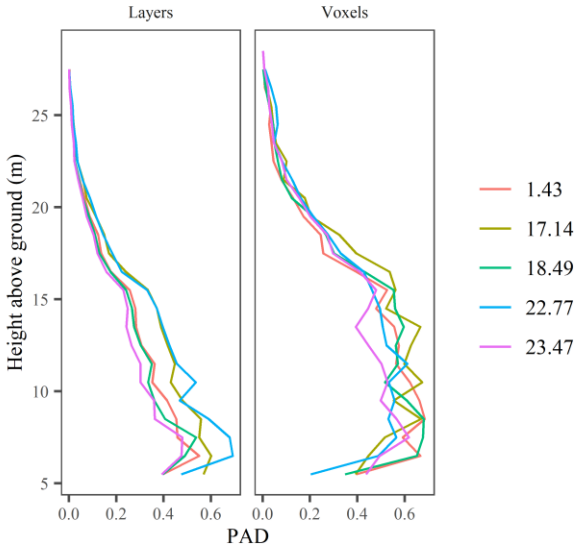

Plot: 209_IRSTEA

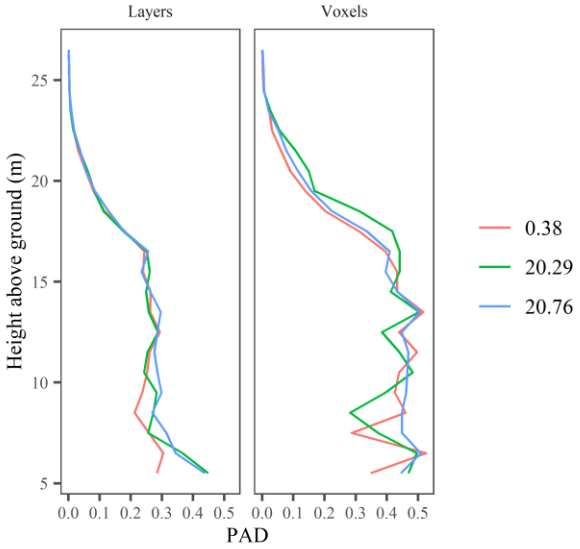

Plot: 213_74_ONF

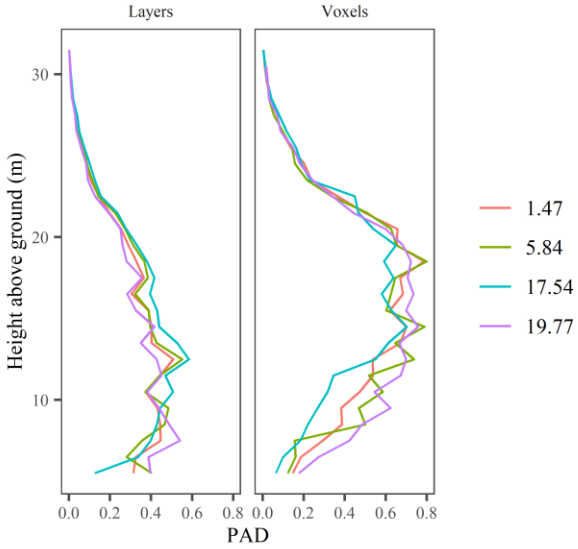

Plot: 218_74_ONF

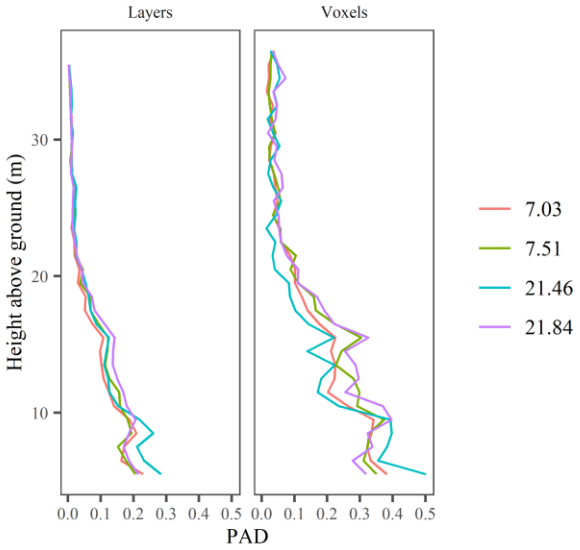

Plot: 219_74_ONF

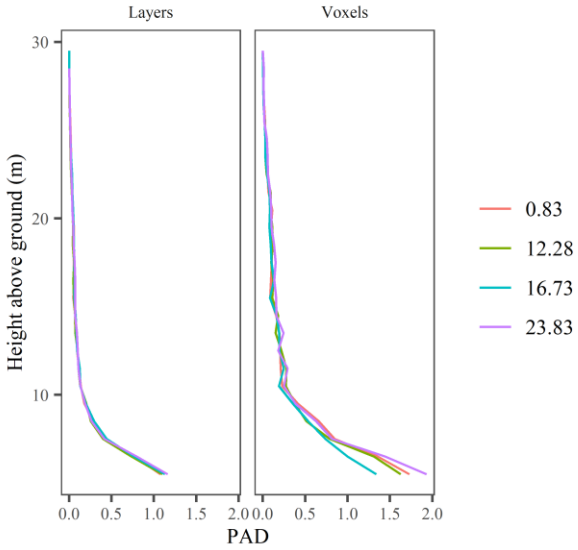

Plot: 220_74_ONF

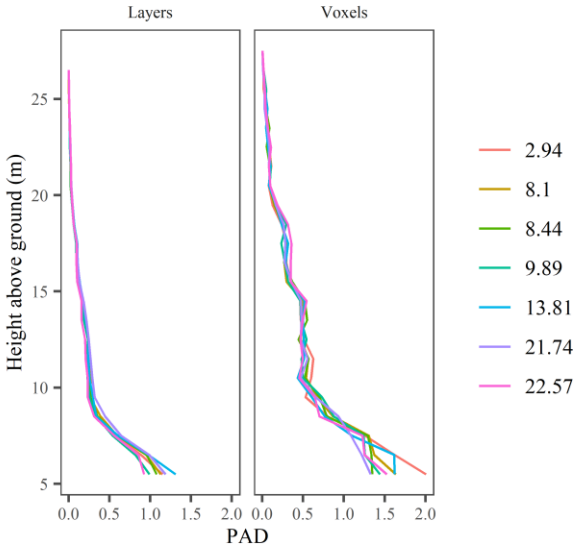

Plot: 232_74_ONF

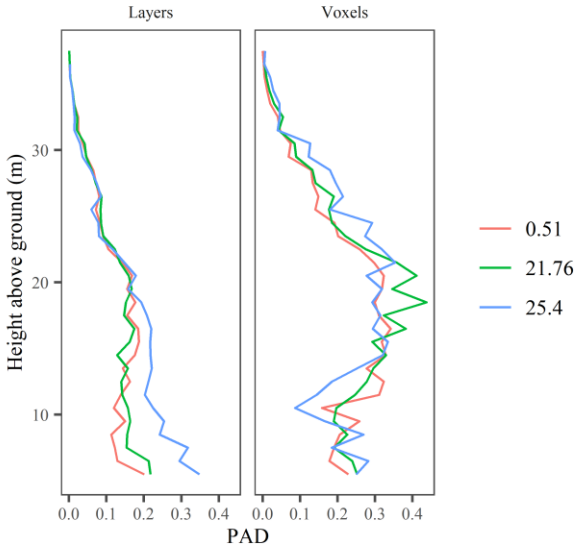

Plot: 258_74_ONF

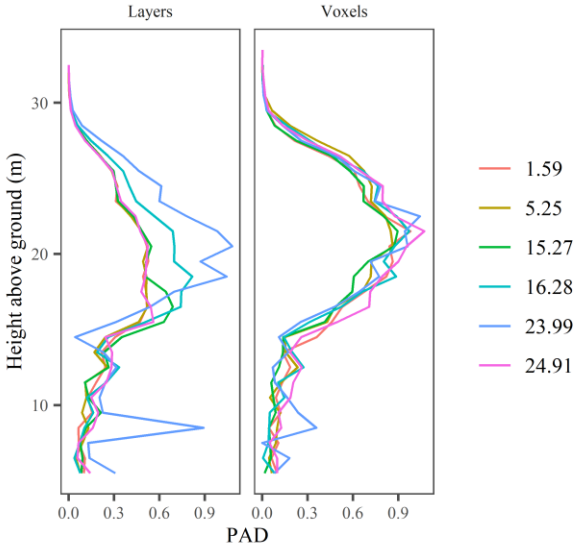

Plot: 264_74_ONF

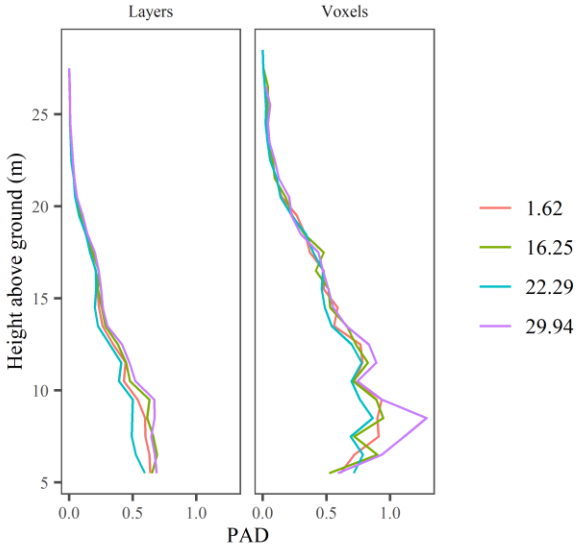

Plot: 267_74_ONF

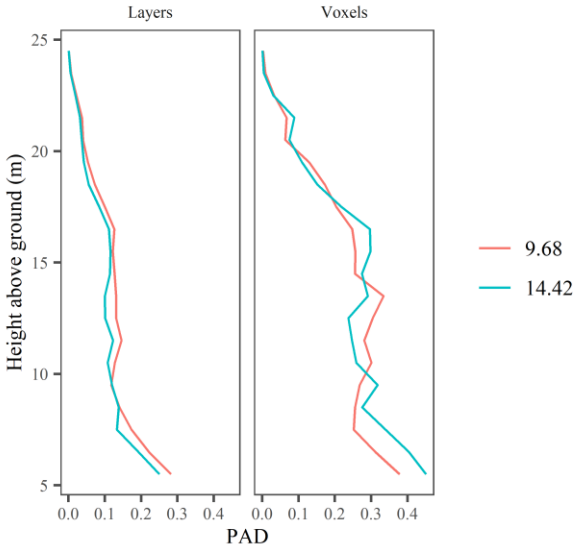

Plot: 268_74_ONF

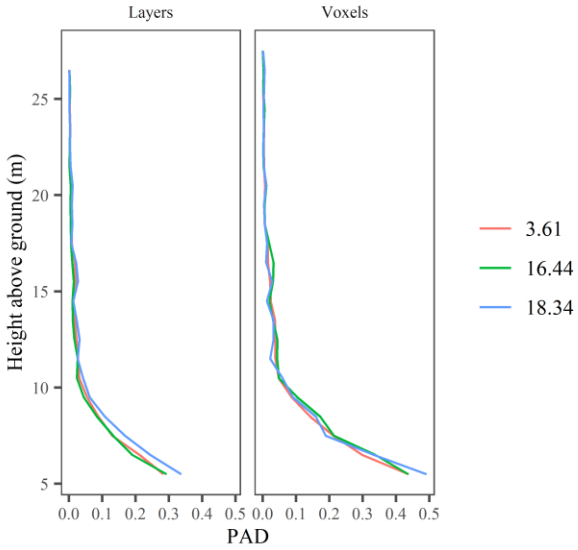

Plot: 46_74_ONF

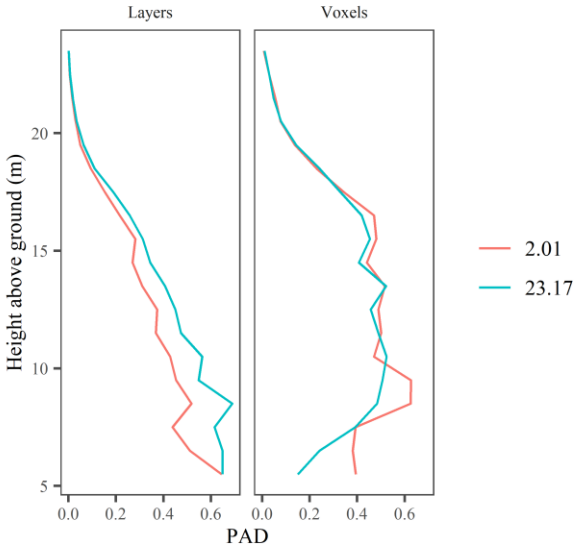

Plot: 48_74_ONF

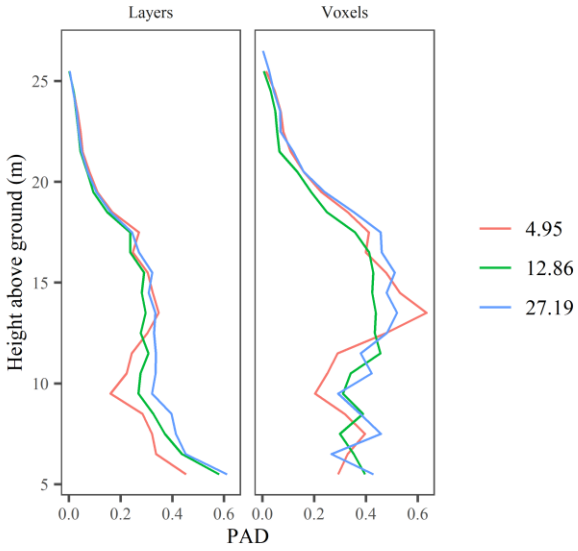

Plot: 52_74_ONF

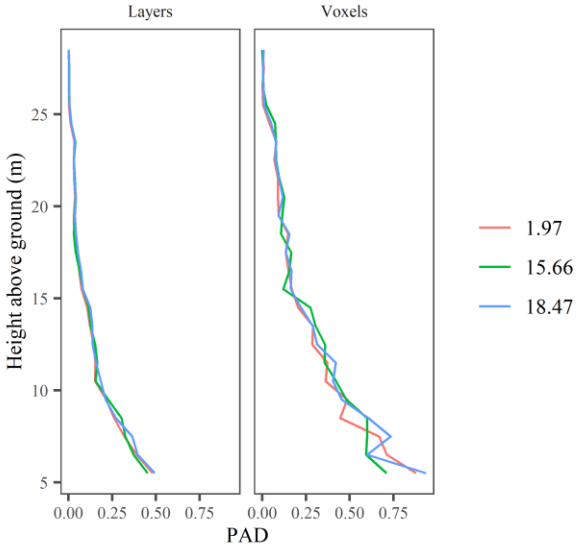

Plot: 62_74_ONF

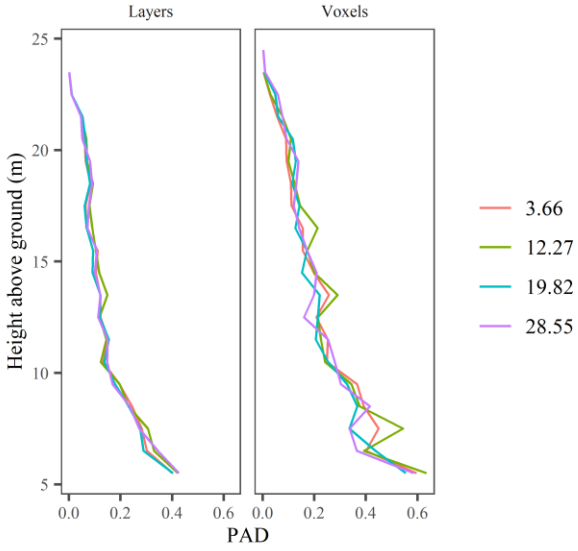

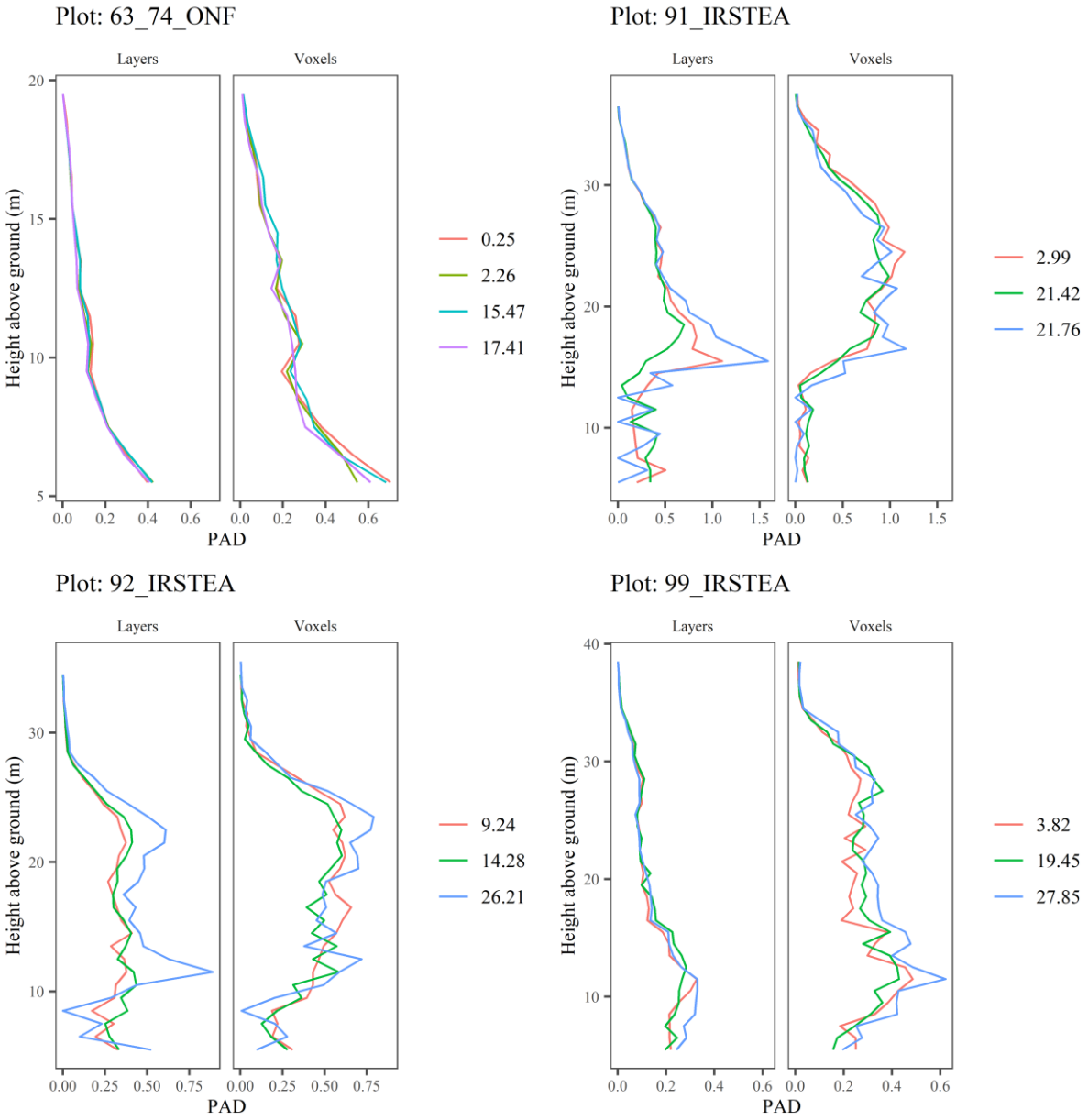
Plot: 63_74_ONF
Layers
Voxels
Height above ground (m)
PAD
0.25
2.26
15.47
17.41
Plot: 91_IRSTEA
2.99
21.42
21.76
Plot: 92_IRSTEA
9.24
14.28
26.21
Plot: 99_IRSTEA
3.82
19.45
27.85

Bibliography

1. ACT, n.d. LiDAR 2019 - Relevé 3D du territoire luxembourgeois [WWW Document]. URL https://data.public.lu/en/datasets/lidar-2019-releve-3d-du-territoire-luxembourgeois/ (accessed 4.26.22).
2. AGENCIJA RS ZA OKOLJE [WWW Document], n.d. URL http://gis.arso.gov.si/evode/profile.aspx?id=atlas_voda_Lidar@Arso (accessed 4.26.22).
3. Ahokas, E., Yu, X., Oksanen, J., Hyyppä, J., Kaartinen, H., Hyyppä, H., 2005. Optimization of the scanning angle for countrywidelaser scanning. Proc. ISPRS Work. Laser Scanning 2005 115–119.
4. Almeida, D.R.A., Stark, S.C., Chazdon, R., Nelson, B.W., Cesar, R.G., Meli, P., Gorgens, E.B., Duarte, M.M., Valbuena, R., Moreno, V.S., Mendes, A.F., Amazonas, N., Gonçalves, N.B., Silva, C.A., Schietti, J., Brancalion, P.H.S., 2019. The effectiveness of lidar remote sensing for monitoring forest cover attributes and landscape restoration. For. Ecol. Manage. 438, 34–43. https://doi.org/10.1016/j.foreco.2019.02.002
5. ASPRS, 2013. LAS SPECIFICATION VERSION 1.4 – R13 28.
6. Atkinson, P.M., Tatnall, A.R.L., 1997. Introduction neural networks in remote sensing. Int. J. Remote Sens. 18, 699–709. https://doi.org/10.1080/014311697218700
7. Barrett, F., McRoberts, R.E., Tomppo, E., Cienciala, E., Waser, L.T., 2016. A questionnaire-based review of the operational use of remotely sensed data by national forest inventories. Remote Sens. Environ. 174, 279–289. https://doi.org/10.1016/j.rse.2015.08.029
8. Bater, C.W., Wulder, M.A., Coops, N.C., Nelson, R.F., Hilker, T., Nasset, E., 2011. Stability of Sample-Based Scanning-LiDAR-Derived Vegetation Metrics for Forest Monitoring. IEEE Trans. Geosci. Remote Sens. 49, 2385–2392. https://doi.org/10.1109/TGRS.2010.2099232
9. Béland, M., Widlowski, J.L., Fournier, R.A., Côté, J.F., Verstraete, M.M., 2011. Estimating leaf area distribution in savanna trees from terrestrial LiDAR measurements. Agric. For. Meteorol. 151, 1252–1266. https://doi.org/10.1016/j.agrformet.2011.05.004
10. Bergeron, Y., Flannigan, M., Gauthier, S., Leduc, A., Lefort, P., 2004. Past, current and future fire frequency in the canadian boreal forest: Implications for sustainable forest management. Ambio 33, 356–360. https://doi.org/10.1579/0044-7447-33.6.356
11. Bernier, P., Schoene, D., 2009. Adapting forests and their management to climate change: An overview. Unasylva 60, 5–11.
12. Bettinger, P., Boston, K., Siry, J.P., Grebner, D.L., 2017. Management of Forests and Other Natural Resources, in: Forest Management and Planning. Elsevier, pp. 1–20. https://doi.org/10.1016/B978-0-12-809476-1.00001-1
13. Bohn, F.J., Huth, A., 2017. The importance of forest structure to biodiversity-productivity relationships. R. Soc. Open Sci. 4, 160521. https://doi.org/10.1098/rsos.160521
14. Bolton, D.K., Tompalski, P., Coops, N.C., White, J.C., Wulder, M.A., Hermosilla, T., Queinnec, M., Luther, J.E., van Lier, O.R., Fournier, R.A., Woods, M., Treitz, P.M., van Ewijk, K.Y., Graham, G., Quist, L., 2020. Optimizing Landsat time series length for regional mapping of lidar-derived forest structure. Remote Sens. Environ. 239, 111645. https://doi.org/10.1016/j.rse.2020.111645
15. Bonan, G.B., 2008. Forests and Climate Change: Forcings, Feedbacks, and the Climate Benefits of Forests. Science (80-.). 320, 1444–1449. https://doi.org/10.1126/science.1155121

16. Bouvier, M., Durrieu, S., Fournier, R.A., Renaud, J.P., 2015. Generalizing predictive models of forest inventory attributes using an area-based approach with airborne LiDAR data. Remote Sens. Environ. 156, 322–334. https://doi.org/10.1016/j.rse.2014.10.004

17. Bouvier, M., Durrieu, S., Fournier, R.A., Saint-Geours, N., Guyon, D., Grau, E., de Boissieu, F., 2019. Influence of Sampling Design Parameters on Biomass Predictions Derived from Airborne LiDAR Data. Can. J. Remote Sens. 45, 650–672. https://doi.org/10.1080/07038992.2019.1669013

18. Breidenbach, J., Astrup, R., 2012. Small area estimation of forest attributes in the Norwegian National Forest Inventory. Eur. J. For. Res. 131, 1255–1267. https://doi.org/10.1007/s10342-012-0596-7

19. Breidenbach, J., Koch, B., Kändler, G., Kleusberg, A., 2008. Quantifying the influence of slope, aspect, crown shape and stem density on the estimation of tree height at plot level using lidar and InSAR data. Int. J. Remote Sens. 29, 1511–1536. https://doi.org/10.1080/01431160701736364

20. Breidenbach, J., Nothdurft, A., Kändler, G., 2010. Comparison of nearest neighbour approaches for small area estimation of tree species-specific forest inventory attributes in central Europe using airborne laser scanner data. Eur. J. For. Res. 129, 833–846. https://doi.org/10.1007/s10342-010-0384-1

21. Cao, L., Coops, N.C., Innes, J.L., Dai, J., Ruan, H., She, G., 2016. Tree species classification in subtropical forests using small-footprint full-waveform LiDAR data. Int. J. Appl. Earth Obs. Geoinf. 49, 39–51. https://doi.org/10.1016/j.jag.2016.01.007

22. Cao, L., Liu, H., Fu, X., Zhang, Z., Shen, X., Ruan, H., 2019. Comparison of UAV LiDAR and digital aerial photogrammetry point clouds for estimating forest structural attributes in subtropical planted forests. Forests 10, 1–26. https://doi.org/10.3390/f10020145

23. Carrasco, L., Giam, X., Papęs, M., Sheldon, K.S., Papeş, M., Sheldon, K.S., 2019. Metrics of lidar-derived 3D vegetation structure reveal contrasting effects of horizontal and vertical forest heterogeneity on bird species richness. Remote Sens. 11, 1–19. https://doi.org/10.3390/rs11070743

24. Cartus, O., Kellndorfer, J., Rombach, M., Walker, W., 2012. Mapping canopy height and growing stock volume using airborne lidar, alos palsar and landsat ETM+. Remote Sens. 4, 3320–3345. https://doi.org/10.3390/rs4113320

25. Chen, X.T., Disney, M.I., Lewis, P., Armston, J., Han, J.T., Li, J.C., 2014. Sensitivity of direct canopy gap fraction retrieval from airborne waveform lidar to topography and survey characteristics. Remote Sens. Environ. 143, 15–25. https://doi.org/10.1016/j.rse.2013.12.010

26. Chirici, G., Mura, M., McInerney, D., Py, N., Tomppo, E.O., Waser, L.T., Travaglini, D., McRoberts, R.E., 2016. A meta-analysis and review of the literature on the k-Nearest Neighbors technique for forestry applications that use remotely sensed data. Remote Sens. Environ. 176, 282–294. https://doi.org/10.1016/j.rse.2016.02.001

27. Coops, N.C., Tompalski, P., Goodbody, T.R.H., Queinnec, M., Luther, J.E., Bolton, D.K., White, J.C., Wulder, M.A., van Lier, O.R., Hermosilla, T., 2021. Modelling lidar-derived estimates of forest attributes over space and time: A review of approaches and future trends. Remote Sens. Environ. 260, 112477. https://doi.org/10.1016/j.rse.2021.112477

28. Corte, A.P.D., Rex, F.E., de Almeida, D.R.A., Sanquetta, C.R., Silva, C.A., Moura, M.M., Wilkinson, B., Zambrano, A.M.A., da Cunha Neto, E.M., Veras, H.F.P., de Moraes, A., Klauberg, C., Mohan, M., Cardil, A., Broadbent, E.N., 2020. Measuring individual tree diameter and height using gatoreye high-density UAV-lidar in an integrated crop-livestock-forest system. Remote Sens. 12. https://doi.org/10.3390/rs12050863

29. Cosenza, D.N., Packalen, P., Maltamo, M., Varvia, P., Räty, J., Soares, P., Tomé, M., Strunk, J.L., Korhonen, L., 2022. Effects of numbers of observations and predictors for various model

types on the performance of forest inventory with airborne laser scanning. Can. J. For. Res. 52, 385–395. https://doi.org/10.1139/cjfr-2021-0192

30. Côté, J.-F., Fournier, R.A., Luther, J.E., van Lier, O.R., 2018. Fine-scale three-dimensional modeling of boreal forest plots to improve forest characterization with remote sensing. Remote Sens. Environ. 219, 99–114. https://doi.org/10.1016/j.rse.2018.09.026

31. Crespo-Peremarch, P., Ruiz, L.A., 2020. A Full-waveform airborne laser scanning metric extraction tool for forest structure modelling. Do scan angle and radiometric correction matter? Remote Sens. 12. https://doi.org/10.3390/rs12020292

32. Dayal, K.R., Durrieu, S., Alleaume, S., Revers, F., Larmanou, E., Renaud, J.-P., Bouvier, M., 2020. Scan angle impact on lidar-derived metrics used in ABA models for prediction of forest stand characteristics: a grid based analysis. ISPRS - Int. Arch. Photogramm. Remote Sens. Spat. Inf. Sci. XLIII-B3-2, 975–982. https://doi.org/10.5194/isprs-archives-XLIII-B3-2020-975-2020

33. Dayal, K.R., Durrieu, S., Lahssini, K., Alleaume, S., Bouvier, M., Monnet, J.M., Renaud, J.P., Revers, F., 2022. An investigation into lidar scan angle impacts on stand attribute predictions in different forest environments. ISPRS J. Photogramm. Remote Sens. 193, 314–338. https://doi.org/10.1016/j.isprsjprs.2022.08.013

34. Deleuze, C., Senga Kiess´e, T., Renaud, J. -P., Morneau, F., Rivoire, M., Santenoise, P., et al. (2013). Rapport final EMERGE sur les mod`eles de volumes. Projet ANR-08- BIOE-003, Programme BIOE 2008.

35. Disney, M.I., Kalogirou, V., Lewis, P., Prieto-Blanco, A., Hancock, S., Pfeifer, M., 2010. Simulating the impact of discrete-return lidar system and survey characteristics over young conifer and broadleaf forests. Remote Sens. Environ. 114, 1546–1560. https://doi.org/10.1016/j.rse.2010.02.009

36. Drake, J.B., Knox, R.G., Dubayah, R.O., Clark, D.B., Condit, R., Blair, J.B., Hofton, M., 2003. Above-ground biomass estimation in closed canopy Neotropical forests using lidar remote sensing: Factors affecting the generality of relationships. Glob. Ecol. Biogeogr. 12, 147–159. https://doi.org/10.1046/j.1466-822X.2003.00010.x

37. Dubayah, R., Blair, J.B., Goetz, S., Fatoyinbo, L., Hansen, M., Healey, S., Hofton, M., Hurtt, G., Kellner, J., Luthcke, S., Armston, J., Tang, H., Duncanson, L., Hancock, S., Jantz, P., Marselis, S., Patterson, P.L., Qi, W., Silva, C., 2020. The Global Ecosystem Dynamics Investigation: High-resolution laser ranging of the Earth's forests and topography. Sci. Remote Sens. 1, 100002. https://doi.org/10.1016/j.srs.2020.100002

38. Dubayah, Ralph O, Drake, J.B., 2000. Lidar Remote Sensing for Forestry. J. For. 98, 44–46. https://doi.org/10.1093/jof/98.6.44

39. Dubayah, Ralph O., Drake, J.B., 2000. Lidar Remote Sensing for Forestry, Journal of Forestry. https://doi.org/10.1093/jof/98.6.44

40. Evans, J., Hudak, A., Faux, R., Smith, A.M.S., 2009. Discrete Return Lidar in Natural Resources: Recommendations for Project Planning, Data Processing, and Deliverables. Remote Sens. 1, 776–794. https://doi.org/10.3390/rs1040776

41. Fassnacht, F.E., Hartig, F., Latifi, H., Berger, C., Hernández, J., Corvalán, P., Koch, B., 2014. Importance of sample size, data type and prediction method for remote sensing-based estimations of aboveground forest biomass. Remote Sens. Environ. 154, 102–114. https://doi.org/10.1016/j.rse.2014.07.028

42. Fedrigo, M., Newnham, G.J., Coops, N.C., Culvenor, D.S., Bolton, D.K., Nitschke, C.R., 2018. Predicting temperate forest stand types using only structural profiles from discrete return airborne lidar. ISPRS J. Photogramm. Remote Sens. 136, 106–119. https://doi.org/10.1016/j.isprsjprs.2017.11.018

43. Fekety, P.A., Falkowski, M.J., Hudak, A.T., Jain, T.B., Evans, J.S., 2018. Transferability of Lidar-derived Basal Area and Stem Density Models within a Northern Idaho Ecoregion. Can. J. Remote Sens. 44, 131–143. https://doi.org/10.1080/07038992.2018.1461557

44. Ferraz, A., Saatchi, S., Mallet, C., Meyer, V., 2016. Lidar detection of individual tree size in tropical forests. Remote Sens. Environ. 183, 318–333. https://doi.org/10.1016/j.rse.2016.05.028

45. Fischer, R., Knapp, N., Bohn, F., Shugart, H.H., Huth, A., 2019. The Relevance of Forest Structure for Biomass and Productivity in Temperate Forests: New Perspectives for Remote Sensing. Surv. Geophys. 40, 709–734. https://doi.org/10.1007/s10712-019-09519-x

46. FAO, 2020. The State of the World's Forests 2020, Forests, Biodiversity and People. FAO and UNEP, Rome. https://doi.org/10.4060/ca8642en

47. Foody, G.M., Boyd, D.S., Cutler, M.E.J., 2003. Predictive relations of tropical forest biomass from Landsat TM data and their transferability between regions. Remote Sens. Environ. 85, 463–474. https://doi.org/10.1016/S0034-4257(03)00039-7

48. Gadow, K. von, Pukkala, T., Tome, M., 2000. Sustainable Forest Management, Managing Forest Ecosystems. Springer Netherlands, Dordrecht. https://doi.org/10.1007/978-94-010-9819-9

49. Gastellu-Etchegorry, J.P., Yin, T., Lauret, N., Cajgfinger, T., Gregoire, T., Grau, E., Feret, J.B., Lopes, M., Guilleux, J., Dedieu, G., Malenovskỳ, Z., Cook, B.D., Morton, D., Rubio, J., Durrieu, S., Cazanave, G., Martin, E., Ristorcelli, T., 2015. Discrete anisotropic radiative transfer (DART 5) for modeling airborne and satellite spectroradiometer and LIDAR acquisitions of natural and urban landscapes. Remote Sens. 7, 1667–1701. https://doi.org/10.3390/rs70201667

50. Gatziolis, D., 2011. Dynamic range-based intensity normalization for airborne, discrete return lidar data of forest canopies. Photogramm. Eng. Remote Sensing 77, 251–259. https://doi.org/10.14358/PERS.77.3.251

51. Gili, P., Civera, M., Roy, R., Surace, C., 2021. An unmanned lighter-than-air platform for large scale land monitoring. Remote Sens. 13. https://doi.org/10.3390/rs13132523

52. Gobakken, T., Næsset, E., 2008. Assessing effects of laser point density, ground sampling intensity, and field sample plot size on biophysical stand properties derived from airborne laser scanner data. Can. J. For. Res. 38, 1095–1109. https://doi.org/10.1139/X07-219

53. Gobakken, T., Næsset, E., 2005. Weibull and percentile models for lidar-based estimation of basal area distribution. Scand. J. For. Res. 20, 490–502. https://doi.org/10.1080/02827580500373186

54. Gopal, S., Woodcock, C., 1996. Remote sensing of forest change using artificial neural networks. IEEE Trans. Geosci. Remote Sens. 34, 398–404. https://doi.org/10.1109/36.485117

55. Grau, E., Durrieu, S., Fournier, R., Gastellu-Etchegorry, J.P., Yin, T., 2017. Estimation of 3D vegetation density with Terrestrial Laser Scanning data using voxels. A sensitivity analysis of influencing parameters. Remote Sens. Environ. 191, 373–388. https://doi.org/10.1016/j.rse.2017.01.032

56. Gu, D., Gillespie, A., 1998. Topographic normalization of Landsat TM images of forest based on subpixel Sun-canopy-sensor geometry. Remote Sens. Environ. 64, 166–175. https://doi.org/10.1016/S0034-4257(97)00177-6

57. Hall, R.J., Skakun, R.S., Arsenault, E.J., Case, B.S., 2006. Modeling forest stand structure attributes using Landsat ETM+ data: Application to mapping of aboveground biomass and stand volume. For. Ecol. Manage. 225, 378–390. https://doi.org/10.1016/j.foreco.2006.01.014

58. Hansen, E.H., Ene, L.T., Gobakken, T., Ole Ørka, H., Bollandsås, O.M., Næsset, E., 2017. Countering negative effects of terrain slope on airborne laser scanner data using procrustean transformation and histogram matching. Forests 8. https://doi.org/10.3390/f8100401

59. He, Q., Chen, E., An, R., Li, Y., 2013. Above-ground biomass and biomass components estimation using LiDAR data in a coniferous forest. Forests 4, 984–1002. https://doi.org/10.3390/f4040984

60. Hervé, M., 2021. RVAideMemoire: Testing and Plotting Procedures for Biostatistics.

61. Hickman, G.D., Hogg, J.E., 1969. Application of an airborne pulsed laser for near shore bathymetric measurements. Remote Sens. Environ. 1, 47–58. https://doi.org/10.1016/S0034-4257(69)90088-1

62. Holmgren, J., Nilsson, M., Olsson, H., 2003. Simulating the effects of lidar scanning angle for estimation of mean tree height and canopy closure. Can. J. Remote Sens. 29, 623–632. https://doi.org/10.5589/m03-030

63. Hopkinson, C., 2007. The influence of flying altitude, beam divergence, and pulse repetition frequency on laser pulse return intensity and canopy frequency distribution. Can. J. Remote Sens. 33, 312–324. https://doi.org/10.5589/m07-029

64. Hopkinson, C., Chasmer, L., 2009. Testing LiDAR models of fractional cover across multiple forest ecozones. Remote Sens. Environ. 113, 275–288. https://doi.org/10.1016/j.rse.2008.09.012

65. Hopkinson, C., Chasmer, L., Young-Pow, C., Treitz, P., 2004. Assessing forest metrics with a ground-based scanning lidar. Can. J. For. Res. 34, 573–583. https://doi.org/10.1139/x03-225

66. Hudak, A.T., Crookston, N.L., Evans, J.S., Falkowski, M.J., Smith, A.M.S., Gessler, P.E., Morgan, P., 2006. Regression modeling and mapping of coniferous forest basal area and tree density from discrete-return lidar and multispectral satellite data. Can. J. Remote Sens. 32, 126–138. https://doi.org/10.5589/m06-007

67. Hudak, A.T., Evans, J.S., Smith, A.M.S., 2009. LiDAR utility for natural resource managers. Remote Sens. https://doi.org/10.3390/rs1040934

68. ICSM, 2010. ICSM LiDAR acquisition specifications and tender template. Version 1.0.

69. IGN, n.d. LIDAR HD [WWW Document].

70. Ioki, K., Tsuyuki, S., Hirata, Y., Phua, M.H., Wong, W.V.C., Ling, Z.Y., Saito, H., Takao, G., 2014. Estimating above-ground biomass of tropical rainforest of different degradation levels in Northern Borneo using airborne LiDAR. For. Ecol. Manage. 328, 335–341. https://doi.org/10.1016/j.foreco.2014.06.003

71. Jaakkola, A., Hyyppä, J., Yu, X., Kukko, A., Kaartinen, H., Liang, X., Hyyppä, H., Wang, Y., 2017. Autonomous collection of forest field reference—The outlook and a first step with UAV laser scanning. Remote Sens. 9, 785. https://doi.org/10.3390/rs9080785

72. Jakubowski, M.K., Guo, Q., Kelly, M., 2013. Tradeoffs between lidar pulse density and forest measurement accuracy. Remote Sens. Environ. 130, 245–253. https://doi.org/10.1016/j.rse.2012.11.024

73. Jandl, R., Spathelf, P., Bolte, A., Prescott, C.E., 2019. Forest adaptation to climate change—is non-management an option? Ann. For. Sci. 76, 1–13. https://doi.org/10.1007/s13595-019-0827-x

74. Jenness, J.S., 2004. Calculating landscape surface area from digital elevation models. Wildl. Soc. Bull. 32, 829–839. https://doi.org/10.2193/0091-7648(2004)032[0829:clsafd]2.0.co;2

75. Jeronimo, S.M.A., Kane, V.R., Churchill, D.J., McGaughey, R.J., Franklin, J.F., 2018. Applying LiDAR individual tree detection to management of structurally diverse forest landscapes. J. For. 116, 336–346. https://doi.org/10.1093/jofore/fvy023

76. Kamoske, A.G., Dahlin, K.M., Stark, S.C., Serbin, S.P., 2019. Leaf area density from airborne LiDAR: Comparing sensors and resolutions in a temperate broadleaf forest ecosystem. For. Ecol. Manage. 433, 364–375. https://doi.org/10.1016/j.foreco.2018.11.017

77. Kangas, A., Gobakken, T., Puliti, S., Hauglin, M., Næsset, E., 2018. Value of airborne laser scanning and digital aerial photogrammetry data in forest decision making. Silva Fenn. 52. https://doi.org/10.14214/sf.9923

78. Kangas, A., Maltamo, M., 2006. Forest Inventory, Springer, Managing Forest Ecosystems. Springer Netherlands, Dordrecht. https://doi.org/10.1007/1-4020-4381-3

79. Kankare, V., Vastaranta, M., Holopainen, M., Räty, M., Yu, X., Hyyppä, J., Hyyppä, H., Alho, P., Viitala, R., 2013. Retrieval of forest aboveground biomass and stem volume with airborne scanning LiDAR. Remote Sens. 5, 2257–2274. https://doi.org/10.3390/rs5052257

80. Kassambara, A., 2021. Rstatix: Pipe-Friendly Framework for Basic Statistical Tests.

81. Kellner, J.R., Armston, J., Birrer, M., Cushman, K.C., Duncanson, L., Eck, C., Falleger, C., Imbach, B., Král, K., Krůček, M., Trochta, J., Vrška, T., Zgraggen, C., 2019. New Opportunities for Forest Remote Sensing Through Ultra-High-Density Drone Lidar. Surv. Geophys. https://doi.org/10.1007/s10712-019-09529-9

82. Keränen, J., Maltamo, M., Packalen, P., 2016. Effect of flying altitude, scanning angle and scanning mode on the accuracy of ALS based forest inventory. Int. J. Appl. Earth Obs. Geoinf. 52, 349–360. https://doi.org/10.1016/j.jag.2016.07.005

83. Ketchum, R.D., 1971. Airborne laser profiling of the arctic pack ice. Remote Sens. Environ. 2, 41–52. https://doi.org/10.1016/0034-4257(71)90076-9

84. Kim, E., Lee, W.K., Yoon, M., Lee, J.Y., Son, Y., Salim, K.A., 2016. Estimation of voxel-based above-ground biomass using airborne LiDAR data in an intact tropical rain forest, Brunei. Forests 7, 1–16. https://doi.org/10.3390/f7110259

85. Knapp, N., Huth, A., Fischer, R., 2021. Tree crowns cause border effects in area-based biomass estimations from remote sensing. Remote Sens. 13. https://doi.org/10.3390/rs13081592

86. Koch, B., Heyder, U., Weinacker, H., 2006. Detection of Individual Tree Crowns in Airborne Lidar Data. Photogramm. Eng. Remote Sens. 72, 357–363. https://doi.org/10.14358/PERS.72.4.357

87. Korhonen, L., Korpela, I., Heiskanen, J., Maltamo, M., 2011. Airborne discrete-return LIDAR data in the estimation of vertical canopy cover, angular canopy closure and leaf area index. Remote Sens. Environ. 115, 1065–1080. https://doi.org/10.1016/j.rse.2010.12.011

88. Krabill, W.B., Collins, J.G., Link, L.E., Swift, R.N., Butler, M.L., 1984. Airborne laser topographic mapping results (Tennessee). Photogramm. Eng. Remote Sens. 50, 685–694.

89. Krabill, W.B., Collins, J.G., Swift, R.N., Butler, M.L., 1980. Airborne laser topographic mapping results from initial joint NASA/US Army Corps of Engineers experiment.

90. Kuuluvainen, T., Angelstam, P., Frelich, L., Jõgiste, K., Koivula, M., Kubota, Y., Lafleur, B., Macdonald, E., 2021. Natural Disturbance-Based Forest Management: Moving Beyond Retention and Continuous-Cover Forestry. Front. For. Glob. Chang. 4, 1–16. https://doi.org/10.3389/ffgc.2021.629020

91. Kwak, D.A., Lee, W.K., Lee, J.H., Biging, G.S., Gong, P., 2007. Detection of individual trees and estimation of tree height using LiDAR data. J. For. Res. 12, 425–434. https://doi.org/10.1007/s10310-007-0041-9

92. Lahssini, K., Teste, F., Dayal, K.R., Durrieu, S., Ienco, D., Monnet, J., 2022. Combining LiDAR metrics and Sentinel-2 imagery to estimate basal area and wood volume in complex forest environment via neural networks. IEEE J. Sel. Top. Appl. Earth Obs. Remote Sens. PP, 1. https://doi.org/10.1109/JSTARS.2022.3175609

93. Lazdinis, M., Angelstam, P., Pülzl, H., 2019. Towards sustainable forest management in the European Union through polycentric forest governance and an integrated landscape approach. Landsc. Ecol. 34, 1737–1749. https://doi.org/10.1007/s10980-019-00864-1

94. Le Toan, T., Beaudoin, A., Riom, J., Guyon, D., 1992. Relating Forest Biomass to SAR Data. IEEE Trans. Geosci. Remote Sens. 30, 403–411. https://doi.org/10.1109/36.134089

95. Lechner, A.M., Foody, G.M., Boyd, D.S., 2020. Applications in Remote Sensing to Forest Ecology and Management. One Earth 2, 405–412. https://doi.org/10.1016/j.oneear.2020.05.001

96. Lee, S., Lee, D.K., 2018. What is the proper way to apply the multiple comparison test? Korean J. Anesthesiol. 71, 353–360. https://doi.org/10.4097/kja.d.18.00242

97. Lefsky, M.A., Cohen, W.B., Harding, D.J., Parker, G.G., Acker, S.A., Gower, S.T., 2002a. Lidar remote sensing of above-ground biomass in three biomes. Glob. Ecol. Biogeogr. 11, 393–399. https://doi.org/10.1046/j.1466-822x.2002.00303.x

98. Lefsky, M.A., Cohen, W.B., Parker, G.G., Harding, D.J., 2002b. Lidar remote sensing for ecosystem studies. Bioscience. https://doi.org/10.1641/0006-3568(2002)052[0019:LRSFES]2.0.CO;2

99. Lei, L., Qiu, C., Li, Z., Han, D., Han, L., Zhu, Y., Wu, J., Xu, B., Feng, H., Yang, H., Yang, G., 2019. Effect of Leaf Occlusion on Leaf Area Index Inversion of Maize Using UAV–LiDAR Data. Remote Sens. 11, 1067. https://doi.org/10.3390/rs11091067

100. Leiterer, R., Furrer, R., Schaepman, M.E., Morsdorf, F., 2015. Forest canopy-structure characterization: A data-driven approach. For. Ecol. Manage. 358, 48–61. https://doi.org/10.1016/j.foreco.2015.09.003

101. LeMay, V., Temesgen, H., 2005. Comparison of nearest neighbor methods for estimating basal area and stems per hectare using aerial auxiliary variables. For. Sci. 51, 109–119.

102. Li, X., Liu, C., Wang, Z., Xie, X., Li, D., Xu, L., 2020. Airborne LiDAR: State-of-the-art of system design, technology and application. Meas. Sci. Technol. 32. https://doi.org/10.1088/1361-6501/abc867

103. Liaw, A., Wiener, M., 2002. Classification and Regression by randomForest. R News 2, 18–22.

104. Lillesand, T.M., Kiefer, R.W., Chipman, J.W., 2004. Remote Sensing and Image Interpretation. John Wiley & Sons, Inc.

105. Link, L.E., 1969. Capability of Airborne Laser Profilometer to Measure Terrain Roughness, in: Proceedings of the Sixth International Symposium on Remote Sensing of Environment, Volume II. pp. 189–196.

106. Liu, H., Shen, X., Cao, L., Yun, T., Zhang, Z., Fu, X., Chen, X., Liu, F., 2021. Deep Learning in Forest Structural Parameter Estimation Using Airborne LiDAR Data. IEEE J. Sel. Top. Appl. Earth Obs. Remote Sens. 14, 1603–1618. https://doi.org/10.1109/JSTARS.2020.3046053

107. Liu, J., Skidmore, A.K., Jones, S., Wang, T., Heurich, M., Zhu, X., Shi, Y., 2018. Large off-nadir scan angle of airborne LiDAR can severely affect the estimates of forest structure metrics. ISPRS J. Photogramm. Remote Sens. 136, 13–25. https://doi.org/10.1016/j.isprsjprs.2017.12.004

108. Liu, K., Shen, X., Cao, L., Wang, G., Cao, F., 2018. Estimating forest structural attributes using UAV-LiDAR data in Ginkgo plantations. ISPRS J. Photogramm. Remote Sens. 146, 465–482. https://doi.org/10.1016/j.isprsjprs.2018.11.001

109. Lopatin, J., Dolos, K., Hernández, H.J., Galleguillos, M., Fassnacht, F.E., 2016. Comparing Generalized Linear Models and random forest to model vascular plant species richness using LiDAR data in a natural forest in central Chile. Remote Sens. Environ. 173, 200–210. https://doi.org/10.1016/j.rse.2015.11.029

110. Lovell, J.L., Jupp, D.L.B., Culvenor, D.S., Coops, N.C., 2003. Using airborne and ground-based ranging lidar to measure canopy structure in Australian forests. Can. J. Remote Sens. 29, 607–622. https://doi.org/10.5589/m03-026

111. Lovell, J.L., Jupp, D.L.B., Newnham, G.J., Coops, N.C., Culvenor, D.S., 2005. Simulation study for finding optimal lidar acquisition parameters for forest height retrieval. For. Ecol. Manage. 214, 398–412. https://doi.org/10.1016/j.foreco.2004.07.077

112. Lu, J., Wang, H., Qin, S., Cao, L., Pu, R., Li, G., Sun, J., 2020. Estimation of aboveground biomass of Robinia pseudoacacia forest in the Yellow River Delta based on UAV and Backpack LiDAR point clouds. Int. J. Appl. Earth Obs. Geoinf. 86, 102014. https://doi.org/10.1016/j.jag.2019.102014

113. Ma, K., Chen, Z., Fu, L., Tian, W., Jiang, F., Yi, J., Du, Z., Sun, H., 2022. Performance and Sensitivity of Individual Tree Segmentation Methods for UAV-LiDAR in Multiple Forest Types. Remote Sens. 14. https://doi.org/10.3390/rs14020298

114. MacDicken, K.G., Sola, P., Hall, J.E., Sabogal, C., Tadoum, M., de Wasseige, C., 2015. Global progress toward sustainable forest management. For. Ecol. Manage. 352, 47–56. https://doi.org/10.1016/j.foreco.2015.02.005

115. Magnussen, S., Boudewyn, P., 1998. Derivations of stand heights from airborne laser scanner data with canopy-based quantile estimators. Can. J. For. Res. 28, 1016–1031. https://doi.org/10.1139/x98-078

116. Magnussen, S., Næsset, E., Gobakken, T., 2010. Reliability of LiDAR derived predictors of forest inventory attributes: A case study with Norway spruce. Remote Sens. Environ. 114, 700–712. https://doi.org/10.1016/j.rse.2009.11.007

117. Magruder, L., Neumann, T., Kurtz, N., 2021. ICESat-2 Early Mission Synopsis and Observatory Performance. Earth Sp. Sci. 8, 1–9. https://doi.org/10.1029/2020EA001555

118. Mallet, C., Bretar, F., 2009. Full-waveform topographic lidar: State-of-the-art. ISPRS J. Photogramm. Remote Sens. 64, 1–16. https://doi.org/10.1016/j.isprsjprs.2008.09.007

119. Martín Abadi, Ashish Agarwal, Paul Barham, Eugene Brevdo, Zhifeng Chen, Craig Citro, Greg S. Corrado, Andy Davis, Jeffrey Dean, Matthieu Devin, Sanjay Ghemawat, Ian Goodfellow, Andrew Harp, Geoffrey Irving, Michael Isard, Jia, Y., Rafal Jozefowicz, Lukasz Kaiser, Manjunath Kudlur, Josh Levenberg, Dandelion Mané, Rajat Monga, Sherry Moore, Derek Murray, Chris Olah, Mike Schuster, Jonathon Shlens, Benoit Steiner, Ilya Sutskever, Kunal Talwar, Paul Tucker, Vincent Vanhoucke, Vijay Vasudevan, Fernanda Viégas, Oriol Vinyals, Pete Warden, Martin Wattenberg, Martin Wicke, Yuan Yu, Xiaoqiang, Zheng, 2015. {TensorFlow}: Large-Scale Machine Learning on Heterogeneous Systems.

120. Martins-Neto, R.P., Maria, A., Tommaselli, G., Imai, N.N., David, H.C., Miltiadou, M., Honkavaara, E., 2021. Identification of Significative LiDAR Metrics and Comparison of Machine Learning Approaches for Estimating Stand and Diversity Variables in Heterogeneous Brazilian Atlantic Forest. Remote Sens. 13, 2444.

121. Maturana, D., Scherer, S., 2015. VoxNet: A 3D Convolutional Neural Network for real-time object recognition, in: 2015 IEEE/RSJ International Conference on Intelligent Robots and Systems (IROS). IEEE, pp. 922–928. https://doi.org/10.1109/IROS.2015.7353481

122. McRoberts, R., Tomppo, E., 2007. Remote sensing support for national forest inventories. Remote Sens. Environ. 110, 412–419. https://doi.org/10.1016/j.rse.2006.09.034

123. Mikolajczyk, A., Grochowski, M., 2018. Data augmentation for improving deep learning in image classification problem, in: 2018 International Interdisciplinary PhD Workshop (IIPhDW). IEEE, pp. 117–122. https://doi.org/10.1109/IIPHDW.2018.8388338

124. Ministry of Forests, Lands, N.R., GeoBC, O. and R.D., 2020. Specifications for Airborne LiDAR for the Province of British COlumbia 1–53.

125. Mitchell, B., Fisk, H., Clark, J., Rounds, E., 2018. Lidar Acquisition Specifications for Forestry Applications. Natl. Lidar Strateg. - USDA 1–27.

126. Mitchell, B., Jacokes-Mancini, R., Fisk, H., 2012. United States Department of Agriculture Forest Service Remote Sensing Applications Center Geospatial Management Office - Considerations for using Lidar Data-A Project Implementation Guide 13.

127. Montaghi, A., 2013. Effect of scanning angle on vegetation metrics derived from a nationwide Airborne Laser Scanning acquisition. Can. J. Remote Sens. 39, 37–41. https://doi.org/10.5589/m13-052

128. Morsdorf, F., Frey, O., Meier, E., Itten, K.I., Allgöwer, B., 2008. Assessment of the influence of flying altitude and scan angle on biophysical vegetation products derived from airborne laser scanning. Int. J. Remote Sens. 29, 1387–1406. https://doi.org/10.1080/01431160701736349

129. Næsset, E., 2009. Effects of different sensors, flying altitudes, and pulse repetition frequencies on forest canopy metrics and biophysical stand properties derived from small-footprint airborne laser data. Remote Sens. Environ. 113, 148–159. https://doi.org/10.1016/j.rse.2008.09.001

130. Næsset, E., 2007. Airborne laser scanning as a method in operational forest inventory: Status of accuracy assessments accomplished in Scandinavia. Scand. J. For. Res. 22, 433–442. https://doi.org/10.1080/02827580701672147

131. Næsset, E., 2002. Predicting forest stand characteristics with airborne scanning laser using a practical two-stage procedure and field data. Remote Sens. Environ. 80, 88–99. https://doi.org/10.1016/S0034-4257(01)00290-5

132. Næsset, E., 1997a. Determination of mean tree height of forest stands using airborne laser scanner data. ISPRS J. Photogramm. Remote Sens. 52, 49–56. https://doi.org/10.1016/S0924-2716(97)83000-6

133. Næsset, E., 1997b. Estimating timber volume of forest stands using airborne laser scanner data. Remote Sens. Environ. 61, 246–253. https://doi.org/10.1016/S0034-4257(97)00041-2

134. Nahorniak, M., Larsen, D.P., Volk, C., Jordan, C.E., 2015. Using Inverse Probability Bootstrap Sampling to Eliminate Sample Induced Bias in Model Based Analysis of Unequal Probability Samples. PLoS One 10, e0131765. https://doi.org/10.1371/journal.pone.0131765

135. Nelson, R., 2013. How did we get here? An early history of forestry lidar 1. Can. J. Remote Sens. 39, S6–S17. https://doi.org/10.5589/m13-011

136. Neumann, M., Ferro-Famil, L., Reigber, A., 2010. Estimation of forest structure, ground, and canopy layer characteristics from multibaseline polarimetric interferometric SAR data. IEEE Trans. Geosci. Remote Sens. 48, 1086–1104. https://doi.org/10.1109/TGRS.2009.2031101

137. Nilson, T., 1971. A theoretical analysis of the frequency of gaps in plant stands. Agric. Meteorol. 8, 25–38. https://doi.org/10.1016/0002-1571(71)90092-6

138. Nilsson, M., Nordkvist, K., Jonzén, J., Lindgren, N., Axensten, P., Wallerman, J., Egberth, M., Larsson, S., Nilsson, L., Eriksson, J., Olsson, H., 2017. A nationwide forest attribute map of Sweden predicted using airborne laser scanning data and field data from the National Forest Inventory. Remote Sens. Environ. 194, 447–454. https://doi.org/10.1016/j.rse.2016.10.022

139. NRC, 2017. Federal airborne LiDAR data acquisition guideline. https://doi.org/10.4095/304669

140. Nurminen, K., Karjalainen, M., Yu, X., Hyyppä, J., Honkavaara, E., 2013. Performance of dense digital surface models based on image matching in the estimation of plot-level forest variables. ISPRS J. Photogramm. Remote Sens. 83, 104–115. https://doi.org/10.1016/j.isprsjprs.2013.06.005

141. O'Malley, T., Bursztein, E., Long, J., Chollet, F., Jin, H., Invernizzi, L., others, 2019. KerasTuner.

142. Ørka, H.O., Bollandsås, O.M., Hansen, E.H., Næsset, E., Gobakken, T., 2018. Effects of terrain slope and aspect on the error of ALS-based predictions of forest attributes. Forestry 91, 225–237. https://doi.org/10.1093/forestry/cpx058

143. Özçelik, R., Diamantopoulou, M.J., Crecente-Campo, F., Eler, U., 2013. Estimating Crimean juniper tree height using nonlinear regression and artificial neural network models. For. Ecol. Manage. 306, 52–60. https://doi.org/10.1016/j.foreco.2013.06.009

144. Packalén, P., Maltamo, M., 2007. The k-MSN method for the prediction of species-specific stand attributes using airborne laser scanning and aerial photographs. Remote Sens. Environ. 109, 328–341. https://doi.org/10.1016/j.rse.2007.01.005

145. Parker, G.G., Russ, M.E., 2004. The canopy surface and stand development: assessing forest canopy structure and complexity with near-surface altimetry. For. Ecol. Manage. 189, 307–315. https://doi.org/10.1016/j.foreco.2003.09.001

146. Pearse, G.D., Watt, M.S., Dash, J.P., Stone, C., Caccamo, G., 2019. Comparison of models describing forest inventory attributes using standard and voxel-based lidar predictors across a range of pulse densities. Int. J. Appl. Earth Obs. Geoinf. 78, 341–351. https://doi.org/10.1016/j.jag.2018.10.008

147. Picard, R.R., Cook, R.D., 1984. Cross-Validation of Regression Models. J. Am. Stat. Assoc. 79, 575–583. https://doi.org/10.1080/01621459.1984.10478083

148. Picos, J., Bastos, G., Míguez, D., Alonso, L., Armesto, J., 2020. Individual tree detection in a eucalyptus plantation using unmanned aerial vehicle (UAV)-LiDAR. Remote Sens. 12. https://doi.org/10.3390/rs12050885

149. Pimont, F., Allard, D., Soma, M., Dupuy, J.-L.L., 2018. Estimators and confidence intervals for plant area density at voxel scale with T-LiDAR. Remote Sens. Environ. 215, 343–370. https://doi.org/10.1016/j.rse.2018.06.024

150. Popescu, S.C., Zhao, K., 2008. A voxel-based lidar method for estimating crown base height for deciduous and pine trees. Remote Sens. Environ. 112, 767–781. https://doi.org/10.1016/j.rse.2007.06.011

151. Prăvălie, R., 2018. Major perturbations in the Earth's forest ecosystems. Possible implications for global warming. Earth-Science Rev. 185, 544–571. https://doi.org/10.1016/j.earscirev.2018.06.010

152. Qin, H., Wang, C., Xi, X., Tian, J., Zhou, G., 2017. Simulating the Effects of the Airborne Lidar Scanning Angle, Flying Altitude, and Pulse Density for Forest Foliage Profile Retrieval. Appl. Sci. 7, 712. https://doi.org/10.3390/app7070712

153. Räty, J., 2020. Prediction of diameter distributions in boreal forests using remotely sensed data. Diss. For. University of Eastern Finland. https://doi.org/10.14214/df.294

154. Rempel, R.C., Parker, A.K., 1964. An information note on an airbornelaser terrain profiler for micro-relief studies, in: Proceedings, 3rd Symposiumon Remote Sensing of Environment. pp. 321–337.

155. Roussel, J.R., Auty, D., Coops, N.C., Tompalski, P., Goodbody, T.R.H., Meador, A.S., Bourdon, J.F., de Boissieu, F., Achim, A., 2020. lidR: An R package for analysis of Airborne Laser Scanning (ALS) data. Remote Sens. Environ. 251, 112061. https://doi.org/10.1016/j.rse.2020.112061

156. Roussel, J.R., Béland, M., Caspersen, J., Achim, A., 2018. A mathematical framework to describe the effect of beam incidence angle on metrics derived from airborne LiDAR: The case of forest canopies approaching turbid medium behaviour. Remote Sens. Environ. 209, 824–834. https://doi.org/10.1016/j.rse.2017.12.006

157. Schutz, B.E., Zwally, H.J., Shuman, C.A., Hancock, D., DiMarzio, J.P., 2005. Overview of the ICESat mission. Geophys. Res. Lett. 32, 1–4. https://doi.org/10.1029/2005GL024009

158. Seidl, R., Rammer, W., Lexer, M.J., 2011. Climate change vulnerability of sustainable forest management in the Eastern Alps. Clim. Change 106, 225–254. https://doi.org/10.1007/s10584-010-9899-1

159. Shi, Y., Wang, T., Skidmore, A.K., Heurich, M., 2018. Important LiDAR metrics for discriminating forest tree species in Central Europe. ISPRS J. Photogramm. Remote Sens. 137, 163–174. https://doi.org/10.1016/j.isprsjprs.2018.02.002

160. Shorten, C., Khoshgoftaar, T.M., 2019. A survey on Image Data Augmentation for Deep Learning. J. Big Data 6. https://doi.org/10.1186/s40537-019-0197-0

161. Silva, C., Hudak, A., Vierling, L., Klauberg, C., Garcia, M., Ferraz, A., Keller, M., Eitel, J., Saatchi, S., 2017. Impacts of Airborne Lidar Pulse Density on Estimating Biomass Stocks and Changes in a Selectively Logged Tropical Forest. Remote Sens. 9, 1068. https://doi.org/10.3390/rs9101068

162. Singh, K.K., Chen, G., Vogler, J.B., Meentemeyer, R.K., 2016. When Big Data are Too Much: Effects of LiDAR Returns and Point Density on Estimation of Forest Biomass. IEEE J. Sel. Top. Appl. Earth Obs. Remote Sens. 9, 3210–3218. https://doi.org/10.1109/JSTARS.2016.2522960

163. Soma, M., Pimont, F., Allard, D., Fournier, R., Dupuy, J.L., 2020. Mitigating occlusion effects in Leaf Area Density estimates from Terrestrial LiDAR through a specific kriging method. Remote Sens. Environ. 245, 111836. https://doi.org/10.1016/j.rse.2020.111836

164. Soma, M., Pimont, F., Dupuy, J.L., 2021. Sensitivity of voxel-based estimations of leaf area density with terrestrial LiDAR to vegetation structure and sampling limitations: A simulation experiment. Remote Sens. Environ. 257, 112354. https://doi.org/10.1016/j.rse.2021.112354

165. Soma, M., Pimont, F., Durrieu, S., Dupuy, J.L., 2018. Enhanced measurements of leaf area density with T-LiDAR: Evaluating and calibrating the effects of vegetation heterogeneity and scanner properties. Remote Sens. 10. https://doi.org/10.3390/rs10101580

166. Soudarissanane, S., Lindenbergh, R., Menenti, M., Teunissen, P., 2009. Incidence Angle Influence on the Quality of Terrestrial Laser Scanning Points. Iaprs XXXVIII, 183–188.

167. Spittlehouse, D.L., Stewart, R.B., 2003. Adaptation to climate change in forest management. BC J. Ecosyst. Manag. Adapt. 4.

168. Sprugel, D.G., 1983. Correcting for Bias in Log-Transformed Allometric Equations. Ecology 64, 209–210. https://doi.org/10.2307/1937343

169. State of Europe's Forests, 2020.

170. Swisstopo, O. fédéral de topographie, n.d. Acquisition de données LiDAR [WWW Document]. URL https://www.swisstopo.admin.ch/fr/connaissances-faits/geoinformation/donnees-lidar.html (accessed 4.22.22).

171. Taylor, L., Nitschke, G., 2019. Improving Deep Learning with Generic Data Augmentation. Proc. 2018 IEEE Symp. Ser. Comput. Intell. SSCI 2018 1542–1547. https://doi.org/10.1109/SSCI.2018.8628742

172. The State of the World's Forests 2020, 2020. , FORESTS, BIODIVERSITY AND PEOPLE. FAO and UNEP, Rome. https://doi.org/10.4060/ca8642en

173. Tompalski, P., White, J.C., Coops, N.C., Wulder, M.A., 2019. Demonstrating the transferability of forest inventory attribute models derived using airborne laser scanning data. Remote Sens. Environ. 227, 110–124. https://doi.org/10.1016/j.rse.2019.04.006

174. Toomajr, S., Tucker, W., 1971. Statistical comparison of airborne laser and stereophotogrammetric Sea Ice profiles. Remote Sens. Environ. 2, 261–272. https://doi.org/10.1016/0034-4257(71)90099-X

175. Torres-Rojo, J.M., Moreno-Sánchez, R., Mendoza-Briseño, M.A., 2016. Sustainable Forest Management in Mexico. Curr. For. Reports 2, 93–105. https://doi.org/10.1007/s40725-016-0033-0

176. Torresan, C., Berton, A., Carotenuto, F., Di Gennaro, S.F., Gioli, B., Matese, A., Miglietta, F., Vagnoli, C., Zaldei, A., Wallace, L., 2017. Forestry applications of UAVs in Europe: a review. Int. J. Remote Sens. 38, 2427–2447. https://doi.org/10.1080/01431161.2016.1252477

177. UN, 1992. Report of the United Nations conference on environment and development,Rio de Janeiro, Brazil: Annex III, NON-LEGALLY BINDING AUTHORITATIVE STATEMENT OF PRINCIPLES FOR A GLOBAL CONSENSUS ON THE MANAGEMENT, CONSERVATION AND SUSTAINABLE DEVELOPMENT OF ALL T.

178. van Lier, O.R., Luther, J.E., White, J.C., Fournier, R.A., Côté, J.-F., 2021. Effect of scan angle on ALS metrics and area-based predictions of forest attributes for balsam fir dominated stands. For. An Int. J. For. Res. https://doi.org/10.1093/forestry/cpab029

179. Vastaranta, M., Wulder, M.A., White, J.C., Pekkarinen, A., Tuominen, S., Ginzler, C., Kankare, V., Holopainen, M., Hyyppä, J., Hyyppä, H., 2013. Airborne laser scanning and digital stereo imagery measures of forest structure: Comparative results and implications to forest mapping and inventory update. Can. J. Remote Sens. 39, 382–395. https://doi.org/10.5589/m13-046

180. Véga, C., Hamrouni, A., El Mokhtari, A., Morel, M., Bock, J., Renaud, J.P., Bouvier, M., Durrieue, S., 2014. PTrees: A point-based approach to forest tree extractionfrom lidar data. Int. J. Appl. Earth Obs. Geoinf. 33, 98–108. https://doi.org/10.1016/j.jag.2014.05.001

181. Véga, C., Renaud, J.P., Durrieu, S., Bouvier, M., 2016. On the interest of penetration depth, canopy area and volume metrics to improve Lidar-based models of forest parameters. Remote Sens. Environ. 175, 32–42. https://doi.org/10.1016/j.rse.2015.12.039

182. Vincent, G., Antin, C., Laurans, M., Heurtebize, J., Durrieu, S., Lavalley, C., Dauzat, J., 2017. Mapping plant area index of tropical evergreen forest by airborne laser scanning. A cross-validation study using LAI2200 optical sensor. Remote Sens. Environ. 198, 254–266. https://doi.org/10.1016/j.rse.2017.05.034

183. Vosselman, G., Maas, H.-G. (Eds.), 2010. Airborne and terrestrial laser scanning. Whittles Publishing.

184. Wallace, L., Lucieer, A., Watson, C., Turner, D., 2012. Development of a UAV-LiDAR system with application to forest inventory. Remote Sens. 4, 1519–1543. https://doi.org/10.3390/rs4061519

185. Wang, C., Luo, S., Xi, X., Nie, S., Ma, D., Huang, Y., 2020. Influence of voxel size on forest canopy height estimates using full-waveform airborne LiDAR data. For. Ecosyst. 7, 31. https://doi.org/10.1186/s40663-020-00243-2

186. Wang, J., Perez, L., 2017. The Effectiveness of Data Augmentation in Image Classification using Deep Learning. https://doi.org/10.48550/ARXIV.1712.04621

187. White, J.C., Coops, N.C., Wulder, M.A., Vastaranta, M., Hilker, T., Tompalski, P., 2016. Remote Sensing Technologies for Enhancing Forest Inventories: A Review. Can. J. Remote Sens. 42, 619–641. https://doi.org/10.1080/07038992.2016.1207484

188. White, J.C., Tompalski, P., Vastaranta, M., Wulder, M.A., Saarinen, N., Stepper, C., Coops, N.C., 2017. A model development and application guide for generating an enhanced forest inventory using airborne laser scanning data and an area-based approach.

189. Williamson, TB and Edwards, J., 2014. Adapting sustainable forest management to climate change. desLibris.

190. Woods, M., Pitt, D., Penner, M., Lim, K., Nesbitt, D., Etheridge, D., Treitz, P., 2011. Operational implementation of a LiDAR inventory in Boreal Ontario. For. Chron. 87, 512–528. https://doi.org/10.5558/tfc2011-050

191. Wulder, M.A., White, J.C., Nelson, R.F., Næsset, E., Ørka, H.O., Coops, N.C., Hilker, T., Bater, C.W., Gobakken, T., 2012a. Lidar sampling for large-area forest characterization: A review. Remote Sens. Environ. 121, 196–209. https://doi.org/10.1016/j.rse.2012.02.001

192. Wulder, M.A., White, J.C., Nelson, R.F., Næsset, E., Ørka, H.O., Coops, N.C., Hilker, T., Bater, C.W., Gobakken, T., 2012b. Lidar sampling for large-area forest characterization: A review. Remote Sens. Environ. 121, 196–209. https://doi.org/10.1016/j.rse.2012.02.001

193. Yang, W., Ni-Meister, W., Lee, S., 2011. Assessment of the impacts of surface topography, off-nadir pointing and vegetation structure on vegetation lidar waveforms using an extended geometric optical and radiative transfer model. Remote Sens. Environ. 115, 2810–2822. https://doi.org/10.1016/j.rse.2010.02.021

194. Yu, X., Hyyppä, J., Karjalainen, M., Nurminen, K., Karila, K., Vastaranta, M., Kankare, V., Kaartinen, H., Holopainen, M., Honkavaara, E., Kukko, A., Jaakkola, A., Liang, X., Wang, Y., Hyyppä, H., Katoh, M., 2015. Comparison of laser and stereo optical, SAR and InSAR point clouds from air- and space-borne sources in the retrieval of forest inventory attributes. Remote Sens. 7, 15933–15954. https://doi.org/10.3390/rs71215809

195. Zhang, Z., Cao, L., She, G., 2017. Estimating Forest Structural Parameters Using Canopy Metrics Derived from Airborne LiDAR Data in Subtropical Forests. Remote Sens. 9, 940. https://doi.org/10.3390/rs9090940

196. Zhen, Z., Quackenbush, L.J., Zhang, L., 2016. Trends in automatic individual tree crown detection and delineation-evolution of LiDAR data. Remote Sens. 8, 1–26. https://doi.org/10.3390/rs8040333

Scientific Contributions

Publication details as first author:

1) **Dayal, K.R.**, Durrieu, S., Alleaume, S., Revers, F., Larmanou, E., Renaud, J.-P., Bouvier, M., 2020. Scan angle impact on lidar-derived metrics used in ABA models for prediction of forest stand characteristics: a grid based analysis. ISPRS - Int. Arch. Photogramm. Remote Sens. Spat. Inf. Sci. XLIII-B3-2, 975–982. https://doi.org/10.5194/isprs-archives-XLIII-B3-2020-975-2020
2) **Dayal, K.R**., Durrieu, S., Lahssini, K., Alleaume, S., Bouvier, M., Monnet, J.M., Renaud, J.P., Revers, F., 2022. An investigation into lidar scan angle impacts on stand attribute predictions in different forest environments. ISPRS J. Photogramm. Remote Sens. 193, 314–338. https://doi.org/10.1016/j.isprsjprs.2022.08.013.

As co-author:

3) K. Lahssini, F. Teste, **K. R. Dayal**, S. Durrieu, D. Ienco and J. -M. Monnet, "Combining LiDAR Metrics and Sentinel-2 Imagery to Estimate Basal Area and Wood Volume in Complex Forest Environment via Neural Networks," in IEEE Journal of Selected Topics in Applied Earth Observations and Remote Sensing, vol. 15, pp. 4337-4348, 2022, doi: 10.1109/JSTARS.2022.3175609.
4) K. Lahssini, **K. R. Dayal**, S. Durrieu and J. -M. Monnet, "Joint Use of Airborne LiDAR Metrics and Topography Information to Estimate Forest Parameters via Neural Networks," 2022 IEEE 21st Mediterranean Electrotechnical Conference (MELECON), 2022, pp. 442-447, doi: 10.1109/MELECON53508.2022.9843039.
5) Lenoir, Jonathan & Gril, Eva & Durrieu, Sylvie & Horen, Hélène & Laslier, Marianne & Lembrechts, Jonas & Zellweger, Florian & Alleaume, Samuel & Brasseur, Boris & Buridant, Jérôme & **Dayal, K.R.** & Frenne, Pieter & Gallet-Moron, Emilie & Marrec, Ronan & Meeussen, Camille & Rocchini, Duccio & Meerbeek, Koenraad & Decocq, Guillaume. (2022). Unveil the unseen: Using LiDAR to capture time-lag dynamics in the herbaceous layer of European temperate forests. Journal of Ecology. 110. 10.1111/1365-2745.13837.

Presentations:

6) Samuel Alleaume, Eric Larmanou, **Karun Dayal**, Sylvie Durrieu, Frederic Revers, et al.. Lidar sur drone pour évaluer la biodiversité des ripisylves. Journées techniques « Les drones en appui aux territoires », Nov 2019, Champs-Sur-Marnes, France. ⟨hal-02953351⟩
7) Poster presentation (ISPRS 2020,2021, 2022). Scan angle impact on lidar-derived metrics used in ABA models for prediction of forest stand characteristics: a grid based analysis
8) MS Silat (AgroParisTech, 2020, 2021, 2022 , 1hr)
9) Oral presentation (ForestSat 2022). Improving ABA models for forest attribute prediction using neural networks by considering effects of terrain and scan angles on 3D lidar point clouds Oral presentation